OCCUPANT-CENTRIC MODELING AND CONTROL FOR LOW-CARBON AND RESILIENT COMMUNITIES

by

JING WANG

B.E., Tongji University, 2013

M.E., Tongji University, 2017

M.S., Technical University of Braunschweig, 2017

A thesis submitted to the

Faculty of the Graduate School of the

University of Colorado in partial fulfillment

of the requirement for the degree of

Doctor of Philosophy

Department of Civil, Environmental and Architectural Engineering

2021

Committee Members:

Wangda Zuo, Chair

Kyri Baker

John Zhai

Yingchen Zhang

Sen Huang

Wang, Jing (Ph.D., Architectural Engineering)

Occupant-Centric Modeling and Control for Low-Carbon and Resilient Communities

Thesis directed by Associate Professor Wangda Zuo

Global climate change and resulting frequent extreme weather events have highlighted the significance of energy sustainability and resilience. Communities, which refer to a group of buildings located geographically together, are important units for energy generation and consumption. Hence, the research of community energy sustainability and resilience has drawn much attention during the past decades. However, there remain many challenges surrounding community energy modeling and control to achieve the low-carbon and resilient goals.

First, few tools are readily available for community-scale dynamic modeling and control-based studies. To address this gap, a community emulator was developed, which was designed to be hierarchical, scalable, and suitable for various applications. Data-driven stochastic building occupancy prediction was integrated into the emulator using logistic regression methods. Based on this work, we publicly released a library for net-zero energy community modeling using the object-oriented equation-based modeling language Modelica.

Second, building load control informed by real-time carbon emission signals is underdeveloped as utility price-driven control has so far been dominant. To better facilitate community energy sustainability through decarbonization, we proposed four rule-based carbon emission responsive building control algorithms to reduce the annual carbon emissions through thermostatically controllable loads. The impact of

carbon net-metering, as well as the evolvement of the future energy generation mix, is analyzed on top of both momentary and predictive rules. Based on the simulation results, the average annual household carbon emissions are decreased by 6.0% to 20.5% compared to the baseline. The average annual energy consumption is increased by less than 6.7% due to more clean hours over the year. The annual energy cost change lies between -4.1% and 3.4% on top of the baseline.

Third, the enhancement of community resilience in an islanded mode through optimal operation strategies is often faced with computational challenges given the large number of controllable loads. To tackle this, we proposed a two-layer model predictive control-based resource allocation and load scheduling framework for community resilience enhancement. Within this framework, the community operator layer optimally allocates the available PV generation to each building, while the building agent layer optimally schedules controllable loads to minimize the unserved load ratio while maintaining thermal comfort. We found that the allocation process is mostly constrained by the building load flexibility. More specifically, buildings with less load flexibility tend to be allocated more PV generation than other buildings. Further, we identified the competitive relationship between the objectives of minimizing unserved load ratio and maximize comfort. Therefore, it is necessary for the building agent to have multi-objective optimization.

Finally, to account for the uncertainties of occupant behavior and its impact on resilient community load scheduling, we developed a preference-aware scheduler for resilient communities. Stochastic occupant thermostat-changing behavior models

were introduced into the deterministic load scheduling framework as a source of uncertainty. KRIs such as the unserved load ratio, the required battery size, and the unmet thermal preference hours were adopted to quantify the impacts. Uncertainties from occupants' thermal preferences and their impact on load scheduling are then studied and addressed through chance constraints. Generally, the proposed controller performs better in terms of the unmet thermal preference hours and the battery sizes compared to the deterministic controller.

Dedication

To my father, Lianghua Wang. Thank you for always being there for me.

To my mother, Weihong Gao. Thank you for your unconditional love and consistent understanding of me.

To my late grandmother, Hongbin Jia. I miss you.

Acknowledgements

I would like to express my deep gratitude to my advisor, Dr. Wangda Zuo for his consistent help and inspirations along this journey. He brought me into the world of research and has ever since taught me how to become an independent researcher. He is always patient, warmhearted, and insightful. His rigorous attitude towards research and easygoing personality will affect me for long.

I am grateful for all my other committee members: Dr. Kyri Baker, Dr. John Zhai, Dr. Sen Huang, and Dr. Yingchen Zhang. Their perceptive comments and feedback have brought this dissertation to this current depth. I have learned a lot from every one of them. Without their contributions and co-authorship, I could not have my research outcomes published so soon.

I would like to thank my manager, Dave Roberts, and colleagues, Prateek Munankarmi and Jeff Maguire, at the National Renewable Energy Laboratory for their support and guidance. Special thanks to my mentor, Dr. Xin Jin, for his patience, inspiring discussions, and trust in me.

I would like to thank all my friends and lab mates at the Sustainable Buildings and Societies Laboratory for their companionship to make this journey more

enjoyable. Among them are Dr. Yunyang Ye, Dr. Yangyang Fu, Dr. Xu Han, Xing Lu, Danlin Hou, Katy Hinkelman, Yingli Lou, Cary Faulkner, Jes Stershic, Mingzhe Liu, Chengnan Shi, Jake Castellini, Saranya Anbarusu, Nasim Mamaghani, Yizhi Yang, David Milner, Tom Sevilla, Angelique Fathy, Qiujian Wang, Shifang Huang, Guang Zhou.

Finally, special thanks to my best friend and life partner, Zichen Liang. Thank you for understanding me and cheering me up when I'm down. Thank you for your love.

Contents

Chapter

Tables

Table

Figures

Figure

Chapter 1. Introduction

1.1 Background

The climate change and global energy crises have driven the energy usage worldwide to become more sustainable. As part of the effort to mitigate the climate change, the Paris Agreement [1] sets out a global framework to limit the global average temperature increase. It also aims for the global emissions to peak as soon as possible and then to undertake rapid reductions thereafter. In the United States, the Biden ministration sets an aggressive goal to reduce 50%--52% of greenhouse gas pollution by 2030 [2]. In China, the world's largest carbon trading market opened in July 2021, where more than 2,000 companies trade carbon emissions quotas there to help the country achieve its carbon emissions reduction goal [3].

The climate change has also led to the increasing frequency of extreme weather events, which put stress on the electric power grid. The 2021 Texas Power Crisis [4] happened as a result of three severe winter storms and caused a massive electricity generation failure, which then led to shortages of water, food, and heat. In 2017, Hurricane Maria left 1.5 million customers across Puerto Rico without electricity, and it took eleven months to restore the power system [5].

Therefore, enhancing energy sustainability and resilience is a significant topic and it should be practiced throughout the energy generation, transmission, distribution, and consumption processes. From the energy generation perspective, the increasing adoption of renewable energy resources helps avoid the carbon emissions associated with traditional fossil fuel-fired plants. Further, the development of microgrids integrated with distributed energy resources (DERs) diminishes the dependence on the power transmission and distribution, which promotes energy resilience. From the energy consumption perspective, buildings and communities are transforming to be more grid-interactive. The U.S. Department of Energy has developed a roadmap with recommendations for how Grid-interactive Efficient Buildings (GEBs) can provide a clean and flexible energy resource [6]. This facilitates energy sustainability and resilience through the control of flexible building loads targeting goals such as building energy decarbonization and resilient building operations.

1.2 Challenges and Research Gaps

Within this context, there remain many challenges and research gaps for the building sector to address. Firstly, though electricity price informed building load control has been extensively studied to reduce building energy costs, building control based on real-time carbon emission signals has not drawn enough attention until recently. Some studies adopt carbon emission reductions as one of the optimization objectives [7–12]. Yet, given the highly demanding computational effort of optimization-based control, rule-based control remains the dominant control method

in building automation systems due to ease of implementation. In addition, unlike energy net-metering, which has been comprehensively studied in building-to-grid related control studies, the inclusion of carbon net-metering is relatively rare. It remains to be explored how the inclusion of carbon net-metering would affect the performance of carbon responsive building control.

Secondly, load management and scheduling are excessively important during emergency situations if buildings want to sustain power outages for longer periods. However, no common rules have been established about how to prioritize loads in buildings during island mode. It remains unclear what principles are there to follow and to what extent can we curtail the loads. In addition, the impact of load scheduling on the built environment and occupant satisfaction remains to be investigated. Moreover, most existing studies limit their work scope to single buildings. When the problem scales to the community level with various building types, the number of controllable loads increases rapidly. If the scheduler tries to optimize the operational status of every appliance at every time step, the problem becomes exponentially complicated, computationally costly, and challenging.

Thirdly, dynamic short-interval interactions between the buildings and the grid require accurate predictions of building loads at a short timestep. Enhanced knowledge about building occupant behavior closes the loop and helps enhance the accuracy of the predicted real-time building loads. However, occupant behavior is a complicated, stochastic mechanism and can be influenced by multiple contextual factors [13, 14]. Due to its stochasticity and the lack of a reliable database for the

protection of occupants' privacy, occupant behavior modeling is still challenging and remains an active research field. Additionally, occupant behavior acts as one of the uncertainty sources in model-based building control such as model-predictive control (MPC). Hence, the existence of certain behaviors might impact the control performance and would require *a priori* interventions to assure a satisfying control result.

Lastly, unlike single building modeling which can be done with readily available commercial software, community-scale modeling often lacks suitable platforms that are extensible and scalable. Further, the complexity of the community model scales up with the number of modeled buildings. This requires the modeling platform to be flexible to allow the users to decide the fidelity of different parts of the model such as the thermal zone models, mechanical systems, and other parameters. Also, a wide range of simulation timesteps should be allowed considering the various dynamics within a community system. For instance, the simulation of DR-related controls could have a timestep of seconds while the thermal reactions of thermal zones are usually sub-hourly to hourly. Additionally, to hide the complexity of a community energy system, a hierarchical modeling structure is often preferred, which is not available in many commercially available software at the time.

1.3 Objectives

Given the aforementioned research gaps, this dissertation aims to address a subset of the identified gaps. The major research objectives and contributions of this dissertation are described below.

(1) An open-source library for Net-Zero Energy Communities (NZEC)

The open-source Modelica library built based on a real NZEC has been publicly released [15]. This library provides a series of Modelica component and subsystem models for community energy systems, including ground source heat pumps, solar thermal water heaters, photovoltaic (PV) panels, to name a few. This library can be easily utilized by users for community energy system modeling and control studies.

Using this library, we built a community emulator which also serves as a virtual testbed [16] for community-scale studies. This emulator is designed and structured in a highly hierarchical way to hide the complexity of the whole community energy system. As a result, it can be easily extended to embrace other systems (e.g., power distribution) or scaled up to model larger communities.

The building occupancy status prediction in this emulator is modeled stochastically. Given that no occupancy sensor data were available, we interpreted building occupancy from measured lighting power data and developed data-driven models to predict occupants' presence in the buildings. The models were validated against the lighting power measurements. The results show that the proposed multi-stage lighting power prediction method can predict daily peak power with a 2.42% relative error. The monthly and weekly NMBEs of lighting power are on average below 8.28%.

(2) Carbon emission responsive building control

To help achieve energy sustainability at a community scale, we consider the energy decarbonization during the buildings' operational phase. We present a rule-

based carbon responsive control framework that controls the setpoints of thermostatically controlled loads responding to the grid's carbon emission signals in real-time. Based on this framework, four controllers are proposed with different combinations of carbon accounting methods and control rules.

To evaluate their performance, we performed simulation studies using models of a 27-home, all-electric, net-zero energy residential community located in Basalt, Colorado, United States. To reduce the operational carbon emissions, the controllers modulate the setpoints of mini-split heat pumps for pre-heating or pre-cooling, and heat pump water heaters for pre-heating when there is excessive PV generation from the rooftop PV systems or when the grid electricity is relatively "clean" (i.e., with low carbon intensities). The carbon intensity data of four future years from the Cambium data set are adopted to account for the evolving resource mix in the power grid. Simulation results indicate that the carbon responsive controllers can reduce the homes' annual carbon emissions by 6.0% to 20.5%.

(3) Optimal load scheduling for resilient communities

To help achieve energy resilience at a community scale, we focus on resilience enhancement through optimal load scheduling for communities in island mode (i.e., disconnected from the main power grid). We designed a methodology for enhancing community resilience through optimal renewable resource allocation and load scheduling to minimize unserved load and thermal discomfort. The proposed control architecture distributes the computational effort and is easier to be scaled up than traditional centralized control. The decentralized control architecture consists of two

layers: The community operator layer (COL) allocates the limited amount of renewable energy resources according to the power flexibility of each building. The building agent layer (BAL) addresses the optimal load scheduling problem for each building with the allowable load determined by the COL. Both layers are formulated as an MPC-based optimization.

Simulation scenarios are designed to compare different combinations of building weighting methods and objective functions to guide real-world deployment by community and microgrid operators. The results indicate that the impact of power flexibility is more prominent than the weighting factor to the resource allocation process. Allocation based purely on occupancy status could lead to an increase in PV curtailment. Further, it is necessary for the building agent to have multi-objective optimization to minimize the unserved load ratio and maximize comfort simultaneously.

(4) Uncertainty of occupant behavior in load scheduling

Since occupant behavior has been identified as one of the major sources of uncertainty in building model-based controls, we propose to analyze and address its impact on load scheduling for resilient communities. Based on the deterministic scheduler proposed above, we developed an occupant preference-aware load scheduler for resilient communities operating in the islanded mode. Chance constraints were adopted to address the occupant-induced uncertainty in room temperature setpoints. Key resilience indicators were selected to quantify the impacts of the uncertainties on community load scheduling.

Results show that the proposed stochastic scheduler performs better in terms of serving the occupants' thermal preference and reducing the required battery size, given the presence of the assumed stochastic occupant behavior. This work indicates that it is necessary to consider the stochasticity of occupant behavior when designing optimal load schedulers for resilient communities.

1.4 Organization of Dissertation

This dissertation is organized as follows: Chapter 1 provides a broad research background of this dissertation with identified research challenges. The contributions of this work are introduced in this chapter as well. Chapter 2 conducts a thorough literature review on the research topics that are related to this dissertation. Chapter 3 discusses the development of the community emulator with stochastic data-driven occupancy prediction. Chapter 4 proposes four carbon emission responsive building controllers and compares their performance. Chapter 5 proposes a hierarchical load scheduling framework for the optimal operation of resilient communities. The uncertainties from occupant behavior are then analyzed in Chapter 6. Finally, Chapter 7 concludes this dissertation with limitations and future work.

Portions of this dissertation have appeared, or will appear, in other publications. Section 2.4, Chapter 5, and Chapter 6 have been published as journal articles. Section 3.3 has been published as a conference paper. Chapter 4 is under review and will be published as a journal article.

Chapter 2. Literature Review

Section 2.4 is based on:

Jing Wang, Wangda Zuo, Landolf Rhode-Barbarigos, Xing Lu, Jianhui Wang, Yanling Lin. “Literature review on modeling and simulation of energy infrastructures from a resilience perspective.” Reliability Engineering & System Safety 183 (2019): 360-373.

2.1 Introduction

This chapter provides a thorough literature review of the state of the art of the research topics discussed in this dissertation. The methods for energy modeling at a community scale are first reviewed with challenges identified. Among the modeling challenges, occupant behavior modeling is then further reviewed in detail. Subsequently, approaches for community decarbonization are reviewed with exemplary studies. Finally, the concept, existing models, and modeling approaches for community energy resilience are investigated comparatively.

2.2 Modeling of Community Energy Systems

2.2.1 Community-scale Energy Modeling

The energy modeling at the community scale is an active and rapidly evolving research area during the past decade. It refers to the computational modeling and simulation of the energy-related performance of a group of buildings [17], which are located geographically close to each other. Given that many communities often share the same energy system, there exist greater flexibility to accommodate large energy infrastructures such as district energy systems and thus richer load diversity to reduce the design capacity of energy systems [16]. The coordination among buildings can potentially provide more opportunities for providing grid services. The goal of community energy modeling is to analyze the short-term performance such as DR potentials or the long-term performance such as carbon emission and energy production/consumption. The analysis results can be further used for guiding the

decision-making of community design and retrofit, decarbonization techniques, as well as community resilience investments, etc.

Existing community energy modeling techniques can be categorized into three types: physics-based modeling [18–20], reduced-order modeling (ROM) [21], and data-driven modeling [17]. The physics-based modeling method typically adopts high-fidelity building modeling tools such as EnergyPlus for the detailed building energy performance prediction. The data-driven modeling method uses building energy data to develop data-driven models (e.g., artificial neural networks) for predicting building energy performance. The ROM method has a fidelity between the aforementioned two methods, where the coefficients of the building ROM models (e.g., RC network models) are predetermined according to building characteristics. Note that for community modeling, the location data also play an important role and can often be represented with the Geographical Information System (GIS).

Many research institutes have developed open-source readily available tools for community/urban scale energy modeling. For instance, URBANopt [22] is a multi-module physics-based modeling tool developed by National Renewable Energy Laboratory (NREL) for high-performance buildings and energy systems at a district scale. The input feature file formatted as a GeoJSON file provides a list of the site information and the building information. Based on Ruby gems, URBANopt then creates the building models automatically as EnergyPlus/OpenStudio models. The integrated REopt [23] module then enables DERs optimal sizing and dispatching.

Additional functionality such as the distribution network modeling is available through the OpenDSS [24] module.

Ali et al. [25] proposed a data-driven approach for multi-scale GIS-based building energy modeling (BEM). Irish building stock data were used in the geocoding procedure to identify archetypes of the building stock. As the next step, data-driven models were developed with a bottom-up approach for predicting building energy performance at a large scale. In the evaluation step, the generated GIS-based building energy performance maps were used for informing district planning and decision-making.

Yu et al. [26] proposed an approach integrating GIS, BEM, and global sensitivity analysis to prioritize key urban planning factors on community energy performance. The residential building prototype models were developed using the clustering tree structure method. EnergyPlus was used for simulating the energy use intensity (EUI) of the developed residential building prototypes. Additionally, a combined data-driven and global sensitivity analysis was conducted with Monte Carlo simulations.

Despite the amount of the emerging development effort, a few challenges remain in the community energy modeling field. First, with the development of building-to-grid integration and electrification in the transportation sector, there lacks a single platform that is capable of simulating multiple infrastructure sectors (e.g., energy, transportation, communication, etc.). Second, very short building simulation intervals down to the minute or second level are becoming essential in the

studies of building DR services. However, traditional BEM tools such as EnergyPlus have a minimum simulation timestep of 1 minute, which is still too large for fast DR services (e.g., frequency regulation). Third, the uncertainties of occupant behavior within single buildings or aggregated at community scales remain underexplored, especially in commercial buildings excluding office buildings.

The first two challenges can be potentially resolved by the object-oriented equation-based modeling language – Modelica [27]. Traditional BEM tools tightly couple numerical solutions with model equations, which makes it difficult to extend these programs to support new use cases [28]. For instance, in a stiff system where the controller with a time constant of seconds is simulated together with an HVAC system with a time constant of hours, such stiff ordinary differential equations would require implicit solvers to efficiently solve the problem [29]. Traditional BEM tools such as EnergyPlus solve such systems in steady-state and do not support adapting the solver based on the use case, which causes inefficient simulation.

In contrast, Modelica users can easily assemble a large system with component models developed by library developers, which enables a more in-depth understanding of the system. A simulation environment then analyzes these models (i.e., equations), optimizes them using computer algebra, translates them to executable codes (e.g., C language), and links them with a numerical solver [28]. This acausal modeling algorithm avoids a tight coupling between the numerical solution methods and the model equations and makes it suitable for modeling any cyber-physical systems of any domain. Further, Modelica has strong solvers with variable

timesteps (e.g., down to millisecond level), which are dependent on the system dynamics [30]. Hence, it is suitable for building control and DR-related simulations [31]. The following section discusses occupant behavior modeling, which addresses the third challenge.

2.2.2 Occupant Behavior Modeling in Buildings

One important aspect of enabling grid interactions in communities is to dynamically value and classify building loads for DR purposes. The uncertainty of occupant behavior is responsible for discrepancies between the simulated building energy consumption and the actual energy consumption [32, 33]. Hence, better knowledge about the occupants' behavior helps enhance the accuracy of real-time building load predictions. However, occupant behavior prediction is a complicated stochastic mechanism and can be influenced by multiple contextual factors [13, 14]. Conventional building energy simulation tools often adopt static schedules for occupants and equipment [34]. However, with the evolvement of other building energy-related fields, scientific and robust methods to model energy-related occupant behavior in buildings are in demand [13].

Many occupant behaviors affect building energy use and thermal comfort. Examples include occupant presence, window opening, window shading, lighting use, thermostat settings, and appliance use [35]. This section focuses on the modeling of the occupant behavior that has direct impacts on building power demand predictions; namely, the light switching, thermostat adjustment, and appliance usage. As an important common input of these behavior models, occupant presence modeling will

be discussed first. Note that other behaviors such as the window opening and closing and shading adjustment, which has an indirect impact on building power demand, are not the focus of this review.

The concept of building occupant behavior modeling consists of two major parts: occupant presence/movement modeling and occupant behavior (i.e., action) modeling. The former one answers the question of whether the occupants are inside the building and where they are. The latter one describes their interactions with the building electrical equipment (e.g., lighting system) in the building. The behavior of the occupants will influence the power demand, internal heat gain, and thermal comfort of the building and vice versa. Compared to conventional static schedules, the generation of dynamic schedules often involves stochastic modeling techniques. This enables real-time predictions of building power demand and its load constitutions and is thus important for the study of grid-interactive buildings and communities.

Occupant presence is a key factor in occupant behavior modeling, and it serves as the input of other behavior models. It describes the number of people inside a room or a building. Some models are capable of simulating the movement of occupants in a large building such as an office. A variety of mathematical methods have been applied to occupant presence modeling, including Markov and Hidden Markov chains, agent-based modeling, and data mining techniques (e.g., clustering and decision trees) [35–38]. According to Annex 66 project [39] final report [35], common data sources for presence models include occupancy, CO_2, and wireless camera sensor data, time-use data, light switching data, etc. [37, 40–42]. The first-order Markov chain

technique has been widely adopted in the development of occupancy models in office buildings [37, 40, 41, 43].

Wilke et al. [36] developed stochastic models, which were calibrated using survey data, to predict three types of time-dependent occupant-related quantities: the probability to be at home, the probability to start an activity, and the probability distribution function of the activity. They adopted first- and higher-order homogeneous Markov chains for modeling the transitions between occupant activities. The higher-order Markov chain extended the first-order chain by involving multiple past values. A Weibull distribution was used to estimate the duration of the occupants being at home.

Wang et al. [44] modeled private office occupancy with a non-homogeneous Poisson process model with two different exponential distributions to simulate the occupancy and vacancy sequence. The model requires three input parameters: mean occupancy duration (default value: 72.78), mean vacancy duration (default value: 42.6), and a seed for a random number generator. They tested the model for 35 private offices and the model has a relative error of around 5%. They also found that the vacant intervals of the 35 rooms were exponentially distributed. The mean vacancy interval was different from room to room. When the mean vacancy intervals were allowed to vary hourly, the fits were improved at some hours, but not at all hours. This model has been implemented in Modelica Buildings library v6.0.0: Buildings.Occupants package [45]. It can also be implemented in EnergyPlus Energy Management Script (EMS).

Tahmasebi and Mahdavi [46] studied the sensitivity of building performance simulation results to the choice of occupants' presence models. They compared the occupancy, lighting, and plug load values of the same building model with fixed or randomized schedules. The conclusion was that random models provide more reliable peak values for occupancy loads. However, they also pointed out that "it is much more important to possess reliable estimations of actual occupancy levels than whether probabilistic or non-probabilistic representations of presence patterns are deployed."

In terms of lighting energy use, studies have shown that the two main effective factors are outdoor illuminance and occupant behavior [47]. In existing occupant light switching models, the common data used include daylight level [48], illuminance level at the workplace [49, 50], occupancy sensor data [49, 50], as well as lighting power demand data [47]. Regarding the modeling approaches, Markov chains have been widely deployed [42, 49, 51].

Table 2.1 lists the major findings for occupant light switching actions. Hunt [48] proposed the earliest model for lighting control. Love's model [52] is similar to Hunt's but categorized occupants' light switching actions into two groups motivated by the expected duration of stay and indoor illuminance levels, respectively. Pigg et al. [53] enriched the previous theories with a statement relevant to occupants' light switch-off action.

Table 2.1 Major findings for occupant light switching actions [54].

Findings	**Reference**
All lights in a room are switched on or off simultaneously.	[48]
Switching mainly takes place when entering or vacating a space.	
The switch-on probability on arrival exhibits a strong correlation with minimum daylighting illuminance in the working area.	

Findings	Reference
People usually pertain to either of the behavioral classes: (a) switch on the lights for the duration of the working day even when temporarily absent (b) use lights only when indoor illuminance levels due to daylighting are low.	[52]
The manual switch-off probability of the lights strongly relates to the expected length of absence.	[53]

More specifically, Hunt's model [48] predicts the state of lights with the occupancy and minimum illuminance on the working plane. The switch-on happens at arrival and depends on the minimum illuminance at the working plane. The switch-off only happens when the occupant is leaving. The model adopts the logistic regression method and can be expressed by Equation (2.1).

$$y = a + \frac{c}{1 + exp\{-b(x - m)\}}, \tag{2.1}$$

where y represents the probability of turning on lights at arrival; x equals the logarithm to base 10 of the minimum work plane illuminances; a, b, c, and m are regression coefficients.

Further, Reinhart and Voss [54] extended Hunt's work by adding a model describing the intermediate switch-on probability. Like Hunt, the switch-on action depends on the minimum work plane illuminance. The switch-off probability is modeled in a logistic relationship with the duration of absence. The tool Lightswitch-2002 [50] was developed based on these models. This tool can be used to simulate occupants' light switching and blind control behavior.

Gunay et al. [55] implemented and compared twelve different sets of light switching behavior models in EnergyPlus EMS. They found that the lighting load peaks earlier when using Hunt's switch-on model, compared to Reinhart's model,

which peaks at the arrival after the last coffee break. Another finding is that people turn off their lights prior to departure about 95% of the time when using Reinhart's switch-off model but tend to forget their lights in Boyce's model [56]. Hence, they concluded that illuminance is less likely to trigger the switch-off action than the expected absent period.

For thermostat adjustment behavior modeling, research in the past relied heavily on user survey data. However, since the early 2010s, thermostat use data from both homes and offices have become available [35]. An example is the Donate Your Data program by ecobee thermostats [57]. In existing thermostat adjustment models, common data used include indoor temperature [58–61], outdoor temperature [59–61], building occupancy [58, 60], and thermal comfort votes [61], to name a few. Markov chains and logistic regression are common modeling approaches.

Ren et al. [58] developed a conditional probability model to predict air-conditioner (AC) usage in a residential apartment. The input data include spot interview, indoor temperature, CO_2 concentration, and AC power. Three types of triggers for AC on-off actions were considered: (1) environmental trigger – indoor air temperature; (2) event trigger – entering/leaving a room, going to bed, getting up; (3) random trigger – unidentified factors. To set up the probability model, Ren first obtained a Markov transfer matrix from historical data. The probability of turning on or off the AC was calculated based on the current on-off condition. Different probabilities were described as constants or discrete Weibull functions. The AC on-

off control actions were then simulated randomly. The validation results show that the R-squared value ranges from 0.89 to 0.99.

Compared with residential thermostat adjustment behavior models, office building models have a larger number of occupants, different schedules and trigger events, and thus higher stochasticity. Sun and Hong [62] simulated office building AC control behavior. The AC is turned on or off when occupants enter or leave the room or when occupants feel hot or cold. The occupant behavior modeling tool obXML [63, 64] adopts the same algorithm.

Gunay et al. [60] developed a thermostat changing behavior model based on the data collected from 38 private offices. The collected dataset consisted of occupancy status, thermostat keypress, indoor temperature, indoor relative humidity, and outdoor temperature. Discrete-time and discrete-event Markov logistic regression models were developed to predict the probability of occupants' setpoint increase and decrease actions during occupied hours. The study identified that the indoor temperature is the best input variable for occupant thermostat changing behavior prediction among the three environmental variables.

Lastly, the usage of household electrical appliances plays an important role in understanding building occupant behavior and has thus received significant attention [65, 66]. The common data used for appliance usage models include time use data [67–69], statistical data [70–72], and monitored appliance usage sensor data [73, 74]. In terms of modeling approaches, Monte Carlo simulation [69, 72, 74]

and Markov chains [67, 71] are two of the most common approaches for predicting the switch-on time of appliances.

Gunay et al. [75] built a data-driven model to predict plug-in equipment load patterns in private office spaces. The input data were occupancy sensor data and load metering data for 10 offices. They directly adopted an existing stochastic occupancy model for private offices [76] to generate the occupancy time series. They then established 10 plug load use patterns from the data and randomly assign them to the rooms in the building. The predicted building plug load distribution profiles were then obtained through Monte Carlo simulations. The model can predict the hourly plug load with a mean absolute error from 1.8 W to 5.7 W. The limitations of this study lie in that the authors did not evaluate the errors caused by occupancy presence models and they neglected the relationship between the occupants and the other plug-in equipment (e.g., vending machines, microwaves, refrigerators).

Mahdavi et al. [77] explored the relationship between inhabitants' presence, installed power for equipment, and electrical energy use in office buildings. The input data included occupancy presence data and load data. Three Weibull distributions were used to describe the plug load fractions. The authors adopted a generalized stochastic occupancy model (i.e., inhomogeneous Markov chain with one input) to generate occupancy presence time series. They then compared and evaluated the annual energy consumption with both measured presence data and stochastically generated presence data through Monte Carlo simulations. Mahdavi found that there

was a linear relationship between the plug load fraction and the presence probability. In addition, the stochastic model performed better in predicting the peak load.

Wang and Ding [78] developed an occupant-based energy consumption prediction model for typical multi-occupant offices (> 8 occupants). The input data included indoor occupant number time series and maximum, minimum, and standby input power of different office equipment. They assumed a cubic polynomial relationship between the occupancy rate and time. The computer input power probability was determined with the Markov chain-Monte Carlo method. Also, they assumed that other office equipment consumed 1% of the energy consumed by the computer. They used the model to predict annual energy consumption and validated the model with relative errors below 5%. The limitations of this work lie in that the authors did not establish a correlation between the occupant behavior and plug load power, where the two parts were simulated separately. Further, the model requires a significant amount of data as input.

Typically, the first step of plug load modeling is to conduct an occupant survey in the simulated building. As mentioned above, the input data usually include occupancy sensor data (e.g., 10-to-15-minute intervals). When no occupancy data is available, data mining techniques can be applied to get occupancy information from energy use data. With these data inputs, an occupancy presence model can be established using regression methods or adapted from an existing presence model. Plug load models are then linked with occupancy presence models, where an appliance is only switched on if there is at least one occupant present [35].

To summarize, based on the literature review, stochastic modeling methods such as the Markov chain have demonstrated their higher accuracy and broader applicability over deterministic methods in occupant behavior modeling. However, data collection remains a fundamental problem. To better describe the occupant behavior in the simulated building, common inputs such as survey data, occupant sensor data, as well as appliance energy use data are required.

There exist some readily available occupant behavior tools. For example, obFMU and obXML [63, 64] enable the co-simulation between occupant behavior and conventional building energy simulation tools. Modelica Buildings library [45] has readily available models for occupant behavior modeling. However, presence modeling for multi-occupied office rooms, as well as other types of commercial buildings, remains a challenge due to its high stochasticity. Its accuracy will further impact the related lighting, thermostat, and appliance use models.

Lastly, no dedicated research was found for plug load interdependency modeling in and residential and commercial buildings. This field awaits more research efforts as the interdependencies affect the power pliability of buildings participating in grid services.

2.3 Community Decarbonization

Buildings account for 35% of carbon dioxide (CO_2) emissions in the United States, which makes buildings important contributors to decarbonization [79]. With the Biden administration's aggressive goal to reduce 50%--52% of greenhouse gas pollution by 2030 [2], a joint effort between the buildings and the electric sector is

emerging to tackle this challenge. Further, the U.S. Department of Energy has developed a roadmap with recommendations for how GEBs can provide a clean and flexible energy resource [6]. On one side, the power generation is adopting more renewable energy, which is cleaner than traditional coal and natural gas-fired plants. On the other side, buildings can reduce their carbon emissions through using less energy (e.g., adoption of energy efficiency measures) or using cleaner energy (e.g., load shifting to cleaner hours).

Building decarbonization can be achieved during various phases of the building life cycle, including design, retrofit, and operation. The design phase often incorporates carbon analysis into early design building energy models [80], and some of the studies focus on embodied carbon emission reduction [81]. For the retrofit phase, several studies have been reported to optimally adopt energy efficiency measures, building system electrification, and high renewable penetration in existing communities for the purpose of enhancing energy performance while attaining carbon neutrality [82–86].

The above two phases are generally static and concern the long-term carbon emission performance of the buildings. During the building operation phase, carbon responsive building control is more flexible, and its deployment requires less capital investment. Adopting carbon emission reductions as one of the objectives or control inputs in optimization-based building control has received increased attention in the last decade [7–12]. Jin et al. [87] proposed a user-centric home energy management system that is based on a multi-objective MPC framework. Carbon emission reduction

serves as one of the objectives along with the minimization of energy cost, thermal discomfort, and user inconvenience. Leerbeck et al. [88] developed an optimal heat pump controller for building space heating. Using weather and CO_2 emission forecasts as inputs to an MPC, approximately 16% of CO_2 emissions were saved compared to typical thermostatic control.

Despite the rapid development of optimization-based control methods, rule-based control is still the dominant control method in building automation systems due to ease of implementation. For example, Clauss et al. [89] investigated predictive rule-based control for reducing the annual CO_2 equivalent greenhouse gas emissions ($CO_{2eq.}$) for a Norwegian single-family detached house. The controlled object was the building heat pump system. Historical weather and $CO_{2eq.}$ emission data from 2015 were used for simulations. The results showed that the carbon responsive control cannot reduce the yearly $CO_{2eq.}$ emission due to the limited daily fluctuations in the average $CO_{2eq.}$ intensity of the Norwegian electricity generation mix.

Carbon accounting methods play an important role in carbon responsive building control. Although electricity net-metering has been broadly taken into account in utility bill calculations, carbon accounting methods have seldom been discussed in the literature. The emissions reduction effect of clean electricity back feeding to the grid has generally been neglected in the design and evaluation of carbon responsive controllers. Additionally, historical CO_2 emission data are typically adopted in existing studies. With the increasing penetration of renewable energy in

the power grid, it is worth exploring evolving emission forecasts and their impact on control strategies.

2.4 Community Energy Resilience

In this section, the concept of resilience is first explored. Then, we conducted a comprehensive review of 30 energy resilience models. We summarized the modeling scenarios and the problems they tackle, as well as their typical assumptions. Based on the literature review, typical approaches to study energy infrastructure resilience are introduced. This review highlights the features and trends of existing models concerning their ability to address the multi-dimensional aspects of energy resilience.

2.4.1 Concept of Resilience

Resilience, as an emerging concept in the area of engineering, was first introduced in 1973 by Holling into the fields of ecology and evolution [90]. This concept was first used to describe the ability of an ecosystem to continue functioning after changes. Today, resilience has been broadly applied across many fields, including natural disasters and risk management [91], civil infrastructure studies [92], system engineering [93], energy systems [94, 95], and more.

Though consensus on the definition of resilience is lacking [96], the essence of resilience definitions is generally the same; that is, it is an overarching concept that encompasses the system performance before and after disastrous events. Francis and Bekera [97] reviewed various approaches to defining and assessing resilience and identified three resilience capacities: adaptive capacity, absorptive capacity, and

recoverability. Resilience therefore can be defined as "the ability of an entity to anticipate, resist, absorb, respond to, adapt to and recover from a disturbance" [98].

Resilience is a multi-dimensional concept. Its qualitative and quantitative studies often involve interdisciplinary efforts. Meerow et al. [99] reviewed the literature on urban resilience and concluded that "applying resilience in different contexts requires answering: Resilience for whom and to what? When? Where? And Why?" They, thus, pointed out the key considerations in the application of resilience: the stakeholder, the stressor, the temporal and spatial scale, and the motivation. Razafindrabe et al. [100] developed a Climate Disaster Resilience Index to measure the existing level of climate disaster resilience of targeted areas. This index utilizes 25 variables in five resilience-based dimensions: natural, physical, social, economic, and institutional. Carlson et al. and McManus et al. [98, 101] provided frameworks for system-level and region-level resilience overview to address personal, business, governmental, and infrastructure aspects of resilience. Roege et al. [102] formulated a scoring matrix to evaluate the system's capability to plan, absorb, recover and adapt from the perspective of physical, information, cognitive and social.

2.4.2 Energy Resilience Models

Energy infrastructures include electric power, natural gas, and fuel networks. Among all critical infrastructure (CI) sectors, energy infrastructure is identified as the most crucial one due to the enabling functions they provide across all other CI sectors (PPD-21). For example, water supply and sewer systems rely on electric power systems to operate their pump stations. Information and telecommunication systems

rely on power networks to carry out information transmission tasks. Transportation systems rely on fuel networks to obtain power for different kinds of vehicles. The dependence of other critical infrastructures on the energy network can lead to its vulnerability: Disruptions in the energy system may trickle down to other dependent infrastructure systems and possibly even back to itself, where the failure originated [103, 104]. This cascading and escalating characteristic of failure adds to the energy network's vulnerability. Energy infrastructures are also vulnerable to climate change. For example, the rising sea level and increasing frequency of major storms lead to severe floods in coastal areas, where a lot of energy infrastructures are located [105], such as power plants, natural gas facilities, and oil and gas refineries. Moreover, high-impact low-probability events, such as hurricanes and terrorist attacks, further threaten the operation of energy infrastructures.

Based on the aforementioned importance and vulnerability, the study of energy infrastructure resilience has become an urgent and significant research topic. Different researchers approach this problem in various ways. Many simulate energy infrastructure resilience as an optimal operation problem [106–110]. Some adopt agent-based modeling (ABM) techniques to reveal the complex interactions among energy system components [111–114]. Others improve traditional topological metrics of the power grid by embodying its physical behavior [115]. In response to the emergence of "big data" resources, some research applies large-scale data analysis in energy resilience studies, especially for power grid studies [116, 117].

To understand what problems are being tackled and how researchers are approaching these problems, this section first summarizes the research problems of the selected models and their corresponding key assumptions. Then, in the following section, the modeling approaches adopted by these models are introduced. They are representative of typical methods for conducting energy infrastructure resilience studies.

Given that resilience describes a system's ability to sustain disruptions and to recover quickly from them, energy infrastructure resilience models concentrate on solving two major problems: 1) resource allocation and hardening planning in the preparation stage, 2) power outage management and service restoration in the immediate aftermath and recovery stage. Due to limited budgets, identifying the most vulnerable components in the system and hardening them with minimized economic costs is one main topic the research community cares about. The second topic aims to mitigate the impacts of the disasters and to recover services quickly. Typical implementations include models that simulate the restoration process or that abstract the restoration process as an optimal control problem [106]. Common restoration measures include repair crew dispatch, distributed generation (DG), and switch device remote control to name a few.

Since the energy infrastructure sector is closely related to other CI sectors, an emerging number of studies focus on the study of interdependencies within the energy infrastructure sector and across CI sectors. Within the energy infrastructure sector, interactions between the natural gas system and the power grid system are

studied [118]. Across different sectors, researchers try to involve energy, water, transportation, and communication systems in the same modeling and simulation framework to find more holistic solutions.

For different application focuses, the models are usually developed under various assumptions of the real world. In models of distributed generation or microgrid technologies, it is typically assumed that the remotely controlled automatic switch devices are available in the distribution network so that lines can be opened/closed, and loads can be connected/disconnected to form multiple microgrids. The switches are assumed to have local communication capabilities to exchange information with their neighboring switches [119]. In most resilience models that simulate defender and attacker activities, the decision-maker has a budget to harden a maximum of power lines and to place a maximum of DG units. The system operators are aware of the status of all the components after the occurrence of the outage [120]. The worst-case attack scenario occurs, and the hardened lines and nodes are assumed to survive the disaster. For models that study weather impacts, it is assumed the system is exposed to the same weather conditions at any given time by modeling the weather event as a standstill event. This reduces the complexity of the modeling procedure because no regional weather aspects are considered. The restoration time during high and extreme wind speed events is equal to the restoration time during normal wind speeds [121, 122]. For models studying interdependencies between power and gas systems, it is assumed that electricity generation consumes gas and

gas compressors consume electricity [120]. Other specific assumptions depend on the modeling objectives and the scale of the model.

Table 2.2 summarizes basic information for the selected models including name, developer/author, scenario, and purpose/problem tackled. "Scenario" gives the specific modeling object of a model. "Purpose/problem tackled" describes the targeted problem the model was developed to solve. Among all the models, 15% are for power outage management and service restoration, 21% are for vulnerability and reliability analysis, 18% are for resource allocation and hardening planning and 12% are for infrastructure interdependency analysis. The rest address problems such as electricity market studies, weather event impact studies, general presentation, and analysis.

Table 2.2 Basic information of the selected energy resilience models.

	Name	**Developer/Author**	**Scenario**	**Purpose/Problem Tackled**
1	Two-stage outage management model (2018)	Arif et al.	Power distribution systems	Improve the computational efficiency in solving outage management problems for large distribution systems, co-optimize the repair, reconfiguration, and DG dispatch to maximize the picked-up loads and minimize the repair time.
2	Microgrids formation scheme (2016)	Chen et al.	Power distribution systems	Create a microgrid operation scheme to restore critical loads from the power outage by controlling the ON/OFF status of the remotely controlled switch devices and DG.
3	Sequential service restoration framework (2018)	Chen et al.	Power distribution systems	Generate a sequential service restoration framework for distribution systems and microgrids in large-scale power outages. A sequence of control actions includes coordinating switches, distributed generators, and switchable loads to form multiple isolated microgrids.
4	Multiple energy resilient operation model (2015)	Manshadi and Khodayar	Electricity and natural gas systems	Identify the vulnerable components and ensure the resilient operation of coordinated electricity and natural gas infrastructures considering multiple disruptions within the microgrid by

	Name	Developer/Author	Scenario	Purpose/Problem Tackled
				improving the resilience of generation and demand scheduling.
5	Two-stage robust optimization model (2016)	Yuan et al.	Power distribution systems	Resilient distribution network planning to coordinate the hardening distributed generation resource allocation with the objective of minimizing the system damage.
6	A risk optimization model (2017)	Nezamoddini et al.	Power transmission networks	Determine the optimal investment decision for the resilient design of transmission systems against physical attacks. The investment costs are minimized such that the load curtailment does not exceed a certain threshold value.
7	The planner-attacker-defender model (2017)	Fang et al.	Power transmission networks	Study the combination of capacity expansion and switch installation in electric systems that ensures optimum performance under nominal operations and attacks. The planner-attacker-defender model is adopted to develop decisions that minimize investment and operating costs, and functionality loss after attacks.
8	Attack structural vulnerability model (2010)	Chen et al.	Power transmission networks	Propose a hybrid approach for structural vulnerability analysis of power transmission networks, in which a DC power flow model with hidden failures is embedded into the traditional error and attack tolerance methodology.
9	CitInES (2013)	Page et al.	Energy generation, storage, transport, distribution systems, and demand	Present a multi-energy modeling environment to simulate and optimize urban energy strategies. Energy demand is modeled to consider the costs and impacts of demand-side measures. Optimization techniques are involved to provide answers to urban energy infrastructure planning issues.
10	An improved model for structural vulnerability analysis (2009)	Chen et al.	Electric power systems	Structural vulnerability analysis of power networks. Depicting a typical power network as a weighted graph based on electrical topology by introducing its bus admittance matrix.
11	Graph Model (2006)	Holmgren	Electric power systems	Model electric power delivery networks as graphs, calculate values of topological characteristics of the networks, and evaluate different strategies to decrease the vulnerability of the system.
12	Tri-level defender-attacker-defender model (2018)	Lin and Bie	Power distribution systems	Find the best hardening plan under malicious attacks given the available defending resources and operational restoration measures for a distribution system. Resilient operational measures include optimal DG islanding formation and topology reconfiguration.

	Name	Developer/Author	Scenario	Purpose/Problem Tackled
13	A "proof-of-concept" model (2011)	TU Delft	The 380kV power network in the Netherlands	Explore the adaptation of energy infrastructures to climate change.
14	Electricity Market Complex Adaptive System (2006)	Argonne National Laboratory (ANL)	Electric power and financial networks	Modeling and simulation of operations in restructured electricity markets.
15	Natural Gas Infrastructure Toolset (2006)	ANL, Infrastructure Assurance Center	Natural gas networks	Provide an analyst with a quick method to access, review, and display components of the natural gas network; perform varying levels of component and systems analysis, and display analysis results.
16	Critical Infrastructure Modeling System (2006)	Idaho National Laboratory	Electric power system, human activity, and supervisory control and data acquisition (SCADA)	Provide decision-makers with a highly adaptable and easily constructed 'wargaming' tool to assess infrastructure vulnerabilities including policy and response plans.
17	Critical Infrastructure Simulation by Interdependent Agents (2006)	University Roma Tre	Electric power system and SCADA	Analyze short-term effects of failures in terms of fault propagation and performance degradation.
18	Integrated energy system reliability evaluation model (2016)	Li et al.	Electricity distribution network, distributed renewable energy system, gas system, cooling, and heating systems	Present a new reliability evaluation approach, in which Smart Agent Communication is based system reconfiguration is integrated into the reliability evaluation process.
19	SynCity (2010)	Imperial College London	Urban energy systems	Provide an integrated, spatially, and temporally diverse representation of urban energy use within a generalized framework across all the design steps and in a variety of problem environments.
20	Resilience evaluation model (2017)	Panteli and Pierluigi	Electric power systems	Provide a conceptual framework for gaining insight into the resilience of power systems with a focus on the impact of severe weather events. The effect of weather is quantified with a stochastic approach. The resilience of the critical power infrastructure is modeled and assessed within a context of system-of-systems that also include human response as a key dimension.
21	Multi-microgrid reliability assessment framework (2017)	Farzin et al.	Multi-microgrid distribution system	Develop a general framework for reliability assessment of multi-microgrid (MMG) distribution systems. Investigate reliability impacts of

	Name	Developer/Author	Scenario	Purpose/Problem Tackled
				coordinated outage management strategies in an MMG distribution network.
22	Critical Infrastructures Interdependencies Integrator (2002)	ANL	Natural gas pipelines	Infrastructure restoration time and/or cost estimation considering an interdependency analysis.
23	Restore (2011)	ANL	Natural gas pipelines	Estimate the time and cost of Infrastructure restoration.
24	A framework for reliability/availability assessment (2017)	Cadini et al.	Electric power transmission networks	Combine an extreme weather stochastic model with a realistic cascading failure simulator based on a direct current power flow approximation and a proportional re-dispatch strategy. The dynamics of the network are completed by the introduction of a restoration model accounting for the operating conditions that a repair crew may encounter during an extreme weather event.
25	Interdependent Energy Infrastructure Simulation System (2006)	Los Alamos National Laboratory	Electric power and natural gas infrastructures	Assist individuals in analyzing and understanding interdependent energy infrastructures.
26	Framework for Electricity Production Vulnerability Assessment (2009)	Shih et al.	Coal distribution network	Use data warehousing and visualization techniques to explore the interdependencies between coal mines, rail transportation, and electric power plants.
27	Critical Infrastructure Protection Modeling and Analysis (CIPMA) Program (2006)	Australian Government - Attorney General's Department	CI networks and high priority precincts	Support business and government decision-making for CI protection, counterterrorism, and emergency management, especially with regard to prevention, preparedness, and planning and recovery.
28	Petroleum Fuels Network Analysis Model (2006)	ANL, Infrastructure Assurance Center	Crude oil and petroleum product transport pipelines	Perform hydraulic calculations of pipeline transport of crude oil and petroleum products. Introduction of pipeline component dependencies into critical infrastructure analyses.
29	Critical energy infrastructures (2014)	Erdener et al.	Electricity, natural gas, and oil systems	Analysis of the impacts of interdependencies between electricity and natural gas systems. Propose an integrated simulation model that reflects the dynamics of the systems in case of disruptions and takes the cascading effects of these disruptions into account.
30	Fast Analysis Infrastructure Tool (2006)	Sandia National Laboratory (SNL)	Electric power, natural gas, and waterway systems	Determine the significance and interdependencies associated with elements of the nation's CI.

2.4.3 Modeling Approaches

In this section, we introduce typical modeling approaches for energy infrastructure resilience problems. The models collected in this work adopt a variety of modeling approaches including optimal operation modeling, topological network modeling, ABM, probabilistic modeling, system dynamics modeling, empirical modeling, and more.

Table 2.3 lists the modeling approaches and the corresponding models that were collected in this work. The most common four approaches will be introduced in detail in the following subsections. The rest of the approaches are introduced briefly in "other approaches". It should be noted that since the review object of this work is numerical models that could conduct simulations and predict system performance in the real world, no surveys or qualitative studies were included. In the remaining part of this section, each modeling approach is introduced with exemplary models to address their characteristics.

Table 2.3 Modeling approaches for energy resilience problems.

	Modeling Approach	**Model Name**
1	**Optimal Operation Modeling**	Two-stage outage management model (Arif et al. 2018)
2		Microgrids formation scheme (Chen et al. 2016)
3		Sequential service restoration framework (Chen et al. 2018)
4		Multiple energy resilient operation model (Manshadi and Khodayar 2015)
5		Two-stage robust optimization model (Yuan et al. 2016)
6		A risk optimization model (Nezamoddini et al. 2017)
7		The planner-attacker-defender model (Fang and Sansavini 2017)
8	**Topological Network Modeling**	Attack structural vulnerability model (Chen et al. 2010)
9		CitInES (Page et al. 2013)
10		An improved model for structural vulnerability analysis (Chen et al. 2009)
11		Graph Model (Holmgren 2006)

	Modeling Approach		Model Name
12			Tri-level defender-attacker-defender model (Lin and Bie 2018)
13	**Agent-Based Modeling**		A "proof-of-concept" model (Bollinger 2011)
14			Electricity Market Complex Adaptive System (Pederson et al. 2006)
15			Natural Gas Infrastructure Toolset (Pederson et al. 2006)
16			Critical Infrastructure Modeling System (Dudenhoeffer et al. 2006)
17			Critical Infrastructure Simulation by Interdependent Agents (Pederson et al. 2006)
18			Integrated energy system reliability evaluation model (Li et al. 2016)
19			SynCity (Keirstead et al. 2010)
20	**Probabilistic Modeling**		Resilience evaluation model (Panteli and Mancarella 2017)
21			Multi-microgrid reliability assessment framework (Farzin et al. 2017)
22			Critical Infrastructures Interdependencies Integrator (Gillette et al. 2002)
23			Restore (ANL 2011)
24			A framework for reliability/availability assessment (Cadini et al. 2017)
25	**Other Approaches**	Actor-Based Modeling	Interdependent Energy Infrastructure Simulation System (IEISS) (Toole and McCown 2008)
26		Empirical Modeling	Framework for Electricity Production Vulnerability Assessment (Shih et al. 2009)
27		System Dynamics Modeling	CIPMA Program (Pederson et al. 2006)
28		Physical Modeling	Petroleum Fuels Network Analysis Model (Pederson et al. 2006)
29		Integrated Simulation Platform	Critical energy infrastructures (Erdener et al. 2014)
30		Integrated Simulation Platform	Fast Analysis Infrastructure Tool (Pederson et al. 2006)

(1) Optimal Operation Modeling

Optimal operation modeling is one of the most widely used methods in the research area of energy infrastructure resilience. In this method, when the system is interrupted, achieving resilience can be interpreted as an optimization problem to restore the system within a short time while minimizing the load shedding ratio.

Arif et al. [106] solved the outage management problem by co-optimizing the repair, reconfiguration, and DG dispatch to maximize the picked-up loads and minimize the repair time considering reconfiguration and repair crew scheduling.

Chen and Ding [108, 119] proposed a microgrid formation mechanism to restore critical loads after major grid faults caused by natural disasters. In this scheme, a mixed-integer linear program was formulated to maximize the total prioritized loads restored while satisfying the self-adequacy and operational constraints of each microgrid. Similarly, Chen et al. [123] formulated a mixed-integer linear program model for the sequential service restoration problem. This model can generate the optimal restoration sequences to coordinate dispatchable DGs and switch gears to energize the system on a step-by-step basis. Manshadi and Khpdayar [110] proposed a bi-level optimization methodology that took into consideration the interdependency between natural gas and electricity infrastructures. Through this model, the identification of most vulnerable components in the system, as well as the resilient generation and demand scheduling could be achieved. Yuan et al. [107] proposed a model for resilient distribution system planning with hardening and DG based on two-stage optimization. In this model, a multi-stage and multi-zone-based uncertainty set was used to capture the uncertainty of natural disasters.

To summarize, existing optimal operation models share common objective functions such as maximizing picked-up loads, minimizing repair time, and economic investments. For restoration strategy development purposes, frequently considered measures include topology reconfiguration, DG dispatch, microgrid formulation, repair crew dispatch, and switch device control. The problem is usually represented by mathematical models with equilibrium equations and certain constraints, including self-adequacy and operation constraints. An emerging number of studies

focus on solving problems of demand scheduling and load flexibility in response to the adoption of building-to-grid and vehicle-to-grid technologies.

However, this type of model usually focuses on one single problem, either protection resource allocation or restoration, which are two separate stages of energy infrastructure resilience. On the other hand, the occurrence of the disaster is usually not simulated. If all of these characteristics are coupled together, the optimization problem might become very complicated, and the computational time problem will arise. Nezamoddini et al. [124] compared the computational time of different scales of test systems. The computational time increases from 3 seconds to 4.2 hours when the system upgrades from the IEEE 6-bus to the IEEE 57-bus test system.

Power networks have been studied as a typical example of real-world complex networks [125]. They can be modeled by extracting their topology. In this type of model, the power networks are represented by a set of vertices connected by a set of edges. The vertices represent buses, and the edges represent transmission lines. This type of model is typically applied in the structural vulnerability analysis of power networks.

(2) Topological Network Modeling

Topological network models are easy to analyze due to their high level of abstraction and simplification. Buldyrev et al. [104] used the topology of the interdependent power system and communication system to demonstrate the cascading fault evolving between the two systems. Page et al. [126] proposed a simplified energy network modeling approach. Based on the topology of the original

network, they used clusters that were aggregations of network nodes to build a less detailed model and calibrated it with detailed simulations. In this way, the number of variables was significantly reduced.

However, purely topological approaches fail to capture the physical properties and operational constraints of power systems and, therefore, can sometimes provide too optimistic of an analysis [115]. Hines et al. [127] compared purely topological network models and higher fidelity models in the vulnerability modeling of electricity infrastructures. They used three measures of vulnerability: characteristic path lengths, connectivity loss, and blackout sizes. They concluded that evaluating vulnerability in power networks using purely topological network models can be misleading. Chen et al. [128] proposed a hybrid model for structural vulnerability analysis of power networks. Their approach embodied the traditional topological methodology and took into account important characteristics of power transmission networks such as the power flow distribution. Consequently, their hybrid model better approximated real power grids compared with a traditional topological network model.

Topology modification, or known as reconfiguration, plays an important role in the study of electric power system resilience, as a section can be reconnected to another power supply when an outage happens. Lin and Bie [129] proposed a tri-level defender-attacker-defender model to harden the distribution system under malicious attacks. In this model, resilient operational measures such as topology

reconfiguration and DG were simulated to study their impact on distribution system resilience.

(3) Agent-based Modeling

Agent-based models consist of dynamically interacting, rule-based agents [130]. A general definition of an agent is: "*an entity with a location, capabilities, and memory. The entity location defines where it is in a physical space… What the entity can perform is defined by its capabilities… the experience history (for example, overuse or aging) and data defining the entity state represent the entity's memory*" [131]. An agent-based model can exhibit complex behavior patterns [132] and provide valuable information about the dynamics of the simulated real-world system [131].

The application of ABM in this domain mainly focuses on analyzing interactions between interdependent systems. Casalicchio et al. [133] used ABM to model a system composed of a power grid and a communication network with agents representing the entire infrastructure, its subsystems, and the humans involved in the scenario. In this model, an agent is described by its attributes, the services it provides to other agents, and the services provided by other agents. Li et al. [114] modeled the integrated energy system of electricity and natural gas. A two-hierarchy smart agent model is built as the basis for the system reliability analysis. The lower hierarchy is the component smart agents including the power lines, transformers, and electricity loads while the higher hierarchy is the zone agents which form the system topology.

Another important application of ABM is to simulate socio-economic activities, such as the electricity market and human activities within the energy infrastructure framework. Zhou et al. [134] simulated an electricity market with DR from commercial buildings. In this model, agents were used to model different market participants such as power generation companies, load-serving entities, commercial building aggregators, and an independent system operator. SynCity [113] is a tool developed by Imperial College London for integrated modeling of urban energy systems. This tool adopts agent-based micro-simulations to simulate the daily activities of citizens of the city. Each citizen makes stochastic decisions based on the pre-defined rules and according to the environment around them. Solanki et al. [135, 136] used agents to model different operators in restoring the electric system.

The ABM technique has proved its advantages in the following aspects: 1) It can capture complicated interdependencies by simulating physical or economic flows among different infrastructures. 2) It enables the study of large-scale problems by avoiding complicated theoretical analysis. 3) It allows behavior analysis of customers or decision-makers by making certain rules. However, this modeling technique still has limitations; it is difficult to validate and not all types of interdependencies can be included in one single model. Most existing agent-based models can only simulate one type of interdependency such as the physical or logical interdependency [137].

(4) Probabilistic Modeling

In energy infrastructure resilience modeling, the probabilistic algorithm is necessarily applied to capture the uncertain characteristics of the system failure.

Many models adopt the sequential Monte Carlo simulation method [121, 122, 138]. A Monte Carlo simulation uses repeated sampling to determine the properties of some phenomenon or behavior [139]. The essential idea is to use randomness to solve problems that might be deterministic in principle. It is useful for gathering information about random objects, estimating certain numerical quantities, and optimizing complicated objective functions [140].

Monte Carlo simulation in the field of energy infrastructure modeling is often employed for the simulation of weather events due to their high stochasticity. Panteli and Marcarella [121] developed a time-series simulation model based on the sequential Monte Carlo method to assess the impact of weather events on power-system resilience. With the knowledge of the hurricane occurrence frequency and its impact on power system components, Li et al. [141] developed an algorithm to evaluate the risks of the power system in face of hurricanes. This method can be expanded to systems under other stochastic natural disasters. Similarly, Cadini et al. Cadini et al. [122] used a sequential Monte Carlo simulation scheme to simulate historical failures caused by both normal and extreme weather events. The simulation results were then used to evaluate the reliability of the studied power transmission system.

Another common application of Monte Carlo simulation in energy infrastructure modeling is to simulate the restoration process of disrupted infrastructures. For example, the software tool Critical Infrastructures Interdependencies Integrator [142] developed by ANL used Monte Carlo simulation

to estimate the time and cost required to restore a given infrastructure component, a specific infrastructure system, or a set of interdependent infrastructures.

It should be noted that Monte Carlo simulation can be integrated into other modeling frameworks, such as optimization-based models, to simulate the performance of energy systems. For example, Farzin et al. [138] evaluated the role of outage management with Monte Carlo simulation while considering the optimal power flow problem of the electric distribution system.

(5) Other Approaches

Actor-based modeling: Similar to an agent-based model, an actor-based model is composed of actors that can make local decisions, create more actors, send messages, and determine how to respond to messages received. The Interdependent Energy Infrastructure Simulation System (IEISS) [143] developed by LANL is an actor-based infrastructure modeling, simulation, and analysis tool designed to understand interdependent energy infrastructures. The actors can realistically simulate the dynamic interactions within each of the infrastructures, with a specialization in simulating the interdependent electric power and natural gas infrastructures.

Empirical modeling: Empirical models are built based on historical data or expert experience. Shih et al. [144] adopted a data warehousing technique to conduct a vulnerability assessment of interdependencies between coal mines, rail transportation, and electric power plants. A data warehouse is a system used for reporting and data analysis. It has the capability of bringing various datasets

together and managing historical data. In this case, the data warehouse allowed an interactive analysis of historical and multi-dimensional data of varied granularities.

System dynamics modeling: System dynamics is a method for studying the behavior and the underlying structure of a complex system over time [145]. It is widely used in the analysis of CI interdependencies. For example, the CIPMA program [146] in Australia adopts the system dynamics model to examine the relationships and dependencies within and between CI systems. It also demonstrates how a failure in one sector can greatly affect the operations of other CI sectors.

Physical modeling: Petroleum Fuels Network Analysis Model (PFNAM) [112] is a physical model developed by ANL to perform hydraulic calculations of pipeline transport of crude oil and petroleum products. The main outputs of the model include pressure and pipeline capacity estimates along the pipeline.

Integrated simulation platform: Some models are implemented in a way that several approaches are adopted for component models and then coupled together. Erdener et al. [118] proposed an integrated simulation model for electricity and gas systems. The electricity and gas systems are first modeled separately and then linked by a MATLAB-based interface. The Fast Analysis Infrastructure Tool (FAIT) developed by SNL [112] consists of a dependency model and an economic model. The dependency model is an object-oriented expert system model of infrastructure interdependencies. The economic model utilizes the input-output method for estimating the economic consequences of the disruption of an asset. An input-output model is a quantitative economic technique that represents the interdependencies

between different branches of a national economy or regional economies [147]. This economics-based method has been applied to CIs to capture the cascading economic effects of a disruption across different sectors [137].

To conclude, the models collected in this work involve representative state-of-the-art energy infrastructure models implemented through various approaches. The addressed problems include optimal resource allocation and hardening planning, interdependency analysis, outage management and restoration, weather impact study, and more. The models intervene across planning, operation, restoration, and adaptation phases of energy infrastructures. Based upon the review, the following observations are gained: The dominant stakeholder of the models are decision-makers, including governments and regulators. Most selected models serve energy consumers indirectly as little attention is paid to energy consumers during the development stage. Most selected models focus on the operation and restoration phases of energy infrastructures. Long-term adaptation strategies are not integrated into the modeling framework by most models. Existent models tend to only consider the immediate effects of system disruptions. The study on the propagated effects of the failure among different sectors is typically neglected. Although many selected models involve economic impact evaluation, only a few models take into account social parameters or consider social impacts of disasters. Concerning other modeling features, physics-based models are still the trend in energy infrastructure modeling, rather than data-driven techniques. Among others, agent-based models tend to have

higher data needs than topological models and optimal operation models. The time horizon and time step vary from several hours to several years.

Based on the discussions above, future trends in the modeling and simulation of energy infrastructures are as follows:

Addressing larger temporal and spatial scale: As most existing energy infrastructure models focus on immediate effects of disruptions but are limited in capturing the dynamic behavior during longer terms, it remains to be explored how the models could be scaled over a larger temporal scale. Also, including the complex interactions across multiple CI sectors over different spatial scales would make the model more realistic. However, the challenge of scalability lies in the computational time. Employing more complexity in the model while reducing the computational time remains a challenge for future researchers.

Integrating more human and social aspects: Though existing models generally serve the needs of decision-makers, energy consumers' behavior and potential in helping to achieve energy infrastructure resilience should be considered more in the future. The emerging focus on human-in-loop control and demand response technologies also implies this trend. Also, since the impact of disasters eventually takes place on the human and the society, this could draw more attention to integrating social characteristics in the modeling frameworks and then study the social impacts of CI disruptions. However, the uncertainty in human behavior and the quantification of social factors remain a challenge.

Employing more smart resources and solutions: Smart technologies such as energy storage and demand response with flexible loads (e.g., electrical vehicles, flexible building loads) are integrated by some models to explore future possibilities of energy resilience. In the future, as these technologies develop and become more accepted, involving them in energy infrastructure models would become a trend.

2.5 Summary

This chapter provides a thorough literature review of the modeling, decarbonization, and resilience of communities. In Section 2.2, the major modeling techniques for community energy modeling are reviewed; namely, physics-based modeling, reduced-order modeling, and data-driven modeling. The advantage of the object-oriented equation-based modeling language Modelica is highlighted through the comparison with traditional BEM tools. As a major source of uncertainties in BEM, approaches for selected occupant behavior are also reviewed in this section.

Section 2.3 first briefly describes building decarbonization measures during the design, retrofit, and operation phases. Subsequently, the reduction of building operational carbon emissions through control methods is discussed in detail. The rule-based carbon responsive control is compared with optimization-based control.

Finally, Section 2.4 reviews the concept of resilience, existing resilience models for energy infrastructures, and approaches for energy resilience. Based on the review, future trends in the resilience modeling of energy infrastructures include addressing larger temporal and spatial scales; integrating more human and social aspects; employing more smart and distributed energy resources.

Chapter 3. Community Emulator with Stochastic Occupant Behavior Predictions

Section 3.3 is based on:

Jing Wang, Wangda Zuo, Sen Huang, Draguna Vrabie. “Data-driven prediction of occupant presence and lighting power: A case study for small commercial buildings.” In Proceedings of the American Modelica Conference 2020. March 23-25, 2020, Boulder, CO, USA.

3.1 Introduction

This chapter first introduces the hierarchical modeling structure for communities with Modelica. An example community emulator based on a real net-zero energy community is used to facilitate the discussion. Further, as part of the community emulator, the stochastic modeling of building occupancy status based on building lighting power data is developed. A case study on small commercial buildings shows that the proposed models can be used for sub-hourly power demand predictions within acceptable deviations of 7%.

3.2 Hierarchical Modeling Structure

3.2.1 System Information

The hierarchical community emulator in Modelica is built based on a real community, Historic Green Village (HGV), located in Anna Maria Island, FL, USA [148]. The main power source of this community consists of two parts: the power grid and the roof-top PV panels (Figure 3.1 (a)). Thanks to the rich solar resources on the island, the community reached net-zero energy in 2014. Energy submeters and ecobee thermostats have been installed to record the energy consumption and generation, indoor air temperature setpoints, and indoor air temperature measurements. A weather station has been installed to measure the outdoor weather conditions (Figure 3.1 (b)). A solar monitoring system monitors the local solar irradiance.

(a)

(b)

Figure 3.1 Photos of the roof-top PV panels (a) and the weather station (b).

There are five mixed-use buildings in HGV as listed in Table 3.1. Building types range from residential apartments to small commercial buildings such as an office, a bakery, and gift shops. The HVAC systems of all buildings are ground source heat pumps (HPs). In summer, cold water is supplied to the HPs serving the building thermal zones, absorbs the heat from the return air, and then is circulated back to a main community heat exchanger where the condensation happens. The heat is then dissipated to the soil through pipes buried underground and in winter vice versa. In total, there are nine thermal zones in the five mixed-use buildings. The HP system capacities are shown in Table 3.1. Different types of domestic hot water (DHW) systems; namely, gas heaters, electric heaters, and solar thermal water heaters, are installed in each building based on their hot water needs.

Table 3.1 Information of buildings, HP systems, and DHW systems in HGV.

Building	**Type**	**Floor area (m^2)**	**HP system capacity (kW)**	**DHW system**
1 (F)	Bakery	410	19.5	Gas heater
2 (G)	Office	95	8.22	Gas heater

Building	Type	Floor area (m^2)	HP system capacity (kW)	DHW system
	Apartment 1	95	8.22	Solar thermal water heater
3 (A)	Gift shop 1	88	8.22	Electric heater
		56	11.07	
	Apartment 2	94	11.07	Solar thermal water heater
4 (D)	Gift shop 2	95	15.07	Electric heater
5 (C)	General store kitchen	120	15.07	Solar thermal water heater
	Ice cream shop	40	15.07	

3.2.2 Model Structure

To model the energy system (e.g., HVAC and DHW) of the community, Figure 3.2 shows a design diagram of the community emulator at the top level. The seven interconnected modules represent the power grid, PV panels, HP system, DHW system, building loads, weather data, and schedules block, respectively. The interactions between each of the modules are indicated by different line types and colors in the diagram. For instance, the grid and the PV system supply power to the HP system, the DHW system, and the building loads. The buildings and the HP systems are connected through the air loop and a temperature sensor measures the indoor air temperature and sends it back to the HP controllers. The HP system and DHW system are connected through the water loop, where waste heat is recovered from the HP loop to preheat the hot water. The buildings, PV, and DHW blocks obtain the outdoor dry-bulb temperature and solar direct and diffuse irradiance information from the weather block. Lastly, the schedules block sends out the schedule information to the buildings, HPs, and DHW system.

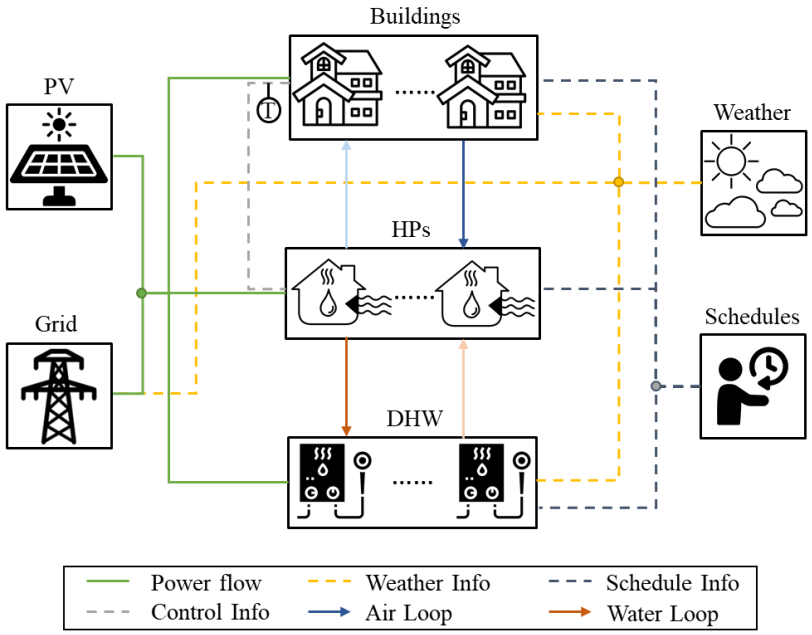

Figure 3.2 Block diagram of the community energy system at the top level.

To account for the dynamics and complexity of the whole community energy system, we chose to use the Modelica language. It is an equation-based object-oriented modeling language that has the advantage of hierarchical modeling structure, object-oriented, and acausal modeling [93, 149]. The main library used for the emulator development is the Modelica Buildings library developed by Laurence Berkley National Laboratory [150]. A Net-Zero Energy Community (NZEC) library was developed based on this work and has been publicly released [15]. Figure 3.3 shows the top-level system Modelica diagram, which has a similar structure to the designed structure in Figure 3.2. In the remainder of this section, the details of each module will be introduced, including the diagram, key assumptions, and controls.

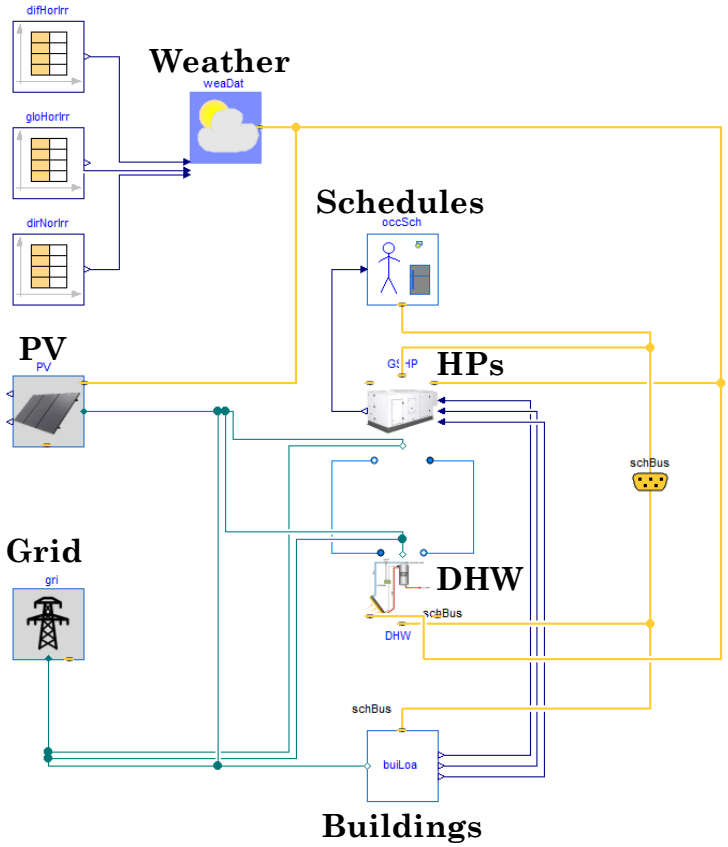

Figure 3.3 Modelica diagram of the community emulator at the top level.

3.2.3 Model Implementation

The power grid in this emulator is modeled as a fixed-voltage power source that generates power at a constant voltage of 120 V and a constant frequency of 60 Hz. This assumption is based on that (1) we are not focusing on the system dynamics of the power grid in the scope of this dissertation; (2) the voltage and frequency of the grid power supply often fluctuate within a very small range, which can be neglected in this work. Figure 3.4 shows the diagram of the PV system in HGV. PV panels are installed on the rooftops of all five buildings as well as the community warehouse and the two carports. As indicated by the diagram, the power generation of all PV panels

is connected through a main PV breaker. The PV power and the grid power are shared by the five buildings together with some campus loads (e.g., irrigation pump, electric vehicle charger).

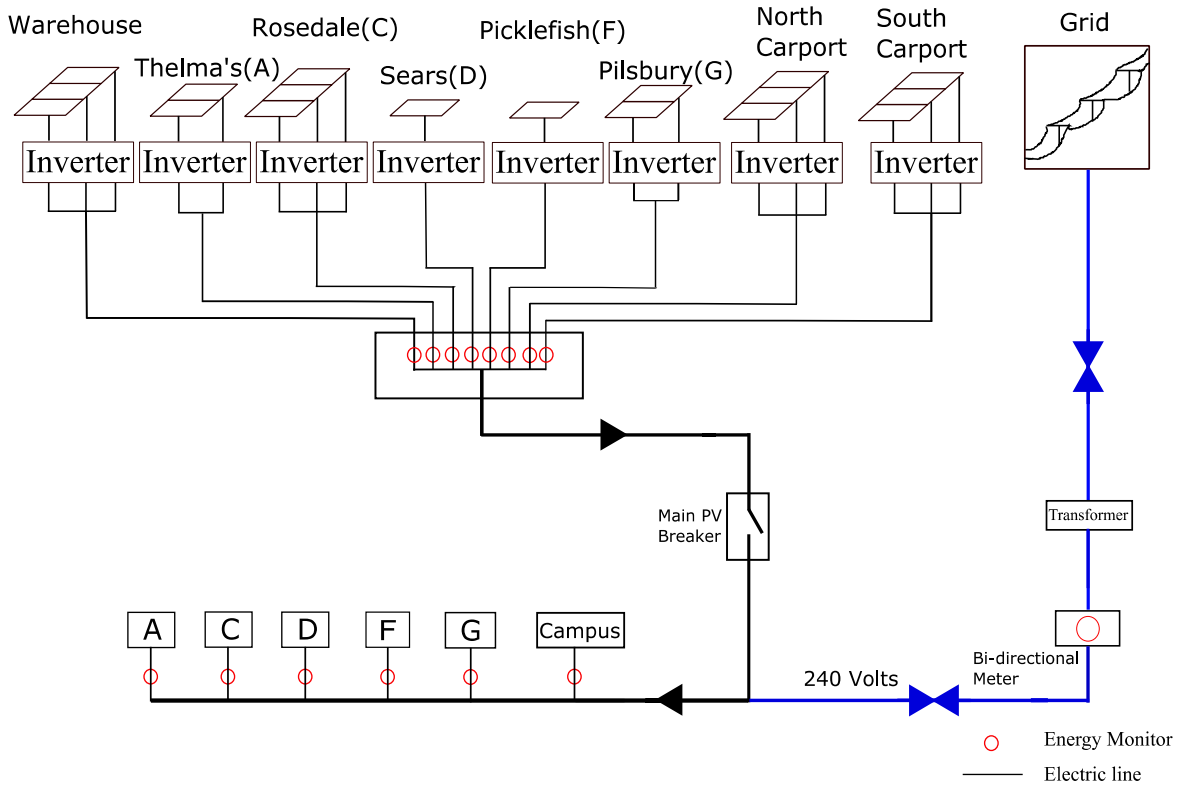

Figure 3.4 One-line diagram of the PV system in HGV.

Figure 3.5 shows the Modelica diagram of the PV system model. The weather bus inputs the direct and diffuse irradiance information based on the measured data, which is then fed into the PV panel models that calculate the power generation. The PV panel areas and tilted angles are based on the system design data. Like the grid model, the PV module generates power flow at a constant voltage of 120 V and a constant frequency of 60 Hz. This system model has been validated against real PV generation data of the community [16, 151].

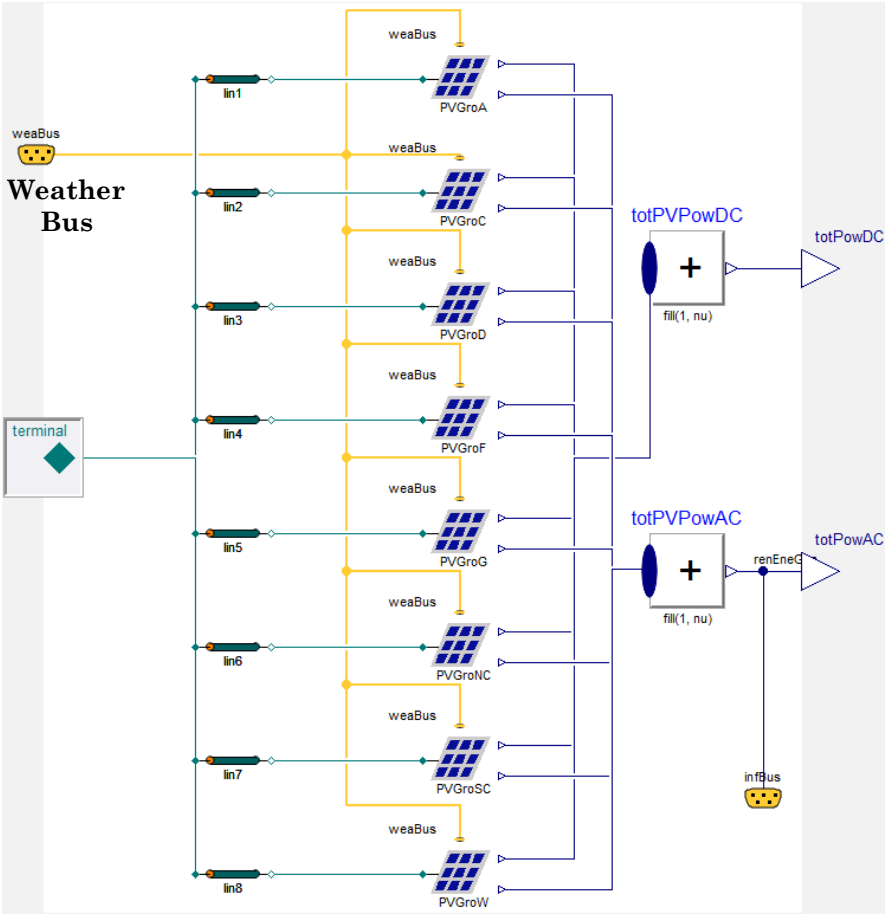

Figure 3.5 Modelica diagram of the PV system model.

The schedules block predicts the hot water usage profile, occupancy schedule, and thermostat setpoint schedule and then outputs the information to the DHW system, buildings, and HP system. The hot water usage is assumed to be constant for now but can be correlated with building occupancy and occupant hot water usage behavior later. Two types of occupancy schedule models are implemented in the emulator. The first type is a fixed schedule model that reads an external prescribed schedule file. The other is an occupancy prediction model that can stochastically predict occupant presence based on the time of day. Details of the presence models can be found in Section 3.3.

We implemented occupancy-based thermostat control in the emulator. As shown in Figure 3.6, the generated occupancy schedule (prescribed or stochastic) is input into the thermostat controller (i.e., T-stat controller). It then switches between two output values: the indoor air setpoint is 24℃ when occupied, and 28℃ while unoccupied. This setpoint is then sent to the local heat pump speed proportional integral derivative (PID) controller. The PID controller calculates the HP speed by comparing the measured room air temperature with its setpoint and then sends the command to the variable frequency driver of the HP.

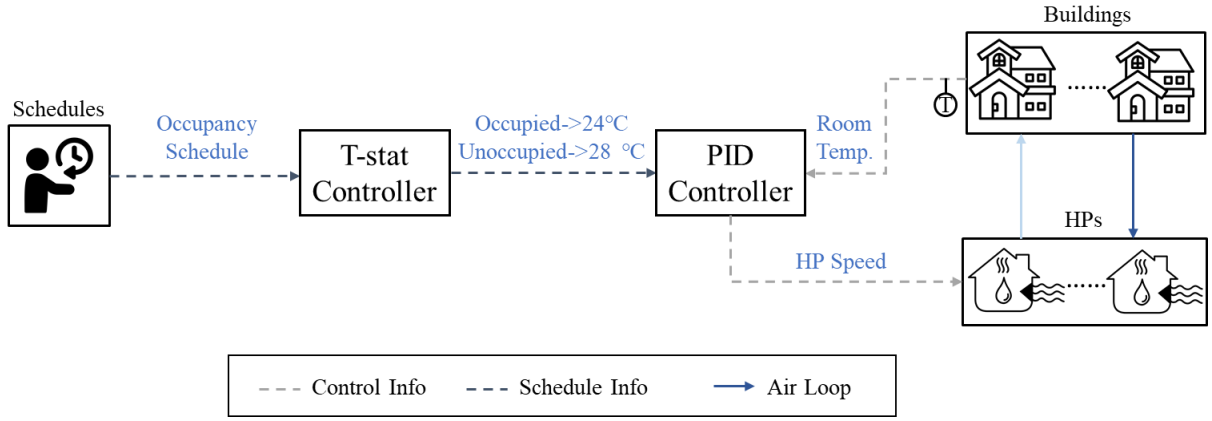

Figure 3.6 Diagram of occupancy-based thermostat control.

The heat pump system Modelica diagram is shown in the figure below. Nine single heat pump models are connected in parallel. Each single heat pump has a corresponding controller, a performance data record, as well as a water circulating pump. The room temperature setpoints, outdoor dry-bulb temperature, and internal heat gain are obtained through the connectors to other modules.

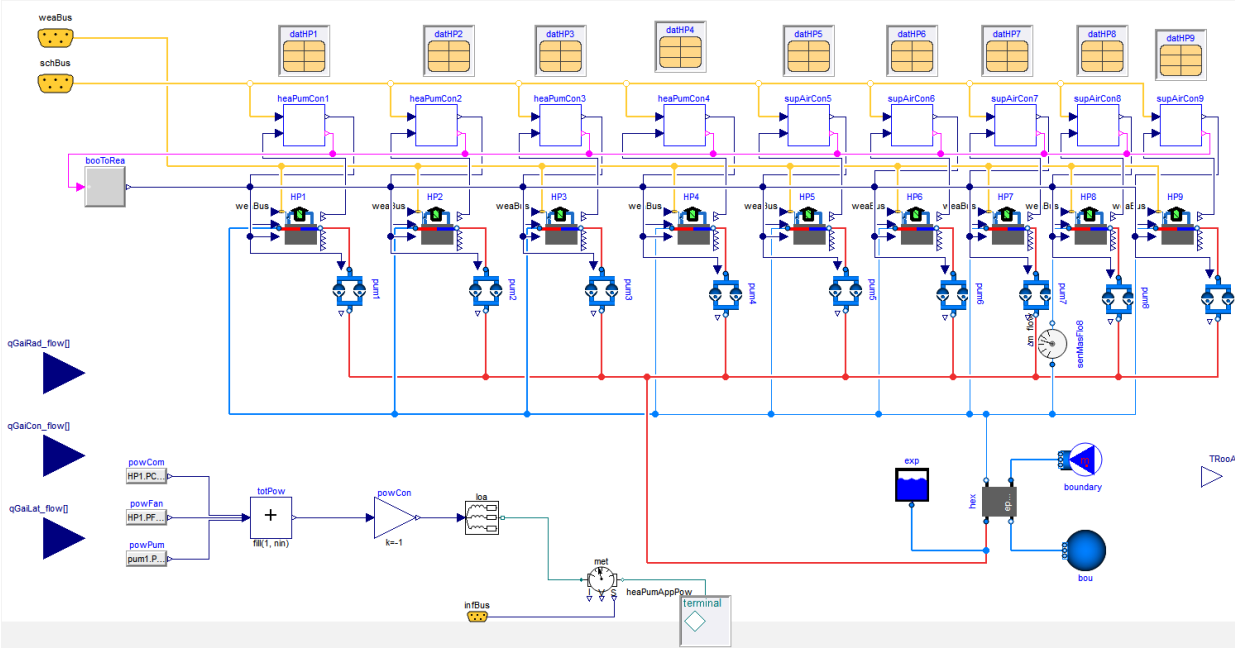

Figure 3.7 Modelica diagram of the heat pump system.

Inside each single heat pump model, there are two major components: a variable speed direct expansion (DX) coil model and a resistance-capacitance (RC) room model (Figure 3.8). The variable speed DX coil model mimics the cooling process of the heat pump. Its speed is controlled by the PID controller implemented at the upper-level system. The RC room model simulates the thermal dynamics of the thermal zone with heat gain from the envelope, occupants, and internal equipment. A constant speed fan supplies cold supply air into the zone.

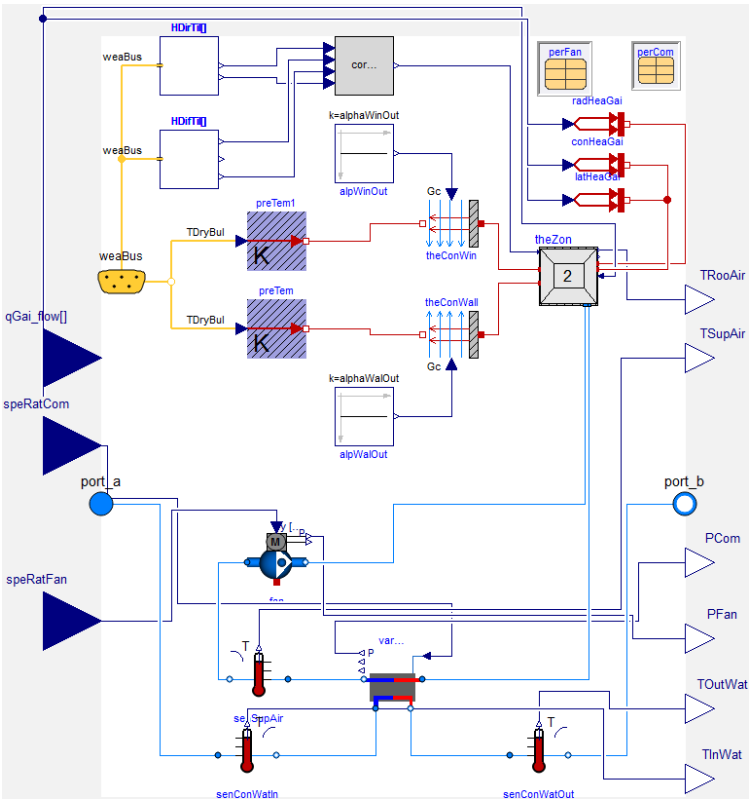

Figure 3.8 Modelica diagram of the single heat pump with thermal zone model.

As shown in Table 3.1, three types of DHW systems are installed in the buildings of HGV: namely, gas heaters, electric heaters, and solar thermal hot water systems. Like the HP system, the DHW system is implemented in a hierarchical way (Figure 3.9). The weather bus inputs the solar irradiance information for the solar thermal units. The schedule bus inputs the hot water usage schedules generated inside the schedule module. The terminal connects all the electricity-consuming components, and the fluid ports supply and return hot water. As gas usage is not modeled in the community emulator, we used text boxes to represent them.

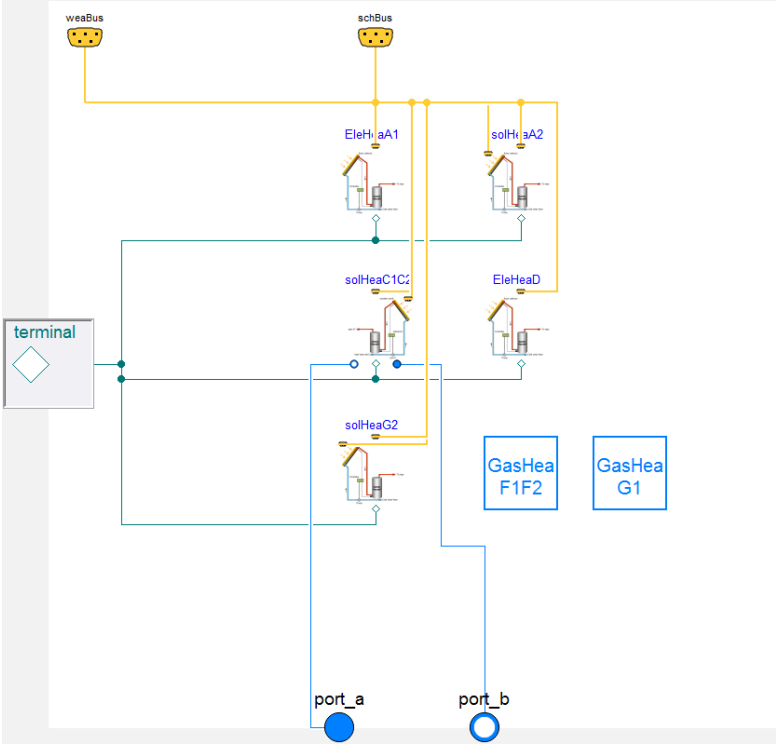

Figure 3.9 Modelica diagram of the HGV DHW system.

Take the solar thermal hot water system with two tanks in Building C (General Store) as an example (Figure 3.10). The city water is first preheated to around 55°C with solar heat and then enters a 120-gallon tank. Then, the water flows to another 30-gallon tank in the kitchen. There, waste heat from two HPs is used to heat the water. The 30-gallon tank has a backup electric heater to make sure the tank water is kept at 50°C.

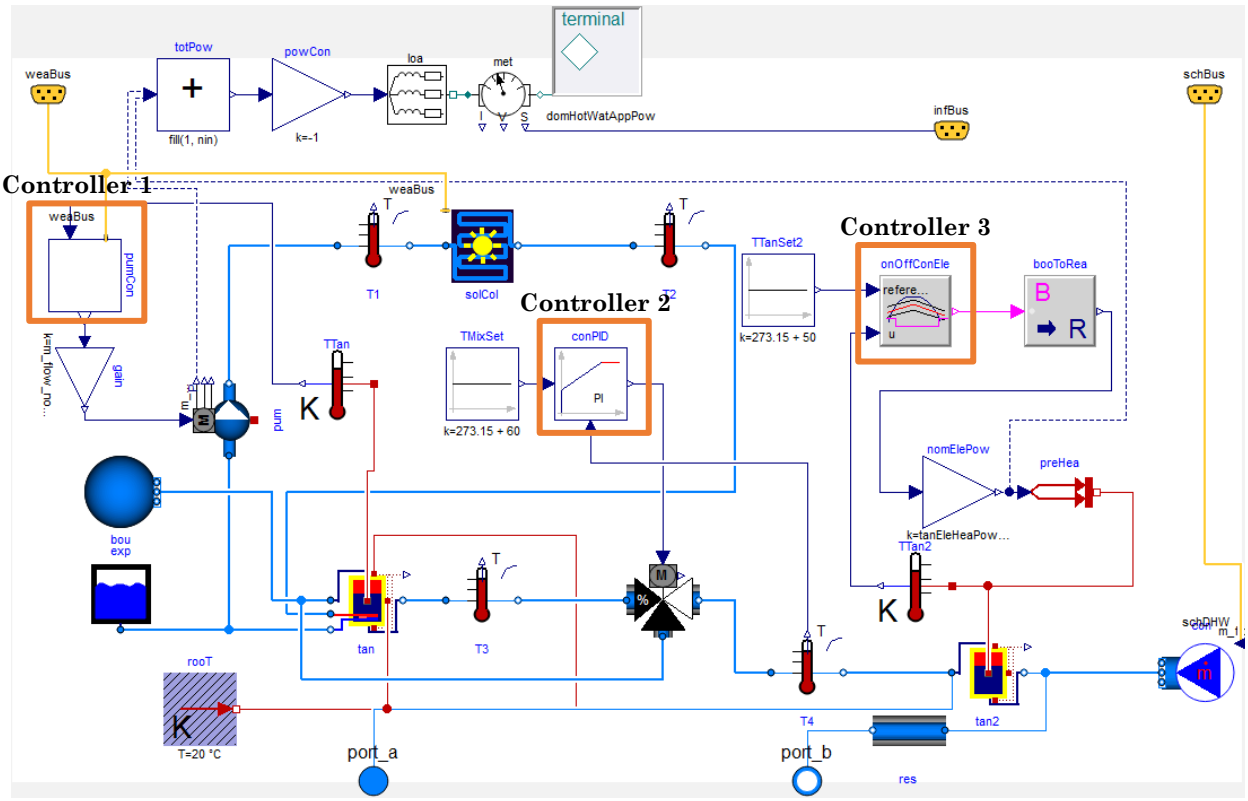

Figure 3.10 Solar thermal hot water system with two tanks in Building C (General Store).

Three local controllers are implemented in this model. Controller 1 controls the ON/OFF status of the circulating pump of the water heated by the solar collector in tank 1 (120 gallons). It is a differential temperature controller. When the temperature difference between the solar collector outlet and the tank water is greater than 5°C and the tank water is lower than 55°C, the water pump is commanded on. Controller 2 dictates the valve position of the three-way mixer that mixes the city water with tank 1 water. The control logic is to increase the ratio of tank 1 water if the mixed water temperature is lower than 50°C. Controller 3 controls the ON/OFF status of the electric heater in tank 2 (30 gallons). The control logic is that if the water temperature is lower than 50°C, the electric heater is commanded on.

The loads inside each building are modeled in an occupancy-based way. As shown in Figure 3.11, each building model receives the occupancy schedule information from the schedule bus. The output is the calculated internal heat gain dissipated by the occupants and the equipment into the spaces. This heat gain is then sent to the thermal zones modeled inside the HP system.

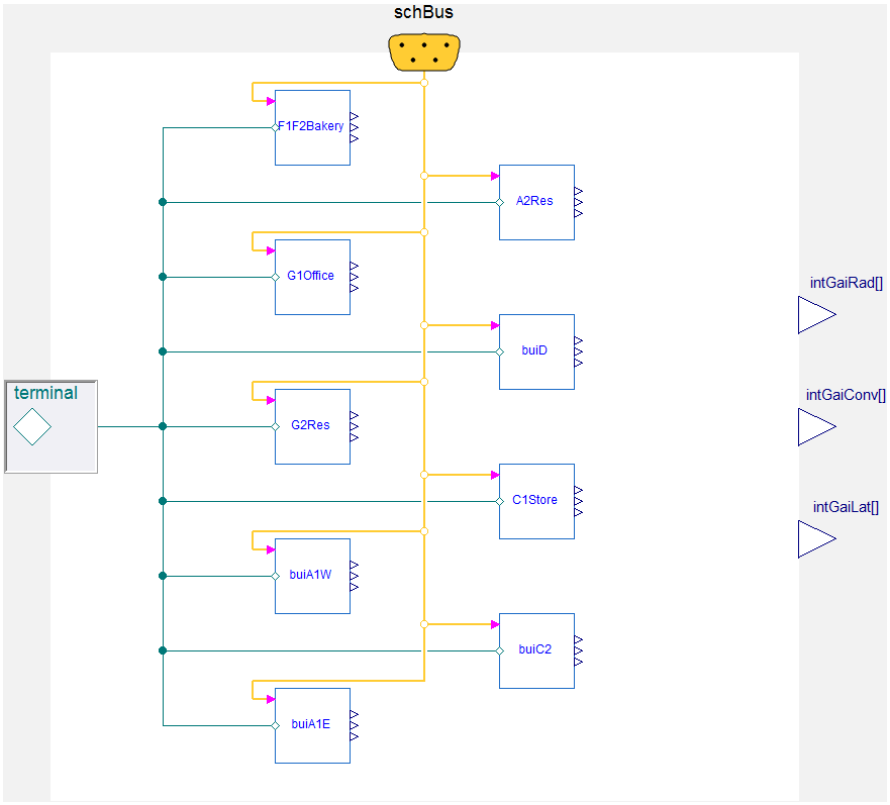

Figure 3.11 Modelica diagram of the building loads at the community level.

Inside each building model, the appliances are modeled separately. For example, the lighting power is modeled as the occupancy (0 or 1 signal) multiplied by the lighting system nominal power. Similar implementation applies to other appliances whose operations depend on the occupancy behavior. The internal heat gain is calculated with the predicted appliance power demand multiplied by the

corresponding heat conversion factor collected in Table A.4. The rest of the appliance power that is not related to DR is modeled as data imported from load profile files.

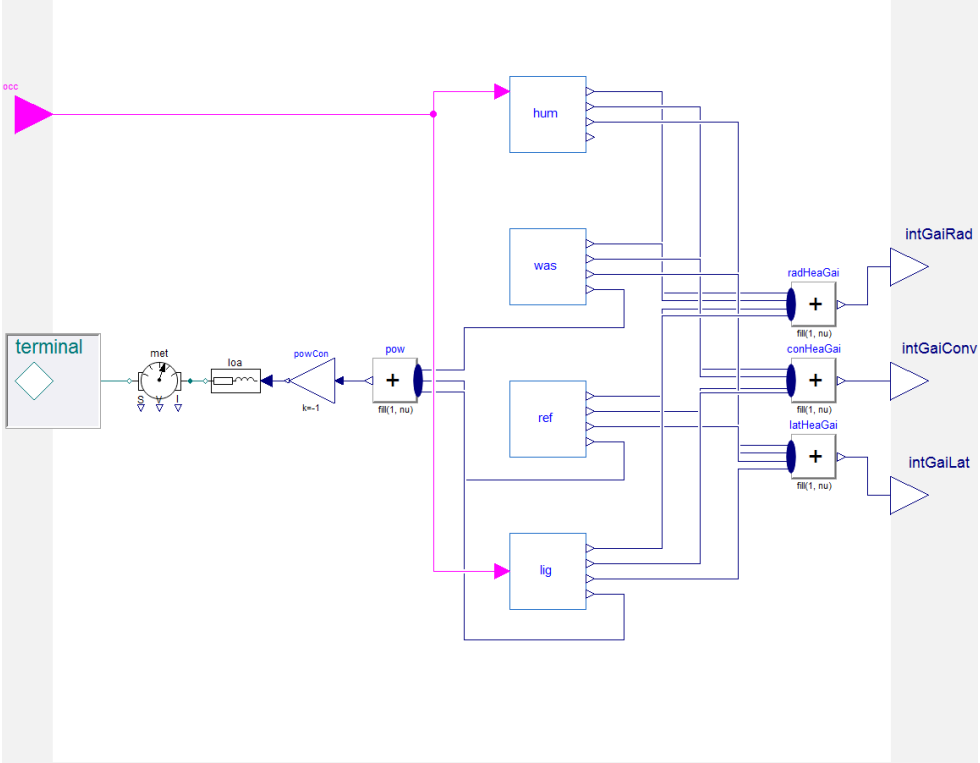

Figure 3.12 Modelica diagram of loads inside each building.

The simulated community aggregated power in July and December is shown in the figures below. The figures indicate that no load pattern difference exists between weekdays and weekends. Also, the community net power follows the “duck curve” for many days of the week due to the PV generation around noon.

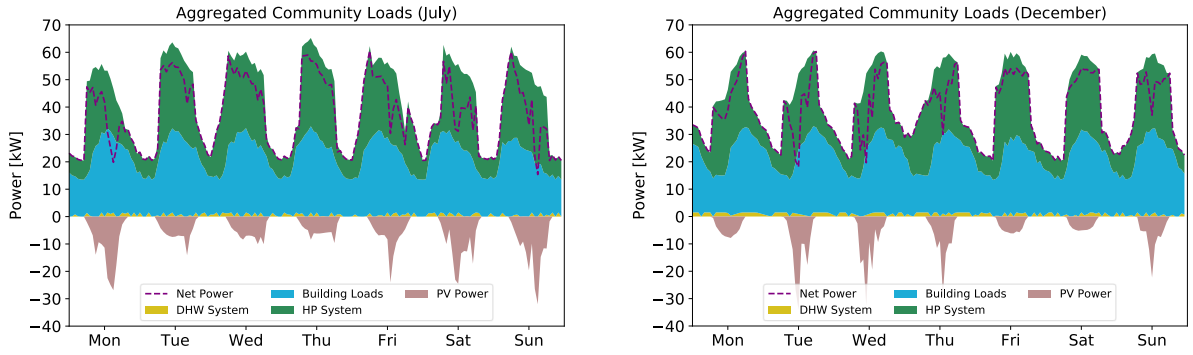

(a) (b)

Figure 3.13 Simulated aggregated community loads in July (a) and December (b).

3.3 Stochastic Building Occupancy Modeling

3.3.1 Introduction

The increasing penetration of renewable energy is introducing more variability within the power grid [152]. To better balance generation and consumption, the power demand side needs to become more flexible and even more controllable. Some studies focus on estimating building load flexibility by controlling thermostatically controllable loads (TCLs) such as HVAC systems and water heaters in buildings [153, 154]. Compared to TCLs, the lighting system has the advantage of shorter response time which makes it more suitable for faster demand response mechanisms (e.g., shimmy).

The stochasticity of occupant behavior and its impact on power and energy consumption presents a challenge to the accurate real-time estimation of building electric loads. Traditional BEM tools use static hourly schedules both for occupant presence and building equipment. This leads to discrepancies between the simulated power shape and the actual consumed power [155, 156], especially for short-term

prediction scenarios such as those needed for fast demand response. Limited data availability is a second challenge, as due to privacy reasons, occupant sensor data is often unavailable. These challenges must be accounted for in theoretical and model-based studies on occupant behavior and its related impacts on the power consumption and flexibility characterization of the built environment.

For commercial buildings, existing occupant presence prediction models have been developed mainly on single office rooms. Wang used exponential distribution to predict the vacancy intervals of single offices [44]. Small commercial buildings have not gained enough attention concerning occupant behavior studies.

Lighting prediction models have been investigated over the past 40 years, and the research points to a strong correlation between occupants' presence and the lighting status in a zone. The first published study for occupants' light switching behavior in office buildings found that switching mainly takes place when entering or vacating a space and the switch-on probability on arrival exhibits a strong correlation with minimum daylighting illuminance in the working area [48]. The manual switch-off probability of lights is strongly correlated with the expected length of absence [53]. Later, this research was expanded by the study of correlations between intermediate switch-on/-off behavior and illuminance levels [54].

In this section, we propose a methodology for occupant presence and lighting power prediction based on minute-level power meter data. We apply the methodology for two small commercial building use cases (one bakery and one ice cream shop) and validate the prediction performance with real data collected from building sites. Here

we present only the prediction of occupant presence and lighting power. In future work, we will extend the methodology to other loads driven by occupant behavior.

The innovation of this work lies in: (1) The proposed method can be applied to occupant presence prediction without occupancy sensor data, and it has been validated against real power meter data. (2) The method can be used for sub-hourly power demand prediction within acceptable deviations of 7%. (3) The method could be applied to other building systems and the Modelica model is extensible and scalable. The rest of this section is organized as follows: Section 3.3.2 presents the methodology. Section 3.3.3 discusses the results. Section 3.3.4 concludes this section with future work and limitations.

3.3.2 Methodology

Our method assumes that the usage of the lighting system and its associated power consumption is strongly determined by the presence of the occupants in the building spaces. This assumption allows us to extract occupant presence schedules from lighting power data. We then use the extracted presence data to train logistic regression models that predict people's arrival and departure times. The trained probability models are then implemented in Modelica language to reproduce building occupancy patterns. The lighting power is then predicted by multiplying the occupant presence value (0 or 1) with the observed nominal lighting power. We then extend the model to address realistic scenarios of multi-stage lighting power. To validate our model, we compare the simulation results with the lighting power data collected at two building sites and evaluate the model performance with respect to several

statistical metrics. The following flowchart (Figure 3.14) shows the research workflow for the results presented in this section.

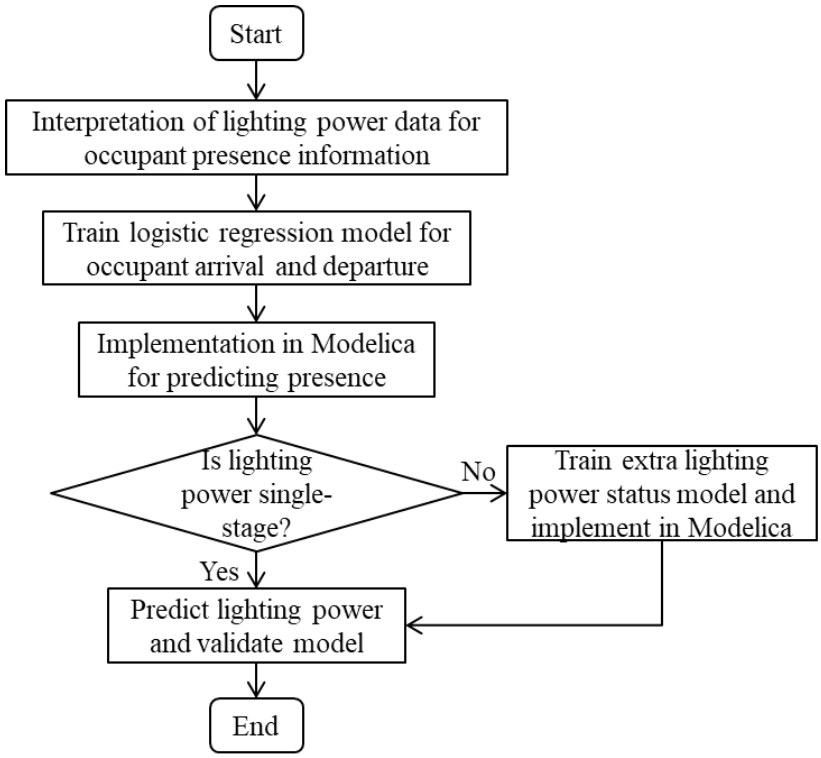

Figure 3.14 Research and modeling workflow.

Next, we discuss the extraction of occupant presence information from the lighting power data. As indicated in the literature review, occupant arrival time and departure time has a strong correlation with the lighting power utilization: According to Hunt's work [48], the action of turning on the lights depends on the minimum illuminance level on the working plane upon arrival and people tend to leave the lights on until the space is fully empty. This is consistent with our observation of the lighting power data in the two studied buildings (i.e., ice cream shop and bakery). As plotted in Figure 3.15, once the lights are turned on, they will remain on for the whole day until all the people leave the space. This means that in this case, the illuminance

level is not a strong driver for light utilization. In our preparation work where we used regression of lighting power based on indoor illuminance levels, prediction accuracy was relatively low. In this work, we will assume that people in the two studied buildings are not sensitive to the illuminance levels and will turn on the lights once they enter the space and will keep the lights on while they are there. Based on this assumption, we extract the occupant presence information from the lighting power data and regard it as the ground truth.

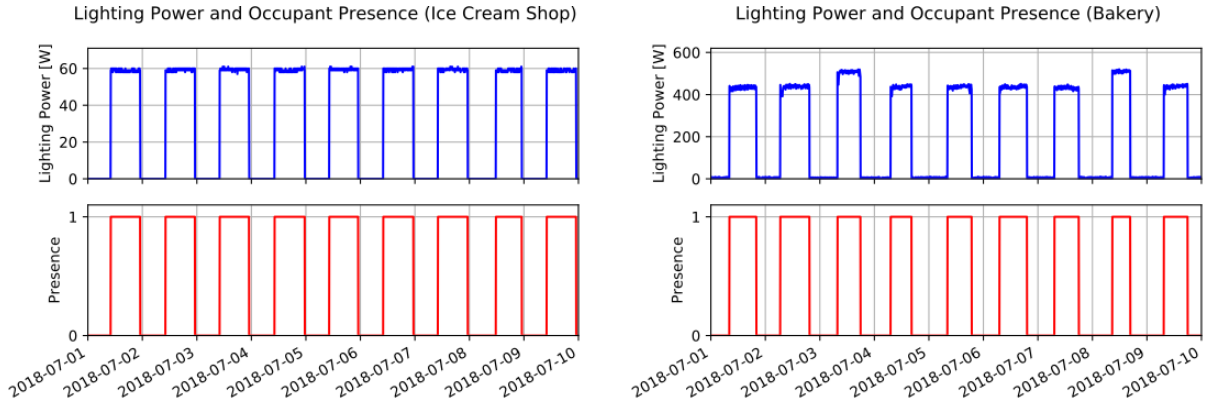

(a) (b)

Figure 3.15 Lighting power and occupant presence in the ice cream shop (a) and bakery (b).

To convert the lighting power data into occupant presence information, we first cleaned the power meter data by removing obvious outliers such as values that are extremely large for lighting systems. Then, we selected the threshold for determining occupant presence (e.g., 0 for absent; 1 for present) to avoid oscillations in presence status. For instance, the threshold for the ice cream shop is selected as 50 W. Any power value above this threshold is converted to 1 and below this threshold into a 0. Because the power data has 1-minute resolutions, we will assume that presence or

absence of 1 minute can be neglected, and we will filter out two consecutive changes of occupant presence to eliminate frequent oscillations in the resulted presence data.

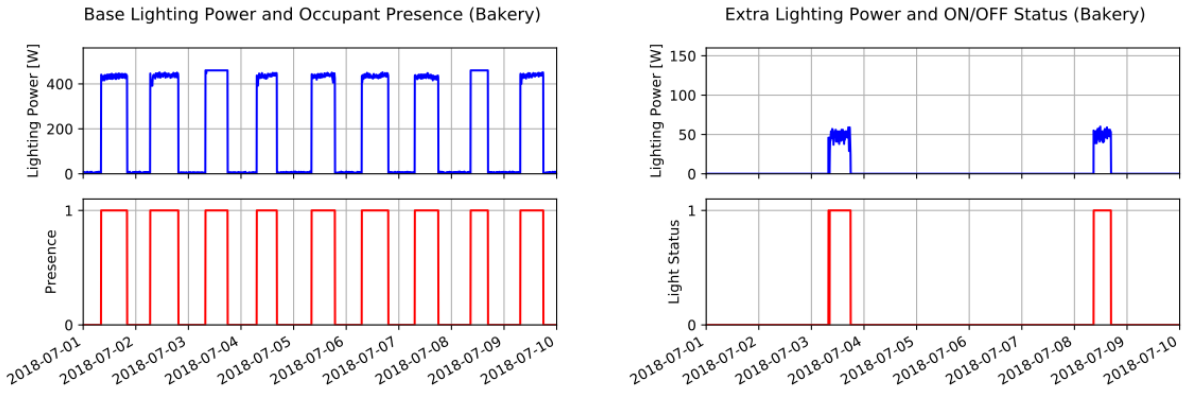

(a) (b)

Figure 3.16 Base lighting power and occupant presence (a); extra lighting power and lighting status (b) in the bakery.

The lighting power shapes shown in Figure 3.15 indicate the different characteristics of the two buildings. For the ice cream shop, only one power value occurs every day regardless of weekday or weekend. However, for the bakery, two distinct levels are observed in the power shape. Hence, for his case, we divide the power shape into two parts namely base lighting power and additional lighting power (Figure 3.16) and we model them separately. This two-stage lighting behavior is probably caused by the zoning of the lighting system. The expression for multi-stage lighting power can be described with Equation (3).

$$P(t) = a_0(t)P_{base} + a_1(t)P_{extr,1} + \cdots + a_{n-1}(t)P_{extr,n-1} \quad (3)$$

P is lighting power; a_i is the binary variable that indicates the status of base or extra lighting; n is the number of stages. For example, the bakery needs a two-stage lighting prediction model, so $n = 2$. The base power and extra power are extracted

from the average power value of each stage. Details are introduced in the following part.

The prediction of occupant presence could be viewed as a classification problem. As discussed before, the arrival and departure behavior in the two studied buildings follows the same pattern for weekdays and weekends regardless of the indoor illuminance level. Hence, the main feature for classifying occupant presence is the time of the day. We chose logistic regression as our model for the training because: (1) it is a linear classifier and is easy to train; (2) it can reach the same level of accuracy as non-linear classifiers; (3) it is easy to implement in Modelica. We divided the arrival and departure behavior into two models and trained them separately as they have opposite trends along time of the day.

To rule out the impact of seasonal change in occupant behavior, the training and validation datasets were selected from the summer of 2018. June and July data were used for the training and August data was used for the validation. During the model training process, the dataset was divided randomly and 10% of the points were used to test the accuracy of the logistic regression classifier. The accuracy is defined as the rate of classifying the data point into the right group. The confusion matrices for the test datasets of all the regression models are shown in Table 3.2. The accuracy of the classifier is then calculated with Equation (3.1).

Table 3.2 Confusion matrices for classification performance.

Model		Predicted No	Predicted Yes	**Model**		Predicted No	Predicted Yes
Ice Cream Shop Arrival	Actual No	3693	44	**Bakery Arrival**	Actual No	2736	132
					Actual Yes	118	1406

Model		Predicted No	Predicted Yes	Model		Predicted No	Predicted Yes
	Actual Yes	31	624	**Bakery Departure**	Actual No	1797	260
Ice Cream Shop Departure	Actual No	283	60		Actual Yes	273	2062
	Actual Yes	4	1849	**Bakery Extra On**	Actual No	16	0
					Actual Yes	3	0

$$Accuracy = \frac{No.\ of\ correctly\ classified\ points}{No.\ of\ total\ data\ points} \tag{3.1}$$

For the bakery, the lighting power is divided into the base power and the extra power. The base part reflects occupants' arrival and departure and is regressed in dependence on the time of the day. The frequency (i.e., number of total times) of extra lights on of the bakery in 2018 is plotted in bars (Figure 3.17). From the figure, we can see that the status of the extra lighting has a correlation with the day of the week. Hence, the feature for this part is chosen as the day of the week. Also, from the figure, we see that the total frequency of extra lights on in 2018 is only 8.8%.

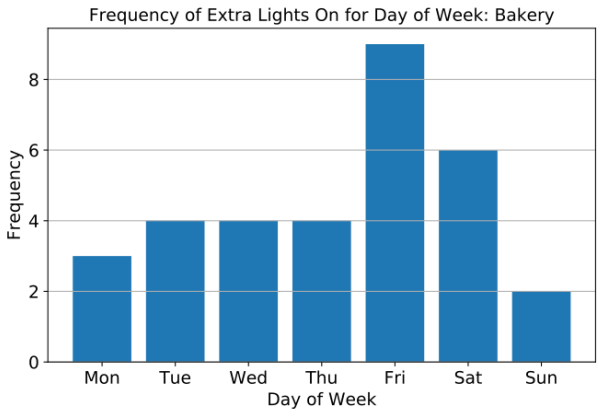

Figure 3.17 Extra lights on frequency for the day of the week in the bakery (2018).

To deal with the imbalance in the training dataset, we adopted the Synthetic Minority Over-sampling Technique (SMOTE) [157], which made the minority (extra lights on) class equal to the majority class (extra lights off) by creating synthetic

samples of the minority class. The logistic regression parameters for each model are listed in Table 3.3.

Table 3.3 Logistic regression parameters.

		Accuracy	β_0	β_1	β_2	β_3	β_4	β_5	β_6	β_7
Ice Cream Shop	Arrival	0.98	-27.198	0.0447	N/A					
	Departure	0.97	34.688	-0.0249						
Bakery	Arrival	0.94	-11.931	0.0254	N/A					
	Departure	0.88	13.777	-0.0125						
	Extra On	0.84	-0.831	-0.483	0.497	-0.259	0.497	-0.117	-0.483	-0.483

The probability function is expressed in Equation (3.2), where p represents the probability of occupant present or extra lights on; e is the natural log base; β is the regression intercept and coefficients; m refers to the number of logistic regression independent variables. The accuracy of all the models is above 84%.

Table 3.4 lists the probability of extra lights on for the day of the week in the bakery.

$$p = \frac{1}{1 + e^{-(\beta_0 + \beta_1 x_1 + \beta_2 x_2 + \cdots + \beta_m x_m)}} \tag{3.2}$$

Table 3.4 Probability of extra lights on for the day of the week from logistic regression.

	Mon	Tue	Wed	Thu	Fri	Sat	Sun
Probability	0.21	0.42	0.25	0.42	0.28	0.21	0.21

Figure 3.18 visualize the training data points and the logistic regression models for arrival and departure in the ice cream shop and bakery. The time of day is in minutes. Based on observations, occupants will arrive before 12 PM and leave after 12 PM. Hence, the arrival models are trained with data points before 720 min (12 PM)

and vice versa. For the ice cream shop departure model, people tend to leave very late: The probability of presence at midnight is around 0.22. To increase the prediction accuracy, we used data after 6 PM to train this model.

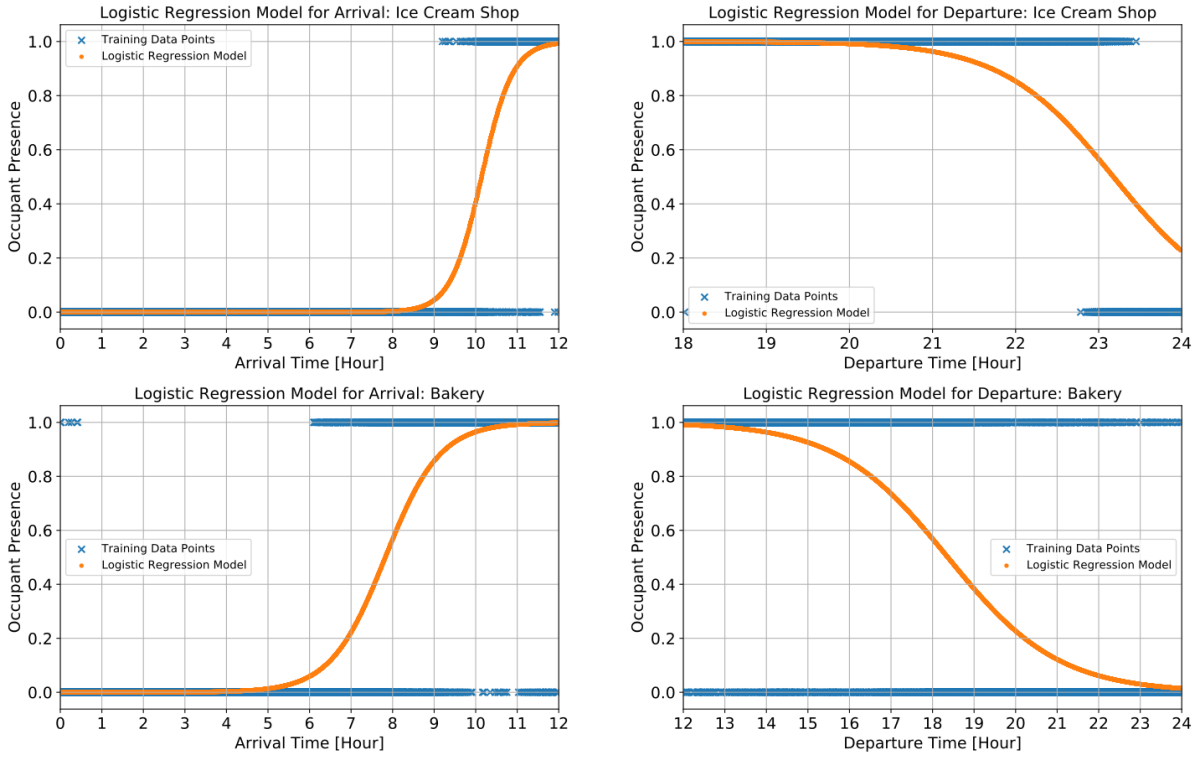

Figure 3.18 Logistic regression models for arrival and departure in ice cream shop and bakery.

The implementation of the presence model and the extra lighting status model is adapted from Buildings.Occupants.Office.Lighting.Hunt1979Light in Modelica Buildings library [150]. The model is implemented as a stochastic simulation model. Every two minutes, a binary variable generator will randomly generate a binary number. The probability of this number being 1 equals the calculated probability of the occupant being present at that time of day based on the logistic regression model. Similarly, in the extra light status model, the probability of the random number being 1 equals the probability of the extra light being on at the simulated day of the week.

Figure 3.19 depicts the layout of the two-stage lighting power prediction model for the bakery. The presence models generate binary signals which will be multiplied with the nominal power of each stage. The nominal powers are the calculated mean values of the lighting power in each stage. The sum of the lighting power of all stages is then compared with the actual lighting power data to validate the performance of the stochastic simulation models. An assumption is made in this model that the extra light will only be on when both of the following conditions are satisfied: (1) The extra light should be on for that day of the week; (2) There are occupants in the building. The simulation was run for the whole month of August 2018 and the time step was set as 10 minutes. The actual time step was picked by Dymola to be 2 minutes due to the stochastic events.

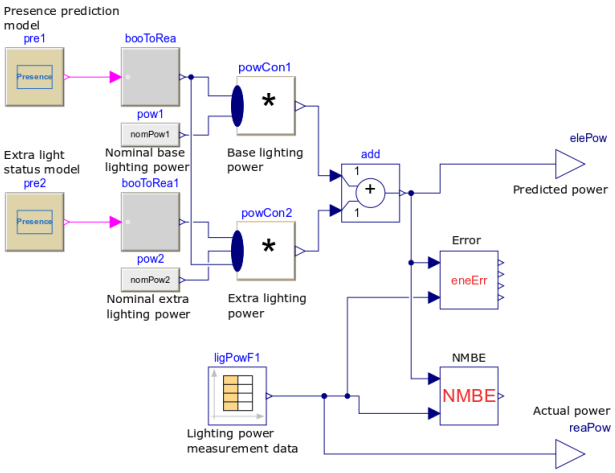

Figure 3.19 Modelica layout of the two-stage lighting power prediction model.

3.3.3 Results and Discussions

We evaluate both the occupant presence prediction performance and the lighting power prediction performance in this section. The presence models are

evaluated with the root mean squared error (RMSE) and the coefficient of variation of RMSE (CVRMSE) of the probability distribution model. The lighting power prediction performance is evaluated with the relative error of the peak power and normalized mean bias error (NMBE). The error in the lighting power prediction is dependent on the presence prediction error as well as the error of nominal power estimation.

The American Society of Heating, Refrigerating and Air-Conditioning Engineers (ASHRAE) Guideline 14-2002 has requirements for whole building energy calibration [158]. The smaller the time scale, the more tolerant the criteria. For example, the criteria for monthly NMBE are 5%, monthly CVRMSE is 15%, and the criteria for hourly NMBE is 10%, hourly CVRMSE is 30%. Though only the lighting system is calibrated in our work, the principle for different time scales should apply.

RMSE represents the standard deviation of the errors and CVRMSE is the ratio of the standard deviation to the mean of the dependent variable. They both describe how concentrated the data is around the line of its best fit. Large errors are especially noticed in these metrics. The equations for calculating the two metrics are listed below. $x_{o,i}$ is the original value of the predicted variable, $x_{f,i}$ is the forecasted value, N is the number of total data points.

Table 3.5 lists the RMSE and CVRMSE of the occupant and extra lighting status prediction models. The CVRMSE for the occupant presence models is below 25%. The CVRMSE for extra lighting prediction is 125%. This is caused by the imbalance of the training data. The probability of the extra lights being on is much lower than the

probability of them being off. Hence, the mean value $\overline{x_o}$ is very small and small errors could cause a large CVRMSE.

$$RMSE = \sqrt{\frac{\sum_{i=1}^{N}\left(x_{f,i} - x_{o,i}\right)^2}{N}} \tag{3.3}$$

$$CVRMSE = \frac{\sqrt{\frac{1}{N}\sum_{i=1}^{N}\left(x_{f,i} - x_{o,i}\right)^2}}{\overline{x_o}} \tag{3.4}$$

Table 3.5 RMSE and CVRMSE of occupant presence and lighting status prediction results.

	Ice Cream Shop	Bakery	
	Occupant Presence	Occupant Presence	Extra Lights
RMSE	0.108	0.101	0.153
CVRMSE	20.9%	25.0%	125%

Figure 3.20 plots the regression model, simulated probability distribution, and the actual probability distribution of arrival and departure in the two buildings. From the figure, we see that the simulated probability distribution aligns with the regression model very well. The actual probability distribution deviates from the regression model especially during the transitional periods in the middle (e.g., 9 to 11 for ice cream shop arrival, 17 to 21 for bakery departure). This could have been caused by the inappropriate selection of the training data. The high accuracy of the classifiers shown in Table 3.3 is partially because more data points are located outside the transitional period. The classifier can distinguish those points easier. Another reason could be that only one feature is used to predict occupant presence. This could have

limited the shape of the logistic regression model to further fit the actual curve. More features should be explored in the future.

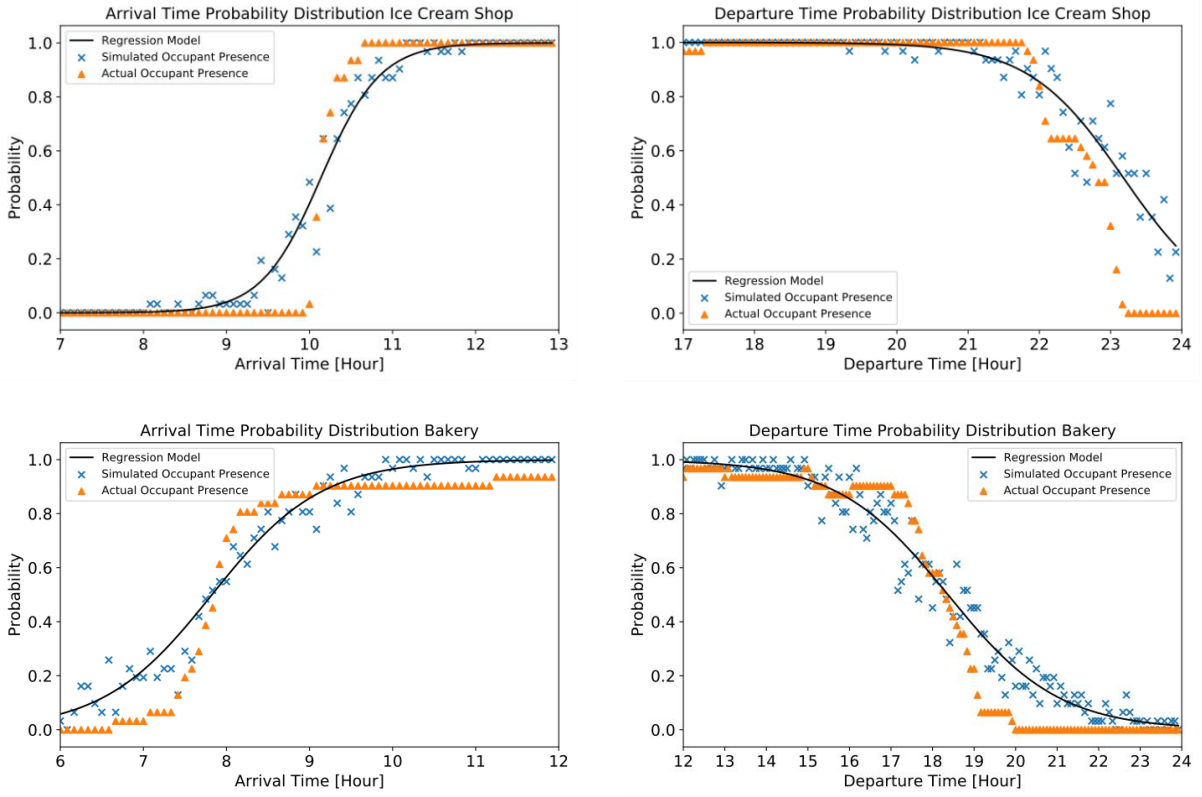

Figure 3.20 Arrival and departure time probability distribution in ice cream shop and bakery.

Table 3.6 compares the probability of extra lights on in the bakery calculated from the simulated results and the actual data. From the table, we see that the simulated and actual results deviate on Tuesday and Wednesday. For other days, the simulation results reproduced the actual probability well.

Table 3.6 Comparison of the simulated and actual probability of extra lights on for the day of the week.

	Mon	Tue	Wed	Thu	Fri	Sat	Sun
Simulated	0	0.29	0.29	0.14	0.29	0.29	0.14
Actual	0	0	0	0.14	0.29	0.29	0.14

To evaluate the lighting power prediction performance of the models, peak power prediction relative error and NMBE are calculated on a monthly, weekly, and daily basis. In this way, the lighting power prediction performance is evaluated for different time scales. As the models in this work are mainly designed for shorter-time demand response scenarios, annual energy consumption is out of scope. Table 3.7 summarizes the peak power prediction accuracy. For the ice cream shop, the errors are all below 2.36%. For the bakery, which is a two-stage prediction, the errors are larger, but all stay below 6.9%. Hence, the multi-stage method performs well in predicting peak power.

Table 3.7 Peak power prediction accuracy.

	Monthly Peak Power	Weekly Peak Power	Daily Peak Power
Ice Cream Shop	2.36%	2.36%~2.36% (Mean: 2.36%)	0.73%~2.36% (Mean: 1.99%)
Bakery	6.90%	2.15%~6.90% (Mean: 5.34%)	1.05%~6.90% (Mean: 2.42%)

To further evaluate the fitness of the power curve to the real power curve, the NMBE metric is adopted, which describes the average bias in the model. NMBE is determined with Equation (3.5). By definition, it is the sum of error over the sum of the actual values. This metric evaluates the fitness of the model over the whole simulation horizon.

$$NMBE = \frac{\sum_{i=1}^{N}\left(x_{f,i} - x_{o,i}\right)}{N \times \overline{x_o}} \tag{3.5}$$

Table 3.8 summarizes the daily, weekly, and monthly NMBE of the lighting power. The lighting power obtained by multiplying the ground truth occupancy data

with nominal power is set as the baseline for better comparison. From the table, the two-stage prediction generally has larger errors than the single-stage model. For the single-stage lighting power in the ice cream shop, the monthly, weekly, and daily NMBE are all within 5%, which indicates a high accuracy for power demand predictions. For the two-stage lighting power in the bakery, the monthly and weekly average errors are within 10%, which is still acceptable. However, we see a big deviation in the daily NMBE, and this leads to a high average value for daily NMBE. This high deviation could have been caused by an uncommon data record on Aug. 19 (see Figure 3.21) when the lights are only on for a short period, but the model simulated it just as usual.

Table 3.8 NMBE of lighting power prediction.

		Baseline	Model
Monthly NMBE	Ice Cream Shop	0.061%	3.92%
	Bakery	-0.55%	8.28%
Weekly NMBE	Ice Cream Shop	-0.27%~0.44% (Mean: 0.060%)	-0.25%~9.84% (Mean: 4.07%)
	Bakery	-2.84%~1.30% (Mean: -0.68)	0.33%~20.4% (Mean: 7.92%)
Daily NMBE	Ice Cream Shop	-0.56%~0.72% (Mean: 0.057%)	-2.59%~23.72% (Mean: 4.03%)
	Bakery	-12.9%~50.9% (Mean: 0.39%)	-21.6%~807% (Mean: 44.1%)

Additionally, as the models are simulated in a stochastic manner and the occupant presence was determined every 2 minutes, we see an obvious oscillation in lighting power in Figure 3.21. This feature of the model leads to that the longer the

simulation time, the closer the expectation of the simulation results will be to the actual data. This explains why the model shows a better performance concerning monthly NMBE. However, the short-term accuracy of the model still needs some improvement.

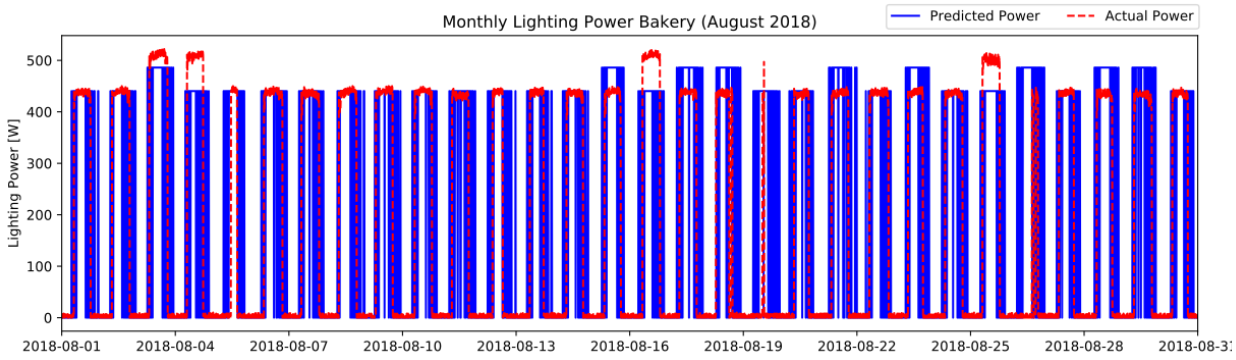

Figure 3.21 Monthly predicted and actual lighting power in the bakery.

3.3.4 Conclusion

This section proposed a methodology for occupant presence learning and reproducing based on lighting power metering data. The method was validated against real data. The results show that the proposed multi-stage lighting power prediction method can predict daily peak power with a 2.42% relative error. The monthly and weekly NMBEs of lighting power are on average below 8.28%.

Through the training and validation process of this work, we found that logistic regression models are sensitive to the quality of the training data. Ideally, the dataset should be more focused on the transitional region of the model and the two classes should be well balanced. Further, increasing the number of independent features should help improve the fitness of the probability model. The stochastic simulation results show that stochastic models can be very accurate for long-term predictions.

However, they cannot predict uncommon events, and this can lead to large short-term prediction errors.

This work has the limitation of not having the ground truth data for occupant presence. The presence generated from lighting power can be delayed when people arrived and did not turn the lights on. This can be cross-validated with other appliance usage data in the future. In the best-case scenario, occupant surveys should be conducted to know their preferences and habits, and occupant sensors should be installed.

3.4 Summary

This chapter introduces the hierarchical modeling structure of a community emulator with stochastic occupancy prediction in Modelica. Section 3.2 first gives an overview of the community energy system and then discusses the modeling details (i.e., implementation, assumptions, control) of each subsystem (i.e., grid, PV, schedule, HP system, DHW system, and building loads). The proposed hierarchical structure is generic and thus can be applied to other community modeling work with appropriate adaptions of the system parameters. Further, it is easily scalable given that the subsystem models are packaged in individual component models, which can be grouped into a larger system through vectorized system modules. The NZEC library can be downloaded from reference [15].

Section 3.3 proposes a methodology for occupant presence learning and prediction based on lighting power metering data. Through a case study with two small commercial buildings, it is found that based on the predicted occupancy status,

the daily lighting peak power can be predicted with 2.42% relative error. Additionally, we found that due to the short-term behavior stochasticity, the model performs better in terms of monthly NMBE than daily NMBE.

Chapter 4. Community Decarbonization Through Carbon Emission Responsive Control

This chapter is based on:

Jing Wang, Prateek Munankarmi, Jeff Maguire, Chengnan Shi, Wangda Zuo, David Roberts, Xin Jin. "Carbon emission responsive building control: A case study with an all-electric residential community in a cold climate." Under review by Applied Energy.

4.1 Introduction

In the United States, buildings account for 35% of total energy-related carbon dioxide emissions, making them important contributors to decarbonization. Carbon intensities in the power grid are time-varying and can fluctuate significantly within hours, so shifting building loads in response to the carbon intensities can reduce a building's operational carbon emissions. This chapter presents a rule-based carbon responsive control framework that controls the setpoints of thermostatically controlled loads responding to the grid's carbon emission signals in real-time. Based on this framework, four controllers are proposed with different combinations of carbon accounting methods and control rules. To evaluate their performance, we performed simulation studies using models of a 27-home, all-electric, net-zero energy residential community located in Basalt, Colorado, United States. To reduce the operational carbon emissions, the controllers modulate the setpoints of mini-split heat pumps for pre-heating or pre-cooling, and heat pump water heaters for pre-heating when there is excessive PV generation from the rooftop PV systems or when the grid electricity is relatively "clean" (i.e., with low carbon intensities). The carbon intensity data of four future years from the Cambium data set are adopted to account for the evolving resource mix in the power grid. Various performance metrics, including energy consumption, carbon emission, energy cost, and thermal discomfort, were used to evaluate the performance of the controllers. Sensitivity analysis was also conducted to determine how the control thresholds and intervals affect the controllers' performance. Simulation results indicate that the carbon responsive

controllers can reduce the homes' annual carbon emissions by 6.0% to 20.5%. However, the energy consumption increased by 0.9% to 6.7%, except in one scenario where it decreased by 2.2%. Compared to the baseline, the change in energy cost was between -2.9% and 3.4%, and thermal discomfort was also maintained within an acceptable range. The little impact on energy cost and thermal discomfort indicates there are no potential roadblocks for customer acceptance when rolling out the controllers in utility programs.

4.2 Methodology

4.2.1 Overview of the Research Methodology

Rule-based carbon emission responsive control, by definition, is to make control decisions in response to real-time carbon emission signals following certain predetermined rules. The control objective is to reduce the carbon emission induced by the power usage of the controlled objects, which are thermostatically controlled loads in this work. The thermostat setpoint is controlled to increase or decrease the load depending on the carbon intensities, predetermined rules, and operation modes.

During the design of the carbon responsive control rule, a fundamental step is to determine how the setpoints change with the emission signal. A common method is to divide the carbon emission data range into several regions, where each region correlates with one setpoint [89]. Evolved from this logic, the ultimate rule form is to establish a function (most likely linear) that maps emissions to a set of setpoints. In this work, we adopt a three-region design of the control rule, which means dividing the carbon emission data range into three regions with two thresholds. Between the

lower threshold (LT) and the higher threshold (HT) is the default zone where the default setpoints $T_{set,default}$ (Table 4.1) will be implemented. Below the LT will be the clean zone and the $T_{set,clean}$ will be implemented, and vice versa. We designed the $T_{set,clean}$ and $T_{set,unclean}$ to be 0.8°C (1.5°F) around $T_{set,default}$ for space heating and cooling, and 8.3 °C (15°F) for the water heater. Here we note that the default setpoints should be dependent on the region and user preferences.

Table 4.1 Control setpoints for heating, cooling, and water heating.

Controlled object	$T_{set,default}$ (°C)	$T_{set,clean}$ (°C)	$T_{set,unclean}$ (°C)
Space heating	21.1	21.9	20.3
Space cooling	23.9	23.1	24.7
Water heater	51.7	60.0	43.4

Unlike energy net-metering, which has been extensively studied in building-to-grid related control studies, the inclusion of carbon net-metering is relatively rare. To address this research gap, we consider different controller designs with and without carbon net-metering to investigate its impact on the control performance.

For electricity prosumers who both consume and produce electricity, carbon net-metering means metering the net carbon emission caused by their electricity consumption and production [159]. In other words, exporting electricity back to the grid will offset carbon emissions from their total emissions. On the contrary, when carbon net-metering is not included, it is more advantageous to use the locally generated electricity from PV systems instead of exporting due to the lack of emission benefits. For controllers considering carbon net-metering, it makes no difference whether to use the clean PV energy locally or to export it to the grid. Both options would bring in the same amount of carbon emission reduction.

According to the information used for making control decisions, rule-based control can be categorized into momentary and predictive control. The momentary rule-based control adopts the current value of the boundary condition (e.g., carbon emission signal) and decides the setpoints for the current control interval [160]. Nevertheless, the predictive rule-based control makes decisions based on both current and future predictions of the boundary condition [89]. Compared to optimization-based controllers such as MPC, predictive rule-based control is simpler but still effective. It is therefore a promising alternative to MPC given that the rules are well designed [161].

In this work, we propose both momentary and predictive carbon responsive controllers. For the predictive controller, the carbon emission information of one future timestep is adopted to facilitate the determination of setpoints for the current timestep. The detailed control algorithms of the four proposed controllers are discussed in the following subsection.

4.2.2 Implementation of Control Algorithms

Figure 4.1 to Figure 4.4 present the flow charts of the four proposed carbon responsive controllers. Here, the LT and HT are predetermined thresholds that are held constant throughout the whole simulation period. In the momentary controller with carbon net-metering (Figure 4.1), the current carbon emission value CO_2^t is compared with the LT and HT sequentially to determine which range it belongs to. If CO_2^t is below the LT, the current timestep will be categorized as clean and the setpoints $T_{set,clean}$ in Table 4.1 will thus be implemented. As a result, the loads P_{hvac}^t

and P_{wh}^{t} will be increased and vice versa. If CO_2^t is between the LT and HT, the default setpoints $T_{set,default}$ will be implemented, which is the same as the baseline setpoints.

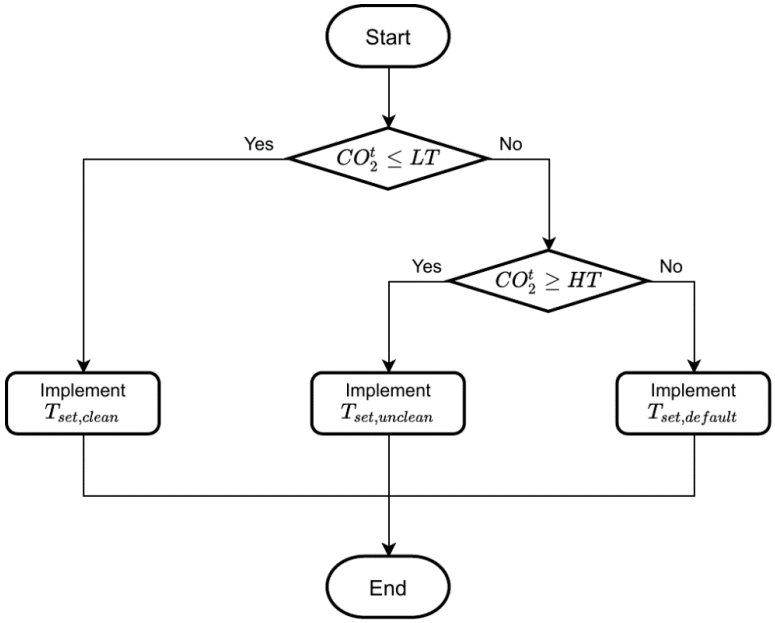

Figure 4.1 Flow chart of momentary control with carbon net-metering.

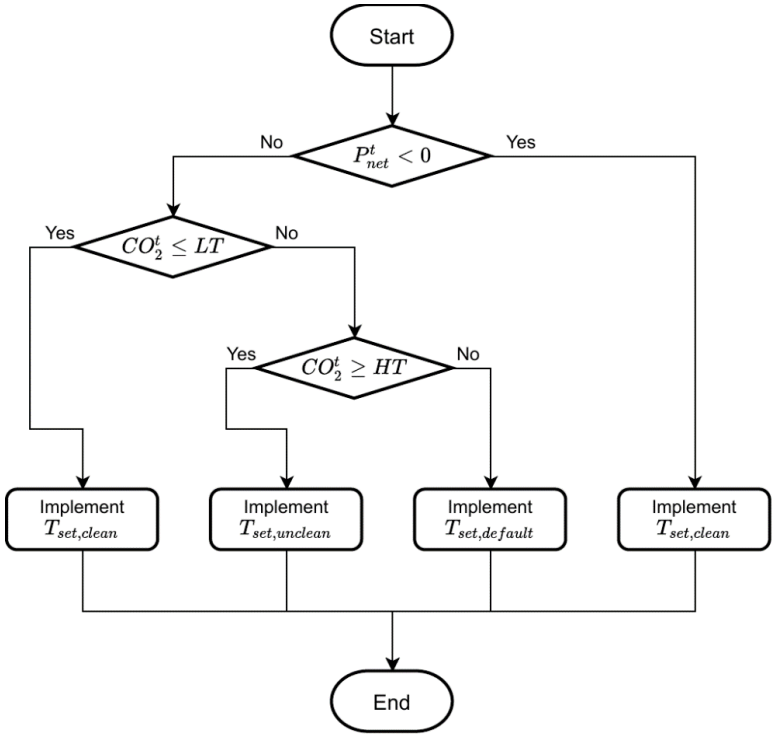

Figure 4.2 Flow chart of momentary control without carbon net-metering.

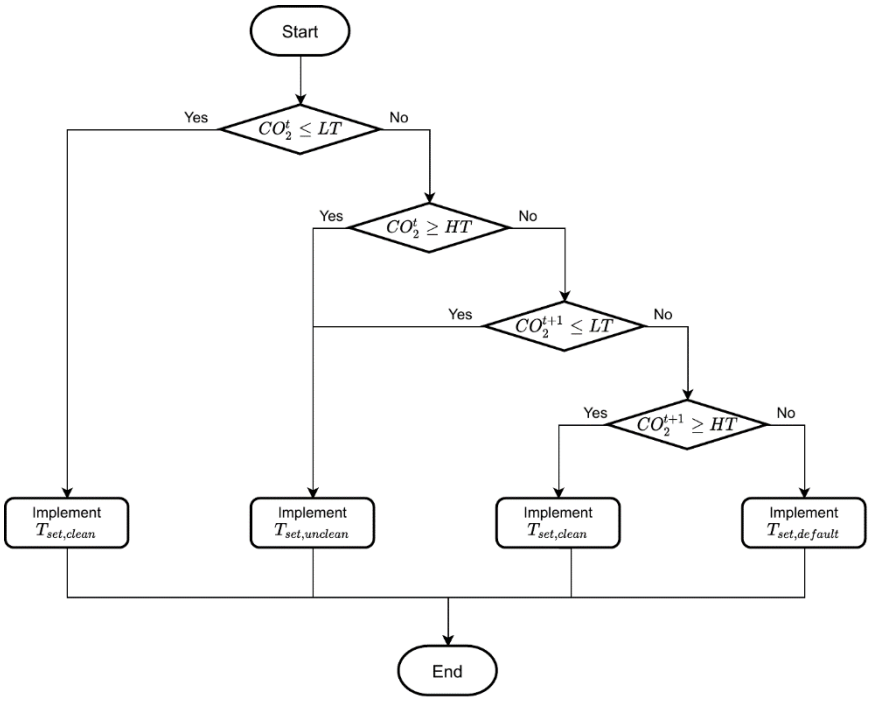

Figure 4.3 Flow chart of predictive control with carbon net-metering.

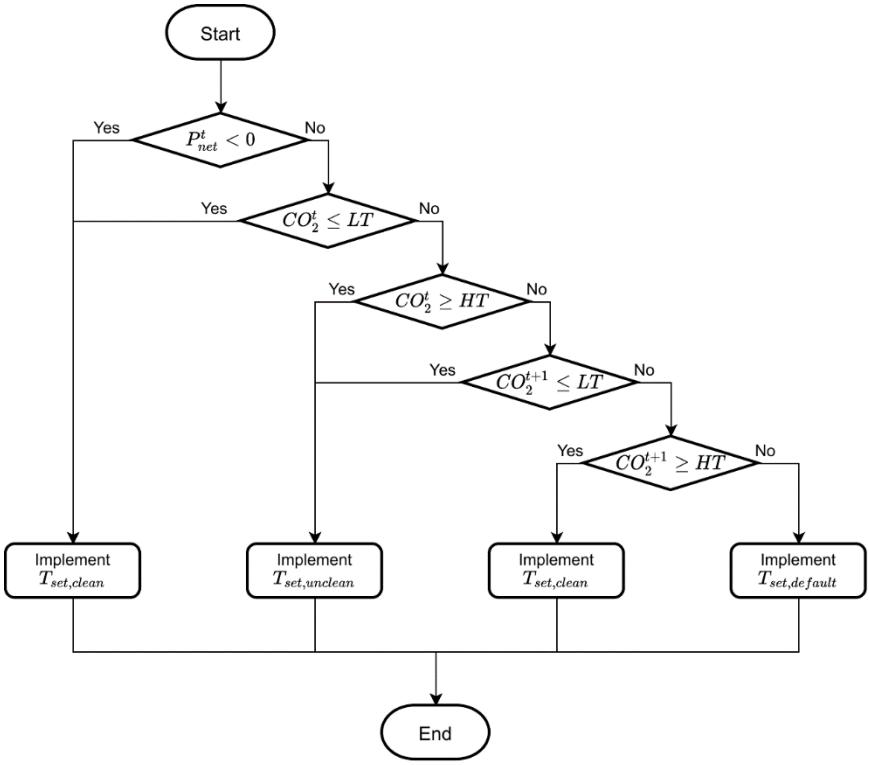

Figure 4.4 Flow chart of predictive control without carbon net-metering.

The momentary controller without net-metering (Figure 4.2) is developed based on the one with net-metering with one more step to increase the PV self-consumption rate. Prior to comparing CO_2^t with the thresholds, the current house net load P_{net}^t is first evaluated. If it is negative, which means the house has surplus PV generation, the setpoints $T_{set,clean}$ will be adopted to increase the loads P_{hvac}^t and P_{wh}^t. In this way, the clean energy can be consumed locally instead of being exported to the grid without any carbon offsetting benefit.

The predictive controllers (Figure 4.3 and Figure 4.4) with and without carbon net-metering are similar to the corresponding momentary controllers in the initial steps. However, the predictive controllers utilize the emission data from the next timestep to further facilitate the control decisions. Essentially, when the emission level of the current timestep falls into the default range, the carbon emission of the next timestep CO_2^{t+1} is then compared with the LT and HT. If the next timestep is categorized as clean, the loads for the current timestep will be decreased to save for later, and vice versa. This algorithm enables more frequent setpoint adjustments and therefore leads to more shifting of loads to cleaner hours.

4.2.3 Co-simulation Platform

A co-simulation platform is used for testing and validating the performance of the proposed control algorithms. The co-simulation platform is built on the hierarchical engine for large-scale co-simulation (HELICS) tool [162]. Key capabilities such as high scalability, cross-platform operability, and modularity make HELICS suitable for developing co-simulation platforms. The co-simulation platform

manages the data communication between different components of the closed-loop co-simulation. It is scalable and creates multiple agents depending on the number of houses in the simulated community.

Figure 4.5 depicts the components of the co-simulation platform and the data exchange flow between different components. Two types of agents are developed in this platform: (1) a building energy simulator (i.e., house agent) and (2) a carbon responsive controller agent. At the beginning of the simulation, an agent for the building simulation and an agent for the controller are instantiated simultaneously for each house.

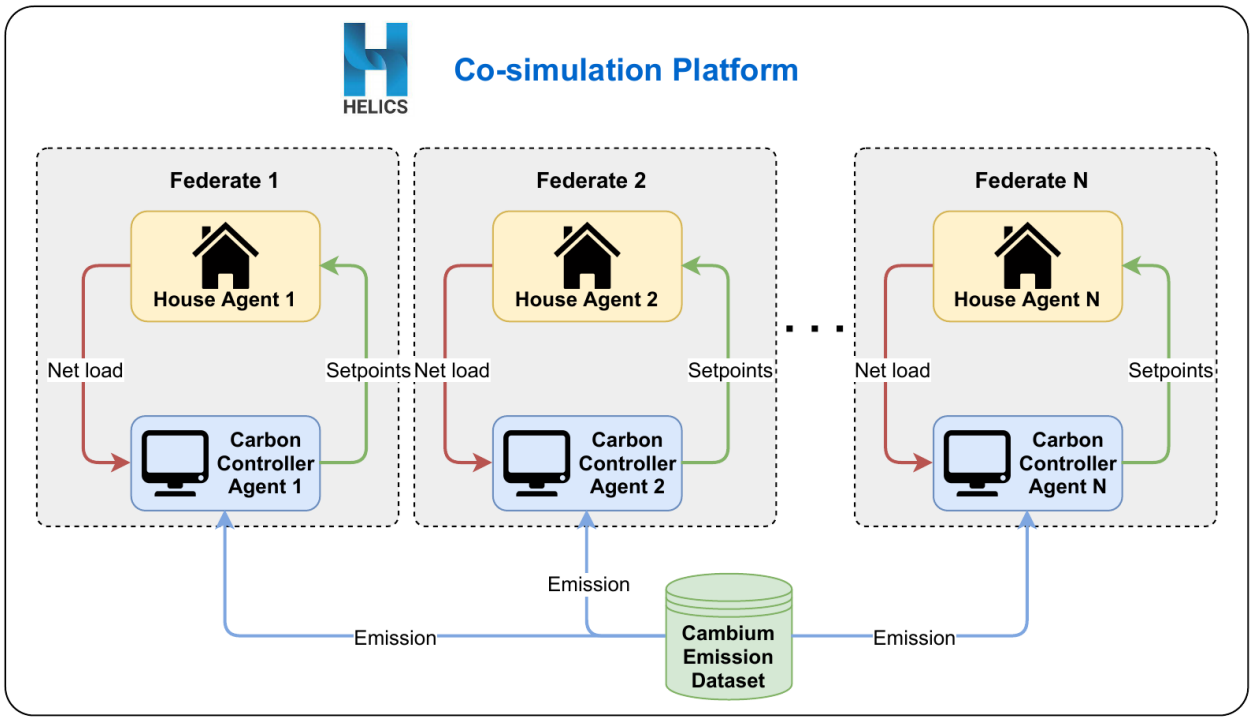

Figure 4.5 Architecture of the co-simulation platform.

Inside each house agent, we used the Operational, Controllable, High-resolution Residential Energy (OCHRE) model [163] for modeling the buildings in this study. OCHRE is capable of implementing the control signals for HVAC, WH,

PV, and battery, and it is designed to be easily integrated into the co-simulation platform. More details about the community modeling are discussed in Section 4.3.2.

The data exchange between the house agent and the controller agent happens in the following order. At the beginning of timestep t, OCHRE computes the net house load (P_{net}^t), and the house agent sends P_{net}^t to the controller. At the same time, the controller agent receives the P_{net}^t together with the current carbon emission data from the Cambium database [164]. For predictive controllers, the future carbon emission data are also received for computing the control actions with the assumption of perfect forecasts. The controller then computes the control setpoints based on the predetermined rules and sends them back to the house agent. After receiving the control action for each device from the controller agent, OCHRE implements the control action and proceeds to the next timestep $t + 1$.

4.3 Case Study

4.3.1 Overview of the Community

The Basalt Vista community, located in Basalt, Colorado, is modeled for the case study. This community is intended to provide affordable housing to schoolteachers in town while also being highly efficient all-electric homes with enough PV to make the community approximately net-zero, as well as batteries for load shifting and resilience. Located at an elevation of 2,015 meters, it is in climate zone 7B, which is very cold and dry [165]. The community consists of 12 multifamily buildings, either duplexes or triplexes, with a total of 27 homes. The homes consist of 2- , 3-, and 4-bedroom units, ranging from 107 to 156 square meters [166].

The HVAC systems of all the units are mini-split heat pump (MSHP) systems. The domestic hot water systems use heat pump water heaters (HPWH). Each unit is installed with rooftop PV systems, except for three units that do not have enough roof space for PV panels. The PV system sizes range from 7.6 to 11.85 kW. Among all the households, six homes are assumed to own electric vehicles and are equipped with Level 1 or Level 2 chargers. Four homes are equipped with home battery systems with capacities of 12 kWh.

4.3.2 Community Modeling

The community is modeled in OCHRE [163], a control-oriented residential building modeling tool. Each building type (i.e., 2-, 3-, and 4-bedroom) shares the same model formation with variant configuration parameters. The building envelope and the controllable loads (i.e., MSHP and HPWH) are described in this section. Models of PV, batteries, electric vehicles, and other electric loads can be found in reference [163].

The RC model is adopted for modeling the building envelope. R represents the thermal resistance between thermal masses, which involves both conduction and convection effects. C represents the thermal mass of different building components such as the air inside a room, exterior and interior walls, furniture, etc. The equation of a node i in the RC network is:

$$C_i \frac{dT_i^t}{dt} = \sum_{j=1}^{M} \frac{T_j^t - T_i^t}{R_{ij}} + H_i^t, \tag{4.1}$$

where C_i is the thermal mass of the node i, T_i^t is the temperature of node i, T_j^t is the temperature of node j adjacent to node i, R_{ij} is the thermal resistance between nodes i and j, H_i^t is the sensible heat injected to node i, and M is the total number of nodes in a house. For each house, approximately 13 Rs and 4 Cs were used to simulate the thermal dynamics. The detailed structure of the RC network model can be found in reference [163].

The MSHP in this work has a variable frequency drive that can modulate to maintain the setpoint of the conditioned space. A local PID controller adjusts the variable frequency drive's speed ratio according to the measured room temperature and the setpoint. For this community, the MSHPs are sized to be larger than might typically be sized according to standard sizing guidance such as the ACCA Manual J [167]. This is to ensure that the heat pump can fully meet the load even during the coldest hours of the year. With the oversized heat pumps, backup heaters are not installed, which makes these homes more energy efficient at the expense of a higher capital cost.

Further, each home has a highly efficient HPWH with a backup electric resistance element installed. The heat pump itself is able to heat the tank more efficiently by removing heat from the ambient air and adding it to the tank. In contrast, the backup electric element is less efficient but can heat the tank more quickly. When there is a demand for water heating, the heat pump turns on first. If there is a sufficiently large draw of hot water that the heat pump is unable to keep up, the backup electric element will then turn on. This will partially recover the tank

temperature before switching back to the heat pump mode to maintain a high level of energy efficiency. The exact control sequence was derived from the detailed laboratory testing of this HPWH unit in response to different typical residential hot water draw profiles [168].

4.3.3 Inputs

The carbon emission data in this work are adopted from the Cambium data set [164]. Based on modeled futures of the U.S. electricity sector, Cambium assembles structured data sets of energy-related metrics (e.g., carbon emissions) to facilitate long-term decision-making. Specifically, the hourly short-run marginal carbon emission data from the Standard Scenarios 2020 Mid-case were adopted in the control development of this work. Though Cambium provides various scenario settings such as high vs. low renewable energy cost, we note that the simulated data are based on certain assumptions about the future projected U.S. electric sector. These assumptions are subject to many uncertainties, such as climate change and policy impacts, which could affect the results and analysis of this work.

Figure 4.6 visualizes the emissions data for the four selected simulation years from Cambium. We selected these four years because only even years are available in Cambium, and we needed to avoid leap years as they are not yet supported in OCHRE. From the figure, we notice that as time goes by, more hours with zero or low carbon emissions emerge. This aligns with the increasing adoption rate of renewable energy and decarbonization measures of the electric sector. Regardless, we still observe some hours of high emission rate in the year 2046, which represent the

operation of coal-fired power plants. Because the emission data for the four years are different, we conducted a sensitivity analysis to determine the control thresholds (Section 4.4.5). As a result, we adopted the absolute values of the 30% and 70% of the emission range in 2022 as the LT and HT for all scenarios.

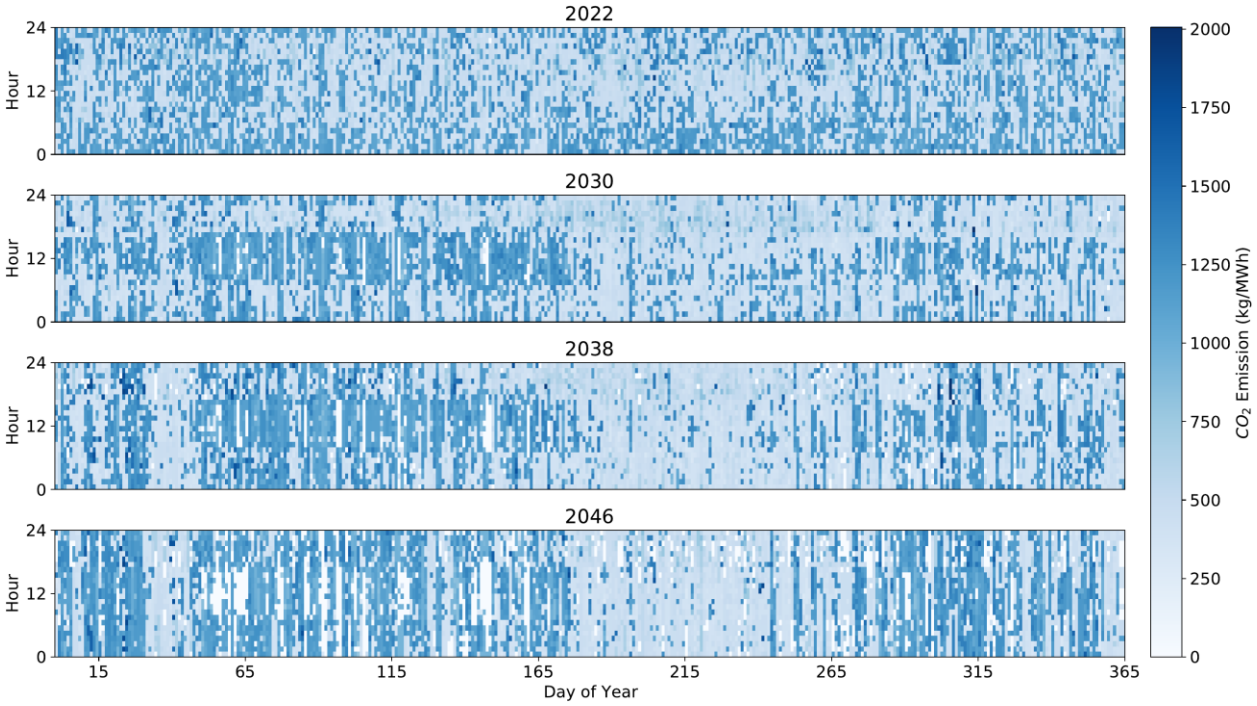

Figure 4.6 Emission data comparison across simulated years.

Similarly, the same weather data were used across all four simulation years to eliminate the impact of weather on building loads so that the results can be directly compared. Actual Meteorological Year (AMY) data of the year 2012 for Pitkin County, Colorado, where the community is located, was used to be consistent with the Cambium weather data file. Here we note that forecasting future weather is an active research topic and is beyond the scope of this work. The occupancy, lighting, and appliance usage schedules for each house were generated from ResStock™ [169]. The time-of-use rate for the local electric utility Holy Cross Energy [170] was used for the

energy cost calculation, where the on-peak (4–9 PM) price is $0.24/kWh and the off-peak (rest of the hours) price is $0.06/kWh.

4.4 Results and Discussions

Based on the case study settings proposed in Section 4.3, we designed five simulation scenarios to evaluate the controller performances. As seen in Table 4.2, the baseline scenario involves no carbon responsive building controller. The remaining four scenarios each adopt one carbon responsive controller proposed in Section 4.2.2, namely momentary or predictive rule-based controller with or without carbon net-metering. Annual energy simulations of the four selected years (2022, 2030, 2038, and 2046) were run with the default setpoints listed in Table 4.1. The house models were run with a timestep of 1 minute, and the control setpoints were updated with a 15-minute interval to avoid excessive cycling of the appliances.

Table 4.2 Description of simulation scenarios in the case study.

Scenario	Carbon accounting method	Rule type	Year
Baseline	N/A	N/A	2022-2046
MO-0	Non-net-metering	Momentary	2022-2046
MO-1	Net-metering		
PR-0	Non-net-metering	Predictive	2022-2046
PR-1	Net-metering		

Next, we present the annual simulation results with four performance metrics: energy consumption, carbon emission, energy cost, and thermal discomfort. Through the comparison of the four proposed controllers, we discuss the impact of carbon net-metering, as well as the effect of prediction in rule-based control. Additionally, we also investigate the evolution of results over the years.

4.4.1 Energy Consumption

Figure 4.7 visualizes the community average annual energy consumption of the controlled loads (HVAC and WH) for different controllers. Compared to the baseline, the annual space heating energy consumption slightly decreases while both the space cooling and water heating energy increases. The divergent heating and cooling energy changes can be attributed to the higher emission levels in the heating season than those in the cooling season (see Figure 4.6), which leads to lower heating energy consumption. In general, carbon responsive building control increases the total household annual energy consumption.

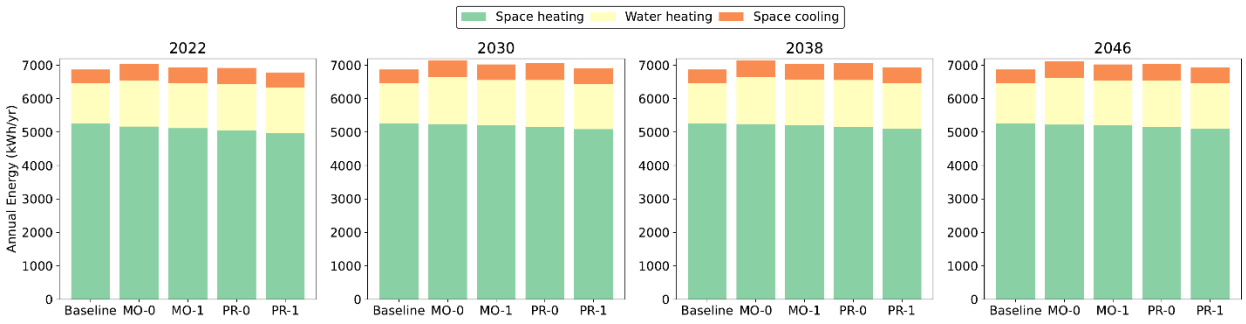

Figure 4.7 Community average annual energy consumption of controlled loads for different controllers across simulated years.

Table 4.3 lists the community average annual energy per household. In the table, the baseline energy consumption is shown in absolute values, whereas the other scenarios are in relative changes compared to the baseline. From the table, the average annual energy increase for the studied community is within 6.7%. For controllers accounting for carbon net-metering, the energy increase is about 2.5% to 3.0% lower compared to scenarios without carbon net-metering. This indicates the incentivizing impact of adopting carbon net-metering, as it encourages the exporting

of power back to the grid. For controllers without carbon net-metering, the energy usage is increased when PV generation is excessive to increase the self-consumption rate, which has led to a higher annual energy consumption.

Table 4.3 Community average annual energy consumption per household for different controllers across simulated years (percentage values are changes relative to the corresponding baseline).

Year	Baseline (kWh/yr.)	MO-0	MO-1	PR-0	PR-1
2022	4,124	3.8%	1.3%	1.1%	-2.2%
2030	4,120	6.6%	3.7%	4.5%	0.9%
2038	4,108	6.7%	4.2%	4.7%	1.6%
2046	4,103	5.8%	3.7%	4.2%	1.6%

Another observation from Table 4.3 is that all predictive controllers perform better than the momentary controllers in terms of energy consumption. This is because the predictive controllers adjust the setpoints based on both current and future emission values. When the current carbon emission falls in the default zone but the future emission falls in the clean zone, it will reduce the current power, and vice versa. Because there are more time instances classified as clean than carbon-intensive over the whole year (as shown in Figure 4.8), the predictive controllers, therefore, reduce energy consumption more often than increase it and save more energy compared to the momentary controllers.

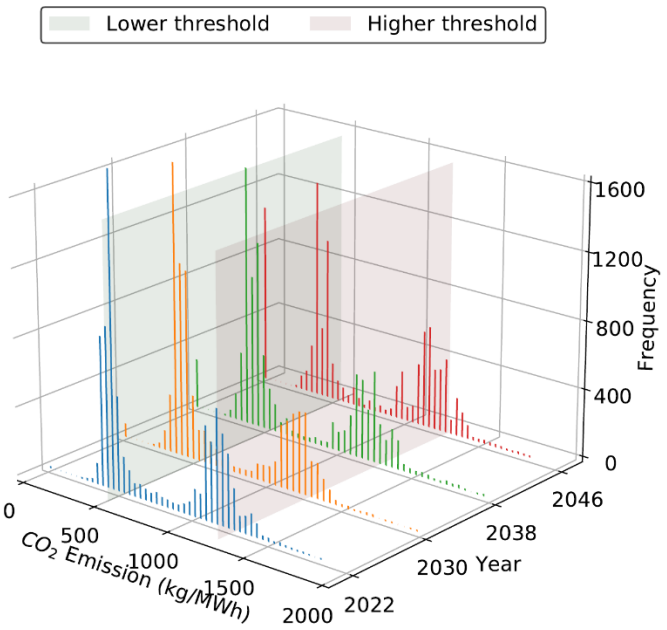

Figure 4.8 Histogram of carbon emission data for the simulated years.

4.4.2 Carbon Emissions

Based on the method of carbon accounting, two ways to calculate the annual carbon emission are adopted. The first method is carbon net-metered, where the power exported to the grid can offset the total carbon emission. The second method does not take account of the exported power back to the grid. The equations for the two methods are as follows:

$$E_{net} = \sum_{t=1}^{N} e^t \, P_{net}^t \Delta t, \tag{4.2}$$

$$E_{non-net} = \sum_{t=1}^{N} e^t \, P_{net}^t \Delta t, \qquad \forall P_{net}^t > 0, \tag{4.3}$$

where E_{net} and $E_{non-net}$ are the annual emission with and without carbon net-metering. t is the timestep, and N is the total number of timesteps in a year. e^t represents the real-time carbon emissions of the grid power. P_{net}^t is the net load of the

house (i.e., total load subtracted by PV and battery power). Δt is the interval length of each timestep.

Figure 4.9 illustrates the community average annual carbon emission of the controlled loads (HVAC and WH). From the figure, it can be seen that in all scenarios, the emissions caused by space heating are reduced through the carbon responsive control. In some scenarios, the emissions produced by cooling and water heating increased due to the corresponding energy increase. This is attributed to the fact that when there are consecutive clean hours, the controllers might pre-cool or pre-heat the space/water tank more than necessary, which leads to an increase in the total operational emissions. Overall, the annual household carbon emissions decreased compared to the baseline.

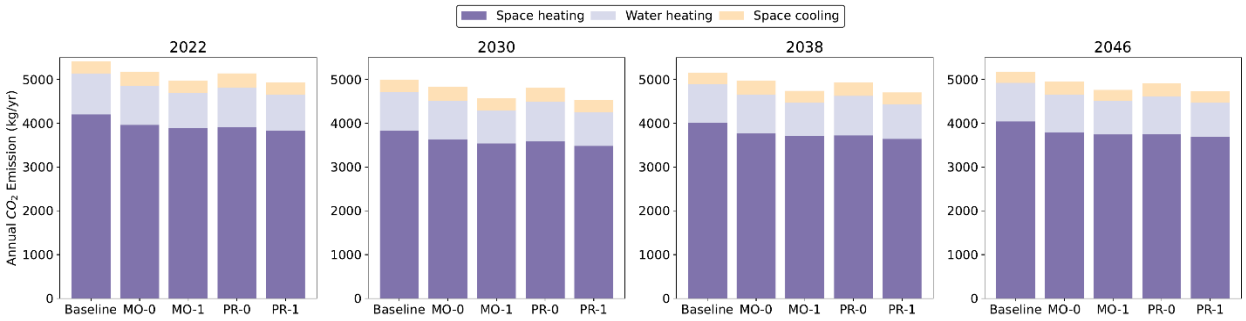

Figure 4.9 Community average annual carbon emission of controlled loads for different controllers across simulated years.

Table 4.4 lists the community average emission per household for different scenarios. In order to eliminate the impact of different carbon accounting methods and focus on the performance variance of the controllers, the carbon emission values listed in Table 4.4 are all net-metered (Equation (4.2)). The emissions results calculated without carbon net-metering are presented in Table A.1 of Appendix A.

Table 4.4 Community average annual carbon emission per household for different controllers across simulated years (net-metered; percentage values are changes relative to the corresponding baseline).

Year	Baseline (kWh/yr.)	MO-0	MO-1	PR-0	PR-1
2022	3,854	-6.0%	-11.0%	-6.8%	-12.1%
2030	2,158	-6.3%	-18.7%	-7.8%	-20.5%
2038	2,650	-6.5%	-15.2%	-7.7%	-16.5%
2046	3,453	-6.3%	-11.6%	-7.1%	-12.6%

Based on Table 4.4, we can see that the controllers that consider carbon net-metering perform better than those that did not. This can be attributed to the logic of the controllers, where the non-net-metered controller increases the loads to do more pre-cooling/pre-heating when the house net-load is negative. This has led to a rise in energy as discussed in former sections, which hinders them from decreasing more carbon emissions.

Similar to the annual energy performance, the emission performance of the predictive controllers is better than the momentary ones. The reason is that predictive controllers make decisions informed by the emissions at the next timestep. This enables a better shifting effect of loads to cleaner periods than the momentary controllers. Cumulatively over a year, more emission is thus reduced by predictive controllers.

Overall, 6% to 20.5% annual carbon emissions reduction is seen by the proposed rule-based controllers compared to the baseline. In terms of the yearly change of emissions, it is interesting that year 2046 is not the one with the lowest emissions. According to Figure 4.8, though the year 2046 has the most hours of zero emission, depending on the power profile of the houses, the zero emission hours might not align

with the high-load hours. Figure 4.10 plots the heat map of a typical house's net load in the year 2046. We see that the high-load hours are mostly in winter and during the nighttime, which aligns with the carbon-intensive hours in Figure 4.6. Therefore, it is safe to infer that the more the high-load hours align with the low-carbon hours, the lower the annual emissions will be.

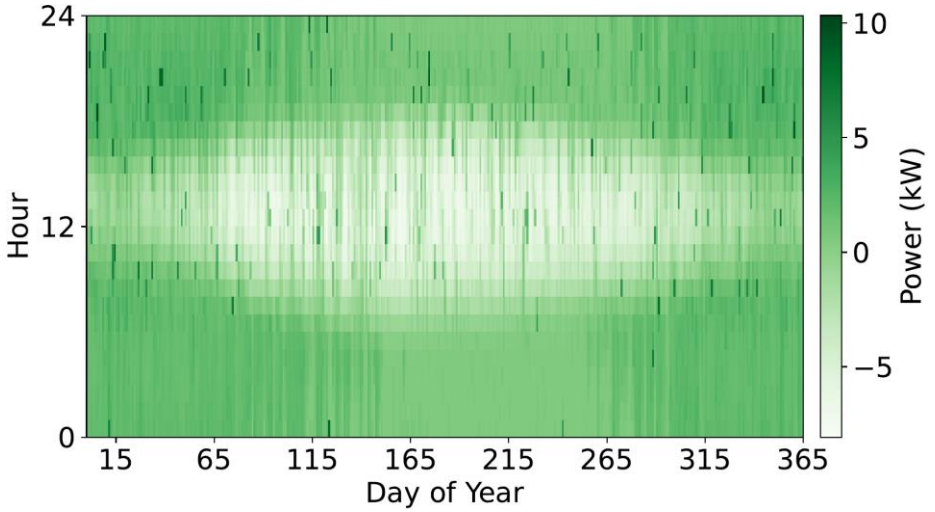

Figure 4.10 Annual house net load heat map (year 2046, house b5).

4.4.3 Energy Cost

Figure 4.11 plots the community average annual energy on-and off-peak costs of the controlled loads in 2022. Similar plots for the other simulation years can be found in Appendix A. From Figure 4.11, we can see that the on-peak energy costs all decreased, and the off-peak costs all increased compared to the baseline. Figure 4.12 plots the house net load in response to the real-time emission signal on a sample winter day of a sample house. The figure shows that when the carbon emission of the on-peak hours exceeds the higher threshold at around 6 PM, the house net load drops below the baseline as all controllers lower the heating and WH setpoints to reduce the loads. However, a certain level of the rebound effect is seen later, where the

controllers consume slightly more energy than the baseline due to the lower setpoints earlier. Overall, during the on-peak hours, more energy is saved due to the high emissions level. Over the whole year of simulation time, the on-peak hours are relatively more carbon-intensive and off-peak hours cleaner, which has led to the reduction of on-peak cost and increase of off-peak cost in Figure 4.11.

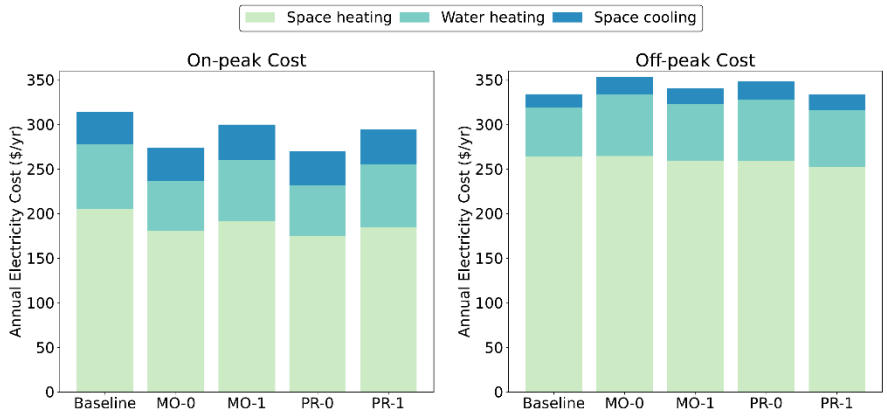

Figure 4.11 Community average annual energy on- and off-peak costs of controlled loads for different controllers in 2022.

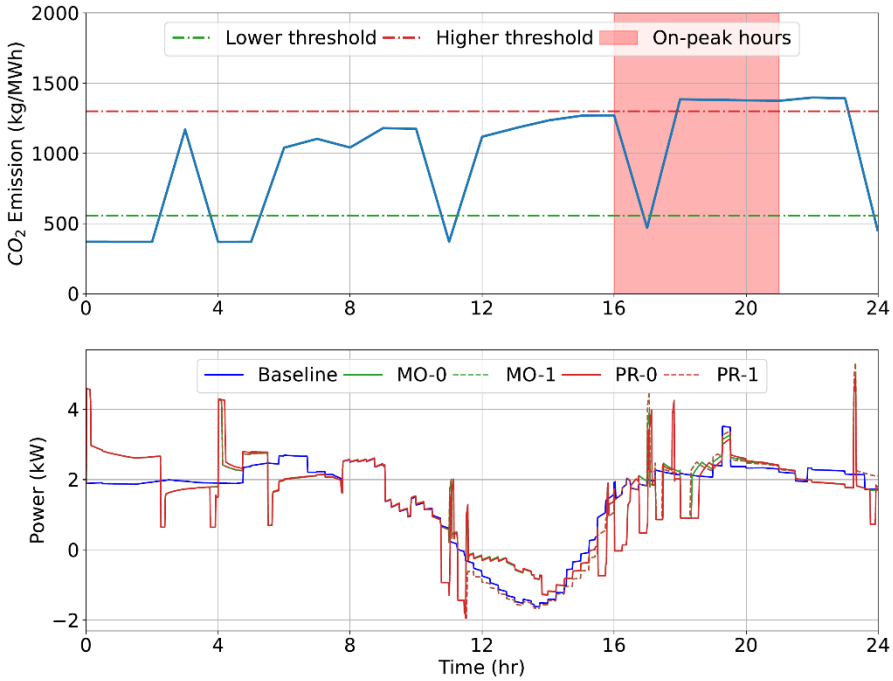

Figure 4.12 House net load in response to the emission signal (winter 2022, house b5).

Table 4.5 summarizes the community average annual energy cost per household for each simulation year. Based on the table, all controllers that do not consider carbon net-metering perform better in terms of the total cost. This can be attributed to the fact that controllers without net-metering tend to use more energy around noon (e.g., 11 AM to 3 PM in Figure 4.12) when the house net load is negative. Because of the rebound effect, they will consume less energy later when PV generation decreases, and the net load is positive. This enables shifting the load from on-peak hours to off-peak hours, which leads to more energy cost savings by the non-net-metered controllers. Additionally, all predictive controllers have more cost savings than the momentary ones. The reason is similar to the energy savings discussion in Section 4.4.1.

Table 4.5 Community average annual energy cost per household for different controllers across simulated years (percentage values are changes relative to the corresponding baseline).

Year	Baseline (kWh/yr.)	MO-0	MO-1	PR-0	PR-1
2022	718	-2.7%	-1.1%	-4.1%	-2.9%
2030	719	1.3%	3.4%	0.1%	1.7%
2038	717	0.5%	2.9%	-0.6%	1.3%
2046	715	-1.0%	1.2%	-1.8%	0.0%

Generally, we see an annual energy cost change of -4.1% to 3.4% on top of the baseline. In terms of the yearly trend of cost savings, we notice that the cleaner the year, the less cost reduction potential. Here, clean means more hours of carbon emission under the lower threshold in Figure 4.8. More specifically, years 2030 and 2038 have more hours under the lower threshold, and the energy cost increased in all scenarios except one.

4.4.4 Thermal Discomfort

Thermal discomfort is quantified by the discomfort degree hours for the HVAC system. For HVAC heating scenarios, when the room temperature is below the heating setpoint, it is considered an uncomfortable period, and vice versa. The switching between heating and cooling is dependent on the outdoor temperature. Note that in this work we consider a setpoint not met as uncomfortable as the actual room temperature deviates from the predetermined setpoint. We did not adopt the ASHRAE recommended comfort range (i.e., 20–28°C) [171] because it is relatively wide compared to our setpoints, which leads to almost the same level of discomfort in all scenarios. A list of the discomfort values according to the ASHRAE Standard is provided in Table A.2 in Appendix A. The discomfort degree hours in this work can be defined by the following equation:

$$U_{hvac} = \sum_{t=1}^{N} |T_{indoor}^{t} - T_{set}^{t}|\,\Delta t, \quad \forall T_{indoor}^{t} < T_{set}^{t}(heating)\ and\ T_{indoor}^{t} > T_{set}^{t}(cooling), \tag{4.4}$$

where T_{indoor}^{t} and T_{set}^{t} are the actual indoor temperature and setpoint, and Δt is the simulation interval of the house model (i.e.,1 minute).

The thermal discomfort for WH is only considered for the shower in this work [172]. It is measured by the unmet thermal energy for any shower draws below 43.3°C (110°F), which is calculated by:

$$U_{wh} = \sum_{t=1}^{N} m_{water}^{t} c_p |T_{water}^{t} - 43.3|\,\Delta t, \qquad \forall T_{water}^{t} < 43.3, \tag{4.5}$$

where m^t_{water} represents the hot water mass flow rate and T^t_{water} is the hot water temperature.

Table 4.6 lists the heating, cooling, and water heating discomfort values for all scenarios across the simulation years. From the table, we see that carbon responsive control brings in a higher level of discomfort in space heating and cooling compared to the baseline, where constant setpoints were implemented annually. However, the hot water discomfort has been slightly improved, which is validated through a higher annual average hot water temperature. Generally, the annual discomfort levels in all the carbon responsive scenarios are maintained within an acceptable range.

Table 4.6 Community average heating, cooling, and water heating discomfort metric values for each simulation scenario.

Year	Heating (°C-hrs./yr.)					Cooling (°C-hrs./yr.)					Hot water (kWh/yr.)				
	Baseline	MO-0	MO-1	PR-0	PR-1	Baseline	MO-0	MO-1	PR-0	PR-1	Baseline	MO-0	MO-1	PR-0	PR-1
2022	8	24	27	30	33	0	2.2	1.9	3.4	3.4	1.3	0.15	0.23	0.19	0.25
2030	8	34	40	31	36	0	4.4	1.0	3.5	3.5	1.3	0.26	0.40	0.26	0.37
2038	8	69	79	64	73	0	7.5	1.5	6.0	6.0	1.3	0.37	0.57	0.39	0.58
2046	8	55	66	51	59	0	6.8	2.4	5.6	5.6	1.3	0.37	0.64	0.31	0.56

When carbon net-metering is considered in the control, the discomfort level increases compared to scenarios without net-metering. This is because when power exporting does not bring emission benefits, the controller tries to increase the self-consumption rate of the surplus PV generation by consuming more energy. This has led to a relatively higher indoor temperature in the heating season and a relatively lower temperature in the cooling season, which means a more comfortable indoor environment for the occupants.

Comparing scenarios with and without predictive control, we notice that predictive control can lead to either an increase or decrease of the discomfort level. There is no direct correlation between the two. Though predictive controllers look ahead for one timestep, the decision to increase or decrease the setpoints is dependent on the emission level at the next timestep, which is rather stochastic in the time frame of one year of simulation time.

4.4.5 Sensitivity Analysis

Control thresholds. The choice of the lower and upper thresholds in rule-based control is essential. To investigate how the thresholds affect the control performance, we conducted a sensitivity analysis. The original lower and upper thresholds were adjusted based on the simulation scenario MO-1 2022. A list of the control performance metrics can be found in Table 4.7. The percentages (e.g., 10&90) here represent the LT and HT, which are based on the emission data range of 2022. The same absolute values of the LT and HT were used across different years.

Table 4.7 Comparison of average performance metric values per household with various control thresholds.

		Lower & upper threshold percentages			
		10&90	20&80	30&70	40&60
Emission (kg/yr.)		3,852	3,819	3,429	3,088
Energy (kWh/yr.)		4,123	4,106	4,177	4,046
Total energy cost ($/yr.)		718	715	711	706
On-peak cost ($/yr.)		627	625	613	617
Off-peak cost ($/yr.)		91	90	97	88
Discomfort	Heating (°C-hrs./yr.)	8	11	27	238
	Cooling (°C-hrs./yr.)	0	0.1	4	21
	Hot water (kWh/yr.)	1.3	1.2	0.2	0.9

From the table, carbon emissions decrease while the control threshold range gets narrower. Specifically, the emission drops drastically from thresholds 20&80 to

30&70 because the latter is more sensitive to emission changes, which leads to more frequent carbon responsive setpoint adjustments.

The relationship between energy consumption and the thresholds is less explicit. Given the same emission signal input, the closer the thresholds, the more hours that fall out of the default zone. Hence, the energy consumption variation depends on the distribution of the emission data. For instance, when the thresholds change from 20&80 to 30&70, more hours are becoming clean compared to hours that are becoming carbon-intensive. This leads to more energy consumed over the whole year.

The annual energy cost sinks with the narrowing threshold range, making the 40&60 thresholds the most cost-effective range. However, the zone thermal discomfort level also reaches the highest in the 40&60 range. This is because the frequent thermostat changes cause the room temperature to swing so that it is more likely to fall outside the comfort zone. The hot water temperature depends not only on the setpoint but also on the water draw profile. There is therefore no explicit correlation between the hot water discomfort level and the thresholds.

To summarize, the 30&70 lower and upper control thresholds chosen in this work best balance the benefits of emissions reduction and energy cost, as well as thermal comfort for the homeowners.

Control interval. The impact of the control interval is studied through varied intervals based on scenario MO-1 2022. From Table 4.8, we observe that the performance of the 15-minute and 30-minute control intervals is very similar to each

other. The 15-minute interval performs better at energy and comfort, whereas the 30-minute is better at emissions and cost. When the interval becomes larger than 30 minutes (e.g., 60 minutes and 120 minutes), then the larger the interval, the worse the control performance. This is probably because in these cases, the controller changes the setpoints too infrequently, which hinders the benefits of carbon responsive control. Considering the balance between control performance and the building thermal dynamics, we chose the control interval to be 15 minutes.

Table 4.8 Comparison of average performance metric values per household with various control intervals.

		Control interval (minute)			
		15	30	60	120
Emission (kg/yr.)		3,429	3,387	3,480	3,740
Energy (kWh/yr.)		4,177	4,184	4,240	4,329
Total energy cost ($/yr.)		711	710	714	724
On-peak cost ($/yr.)		613	612	613	619
Off-peak cost ($/yr.)		97	98	101	105
Discomfort	Heating (°C-hrs./yr.)	27	31	38	49
	Cooling (°C-hrs./yr.)	4	5	6	12
	Hot water (kWh/yr.)	0.2	0.2	0.2	0.3

4.5 Conclusion

In this chapter, we propose a carbon emission responsive control framework for thermostatically controlled loads. Within this framework, the four various controllers adjust thermostat setpoints according to projected carbon emission signals. The impact of carbon net-metering in both momentary and predictive rule-based controllers is investigated through the controller design and a case study. Sensitivity analysis is conducted to evaluate the role of control thresholds and control intervals in the controller design.

Based on the simulation results, the average annual household carbon emissions are decreased by 6.0% to 20.5% compared to the baseline. The average annual energy consumption is increased by less than 6.7% due to more clean hours over the year. The annual energy cost change lies between -4.1% and 3.4% on top of the baseline. All on-peak energy costs decreased while all off-peak costs increased, indicating that the carbon intensities during on-peak hours are higher than those during off-peak hours. Generally, the annual discomfort levels in all the carbon responsive scenarios are maintained within an acceptable range.

Evaluating the impact of carbon net-metering, we found that controllers with carbon net-metering show 2.5% to 3.0% less energy consumption and 5% to 12.7% less emission than controllers without carbon net-metering. This indicates the incentivizing impact of adopting carbon net-metering, as it encourages the exporting of power back to the grid. For controllers without carbon net-metering, higher annual energy consumption and carbon emissions result from attempting to increase the PV self-consumption rate. However, all controllers that do not consider carbon net-metering perform better in terms of the total cost. Due to the rebound effect, they tend to be shifting loads from on-peak hours to off-peak hours, causing the total cost to sink. Further, because more energy is consumed, non-net-metering controllers tend to create a more comfortable indoor environment for the occupants.

All predictive controllers perform better than the momentary controllers in terms of energy consumption, carbon emission, and energy cost. This is attributed to the enhanced load shifting effect by the predictive controller design. Also, this finding

verifies the claim made by Fischer [161] that predictive rule-based controllers are promising alternatives to optimization-based controllers because they are simpler and still effective.

We notice in some scenarios the emissions produced by space cooling and water heating are higher compared to the baseline due to the increased energy consumption from load shifting. This indicates rule-based control solely informed by carbon emission signals may end up with higher emissions, which could be overcome by using optimization-based control methods such as MPC. Additionally, we note that another limitation of this work, which is also a general limitation of rule-based control, is that the rule thresholds might be case-dependent and thus need to be carefully selected for the specific use case. Future work includes:

- Investigating better designs of the control rules to achieve synergetic emission, energy, and cost reductions.
- Incorporating other types of controllable devices such as battery and schedulable loads into the carbon emission responsive control framework to enable more emission reductions.
- Comparing the performance of the developed rule-based control to optimization-based control.
- Incorporating real-time electricity pricing rates for the cost analysis to better reflect the relationship between carbon intensity and electricity price (i.e., lower intensity, lower price).

- Conducting lifecycle cost analysis for the controlled equipment to account for the impact of equipment short cycling on equipment life and replacement cost.
- Discussing the trade-off between the reduction of operational carbon emissions and the potential sacrificing of equipment energy efficiency.

Chapter 5. Community Resilience Enhancement Through a Hierarchical Scheduling Framework

This chapter is based on:

Jing Wang, Kaitlyn Garifi, Kyri Baker, Wangda Zuo, Yingchen Zhang, Sen Huang, Draguna Vrabie. "Optimal renewable resource allocation and load scheduling of resilient communities." Energies 13, no. 21 (2020): 5683.

Jing Wang, Kaitlyn Garifi, Kyri Baker, Wangda Zuo, Yingchen Zhang. "Optimal operation for resilient communities through a hierarchical load scheduling framework." In Proceedings of the 2020 Building Performance Analysis Conference & SimBuild, Virtual Conference, Chicago, IL, USA, vol. 9. 2020.

This chapter presents a methodology for enhancing community resilience through optimal renewable resource allocation and load scheduling in order to minimize unserved load and thermal discomfort. The proposed control architecture distributes the computational effort and is easier to be scaled up than traditional centralized control. The decentralized control architecture consists of two layers: The community operator layer (COL) allocates the limited amount of renewable energy resources according to the power flexibility of each building. The building agent layer (BAL) addresses the optimal load scheduling problem for each building with the allowable load determined by the COL. Both layers are formulated as an MPC-based optimization. Simulation scenarios are designed to compare different combinations of building weighting methods and objective functions to provide guidance for real-world deployment by community and microgrid operators. The results indicate that the impact of power flexibility is more prominent than the weighting factor to the resource allocation process. Allocation based purely on occupancy status could lead to an increase in PV curtailment. Further, it is necessary for the building agent to have multi-objective optimization to minimize the unserved load ratio and maximize comfort simultaneously.

5.1 Introduction

In the past several decades, the degrading power grid infrastructure has been faced with higher stress. On one hand, the frequency of human-made disasters as well as extreme weather events is increasing, causing more frequent power outages [152]. On the other hand, the rapid technological advancement and

increasing adoption of renewable energy is bringing more uncertainty and variability, posing new challenges to the grid. These factors impact the resilience of the power supply and, thus, require the demand side to become actively involved in grid resilience management.

In 2017, Hurricane Maria left 1.5 million customers across Puerto Rico without electricity and it took 11 months to fully restore the power system [5]. In such extreme cases, outages not only cause inconvenience to occupants' daily life but also compromise their health or even lives. The power loss of the HVAC system in a nursing home located in Florida caused 12 patients' deaths after Hurricane Irma in 2017 [173]. This has motivated the research towards more resilient communities.

Studies have proven that communities with on-site PV power and batteries have the potential to sustain power outages for a certain period if the energy resources are properly managed and the controllable loads are well scheduled [174]. Some research efforts focus on microgrid operation with selected distributed generation technologies and energy storage systems. Marnay et al. [175] illustrated that the adoption of combined heat and power together with heat and electrical storage in a hypothetical San Francisco hotel can lead to 11% cost savings and 8% carbon emission reductions. Similarly, Bozchalui et al. [176] developed mathematical models of combined cooling, heating, and power system for a commercial building microgrid, together with PV generation, thermal energy storage, and battery storage devices. Results in [174–176] show that adopting the above technologies can reduce total costs and help achieve efficiency and emission reduction targets.

Some research focuses on restoring the power generation, transmission, and distribution promptly after power outages [152]. Arif et al. [106] co-optimized the topology reconfiguration, repair crew scheduling, and distributed generator (DG) dispatching to maximize the picked-up loads while minimizing the repair time. Chen [119] and Ding [108] proposed a mechanism for microgrid formation to restore critical loads after major disruptions in the power grid. In their scheme, a mixed-integer linear program (MILP) was formulated to maximize the total restored critical loads. The problem was constrained by each microgrid's self-adequacy and operation constraints. Similarly, Chen et al. [123] proposed a MILP model for the optimal sequential service restoration, which coordinates dispatchable DGs and switch gears to restore the power system service step by step.

Other studies consider flexible load scheduling as an important avenue to enhance resilience. In this case, the power demand from buildings can be ramped up or down in response to exterior signals, such as available PV power and occupancy prediction. Hussain et al. [177] classify proactive scheduling, such as revising schedules of dispatchable generators, flexible loads, and energy storages, as the first step for enhancing grid resilience. Kallel et al. [178] proposed a demand-side management control strategy through the modification of the household load profile to satisfy the demand and reduce the size of system components in a stand-alone hybrid PV system. Results show that the proposed strategy led to minimum loss of power supply probability and system cost, as well as extended battery life.

Among the optimal load scheduling studies, some researchers approach load management through a rule-based methodology. Ayodele et al. [179] proposed a rule-based load management scheme for a stand-alone PV battery system, where residential loads are classified into critical and non-critical loads. The critical loads are given higher priority and therefore can operate at their scheduled time while the uncritical loads can be shifted to other times. However, this type of method is not suitable for problems with a large number of variables (i.e., controllable appliances), where manually defining the algorithms becomes difficult.

Many other studies formulate load scheduling as an optimization problem. Garifi et al. [180] adopted a stochastic MPC-based algorithm for demand response in a home energy management system (HEMS). The HEMS optimally schedules controllable appliances given user preferences and available residentially owned power sources such as PV and battery. Zhao et al. [181] applied a genetic algorithm (GA) in a HEMS controller where the optimal power scheduling schemes under various electricity pricing models are compared. Pathak et al. [182] developed a scheduling strategy for demand response management of residential loads using a particle swarm optimization algorithm. Additionally, machine learning techniques have been emerging in the optimal load scheduling field. Zhang et al. [183] proposed a learning-based HEMS, where neural network and regression-based learning are adopted to predict the energy consumption of the HVAC system. Mazzeo et al. [184] applied an energy reliability-constrained method for the multi-objective optimization

of hybrid photovoltaic-wind-battery systems. The proposed method permits choosing the most proper indicator combination to be constrained or optimized.

Noticeably, occupants' preferences are widely considered in the problem formulation of load scheduling as either constraints or objectives. Jin et al. [87] presented a user-centric HEMS that is built on a multi-objective MPC framework, wherein the objectives consist of thermal comfort and user convenience. In Zhao's work [181], the delay time rate of home appliances, i.e., the deviation between an appliance's actual operation time and its scheduled time, is minimized to increase the satisfaction of user preferences.

Optimal load scheduling in single buildings, especially residential buildings, has been studied extensively [87, 180–183]. Quantifying load flexibility and optimal load scheduling in other building types, however, needs further exploration. Larger-scale studies, such as those for microgrids, often focus on identifying enabling energy technologies or operating energy resources from a higher level. The scheduling of each controllable load in every building of a community can be computationally challenging due to the increased number of variables. However, this also provides more possibilities for load scheduling due to the heterogeneity of different building load shapes in the community. If building loads in the same community are scheduled simultaneously by a single operator, power-sharing is possible. Further, under certain circumstances, buildings of lower priority could reduce their loads to satisfy the demand of higher priority building loads.

Therefore, this chapter proposes a new methodology for optimal renewable resource allocation and load scheduling in resilient communities. The methodology adopts a hierarchical architecture consisting of a COL and a BAL. The COL enables dynamic renewable resource sharing among buildings in the same community according to various weighting methods. The BAL then achieves the locally optimal operation solution by controlling its HVAC system, loads and battery storage with the allowable load decided by the COL. The innovation of this work is that it proposes an easy-to-deploy optimization scheme for large-scale communities, which embraces both high-level resource allocation and low-level high-fidelity BEM. The hierarchical control architecture distributes the computational effort and is easier to be scaled up than traditional centralized control, which is not robust for large-scale deployment. The hierarchical structure also helps hide the complexity of the whole scheduling system through the separated layers. In the case study, different building types are considered, including residential and small commercial buildings.

The remainder of the chapter is organized as follows: Section 5.2 introduces the concept and architecture developed for community resource allocation and load scheduling. Section 5.3 provides the mathematical formulation of the optimization problem. Section 5.4 demonstrates the proposed methodology through a case study based on a real community. Finally, concluding remarks and future work are provided in Section 5.5.

5.2 Methodology

In this work, we consider an islanded community during a power outage. The only energy resource accessible to the community is the on-site PV generator and the batteries. Under this problem setting, the research question is how to optimally allocate the limited PV generation among different buildings and schedule the loads to meet occupants' essential needs for a certain period. Here, we confine occupants' essential needs to be physiological (i.e., food and shelter) and safety needs (i.e., lighting at night), which align with the two bottom levels of Maslow's Hierarchy of Needs [185].

To address this problem, we propose a hierarchical control architecture that consists of two layers. The top layer is the COL which mimics the perspective of the community operator and seeks the optimal solution for allocating the limited PV power among buildings. The bottom layer is the BAL which satisfies its occupants' needs through optimal load scheduling. In this way, the cooperation among buildings is achieved through their individual but simultaneous communication with the operator, and the global optimum of the whole community is also achieved through decentralized control. The operation in both layers is formulated as MPC problems. The proposed architecture with data exchange flow is visualized in Figure 5.1.

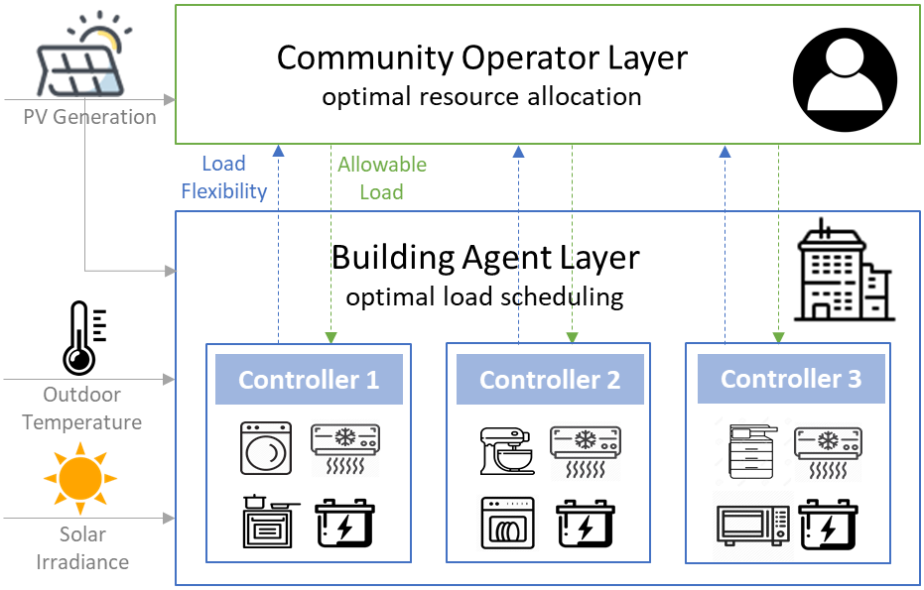

Figure 5.1 Proposed architecture with data exchange flow.

As can be seen from the figure, the COL determines the allowable load based on the forecast of the total PV power generation and the load flexibility of each building. The determined allowable load of each building is then passed down to the building smart controllers in BAL. Other inputs of the BAL consist of the outdoor temperature and solar irradiance forecasts. This decentralized control architecture distributes the computational efforts to local controllers. Compared with centralized control, this structure is more robust, scales up easily, and allows the use of inexpensive and simple agents at the BAL [186]. The data exchange between the COL and the BAL can be implemented through a multi-agent communication system [187]. The detailed mechanisms of the two layers are introduced in the remainder of this section.

The COL allocates the limited amount of available generation from a renewable energy resource; namely, PV power, according to the load flexibility of each building, within which range the building's power demand can fluctuate. The operator decides

the optimal way to allocate the current PV power to avoid PV curtailment and building load shedding. We assume that the operator does not take into account the detailed building equipment information, extra building-owned energy resources (i.e., battery), or building thermal dynamics in its allocation process. This assures the scalability of the control framework. The allocated PV power to building i is defined as the allowable load:

$$P_{allow,i}^{t} = \alpha_i^t * P_{pv}^{t}, \tag{5.1}$$

where α_i^t is the ratio of the allowable load of building i to the current total PV generation P_{pv}^{t}. Since it is directly related to the allocated PV power, α_i^t is referred to as the allocation factor in the rest of the chapter.

To investigate a logical way to allocate the PV power besides the baseline, where the allocation is done only with information of building load flexibility, we introduce weighting factors into the problem. The weighting factor reflects the priority of each building. Two types of weighting factors are considered: constant versus dynamic. The constant weighting factor is adopted when a building is naturally more important than other buildings. For example, health facilities are naturally prioritized over other types of buildings during emergencies. The dynamic weighting factor is time-varying based on occupancy, e.g., when a building is occupied, it has a higher weighting factor.

Therefore, the COL decides the allowable load of each building through three methods: (1) equally weighted, (2) weighted based on priority, (3) weighted based on occupancy. The determined allowable load is then passed to the smart controllers in

BAL, where each building performs its local detailed optimization to achieve its own objectives.

The BAL addresses the optimal load scheduling problem with the predetermined allowable load. Each building is simulated as an agent that has various electrical loads, an HVAC system, and a battery. The HVAC system is modeled with a linear regression model trained from data. The battery is modeled with a linear convex model. By adopting linear room temperature models and battery models, the optimization problem becomes linear. This method has the advantage of shorter computational time. However, compared to high-fidelity nonlinear models, it may lose some model fidelity and the ability to simulate certain system dynamics by making simplifications. In this work, linear models are accurate enough for our application scenario.

In this work, following methods found in the literature [178, 179, 181, 183, 188], the building's electrical loads are categorized into four types: sheddable, modulatable, shiftable, and critical. The primary classification criteria include the assumed occupants' preference during emergency circumstances and the electrical characteristics of different appliances. Only loads that are related to safety (e.g., lighting at night) or food preservation (e.g., refrigerator) are considered critical. Sheddable loads are those that can be fully disconnected without impacting the occupant's essential needs during the studied period, such as coffee makers. Modulatable loads are those categorized by varying power amplitudes such as the HVAC system. Shiftable loads are those that need to be operated but are flexible with

respect to the time of day that they are scheduled. Examples are washers and driers. From a practical point of view, categorizing building loads can help avoid dealing with thousands of individual load models especially when the problem scales up. It can significantly reduce the computational effort. Figure 5.2 visualizes the logic we followed to categorize the loads.

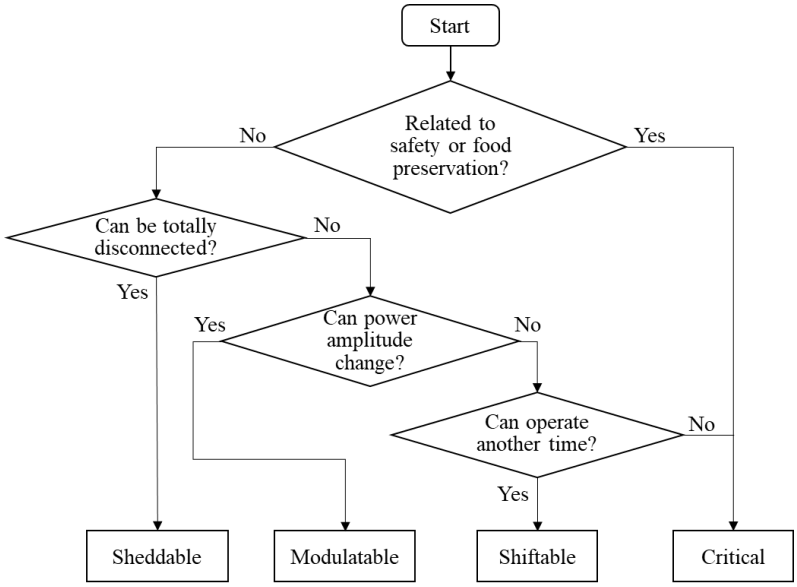

Figure 5.2 Flow chart of the load categorization logic.

Additionally, at this layer, different optimization objective functions are compared to evaluate their performance in satisfying selected key performance indices (KPIs); namely, unserved load ratio, thermal comfort, PV curtailment, and required battery installation size. Two objectives are considered: (1) minimizing unserved load ratio, and (2) maximizing thermal comfort.

It is to mention that we included uncertainty in the weather-related parameter forecasts to account for prediction errors. Chance constraints for the indoor temperature range are, thus, implemented to ensure thermal comfort is maintained

with high probability. The following section presents the detailed mathematical formulation of the two-layered control architecture with equations.

5.3 Formulation of the Optimization Problem

5.3.1 Community Operator Layer

The COL determines the allowable load of each building through MPC-based optimization that takes into account forecasted PV generation, building load flexibility, priority, and occupancy of each building. The flexibility of building loads depends on the power demand of the controllable loads, i.e., the sum of sheddable, modulatable, and shiftable loads. Note that the HVAC load flexibility is reflected in the temperature range constraints and is not summed here. The mathematical formulation of the load flexibility for each building i is given by:

$$P^t_{load,flex,i} = \sum_{j=1}^{N_{shed,i}} \hat{P}^t_{shed,i,j} + \sum_{j=1}^{N_{modu,i}} \hat{P}^t_{modu,i,j} + \sum_{j=1}^{N_{shif,i}} \hat{P}^t_{shif,i,j}, \tag{5.2}$$

where $\hat{P}^t_{shed,i,j}$, $\hat{P}^t_{modu,i,j}$, and $\hat{P}^t_{shif,i,j}$ denote the prediction data of each sheddable, modulatable, and shiftable load in building i, respectively. The $N_{shed,i}$, $N_{modu,i}$, and $N_{shif,i}$ represent the number of appliances under each category. The constraints of the flexible load are defined as:

$$\underline{P}^t_{load,i} = \sum_{j=1}^{N_{crit,i}} \hat{P}^t_{crit,i,j}, \tag{5.3}$$

$$\overline{P}^t_{load,i} = \underline{P}^t_{load,i} + P^t_{load,flex,i}, \tag{5.4}$$

$$\underline{P}^t_{load,i} \le P^t_{load,i} \le \overline{P}^t_{load,i}, \tag{5.5}$$

where $\hat{P}^t_{crit,i,j}$ stands for the prediction data of each critical load in building i. $P^t_{load,i}$ is an optimization variable that represents the actual consumed power at each timestep, which is bounded by the critical load $\underline{P}^t_{load,i}$ and the total desired load $\overline{P}^t_{load,i}$. Equations (5.6)-(5.10) define the power balance and its constraints at the community level:

$$\alpha^t_i * P^t_{pv} - P^t_{curt,i} = P^t_{load,i} - P^t_{shed,i}, \tag{5.6}$$

$$\text{s.t. } 0 \leq P^t_{curt,i} \leq \alpha^t_i * P^t_{pv}, \tag{5.7}$$

$$0 \leq P^t_{shed,i} \leq \underline{P}^t_{load,i}, \tag{5.8}$$

$$0 \leq \alpha^t_i \leq 1, \tag{5.9}$$

$$\sum_{i=1}^{I} \alpha^t_i = 1, \tag{5.10}$$

where $\alpha^t_i * P^t_{pv}$ is the PV power allocated to building i at timestep t. Equation (5.7) defines the range of the PV curtailment, where the variable $P^t_{curt,i}$ denotes the curtailment of allocated PV power in the case that allocated PV power exceeds the upper bound of $P^t_{load,i}$. Similarly, $P^t_{shed,i}$ is the variable of load shedding for situations when the available PV power is less than the lower bound of $P^t_{load,i}$. Equation (5.8) enforces that the value of load shedding cannot exceed the lower bound of $P^t_{load,i}$. Equations (5.9) and (5.10) define the range of the PV allocation factor α^t_i and the sum of all allocation factors at any timestep must equal 1. The total number of buildings in the community is given by parameter I.

The objective of the COL is to minimize the total PV curtailment and load shedding over the whole MPC prediction horizon at the community level. The mathematical formulation of the objective function is defined as:

$$f_{cost}(t, \{x^t\}_{t=1}^{H}) = \sum_{i=1}^{\mathrm{I}} \sum_{t=1}^{H} (P_{curt,i}^{t} + P_{shed,i}^{t}), \tag{5.11}$$

$$\min_{\{x^t\}_{t=1}^{H}} f_{cost}(t, \{x^t\}_{t=1}^{H}), \tag{5.12}$$

where H denotes the prediction horizon. Let x^t be the vector of all optimization variables of the COL:

$$x^t = \left[\{P_{curt,i}^{t}\}_{t=1}^{H}, \{P_{shed,i}^{t}\}_{t=1}^{H}, \{P_{load,i}^{t}\}_{t=1}^{H}, \{\alpha_i^t\}_{t=1}^{H}\right], i \in \{1, 2, \dots, \mathrm{I}\}, \mathrm{t} \in \{1, 2, \dots, \mathrm{H}\}. \tag{5.13}$$

For scenarios where a certain building is prioritized over other buildings, a weighting factor $w_i^t > 1$is introduced into the cost function shown in Equation (5.11) to obtain:

$$f_{cost}(t, \{x^t\}_{t=1}^{H}) = \sum_{i=1}^{I} \sum_{t=1}^{H} (P_{curt,i}^{t} + w_i^t * P_{shed,i}^{t}). \tag{5.14}$$

This will ensure that a prioritized building will experience less load shed $P_{shed,i}^{t}$. For constant weighting scenarios, w_i^t of the prioritized building is twice as large as the rest of the buildings over the whole simulation. For occupancy-based time-varying weighting scenarios, w_i^t of any building is doubled when that building is occupied.

5.3.2 Building Agent Layer

The BAL performs MPC-based optimal load scheduling with detailed device models. The overall optimization problem is a MILP since our device models include binary variables. Each building agent coordinates the electricity usage of an HVAC

model, four types of building loads, and a battery. Since all the equations in this section apply for every individual building i, to avoid redundancy, we have removed the notation of building index i in the following discussion. For each of the studied buildings, the power balance that must be satisfied at each timestep is given by:

$$P_{pv}^{t} - P_{curt}^{t} = P_{ch}^{t} - P_{dis}^{t} + P_{load}^{t} + P_{hvac}^{t}, \tag{5.15}$$

where PV curtailment is limited by how much PV generation is available:

$$\text{s.t. } 0 \le P_{curt}^{t} \le P_{pv}^{t}. \tag{5.16}$$

Two different cost functions are designed to be compared: (1) to minimize unserved load ratio:

$$f_{cost}(t, \{x^t\}_{t=1}^{H}) = \sum_{t=1}^{H} \left(\overline{P}_{load}^{t} - P_{load}^{t}\right) + \sum_{t=1}^{H} \gamma P_{ch}^{t} + \sum_{t=1}^{H} \gamma' P_{curt}^{t}, \tag{5.17}$$

$$\min_{\{x^t\}_{t=1}^{H}} f_{cost}(t, \{x^t\}_{t=1}^{H}), \tag{5.18}$$

and (2) to maximize thermal comfort:

$$f_{cost}(t, \{x^t\}_{t=1}^{H}) = \sum_{t=1}^{H} \left(T_{room}^{t} - \frac{\underline{T}_{room} + \overline{T}_{room}}{2}\right)^2 + \sum_{t=1}^{H} \gamma P_{ch}^{t} + \sum_{t=1}^{H} \gamma' P_{curt}^{t}, \tag{5.19}$$

$$\min_{\{x^t\}_{t=1}^{H}} f_{cost}(t, \{x^t\}_{t=1}^{H}). \tag{5.20}$$

In Equation (5.17), $\overline{P}_{load}^{t}$ is the same predicted load upper bound discussed in Section 5.3.1 in Equation (5.4). The difference between this upper bound and the actual operated loads P_{load}^{t} is minimized to achieve maximum served load. In Equation (5.19), the first term penalizes when the indoor air temperature T_{room}^{t} deviates from the desired temperature range given by $\underline{T}_{room}$ and $\overline{T}_{room}$, which are the

lower and upper bounds of the indoor air temperature. To avoid simultaneous charging and discharging of the battery as well as PV curtailment, the objective function also includes small penalizations of charging γP_{ch}^{t} and curtailment $\gamma' P_{curt}^{t}$ [189].

The room temperature is predicted with a linear regression model shown in Equations (5.21)-(5.23). The independent variables include the ambient temperature T_{amb}^{t}, indoor room temperature T_{room}^{t}, and solar irradiance Q_{sol}^{t} of the past two timesteps, and the speed of the HVAC equipment of the past one timestep r_{hvac}^{t}. The normalized speed ranges from 0 to 1. The resulted HVAC system power is thus the product of the speed ratio r_{hvac}^{t} and the nominal power $P_{hvac,nom}$. The choice of regression over two past terms is to reflect the impact of building thermal mass on indoor temperature evolution while balancing prediction accuracy and computational time [190]. In this model, the internal heat gain was not included as it is calculated from the actual operated devices (i.e., optimization variables). Having it in the temperature prediction model will further couple the temperature calculation and the load scheduling, causing the computational effort to be greater. Additionally, compared to the solar heat gain, the internal heat gain accounts for less than 10% of the total heat gain in our case. Due to the above reasons, we did not include the internal heat gain in this model.

$$T_{room}^{t+1} = \beta_1 T_{amb}^{t} + \beta_2 T_{amb}^{t-1} + \beta_3 T_{room}^{t} + \beta_4 T_{room}^{t-1} - \beta_5 r_{hvac}^{t} + \beta_6 Q_{sol}^{t} + \beta_7 Q_{sol}^{t-1} \tag{5.21}$$

$$0 \leq r_{hvac}^{t} \leq 1 \tag{5.22}$$

$$P_{hvac}^{t} = r_{hvac}^{t} * P_{hvac,nom} \tag{5.23}$$

To account for the uncertainty in the outdoor air temperature and solar irradiance forecasts, we use chance constraints to ensure that thermal comfort is maintained with a high probability [191]. The chance constraints are given by:

$$Pr\left(\underline{T}_{room} \leq T_{room}^{t}\right) \geq 1 - \varepsilon_T, \tag{5.24}$$

$$Pr\left(T_{room}^{t} \leq \overline{T}_{room}\right) \geq 1 - \varepsilon_T, \tag{5.25}$$

where ε_T is the maximum violation probability of the chance constraint. We assume that the forecasting errors for all timesteps follow the same normal distribution and are independent for each timestep:

$$T_{amb,e}^{t} \sim \mathcal{N}(\mu_T^t, (\sigma_T^t)^2), \tag{5.26}$$

$$Q_{sol,e}^{t} \sim \mathcal{N}\left(\mu_Q^t, (\sigma_Q^t)^2\right). \tag{5.27}$$

The outdoor temperature and solar irradiance predictions can, thus, be represented as:

$$T_{amb}^{t} = T_{amb,f}^{t} + T_{amb,e}^{t}, \tag{5.28}$$

$$Q_{sol}^{t} = Q_{sol,f}^{t} + Q_{sol,e}^{t}, \tag{5.29}$$

where $T_{amb,f}^{t}$ and $Q_{sol,f}^{t}$ are the forecasts of ambient temperature and solar irradiance while $T_{amb,e}^{t}$ and $Q_{sol,e}^{t}$ are the forecast errors. The chance constraint shown in Equation (5.25) can be rewritten as:

$$Pr(\chi_T^{t+1} \leq 0) \geq 1 - \varepsilon_T, \tag{5.30}$$

where:

$$\chi_T^{t+1} = T_{room}^{t+1} - \overline{T}_{room}. \tag{5.31}$$

Then, by substituting Equations (5.21), (5.28), and (5.29) for T_{room}^{t+1}, the above equation becomes:

$$\begin{aligned}\chi_T^{t+1} = \beta_1\left(T_{amb,f}^t + T_{amb,e}^t\right) + \beta_2\left(T_{amb}^{t-1} + T_{amb,e}^{t-1}\right) + \beta_3 T_{room}^t + \beta_4 T_{room}^{t-1} - \beta_5 r_{hvac}^t \\ + \beta_6\left(Q_{sol,f}^t + Q_{sol,e}^t\right) + \beta_7\left(Q_{sol}^{t-1} + Q_{sol,e}^{t-1}\right) - \overline{T}_{room}.\end{aligned} \tag{5.32}$$

Since $T_{amb,e}^t$ and $Q_{sol,e}^t$ are normally distributed, χ_T^{t+1} is also normally distributed with the following mean μ^t and standard deviation σ^t:

$$\begin{aligned}\mu^t = \beta_1\left(T_{amb,f}^t + \mu_T^t\right) + \beta_2(T_{amb}^{t-1} + \mu_T^t) + \beta_3 T_{room}^t + \beta_4 T_{room}^{t-1} - \beta_5 r_{hvac}^t \\ + \beta_6\left(Q_{sol,f}^t + \mu_Q^t\right) + \beta_7\left(Q_{sol}^{t-1} + \mu_Q^t\right) - \overline{T}_{room},\end{aligned} \tag{5.33}$$

$$\sigma^t = \sqrt{(\beta_1\sigma_T^t)^2 + (\beta_2\sigma_T^t)^2 + (\beta_6\sigma_Q^t)^2 + (\beta_7\sigma_Q^t)^2}. \tag{5.34}$$

Hence, the chance constraint in Equation (5.30) can be reformulated as:

$$Pr(\chi_T^{t+1} \leq 0) = \Phi\left(\frac{0 - \mu^t}{\sigma^t}\right) \geq 1 - \varepsilon_T, \tag{5.35}$$

where $\Phi(\cdot)$ is the cumulative distribution function (CDF) of the standard normal distribution $\mathcal{N}(0,1)$. Finally, by taking the inverse CDF of both sides in Equation (5.35), we obtain the chance constraint for ensuring the indoor temperature not exceeding the upper bound of $\overline{T}_{room}$ with the probability of $(1 - \varepsilon_T)$ as follows:

$$\begin{aligned}\overline{T}_{room} - \beta_1\left(T^t_{amb,f} + \mu^t_T\right) - \beta_2(T^{t-1}_{amb} + \mu^t_T) - \beta_3 T^t_{room} - \beta_4 T^{t-1}_{room} + \beta_5 r^t_{hvac} \\ - \beta_6\left(Q^t_{sol,f} + \mu^t_Q\right) - \beta_7\left(Q^{t-1}_{sol} + \mu^t_Q\right) \\ \geq \Phi^{-1}(1-\varepsilon_T)\sqrt{(\beta_1\sigma^t_T)^2 + (\beta_2\sigma^t_T)^2 + \left(\beta_6\sigma^t_Q\right)^2 + \left(\beta_7\sigma^t_Q\right)^2}.\end{aligned} \tag{5.36}$$

Taking a similar derivation process for Equation (5.24), we obtain the chance constraint for the temperature lower bound:

$$\begin{aligned}\beta_1\left(T^t_{amb,f} + \mu^t_T\right) + \beta_2(T^{t-1}_{amb} + \mu^t_T) + \beta_3 T^t_{room} + \beta_4 T^{t-1}_{room} - \beta_5 r^t_{hvac} + \beta_6\left(Q^t_{sol,f} + \mu^t_Q\right) \\ + \beta_7\left(Q^{t-1}_{sol} + \mu^t_Q\right) - \underline{T}_{room} \\ \geq \Phi^{-1}(1-\varepsilon_T)\sqrt{(\beta_1\sigma^t_T)^2 + (\beta_2\sigma^t_T)^2 + \left(\beta_6\sigma^t_Q\right)^2 + \left(\beta_7\sigma^t_Q\right)^2}.\end{aligned} \tag{5.37}$$

As mentioned above, the electrical loads consist of four types: sheddable, modulatable, shiftable, and critical, which are summed in the following equation:

$$P^t_{load} = \sum_{j=1}^{N_{shed}} P^t_{shed,j} + \sum_{j=1}^{N_{modu}} P^t_{modu,j} + \sum_{j=1}^{N_{shif}} P^t_{shif,j} + \sum_{j=1}^{N_{crit}} P^t_{crit,j}. \tag{5.38}$$

where $P^t_{shed,j}$, $P^t_{modu,j}$, $P^t_{shif,j}$, and $P^t_{crit,j}$ are the optimization variables for individual loads in each category. The mathematical formulation of the sheddable load is shown in Equation (39), where $u^t_{shed,j}$ is a binary optimization variable and $\hat{P}^t_{shed,j}$ is the original sheddable load power demand data. The actual sheddable load after optimization $P^t_{shed,j}$ is determined by the ON/OFF status represented by the binary variable.

$$P^t_{shed,j} = u^t_{shed,j} * \hat{P}^t_{shed,j}, \qquad j \in \{1, \dots, N_{shed}\} \tag{5.39}$$

Equation (5.40) sets the lower and upper bound of the optimization variable $P^t_{modu,j}$, which represents the modulatable load power demand. The actual demand is modulated between zero and the original demand data $\hat{P}^t_{modu,j}$.

$$0 \le P^t_{modu,j} \le \hat{P}^t_{modu,j}, \qquad j \in \{1, \dots, N_{modu}\} \tag{5.40}$$

Equation (5.41) states that the actual critical load $P^t_{crit,j}$ must be exactly equal to the critical power demand data $\hat{P}^t_{crit,j}$.

$$P^t_{crit,j} = \hat{P}^t_{crit,j}, \qquad j \in \{1, \dots, N_{crit}\} \tag{5.41}$$

The shiftable loads are scheduled through scheduling matrices [181]. First, using the power data [192], we extracted the average cycle time $n_{shif,j}$ and the average power demand $P_{shif,j,avg}$ of each shiftable load. The starting time of a shiftable load $t_{shif,j,s}$ is optimized over the MPC horizon. At the scheduled starting time, the binary variable $v^t_{shed,j}$ equals 1 and is 0 otherwise:

$$\begin{gathered} v^t_{shif,j} = \begin{cases} 1, t = t_{shif,j,s} \\ 0, t \neq t_{shif,j,s} \end{cases}, \\ \forall t \in \{1, \dots, H - n_{shif,j} + 1\}, j \in \{1, \dots, N_{shif}\}. \end{gathered} \tag{5.42}$$

Once the starting time of a load is selected, the power demand of the load is then fixed until it finishes its cycle. The appliance must finish its cycle before the horizon ends ($t \in \{1, \dots, H - n_{shif,j} + 1\}$). Here, we assume that each shiftable load operates once and only once in each horizon, which is enforced by:

$$\sum_{t=1}^{H-n_{shif,j}+1} v^t_{shif,j} = 1. \tag{5.43}$$

Next, a scheduling matrix $\boldsymbol{S}_{shif,j}$ of shape $H \times (H - n_{shif,j} + 1)$ is generated for each shiftable load. The actual power shape of the load, denoted $P^t_{shif,j}$, is calculated by:

$$P^t_{shif,j} = \boldsymbol{S}_{shif,j} \times \begin{bmatrix} v^1_{shif,j} \\ \vdots \\ v^{H-n_{shif,j}+1}_{shif,j} \end{bmatrix} \times P_{shif,j,avg}. \tag{5.44}$$

For instance, when $H = 12, n_{shif,j} = 3$, an appliance scheduling matrix of shape 12×10 is generated as follows:

$$\boldsymbol{S}_{shif,j} = \begin{bmatrix} 1 & 0 & & 0 & 0 \\ 1 & 1 & & 0 & 0 \\ 1 & 1 & & 0 & 0 \\ 0 & 1 & & 0 & 0 \\ \vdots & 0 & \cdots & \vdots & 0 \\ 0 & \vdots & & 0 & \vdots \\ 0 & 0 & & 1 & 0 \\ 0 & 0 & & 1 & 1 \\ 0 & 0 & & 1 & 1 \\ 0 & 0 & & 0 & 1 \end{bmatrix} \tag{5.45}$$

The linear battery model adopted in this work is shown in Equations (5.46)-(5.48). The battery state of charge (SOC) E^{t+1}_{bat} depends on the SOC of the previous timestep E^t_{bat}, as well as the battery charging or discharging during each step and the battery charging/discharging efficiencies η_{ch} and η_{dis}. Constraints in Equations (5.47)-(5.48) enforce the acceptable limits for charging/discharging power and battery SOC:

$$E^{t+1}_{bat} = E^t_{bat} + \eta_{ch} P^t_{ch} \Delta t - \frac{1}{\eta_{dis}} P^t_{dis} \Delta t \tag{5.46}$$

$$0 \leq P^t_{ch}, P^t_{dis} \leq \overline{P}_{bat} \tag{5.47}$$

$$0 \leq E^t_{bat} \leq \overline{E}_{bat} \tag{5.48}$$

The optimization variables in each building agent are collected in vector x^t:

$$x^t = \begin{bmatrix} \{P^t_{curt}\}^H_{t=1}, \{P^t_{ch}\}^H_{t=1}, \{P^t_{dis}\}^H_{t=1}, \{r^t_{hvac}\}^H_{t=1}, \{u^t_{shed,j}\}^H_{t=1}, \\ \{P^t_{modu,j}\}^H_{t=1}, \{v^t_{shif,j}\}^{H-n_{shif,j}+1}_{t=1}, \{T^t_{room}\}^H_{t=1}, \{E^t_{bat}\}^H_{t=1} \end{bmatrix}. \quad (5.49)$$

5.4 Case Study

The proposed architecture has been tested with a case study based on a real-world community located in Anna Maria Island, FL [148]. It is a net-zero energy community made up of residential units and small commercial buildings with on-site PV panels. To demonstrate the idea of dynamic power-sharing among buildings, the data for three buildings of different types are used in the case study [192]. The selected buildings are one residential building (area: 93.8 m^2), one ice cream shop (area: 160.5 m^2), and one bakery (area: 410 m^2). All buildings use heat pumps as HVAC equipment. All data for the case study have been exported from a validated physics-based model of the studied community [151]. The weather file embedded in the model is typical meteorological year (TMY) data for the weather station at Tampa International Airport [193]. The load data consists of power submetering data provided by the community [192]. The solar irradiance data are collected through a local solar station. The indoor temperature data are simulation results generated by the physics-based room models [15]. The simulations are run in Python 2.7 with Gurobi 9.0 [194] as the optimization engine. The average simulation time of each scenario is about 20 s in Windows 7 operating system on a DELL T5810 workstation with 32 GB RAM and a 3.50 GHz Intel Xeon CPU (E5-1620 v4) processor.

5.4.1 Simulation Scenario Design

The optimal resource allocation and load scheduling MPC algorithm for the community when disconnected from the grid was simulated for 48 h within Florida's hurricane season on August 4 and 5. The timestep Δt for both COL and BAL is 1 h and the MPC horizon $H = 12$ h to balance the trade-off between forecast information and computational time. Table 5.1 lists the 10 scenarios covering various weighting methods at the operator layer and two different objectives at the building layer. In the following discussion, R stands for Residential, I stands for Ice Cream Shop, and B stands for Bakery. Each scenario was run for all three buildings. In total, 30 simulations were run and analyzed.

Table 5.1 Designed simulation scenarios with varied weighting factors and objective functions.

		Community Operator Layer				
			Priority-Based Weighting			Occupancy-Based Weighting
		Equal Weighting	Prioritize Residential	Prioritize Ice Cream Shop	Prioritize Bakery	
Building Agent Layer	Minimize unserved load ratio	S11	S21_R	S21_I	S21_B	S31
	Maximize thermal comfort	S12	S22_R	S22_I	S22_B	S32

In the room temperature constraints, the lower and upper temperature limits $\underline{T}_{room}$ and $\overline{T}_{room}$ are governed by ASHRAE Standard 55–2017 [171], which recommends the temperature range for thermal comfort to be approximately between 67°F and 82°F (20–28°C). Thus, $\underline{T}_{room}$ is 20°C and $\overline{T}_{room}$ is 28°C. Table 5.2 summarizes the coefficients of the HVAC linear regression models. The prediction accuracy is

measured with the RMSE. The nominal power of each heat pump is listed in the last row of Table 5.2.

Table 5.2 Coefficients, accuracy, and nominal power of HVAC linear regression models.

	Regression Variables	Residential	Ice Cream Shop	Bakery
Coefficients	T_{room}^{t-1}	1.527	1.579	1.530
	T_{room}^{t-2}	−0.532	−0.586	−0.536
	T_{amb}^{t-1}	0.037	0.044	0.050
	T_{amb}^{t-2}	−0.032	−0.036	−0.044
	r_{HVAC}^{t-1}	−0.324	−0.688	−0.393
	Q_{sol}^{t-1}	0.350	0.486	0.206
	Q_{sol}^{t-2}	−0.072	−0.219	0.098
RMSE (°C)		0.196	0.230	0.295
Nominal Power (kW)		4.0	5.5	6.8

Table 5.3 summarizes the load categorization results following the classification proposed in Section 5.2. In this study, we determine whether a load is sheddable from the building owner's perspective. For instance, the coffee maker and the soda dispenser in the ice cream shop are classified as sheddable during the outage. Mixers with variable speed options, as well as the HVAC system, are classified as modulatable loads due to their varying power amplitudes. Since some plug loads in the dataset are unspecified, we sum those loads into one modulatable load. The washer, dryer, and stovetop range are considered shiftable loads in this work as their operation schedules can be flexible if needed. Lights, coolers, and display cases are classified as critical because they are related to occupants' need for safety and food preservation. Due to the islanded circumstances, some loads commonly categorized as critical are considered to be sheddable (e.g., computer) in this work.

Table 5.3 Summary of load types in studied buildings.

Load Type	Residential	Ice Cream Shop	Bakery
Sheddable	Computer	Coffee maker, soda dispenser, outdoor ice storage	Microwave
Modulatable	HVAC	HVAC	Mixer, unspecified room plugs, HVAC
Shiftable	Range, washer, dryer	None	Range, oven, dishwasher
Critical	Lights, refrigerator	Lights, cooler, display case	Lights, cooler, display case

Parameters related to battery configuration and penalty coefficients are summarized in Table 5.4. We assumed the maximum charging/discharging power $\overline{P}_{bat}$ to be 40% of the battery energy bound $\overline{E}_{bat}$. Further, the initial battery SOC is assumed to be 50% of $\overline{E}_{bat}$. The charging/discharging efficiencies are $\eta_{ch} = \eta_{dis} = 0.9$.

Table 5.4 Parameters of battery configuration and penalty coefficients.

Parameter	Residential	Ice Cream Shop	Bakery
Battery energy upper bound $\overline{E}_{bat}$ (kWh)	70	270	280
Maximum charging power $\overline{P}_{bat}$ (kW)	28	108	112
Penalty of charging γ	1.00×10^{-3}	1.00×10^{-6}	1.00×10^{-4}
Penalty of curtailment γ'	5.00×10^{-3}	1.00×10^{-5}	1.00×10^{-3}

5.4.2 Validation of the Chance Constraint

Before further evaluating the simulation results, we first need to validate the chance constraints. The normally distributed error we introduced into the outdoor temperature forecast is assumed to be $T^t_{amb,e} \sim \mathcal{N}(0, (0.2)^2)$ and the solar irradiance forecast error is assumed to be $Q^t_{sol,e} \sim \mathcal{N}(0, (0.01)^2)$. The tolerance ε_T is 0.05, meaning

that with the given error distribution of forecast, the temperature range can be violated 5% of the time in the independent experiments.

Monte Carlo simulations were adopted for the constraint validation. For each timestep of the simulation, normally distributed errors were generated randomly 1000 times and then added into the temperature prediction model in Equation (5.21) with the optimal HVAC operation decisions. Results showed that all temperature predictions of 10 scenarios in all three buildings are within the range of 20–28℃. As an example, Figure 5.3 compares the temperature predictions with and without uncertainty using the simulation results for scenario S11. We see that, with the accumulation of prediction errors (both positive and negative), the absolute difference between the temperature trajectories with and without forecast error lies within the 0–0.5℃ range.

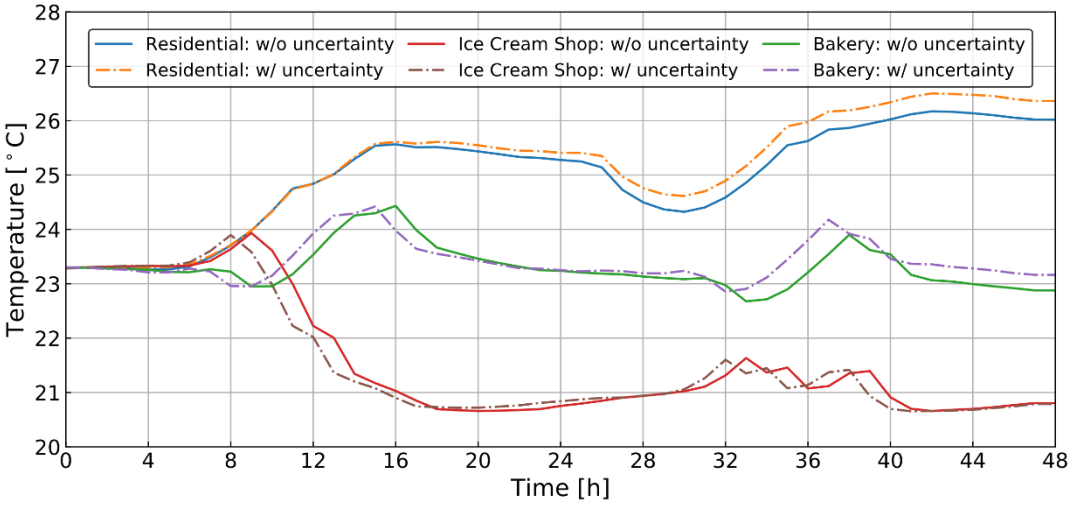

Figure 5.3 Comparison of predicted indoor air temperature with and without the inclusion of uncertainty in Scenario S11.

5.4.3 Impact of Weighting Factor

This section first discusses the allocation factors α_i^t generated by the operator layer, which later serves as the input for the smart controllers at the building layer. Then, we compare the scheduled load shapes, battery behavior, and indoor temperature of each building in different scenarios to further discuss the impact of weighting factors on the KPIs.

Figure 5.4 compares the allocation factors for equally weighted buildings (baseline) with weightings that prioritize each building over the others. Qualitatively, when all buildings are equally weighted in the allocation process (second plot from top), we see a rather random behavior for the PV allocation during the night time when no PV power is available. All three buildings take turn to get full PV power ($\alpha_i^t = 1$) because they have the same objective function value. On the contrary, for the scenarios when a single building is prioritized, the prioritized building gets full PV power alone during the nighttime (bottom three plots). During the daytime, when more PV generation is available, the allocation results follow similar trends for all scenarios regardless of the weighting method. Although generally, we see less load shedding in the prioritized building, as well as a higher value of the allocation factor, the allocation process is mostly constrained by the building load flexibility ranges. More specifically, buildings with a higher load flexibility lower bound (i.e., ice cream shop) tend to get more allowable load than other buildings.

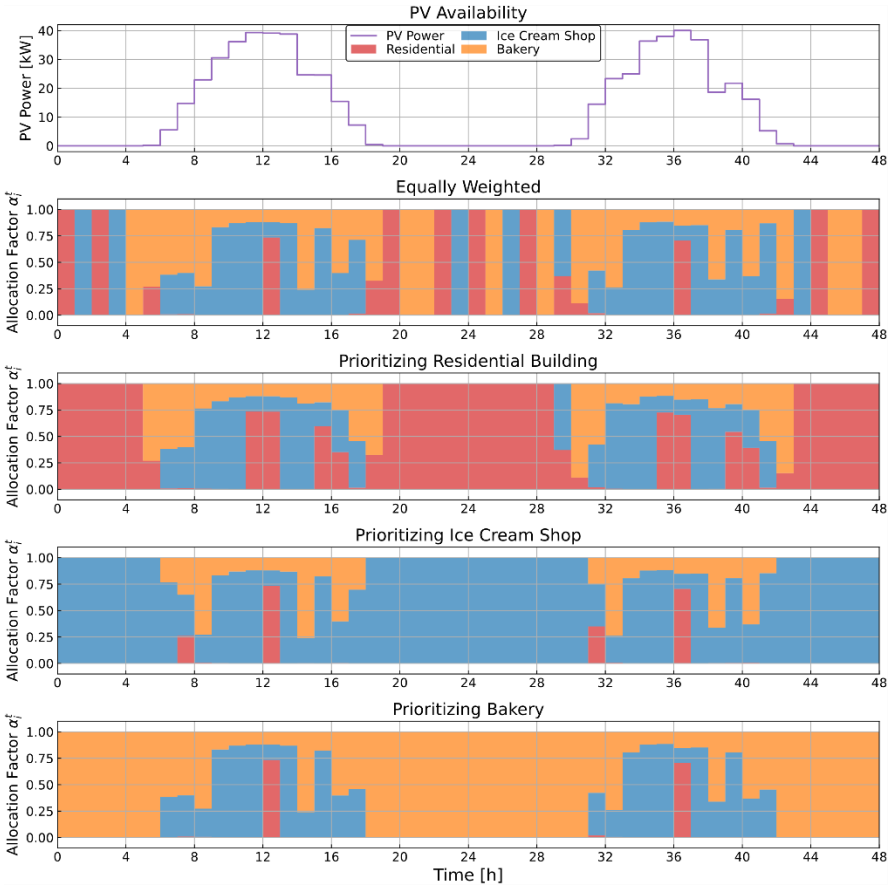

Figure 5.4 Allocation factors for each COL PV allocation scenario.

Figure 5.5 plots the allocation factors for the occupancy-based weighting method against building occupancy. Here, occupancy indicates whether the building is occupied. In this work, we do not consider the number of people in the building as we don't have access to this level of data. From the middle plot, we see that the residential building is mostly occupied during the night from about 7 PM to 8 AM Ice cream shop and bakery are occupied during the day from 10 AM–11 PM and 6 AM–7 PM, respectively. From the bottom plot, we see that similar to single building prioritized scenarios, when at night the only residential building is occupied, it gets full PV allocation. However, when the time reaches 5 AM, the allocation factor of the residential building starts to decrease and during the day only a few hours will it get

PV power due to its unoccupied status. During the daytime, when both the bakery and ice cream shop are occupied, the allocation follows the buildings' power flexibility lower bounds as discussed before.

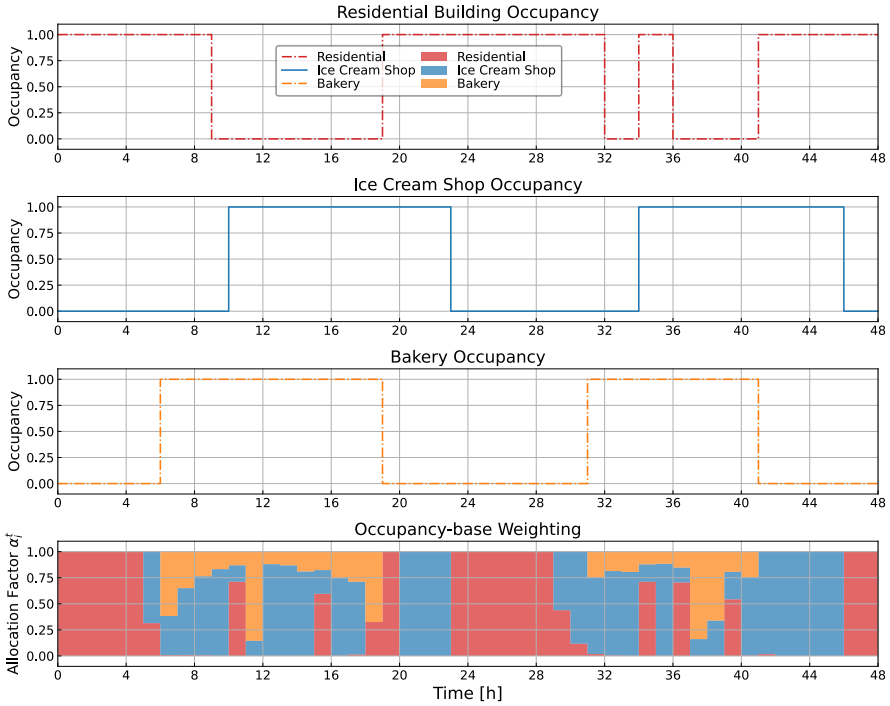

Figure 5.5 Allocation factors for occupancy-based weighting against building occupancy.

To further quantify the impact of different weighting methods, the mean values of the allocation factors $\overline{\alpha_i^t}$, as well as the total allocated PV energy are listed in Table 5.5. Due to the highly stochastic allocation during nighttime when no PV power is available, we only counted hours when PV generation is greater than zero in the calculation of $\overline{\alpha_i^t}$. From the table, we noticed that having a lower mean allocation factor does not necessarily mean less PV energy allocation. For example, in the scenario where the residential building is prioritized, its $\overline{\alpha_i^t}$ is less than 22% while for the bakery it is almost 33%. However, the total PV energy allocated to the residential

building is 33.42% more than that allocated to the bakery. This is because the residential building has higher α_i^t values during hours with the most PV generation (i.e., around noon). This indicates that having a higher allocation factor when more PV power is generated is more crucial. When looking at the occupancy-based weighting scenario, the residential building PV energy exceeds that of the equal weighting scenario since the shortly occupied hours during the day (e.g., hours 34–36) bring more allocation. Overall, no matter which weighting method is adopted, the ice cream shop is always allocated the most PV energy due to its large refrigeration loads, while the residential building is always allocated the least amount of PV energy (except when it is prioritized in scenarios S21_R and S22_R). This indicates that the impact of power flexibility is more prominent than the weighting factors during the resource allocation.

Table 5.5 Mean values of allocation factors and PV energy allocation for different weighting methods.

Building	**Equal Weighting**		**Priority-Based Weighting**						**Occupancy-Based Weighting**	
			Prioritize Residential		**Prioritize Ice Cream Shop**		**Prioritize Bakery**			
	$\overline{\alpha_i^t}$	$E_{pv}(kWh)$	$\overline{\alpha_i^t}$	$E_{pv}(kWh])$	$\overline{\alpha_i^t}$	$E_{pv}(kWh])$	$\overline{\alpha_i^t}$	$E_{pv}(kWh])$	$\overline{\alpha_i^t}$	$E_{pv}(kWh])$
Residential	0.099	59.52	0.218	153.85	0.075	67.18	0.054	58.67	0.163	108.61
Ice Cream Shop	0.499	350.07	0.455	309.51	0.669	356.00	0.454	346.20	0.581	308.51
Bakery	0.402	169.08	0.326	115.31	0.256	155.50	0.492	173.80	0.255	161.56

Next, the simulation results will be discussed for the various PV allocation methods. In the following discussion, we highlight a subset of the results; however, the complete set of results are available in Appendix A and quantitative results for all 30 simulations are summarized in Table A.3. In the following simulation results,

the baseline power is the original load shape from the data. The positive battery power means charging and the negative means discharging. The scheduled sheddable, modulatable, shiftable, and critical loads are represented by color blocks. When evaluating the thermal comfort results, the baseline temperature is the original indoor temperature with a setpoint of 24°C without optimization. For clarity, the label S21 in the temperature plots represents the scenario of the discussed building being prioritized, as described in Table 5.1.

The residential building operation is compared in the scenario where all buildings are equally weighted and where the residential building is prioritized in Figure 5.6 and Figure 5.7, respectively. In both scenarios, we see that shiftable loads are scheduled during the day when more PV power is available. All sheddable and modulatable loads are satisfied in both cases (see Table A.3 for details). When the allocated PV power is more than doubled in the residential building due to it being prioritized, we see more battery charging and discharging in Figure 5.7. However, more than enough PV power is allocated to the residential building in this case due to its high priority, resulting in 31.25% of the allocated PV power being curtailed. Additionally, more power is allocated to the HVAC system in Figure 5.7, causing the indoor temperature to be closer to the lower bound (Figure 5.8). Comparing S11, S21, S31 with various weighting factors in Figure 5.8, we see that scenarios with more allocated PV power results in a lower indoor temperature since more power is available for the HVAC load. In Figure 5.8, all temperatures are within the comfort

bounds. It is noted that in Figure 5.8, S12, S22, and S32 temperature curves have almost the same trend that cannot be differentiated from the plot.

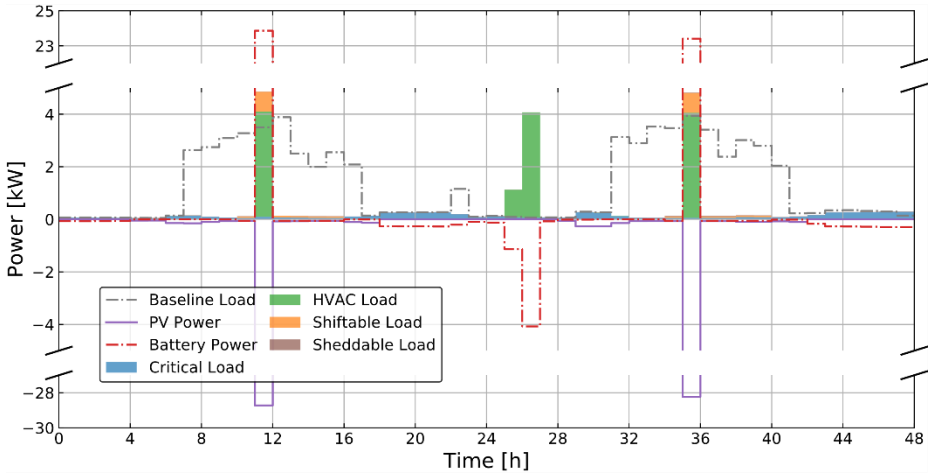

Figure 5.6 Residential building load shape, battery behavior, and PV power (S11: equal weighting, minimizing unserved load ratio).

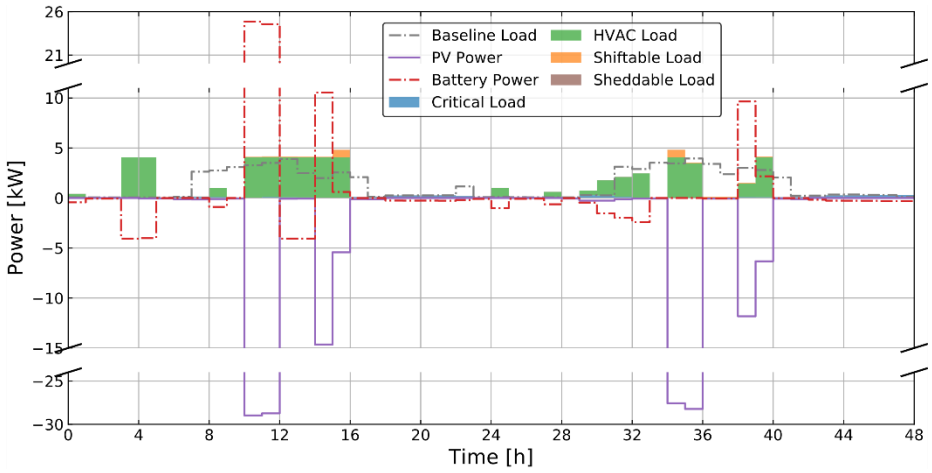

Figure 5.7 Residential building load shape, battery behavior, and PV power (S21_R: prioritizing residential, minimizing unserved load ratio).

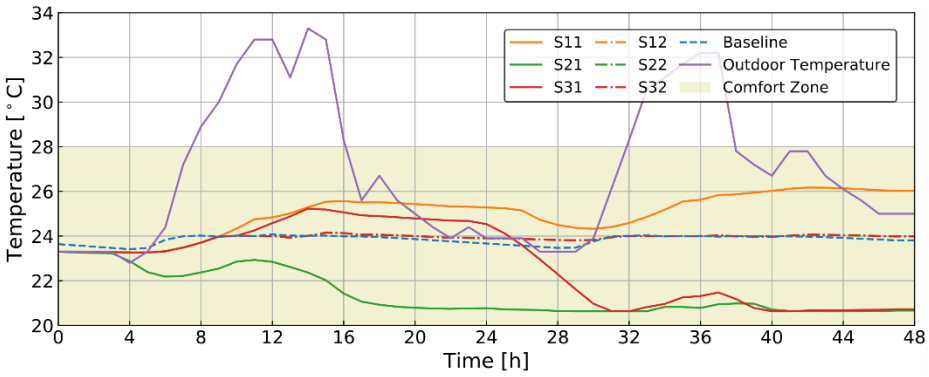

Figure 5.8 Residential building indoor and outdoor temperature for all scenarios.

Figure 5.9 depicts the results for the ice cream shop with equal weighting while Figure 5.10 shows the results with occupancy-based weighting. Since the total allocated PV energy in Figure 5.10 is reduced by about 12% compared to Figure 5.9, we see much less battery charging and a slight reduction of HVAC power in Figure 5.10. All sheddable loads are satisfied in both cases (see Table A.3 for details). In Figure 5.11, the indoor temperature trajectories of S11 and S21 overlap with each other as almost the same amount of PV power is allocated to the ice cream shop in these two scenarios. The indoor temperature in simulation scenario S31 first drops below those of scenarios S11 and S21 in the morning due to a precooling between 6 to 9 AM, and then exceeds them in the afternoon due to less power available to operate the HVAC system. A similar trend is also seen in the following simulation day. As in the residential building, Figure 5.11 shows that the indoor thermal comfort of the ice cream shop was maintained within the given temperature bounds. It is noted that in Figure 5.11, S12, S22, and S32 temperature curves have almost the same trend that cannot be differentiated from the plot.

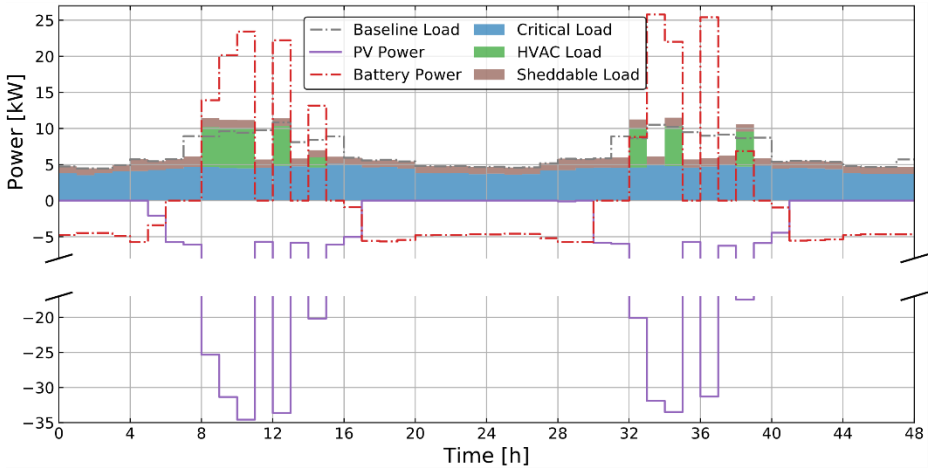

Figure 5.9 Ice cream shop load shape, battery behavior, and PV power (S11: equal weighting, minimizing unserved load ratio).

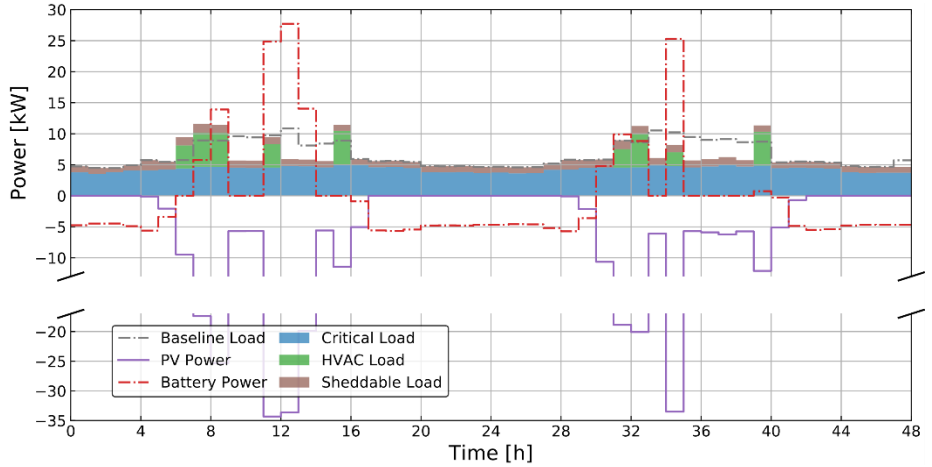

Figure 5.10 Ice cream shop load shape, battery behavior, and PV power (S31: occupancy-based weighting, minimizing unserved load ratio).

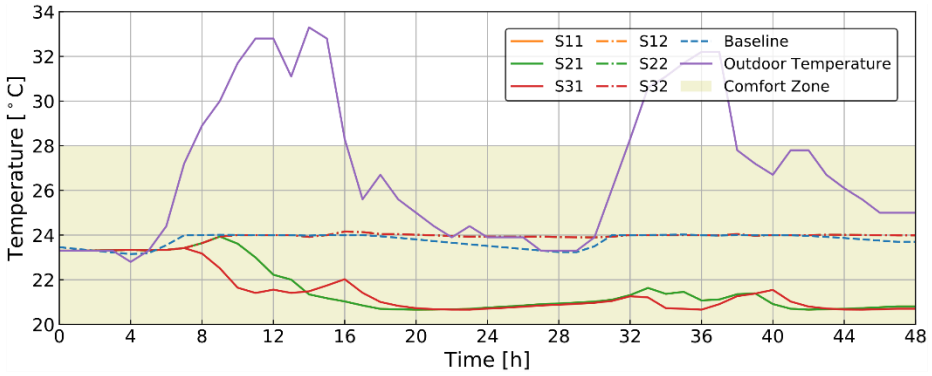

Figure 5.11 Ice cream shop indoor and outdoor temperature for all scenarios.

Figure 5.12 plots the results for bakery with equal weighting while Figure 5.13 with occupancy-based weighting. Due to a reduction of PV power in Figure 5.13, much less power is allocated to the HVAC system, especially during the late afternoon (e.g., hours 16 and 40). The battery discharging is almost the same in the two scenarios, both to satisfy the four types of loads present in this building. All sheddable and modulatable loads are satisfied in both cases (see Table A.3 for details). However, battery charging only happens about once a day in scenario S31 given the focused allocated PV power shape. In Figure 5.14, the indoor temperature for S31 is higher than S11 due to less power available to operate the HVAC system. All temperatures are within the comfort temperature bounds. It is noted that in Figure 5.14, S12, S22, and S32 temperature curves have almost the same trend that cannot be differentiated from the plot.

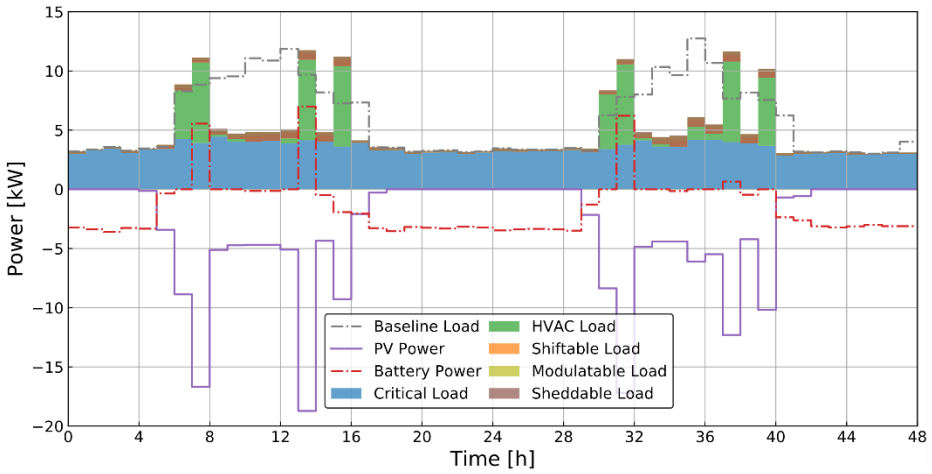

Figure 5.12 Bakery load shape, battery behavior, and PV power (S11: equal weighting, minimizing unserved load ratio).

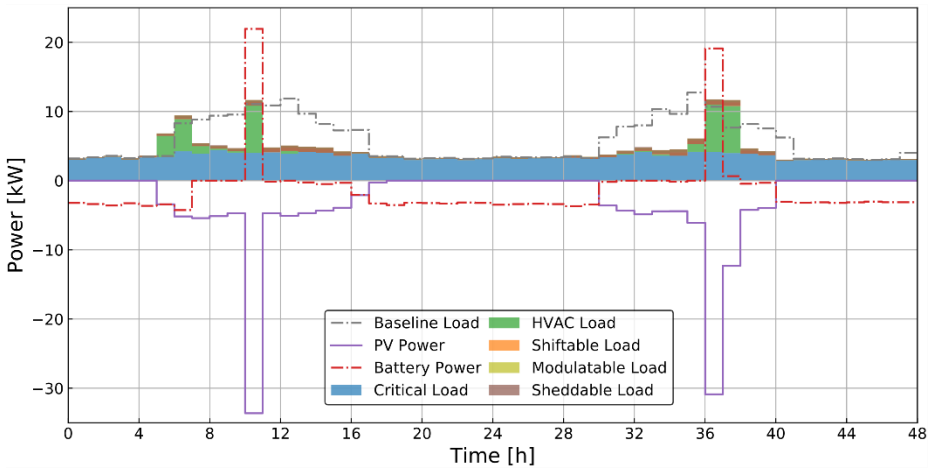

Figure 5.13 Bakery load shape, battery behavior, and PV power (S31: occupancy-based weighting, minimizing unserved load ratio).

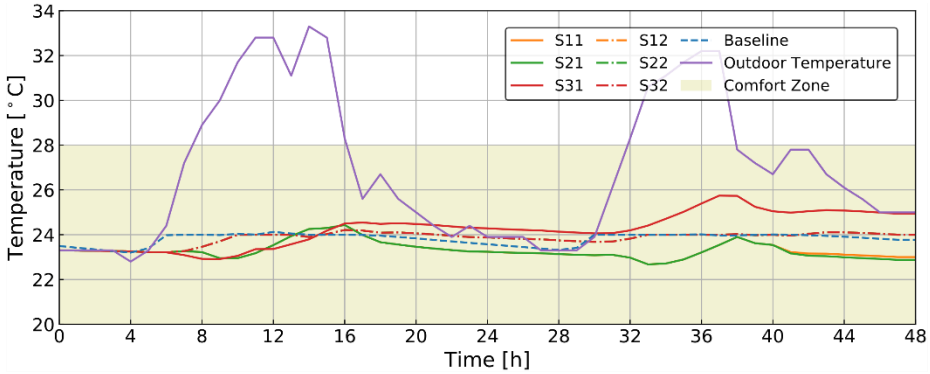

Figure 5.14 Bakery indoor and outdoor temperature for all scenarios.

To summarize, in this section, we discussed the PV resource allocation results under different weighting methods. The resulted load shape, battery behavior, and indoor temperatures are also discussed qualitatively. From the discussion, we found that the weighting method of the operator layer directly affects the mean allocation factor of each building. When one building is prioritized, we see an obvious increase of $\overline{\alpha_i^t}$. However, a higher $\overline{\alpha_i^t}$ does not necessarily mean more PV energy allocation. A higher allocation factor during periods with more PV generation (e.g., around noon) is more crucial than a higher mean value of the allocation factor overall. Additionally, we noticed that the allocation process is mostly constrained by the building load

flexibility ranges. More specifically, buildings with a higher load flexibility lower bound (i.e., ice cream shop with large critical loads) tend to get more allowable load than other buildings. Additionally, when prioritizing buildings according to occupancy status, the building with a longer occupant presence gets more PV power, which is not necessarily a fair allocation method. For instance, in S31, 5.5% of the PV energy allocated to the residential building was curtailed. Since the allocation process was according to building occupancy time, more than enough power is allocated to the residential building in this case. Lastly, the resulting load schedule, battery behavior, and indoor temperature are directly correlated with the available PV power when other system settings are the same (e.g., battery charging constraints and penalty coefficients).

5.4.4 Impact of Objective Function

This section discusses the impact of different objective functions on the scheduled load shapes, battery behavior, and indoor temperature. Similar to the last section, qualitative discussions will first be provided.

Figure 5.15 plots the results of the residential building with equal weighting and the objective is to maximize thermal comfort. Compared with Figure 5.6, we see that when the objective switches from minimizing unserved load to maximizing comfort, there is an obvious increase of HVAC power, and the temperature gets closer to the temperature setpoint of 24℃ (Figure 5.8). When comparing Figure 5.16 with Figure 5.7, we see a decrease in HVAC power usage because before (S21 in Figure 5.8), the indoor temperature was below 24℃; when the objective is to minimize the

temperature deviation from 24℃, the required cooling power is actually less. The HVAC power is saved to get the indoor temperature closer to the temperature setpoint.

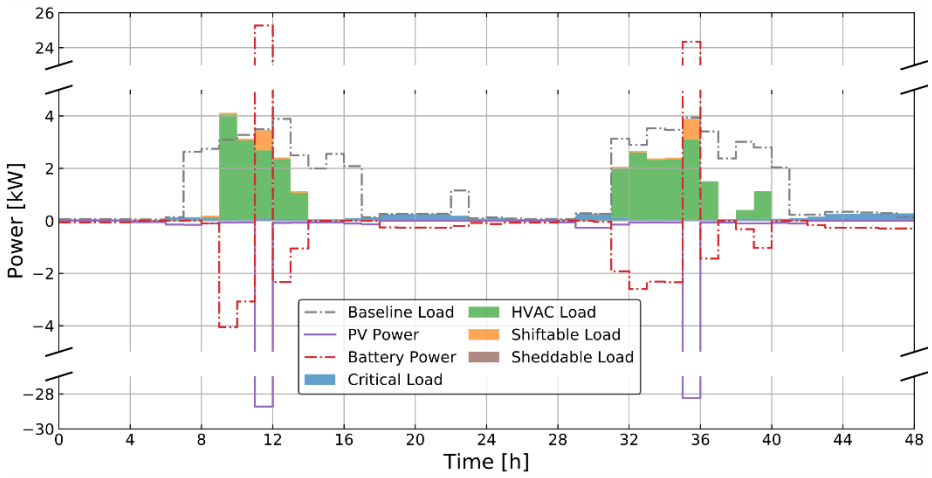

Figure 5.15 Residential building load shape, battery behavior, and PV power (S12: equal weighting, maximizing thermal comfort).

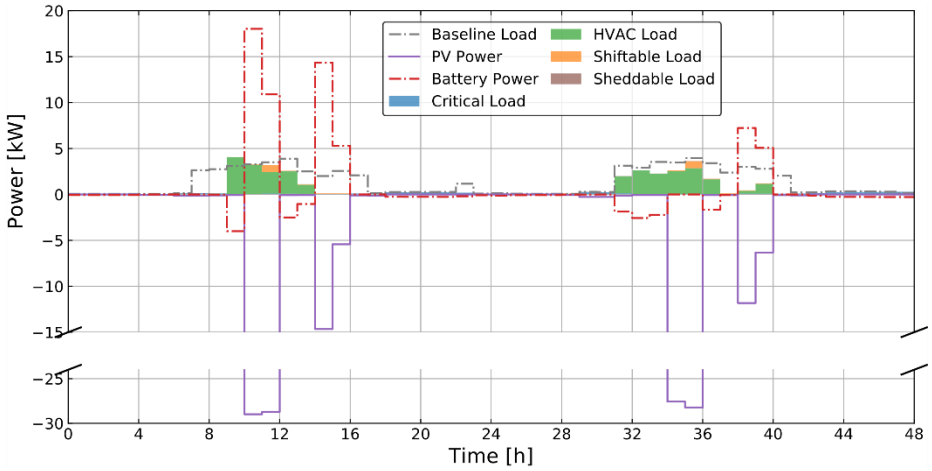

Figure 5.16 Residential building load shape, battery behavior, and PV power (S22_R: prioritizing residential, maximizing thermal comfort).

Comparing Figure 5.17 with Figure 5.9, we see a decrease of serving in sheddable load when the objective switches from minimizing unserved load to maximizing comfort. As a result, 63.72% of the sheddable load is unserved in this scenario (Table A.3). However, the HVAC power also decreases in order to increase

the indoor temperature to the temperature setpoint. The saved PV power is charged into the battery as we see an increase in battery charging in Figure 5.17. A similar observation can be found if we compare Figure 5.18 with Figure 5.12, where the unserved ratio of sheddable load increases to 99.03% and modulatable to 68.89% due to the change of the objective function (Table A.3).

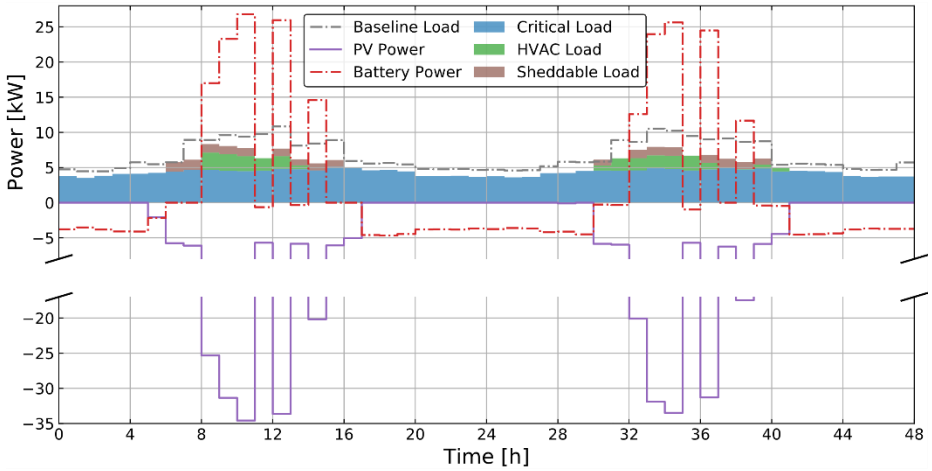

Figure 5.17 Ice cream shop load shape, battery behavior, and PV power (S12: equal weighting, maximizing thermal comfort).

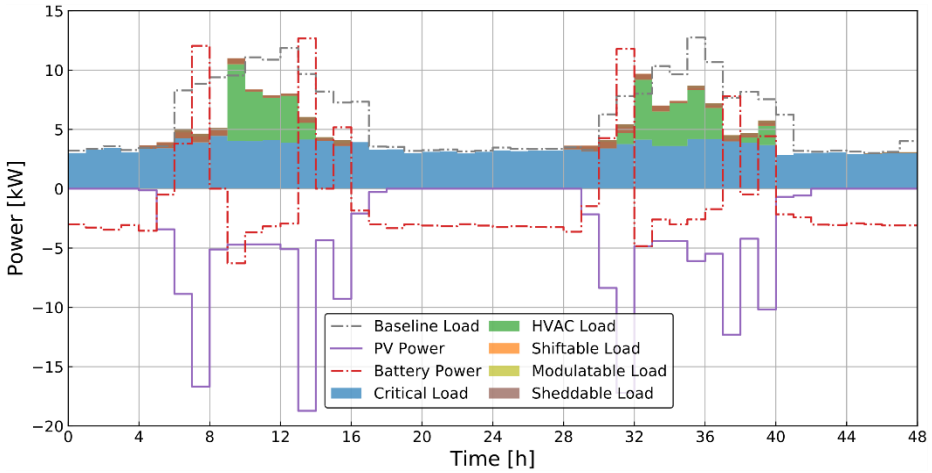

Figure 5.18 Bakery load shape, battery behavior, and PV power (S12: equal weighting, maximizing thermal comfort).

To further quantify the impact of the weighting factor and objective function, we summarized the community overall KPIs in Table 5.6 and Table 5.7. The KPIs

include PV curtailment ratio, unserved load ratio, temperature deviation from setpoint, and required battery size. The definition of the PV curtailment ratio is the total curtailed PV energy over the generated energy during the simulation horizon. The unserved load ratio is calculated by dividing the total unserved load by the total original load over the simulation horizon. The definition of the temperature deviation from the setpoint is adapted from the root mean square deviation (RMSD), which is the root mean of the square of the deviation between the indoor temperature and the temperature setpoint over the 48-h simulation denoted by:

$$RMSD = \sqrt{\frac{\sum_{t=1}^{H}\left(T_{room}^{t} - \frac{\underline{T}_{room} + \overline{T}_{room}}{2}\right)^2}{N}}, \tag{5.50}$$

where $N = 48$ is the simulation horizon. Here, the temperature setpoint is selected to be the middle of the comfort temperature range: 24℃. Lastly, the required battery size is obtained by subtracting the minimum battery SOC from the maximum value. This gives us a sense of how much of the battery capacity has been utilized under different scenarios. Further, this could help to guide the battery sizing to enhance community resilience.

Table 5.6 Community overall PV curtailment and unserved load ratio of each scenario.

Scenario	PV Curtailment Ratio	Unserved Load Ratio				
		Sheddable	Shiftable	Modulatable	Critical	Overall
S11	0.00%	0.00%	10.94%	0.00%	0.00%	0.27%
S21_R	8.31%	0.00%	10.94%	0.00%	0.00%	0.27%
S21_I	0.00%	0.00%	10.94%	0.00%	0.00%	0.27%
S21_B	0.00%	0.00%	10.94%	0.00%	0.00%	0.27%
S31	1.03%	0.00%	10.94%	0.00%	0.00%	0.27%
S12	0.00%	64.14%	10.94%	68.89%	0.00%	9.25%
S22_R	13.18%	65.06%	10.94%	77.00%	0.00%	9.54%
S22_I	0.00%	64.13%	10.94%	72.83%	0.00%	9.34%

Scenario	PV Curtailment Ratio	Unserved Load Ratio				
		Sheddable	Shiftable	Modulatable	Critical	Overall
S22_B	0.00%	64.14%	10.94%	69.23%	0.00%	9.26%
S32	5.43%	65.49%	10.94%	73.64%	0.00%	9.51%

From Table 5.6, we see that PV curtailment only happens when the residential building is prioritized (S21_R and S22_R) or when occupancy-based weighting is implemented (S31 and S32). This is because the residential building has a relatively small power demand compared to the other two commercial buildings. When it is prioritized by the operator layer, more PV generation is allocated than needed, resulting in PV curtailment. This also echoes our discussions above that allocating purely based on building occupancy status could lead to unfair allocation situations. In the table, the shiftable load unserved load ratio is the same for all scenarios. This is because of our assumption that each shiftable load operates once and only once every day. However, in the original data, some loads might have operated more than once, causing "unserved load" for shiftable loads. Given this, we can consider that all loads are satisfied for the scenarios to minimize unserved load (S11 to S31 in Table 5.6). When looking at scenarios S12–S32 in Table 5.6, we see an increase of unserved load as the objective switches to maximizing comfort. The largest unserved load ratio appears in the scenario where the residential building is prioritized. From Table 5.6, the scenarios that perform the best would be S11, S21_I, and S21_B if we only consider PV curtailment and unserved load ratio. In these scenarios, the PV allocation is either equally weighting all buildings or prioritizing those with larger power demand while minimizing the unserved load ratio.

Table 5.7 Community overall room temperature deviation and required battery size of each scenario.

Scenario	Temperature Deviation (℃)	Battery Size (kWh)
S11	3.04	199.8
S21_R	4.05	215.55
S21_I	2.78	209.64
S21_B	3.10	194.61
S31	3.48	182.91
S12	0.53	218.07
S22_R	0.53	242.05
S22_I	0.53	237.91
S22_B	0.53	210.19
S32	0.53	199.52

Next, we analyze the temperature deviation and necessary battery size shown in Table 5.7. We see that all scenarios with the thermal comfort objective experience the fewest temperature deviations. This means that the indoor temperature is well controlled to stay near the temperature setpoint. In the remaining scenarios with the unserved load objective, large deviations in temperature can be seen. For many scenarios, this is due to lower indoor temperatures than the temperature setpoint. Hence, setting the temperature setpoint appropriately can save HVAC energy. However, in our case, the saved energy was either curtailed or charged into the battery instead of satisfying the other loads. This also leads to larger battery sizes in scenarios to maximize comfort (average size: 221.5 kWh) than scenarios to minimize unserved load (average size: 200.5 kWh). Therefore, a co-optimization of thermal comfort and unserved load is necessary with the benefit of less curtailment, smaller unserved load ratio, assured thermal comfort, as well as smaller battery size.

The above simulation results highlight the impact of the objective function on KPI outcomes. From the above discussions, we identified that if only PV curtailment

and unserved load ratio are considered, the best option is to allocate the PV resource either equally weighting or prioritizing buildings with larger power demand while minimizing the unserved load ratio. After further looking at other indices, we noticed that choosing the optimization objective to track an appropriately selected indoor room temperature setpoint will save HVAC energy. However, this will not lead to a lower unserved ratio for other load types. Instead, the PV curtailment could increase. The two objectives have a competitive relationship: serving more HVAC power to increase thermal comfort will decrease the other served load.

5.5 Conclusion

We proposed a novel decentralized control architecture for renewable resource allocation and load scheduling of resilient communities. This MPC-based optimization architecture consists of a community operator layer that allocates the daily PV power generation to achieve the community-wide optimum and a building agent layer that schedules building loads to achieve its local optimum in each building. Three allocation methods were tested for the operator layer: equally weighted, weighted based on building priority, and weighted based on building occupancy. At the building level, two objective functions were compared: minimizing unserved load ratio versus maximizing thermal comfort. The proposed framework has the advantage of distributed computational effort and is easier to be scaled up than traditional centralized control, which is not robust for large-scale deployment. Additionally, the comparison between different combinations of allocation methods

and objective functions provides guidance for real-world deployment by community and microgrid operators.

Through a case study for an islanded community in FL for 48 h, we evaluated the proposed architecture with respect to user-centric performance metrics. We found that the allocation process is mostly constrained by the building load flexibility. More specifically, buildings with less load flexibility (i.e., ice cream shop with large critical loads) tend to be allocated more PV generation than other buildings. Additionally, when prioritizing buildings according to occupancy status, the building with a longer occupancy duration is allocated more PV power, which may not result in a fair allocation method and could lead to more PV curtailment.

Additionally, through the analysis of different objective functions, we found that setting the objective to target at an appropriately selected indoor temperature setpoint will result in increased HVAC energy savings. However, in our case study, this did not lead to a lower unserved ratio for other load types. Instead, the PV curtailment increased. The two objectives have a competitive relationship: serving more HVAC power to increase thermal comfort will decrease the other served load. Therefore, it is necessary for the building agent to have multi-objective optimization to minimize the unserved load ratio and maximize comfort simultaneously. This will bring the benefit of less curtailment, a smaller unserved load ratio, assured thermal comfort, as well as smaller battery size. However, the weighting between the two objectives needs to be carefully selected as their scales are quite different.

Limitations of this work lie in that all load models (e.g., HVAC system) have been linearized for the reduction of the computational effort, which can be improved in the future. Further, the decentralized MPC problem was not solved iteratively with data exchanged between the two layers. This is reasonable in this work because the same model was used for both prediction and evaluation. However, for more realistic cases, the problem should be solved iteratively with information exchanged at every timestep to better account for uncertainties.

For future work, we will conduct multi-objective optimization for the building agent layer to investigate the trade-off between minimizing the unserved load ratio and maximizing thermal comfort. Uncertainty of PV generation should also be included to reflect the impact of different weather conditions. Nonlinear models for controllable devices could be incorporated into the framework to better reflect the system dynamics in the future.

Chapter 6. Uncertainties of Occupant Behavior and Its Impact on Resilient Community Scheduling

This chapter is based on:

Jing Wang, Sen Huang, Wangda Zuo, Draguna Vrabie. “Occupant preference-aware load scheduling for resilient communities.” Energy and Buildings, 252, pp. 111399.

The load scheduling of resilient communities in the islanded mode is subject to many uncertainties such as weather forecast errors and occupant behavior stochasticity. To date, it remains unclear how occupant preferences affect the effectiveness of the load scheduling of resilient communities. This chapter proposes an occupant preference-aware load scheduler for resilient communities operating in the islanded mode. The load scheduling framework is formulated as a model predictive control problem. Based on this framework, a deterministic load scheduler is adopted as the baseline. Then, a chance-constrained scheduler is proposed to address the occupant-induced uncertainty in room temperature setpoints. Key resilience indicators are selected to quantify the impacts of the uncertainties on community load scheduling. Finally, the proposed preference-aware scheduler is compared with the deterministic scheduler on a virtual testbed based on a real-world net-zero energy community in Florida, USA. Results show that the proposed scheduler performs better in terms of serving the occupants' thermal preference and reducing the required battery size, given the presence of the assumed stochastic occupant behavior. This work indicates that it is necessary to consider the stochasticity of occupant behavior when designing optimal load schedulers for resilient communities.

6.1 Introduction

Due to the increasing frequency of extreme weather events such as the 2021 Texas Power Crisis [4], there is an emerging need for community resilience studies. Resilient communities refer to those that can sustain disruptions and adapt to them

quickly by continuing to operate without sacrificing the occupants' essential needs [152, 174]. Enabling technologies for resilient communities often involve distributed energy resources such as PV and electrical energy storage (EES) systems. When disconnected from the main grid, the adoption of advanced control techniques can help enhance community resilience.

As an advanced control technique, optimal load scheduling determines the operation schedules of controllable devices in the community to achieve optimization objectives. For a resilient community, typical controllable assets include the EES, PV, and thermostatically controllable devices in buildings such as the HVAC system. Building plug loads that are sheddable, shiftable, or modulatable can also be considered flexible loads in islanded circumstances [195]. The objectives of the load scheduling for resilient communities often involve maximizing the self-consumption rate of locally generated PV energy, minimizing PV curtailment, and minimizing the unserved ratio to critical loads.

It is important to account for uncertainties when designing a load scheduler for resilient communities. Moreover, due to the limited amount of available PV generation during off-grid scenarios, the uncertainties need to be more carefully dealt with to ensure a satisfying control performance. Sources of uncertainties for a community load scheduling problem mainly lie in two aspects: power generation and consumption. For renewable energy generation, weather forecast errors play a prominent role in the cause of uncertainty. Whereas, for energy consumption, occupant behavior stochasticity is a major source of uncertainty.

Much of existing load scheduling research has considered the uncertainty of weather forecasts [191, 196–203]. Kou et al. [196] proposed a comprehensive scheduling framework for residential building DR considering both day-ahead and real-time electricity markets. The results demonstrated the effectiveness of the proposed approach for large-scale residential DR applications under weather and consumer uncertainties. Garifi et al. [191] adopted stochastic optimization in an MPC-based home energy management system. The indoor thermal comfort is ensured at a high probability with uncertainty in the outdoor temperature and solar irradiance forecasts. Faraji et al. [197] proposed a hybrid learning-based method using an artificial neural network to precisely predict the weather data, which eliminated the impact of weather forecast uncertainties on the scheduling of microgrids. Similarly, in the authors' previous publication [198], normally distributed outdoor temperature and solar irradiance forecast errors were introduced into the community control framework, which accounted for the uncertainties in the weather forecasts.

However, the uncertainties from the power consumption perspective, especially the occupant behavior uncertainty, is rarely accounted for in load scheduling research [204–208]. Some efforts to integrate occupant behavior modeling can be found in studies of building optimal control [209–212]. Aftab et al. [209] used video-processing and machine-learning techniques to enable real-time building occupancy recognition and prediction. This further facilitated the HVAC system operation control to achieve building energy savings. Lim et al. [210] solved a joint occupancy

scheduling and occupancy-based HVAC control problem for the optimal room booking (i.e., meeting scheduling) in commercial and educational buildings. Both the occupancy status of each meeting room and the HVAC control variables were decision variables. Mixed-integer linear programming was adopted to optimally solve the optimization problem.

Notably, all of the preceding control work considered the stochasticity of building occupancy schedules, but the integration of other types of occupant behavior into building optimal control is not well studied in the existing literature. Some researchers integrate the occupant thermal sensation feedback into the MPC for buildings [213, 214]. For instance, Chen et al. [213] integrated a dynamic thermal sensation model into the MPC to help achieve energy savings using the HVAC control. For the occupant sensation model, the predictive performance of certainty-equivalence MPC and chance-constrained MPC were compared.

To summarize, the literature review shows that current research mainly focuses on the load scheduling of single buildings under grid-connected scenarios. There is a lack of research on the optimal load scheduling of resilient communities informed by occupant behavior uncertainties in the islanded mode [215]. Given this gap, this chapter proposes an occupant preference-aware load scheduling framework for resilient communities in the islanded mode. The occupants' thermal preference for indoor air temperature will be reflected in the integration of thermostat adjustment probabilistic models. The optimal load scheduling is formulated as an MPC problem,

so the stochastic thermostat-changing behavior will be regarded as the uncertainty in the MPC problem.

Different methods, such as the offset-free method and robust method, can be used to handle the uncertainties in MPC problems [216]. The chance-constraint method, also known as the stochastic MPC, was selected to deal with the uncertainty in occupant preference in our study. It allows the violation of certain constraints at a predetermined probability. It thus enables a systematic trade-off between the control performance and the constraint violations [180]. The advantage of addressing occupant preference uncertainty by using the chance-constraint method lies in the *a priori* handling of the uncertainty, which does not require the extra error-prediction models needed by other methods (i.e., offset free method), and thus simplifies the control problem [217]. Therefore, less computational effort is required after the control design phase. Though it requires the controller to know the estimated uncertainty distribution beforehand, the development of occupant behavior probabilistic modeling will make knowing this less challenging.

In this work, we consider the load scheduling of a resilient community in islanded mode during power outages. The goal is to study the impact of occupants' thermal preference on the operation of an islanded community. The load scheduling problem of the community will be solved using an optimization-based hierarchical control framework. Occupant thermal preference will be integrated through thermostat changing behavioral models to inform the development of the load scheduler. The major contributions of this work include (1) a proposed new

preference-aware load scheduler for resilient communities, which assures better control performance related to satisfying occupants' thermal preferences and reducing the battery size; (2) the quantification of the impact of occupant thermostat-changing behavior on resilient community optimal scheduling using selected key resilience indicators (KRIs); and (3) the testing of the proposed scheduler on a high-fidelity virtual testbed for resilient communities.

The remainder of this chapter is organized as follows: Section 6.2 details the research methodology. Section 6.3 describes the controllable device models used in this work involving the building HVAC models, load models, and battery models. Section 6.4 then discusses the deterministic versus stochastic scheduler formulations and proposes a chance-constrained controller for preference-aware load scheduling of resilient communities. Section 6.5 applies the theoretical work to a case study community and quantifies the impact of occupant preference uncertainty. Simulation results and discussions are presented in this section. Finally, Section 6.5 concludes the chapter by identifying future work.

6.2 Methodology

In this section, we first introduce a hierarchical optimal control structure for resilient community load scheduling. Based on the structure, a deterministic scheduler will be implemented as the baseline. Further, we propose a research workflow to implement a stochastic preference-aware scheduler for addressing uncertainties in occupant thermostat-changing behavior. KRIs are proposed at the end of this section.

6.2.1 Hierarchical Optimal Control for Resilient Communities

In this study, we assume that the only energy resource accessible to the islanded community is on-site PV generation and the batteries for an extended period of more than 24 hours. In this problem setting, in order to make full use of the limited amount of PV generation and satisfy the occupants' essential needs, the building loads need to be shifted or modulated. The battery works as a temporal arbitrage for meeting the demand at night. In addition, the occupant thermal preference will affect the energy consumption of the HVAC system through the stochastic thermostat-changing behavior. To optimally control such a community, considering the above factors, we adopted a hierarchical control structure.

As illustrated in Figure 6.1, two layers of control are formulated: a community operator layer (COL) and a building agent layer (BAL). The COL optimally allocates the limited amount of the on-site PV generation based on the load flexibility provided by each building. The calculated allowable load for each building is then passed down to the BAL, where each building optimally schedules its controllable devices (i.e., HVAC, battery, and controllable loads) to achieve its local optimization goals. Both layers are formulated as MPC-based optimization problems.

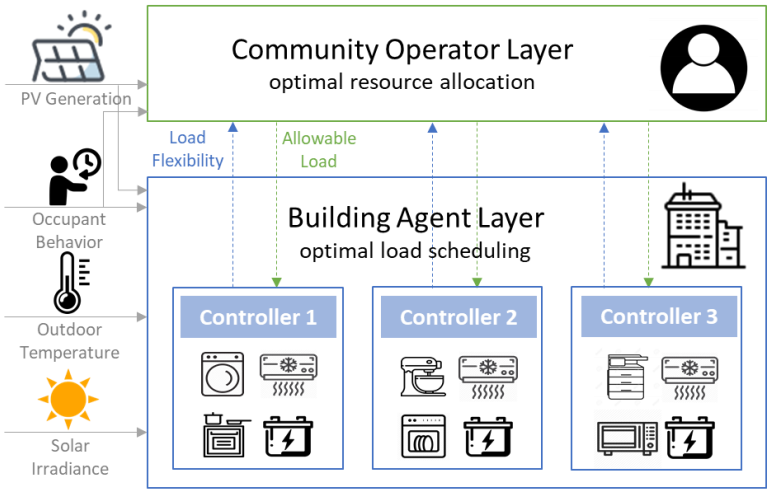

Figure 6.1 The hierarchical optimal control structure for community operation.

The input of the hierarchical control involves the predicted PV generation data, outdoor air dry-bulb temperature, and solar irradiance. The PV generation data are used by the COL to determine the optimal allocation among buildings. The temperature and irradiance data are used by the HVAC models for updating the indoor room temperature predictions. The occupant behavior affects the two layers differently. The COL uses building occupancy schedules to decide the weights of different buildings during the PV allocation (details can be found in Section 5.2). The BAL considers occupant thermal preference to be the uncertainty in the indoor room temperature prediction.

6.2.2 Proposed Workflow

Figure 6.2 depicts the workflow of this work. A deterministic optimal load scheduler without the occupant thermal preference uncertainty is implemented in the hierarchical control structure. Further, to account for the uncertainties, we propose a chance-constrained controller. It is developed based on the deterministic controller and involves an alteration of the room temperature constraints, which

accounts for the uncertainties in room temperature prediction errors caused by the occupants' thermostat-changing behavior. The Monte Carlo simulation method was adopted to cover a wide range of simulation results.

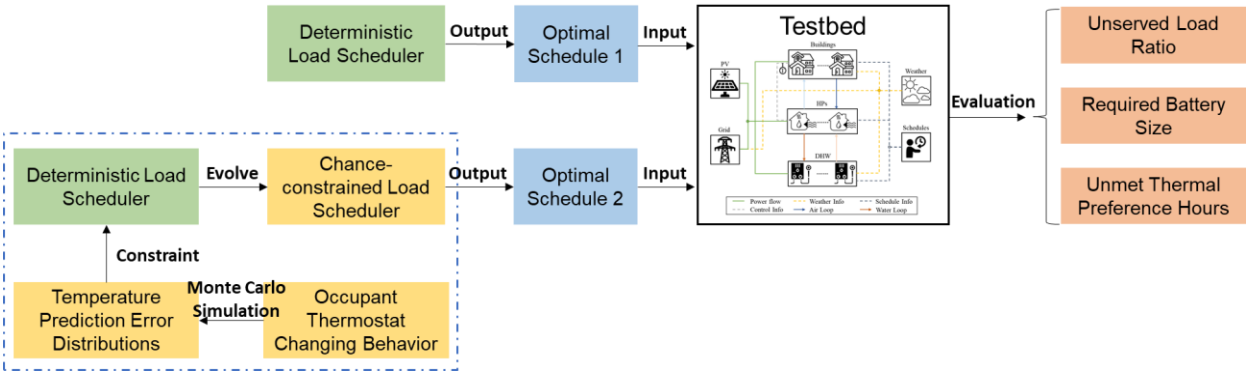

Figure 6.2 Diagram of the proposed workflow.

Further, to reflect various styles of occupant behavior, three types of occupant thermostat-changing models were adopted: low, medium, and high, which represent three levels of frequencies of the thermostat-changing activities. Here, we assume that when the occupant decides to change the indoor air temperature setpoint according to their preference, the predetermined optimal HVAC equipment control setting at the current timestep will be overridden. Instead, a new control setting will be calculated to achieve the occupants' setpoint at the current timestep. At the next timestep, the predetermined optimal setting will still be used if the occupant is not changing the setpoint consecutively.

Finally, the optimal schedules determined by the chance-constrained controller and the deterministic controller are tested on a high-fidelity virtual testbed [16] with respect to their individual performances. KRIs such as the unserved load ratio, the

required battery size, and the unmet thermal preference hours were adopted to quantify the results.

The *unserved load ratio* in this work is defined as the relative discrepancy between the served load P_{load}^{t} and the originally predicted load $\overline{P}_{load}^{t}$:

$$Unserved\ load\ ratio = \frac{\sum_{t=1}^{N}\left(\overline{P}_{load}^{t} - P_{load}^{t}\right)}{\sum_{t=1}^{N}\overline{P}_{load}^{t}}, \tag{6.1}$$

where N is the MPC simulation horizon of 48 hours. The *required battery size* is obtained by subtracting the minimum battery SOC from the maximum SOC. This gives us a sense of how much of the battery capacity has been used under different scenarios. Finally, we define the *unmet thermal preference hours* metric for the cumulative absolute difference between the actual and the preferred room temperature over the optimization horizon:

$$Unmet\ thermal\ preference\ hours = \sum_{t=1}^{N}\left|T_{room}^{t} - T_{prefer}^{t}\right|\Delta t. \tag{6.2}$$

It quantifies how well the controller performs to satisfy the occupants' thermal preference and has the unit of ºC-hrs. (degree hours).

6.2.3 Models for Controllable Devices

This study assumes that heating and cooling is provided by heat pumps and the heat pump energy consumption represents the HVAC system energy consumption. We adopted linear regression models for the HVAC system to predict room temperatures at each timestep. To precisely model the building thermal reactions, two types of parameters that contribute to the heat gain of the building space are considered. The first type is environmental parameters such as the outdoor air dry-

bulb temperature and solar irradiance. The second type represents the internal heat gain due to the presence of the occupants and the operation of appliances. We assumed that the simulated buildings are well sealed and thus the interference from the infiltration can be omitted. Therefore, the HVAC model updates the indoor room temperature based on the room temperature at the last timestep, the abovementioned heat gains, and the heating/cooling provided by the heat pump system at every timestep. The control variable is the heat pump speed ratio, which ranges from 0 to 1 continuously. The resulting HVAC power is equal to the speed ratio multiplied by the nominal heat pump power. Additionally, to better account for the effect of building thermal mass, for each heat gain parameter, two past terms are adopted, respectively [190]. The equations for the HVAC model are as follows:

$$T_{room}^{t+1} = \beta_1 T_{room}^{t} + \beta_2 T_{room}^{t-1} + \beta_3 T_{amb}^{t} + \beta_4 T_{amb}^{t-1} + \beta_5 r_{hvac}^{t} + \beta_6 Q_{sol}^{t} + \beta_7 Q_{sol}^{t-1} + \beta_8 Q_{gain}^{t} + \beta_9 Q_{gain}^{t-1}, \tag{6.3}$$

$$\text{s.t. } 0 \le r_{hvac}^{t} \le 1, \tag{6.4}$$

$$P_{hvac}^{t} = r_{hvac}^{t} P_{hvac,nom}, \tag{6.5}$$

where $T_{room}^{t}, T_{amb}^{t}, Q_{sol}^{t}$, and Q_{gain}^{t} represent the room temperature, ambient dry-bulb temperature, solar irradiance, and internal heat gain at timestep t, respectively. The r_{hvac}^{t} and $P_{hvac,nom}$ are the heat pump speed ratio and the nominal HVAC system power. The linear regression coefficients are represented by β. For β_5, a negative value means cooling, and positive means heating.

In the model, Q_{gain}^{t} and Q_{gain}^{t-1} are related to the occupant presence and the operation of the building appliances. When the building is occupied, 70% of the total heat rate of a person (i.e., 100 W) is dissipated as sensible heat into the space and the rest 30% is latent heat [218]. The heat gain from appliances is calculated by the power of the appliance multiplied by its heat gain coefficient, which reflects how much of the consumed electric power is dissipated into the space as heat. Table A.4 in Appendix A lists the heat gain coefficients adopted from the literature [219–221].

Note that the controllable loads are optimization variables of the scheduling problem, which will be iteratively calculated at each optimization timestep. Therefore, to speed up the optimization, we reduced the coupling between the thermal models and the electric demand models. This was done by calculating the weighted average heat gain coefficients for each building based on the capacity of each appliance (Table A.4).

The building load models in this work are categorized into four types according to their power flexibility characteristics: sheddable, modulatable, shiftable, and critical (Figure 6.3). The load categorization process has been introduced in Section 5.2. The critical loads account for about 20% to 90% of the total building loads depending on building type and time of day. The mathematical formulation of the loads and the battery model can be found in Section 5.3.2.

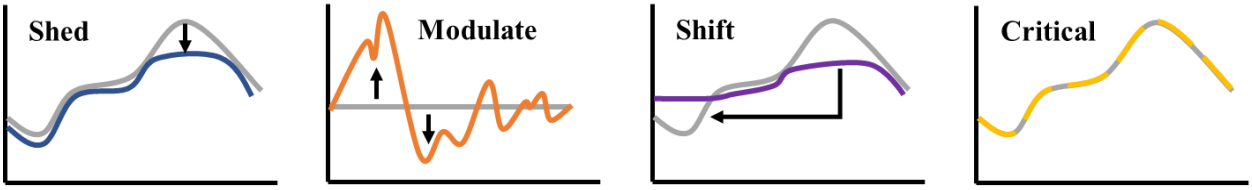

Figure 6.3 Power flexibility characteristics of the four load types [222].

6.3 Optimal Load Scheduling

This section first presents the mathematical formulation of the deterministic load scheduler. After that, we will introduce the formulation of the occupant preference-aware stochastic scheduler containing three parts: the thermostat-changing model, the uncertainty introduction mechanism, and the method to address the uncertainty.

6.3.1 Deterministic Scheduler

As introduced in Section 6.2.1, the deterministic scheduler adopts a two-layer structure with COL and BAL. The objective of the COL is to minimize the community-level PV curtailment to facilitate better use of the limited PV power during the outage. The main constraints are the load flexibility of each building, building occupancy, and building priority, etc. No detailed building assets are simulated at the community layer. This ensures that the COL is computationally tractable, especially when the problem scales up and the number of controllable building assets scales up. The detailed mathematical formulation of the COL can be found in Section 5.3.1.

The objective of the BAL is to minimize the unserved load ratio of each building within the allowable load range allocated by the COL. This is achieved through MPC-based optimal scheduling of the building-owned HVAC system, controllable loads, and battery. The optimization is a mixed-integer linear programming problem

because the sheddable and shiftable load models contain binary variables. Next, the mathematical formulation of the optimization problem is presented. Note that the formulation applies to every individual building in the community.

The cost function to minimize the unserved load ratio is formulated as:

$$f_{cost}(t, \{x^t\}_{t=1}^{H}) = \sum_{t=1}^{H} \left(\overline{P}_{load}^{t} - P_{load}^{t}\right) + \sum_{t=1}^{H} \gamma P_{ch}^{t} + \sum_{t=1}^{H} \gamma' P_{curt}^{t}, \tag{6.6}$$

$$\min_{\{x^t\}_{t=1}^{H}} f_{cost}(t, \{x^t\}_{t=1}^{H}), \tag{6.7}$$

where $\overline{P}_{load}^{t}$ is the predicted load upper bound from data. The difference between this upper bound and the actual operated loads P_{load}^{t} is minimized to achieve a maximum served load to the building. To avoid simultaneous battery charging and discharging as well as PV curtailment, the objective function also includes small penalizations of charging $\gamma \mathrm{P}_{\mathrm{ch}}^{\mathrm{t}}$ and curtailment $\gamma' \mathrm{P}_{\mathrm{curt}}^{\mathrm{t}}$ [189], where γ and γ' are the penalization coefficients. The power balance of each building that must be satisfied at each timestep is given by:

$$P_{pv}^{t} - P_{curt}^{t} = P_{ch}^{t} - P_{dis}^{t} + P_{load}^{t} + P_{hvac}^{t}, \tag{6.8}$$

where PV curtailment P_{curt}^{t} is limited by how much PV generation P_{pv}^{t} is available:

$$0 \leq P_{curt}^{t} \leq P_{pv}^{t}. \tag{6.9}$$

The left-hand side of Equation (6.8) represents power generation, whereas the right-hand side represents consumption. The P_{ch}^{t} and P_{dis}^{t} stand for the battery charging and discharging power as in Equation (5.46). The P_{load}^{t} and P_{hvac}^{t} are the total building loads and the HVAC power calculated in Equations (5.38) and (5.23),

respectively. To assure thermal comfort of the indoor environment, a temperature constraint is given by:

$$\underline{T}_{room} \leq T_{room}^{t} \leq \overline{T}_{room}, \tag{6.10}$$

where $\underline{T}_{room}$ and $\overline{T}_{room}$ are the lower and upper room temperature bounds implemented as hard constraints. The optimization variables in each building agent are collected in vector x^t:

$$x^t = \begin{bmatrix} \{P_{curt}^t\}_{t=1}^H, \{P_{ch}^t\}_{t=1}^H, \{P_{dis}^t\}_{t=1}^H, \{r_{hvac}^t\}_{t=1}^H, \{u_{shed,j}^t\}_{t=1}^H, \\ \{P_{modu,j}^t\}_{t=1}^H, \{v_{shif,j}^t\}_{t=1}^{H-n_{shif,j}+1}, \{T_{room}^t\}_{t=1}^H, \{E_{bat}^t\}_{t=1}^H \end{bmatrix}. \tag{6.11}$$

6.3.2 Stochastic Preference-aware Scheduler

To address the uncertainties of occupant thermal preference in the scheduling problem of resilient communities, this section introduces the stochastic preference-aware scheduler. First, we discuss the modeling of the occupant behavior uncertainties as a probability function. Then we show the mechanism by which this uncertainty might affect the optimal control of the HVAC system. After that, we propose using the chance-constraint method to address the uncertainty.

The stochastic occupant thermostat-changing model adopted in this work was proposed by Gunay et al. [60]. Through continuous observation of the occupants' thermostat keypress actions in private office spaces, the relationship between the thermostat-changing behavior and the concurrent occupancy, temperature, and relative humidity was analyzed. It was noted that the frequency of thermostat interactions (i.e., increasing or decreasing) can be approximated as a univariate logistic regression model with the indoor temperature as the independent predictor

variable. Though the original data set was obtained from two office buildings, Gunay et al. generalized the study to understand occupants' thermostat user behavior and temperature preferences. Given the universality of their work, we have adapted their models based on our use cases. Note that occupants might have varied (e.g., higher) tolerance of indoor temperature during an emergency. The exact thresholds need further experimental study and validation, which is out of the scope of this work.

The thermostat-changing behavior models determine whether the occupants will change the setpoint temperature based on the concurrent indoor air temperature. The probability of increasing and decreasing the temperature setpoint is predicted with a logistic regression model:

$$p = \frac{1}{1 + e^{-(a+bT_{room})}}, \tag{6.12}$$

where p is the probability of the changing action, T_{room} is the indoor room temperature, and a and b are coefficients. To investigate different uncertainty levels, we proposed three different active levels by revising the coefficients of the model in Equation (6.12). As shown in Table 6.1, the low active level adopts the original coefficients in [60]. Then, we proposed the medium and high active levels to represent various occupant thermal preference styles. The standard errors and p-values of the low active level coefficients are also provided in the table. As for the medium and high levels, we do not have measurement data for the statistical analysis since we adapted the coefficients from the original reference [60].

Table 6.1 Coefficients in different active levels of the occupant thermostat-changing behavior model.

Active Level	**Coefficients**			
	Increasing		Decreasing	
	a	b	a	b
Low [60]	-0.179	-0.285	-17.467	0.496
Medium	7.821	-0.485	-20.667	0.696
High	15.821	-0.685	-23.867	0.896
Standard Error	1.047	0.048	0.684	0.028
p-value	0.864	0.000	0.000	0.000

Note that the adaptation of the original logistic regression models was made under the following assumptions to ensure the adapted models remained realistic. For the setpoint increasing scenario, the slope coefficient of b is varied linearly to reflect a higher frequency of the changing behavior. The intercept coefficient a is then calculated to make sure that all active levels have the same value of probability at the temperature of 40ºC. For the setpoint decreasing scenario, a similar approach is taken to make sure the same value of probability at 16ºC is shared by all active levels. At each thermostat interaction, we assume that 1ºC of setpoint change would take place. Figure 6.4 depicts the probabilities of the three active levels. Note that this figure contains a wider temperature range than 16ºC-40ºC to show a more comprehensive performance of the behavior models.

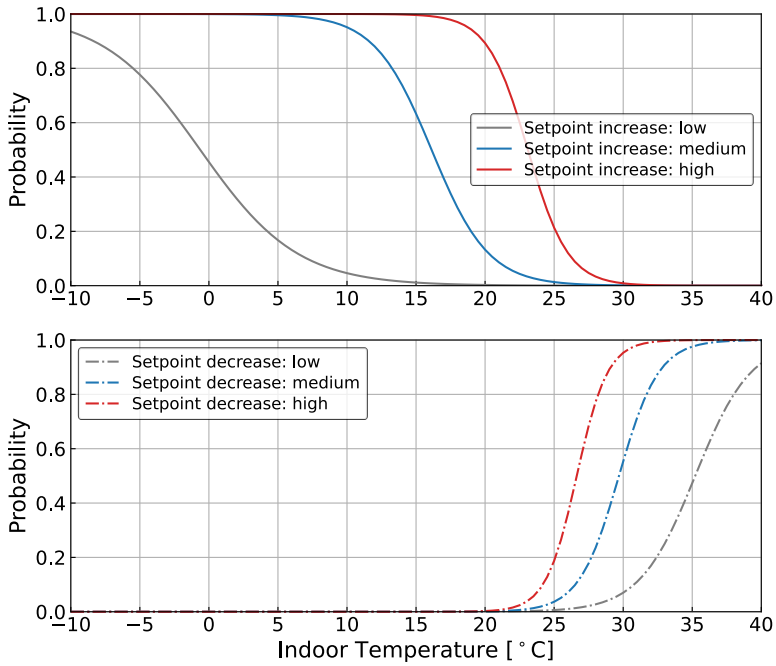

Figure 6.4 Probability of different thermostat-changing behavior.

Once the probability of the thermostat-changing behavior is determined using the above models, the increasing or decreasing action is determined by comparing the probabilities with a randomly generated number. At each optimization timestep, a random number between 0 and 1 is generated. If the number is larger than $1 - \Pr(increase)$, the action will be to increase. On the contrary, if it is smaller than $\Pr(decrease)$, the action will be to decrease. Because the sum of the increase and decrease probabilities is smaller than 1 in our case, this algorithm assures at most one action will be taken at each timestep.

To introduce the occupant thermostat-changing uncertainties to the load scheduling problem, a stochastic simulation model representing the behavior needs to be incorporated into the optimization. Figure 6.5 shows the control signal flow for the typical indoor air temperature control, which affects the HVAC system's operational status and its power consumption. The occupant sets the temperature

setpoint according to his/her preference through the thermostat. Behind the thermostat, a PID controller decides the next heat pump speed to offset the difference between the measured room temperature and the setpoint. This heat pump speed signal is then fed into the heat pump system to provide cooling for the conditioned space. Due to the presence of dynamic environmental and behavioral disturbances, this process will need to be repeated until the measured room temperature reaches the setpoint.

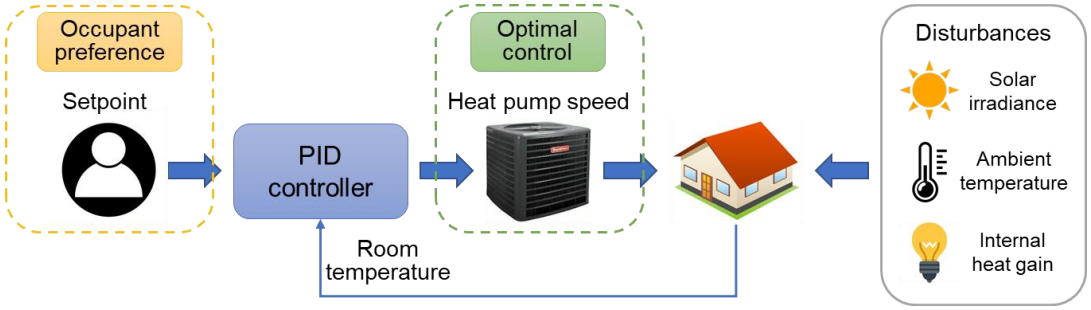

Figure 6.5 Diagram showing the introduction of occupant thermostat-changing behavior to the optimization.

However, in the optimal control mechanism, the optimal scheduler takes over the control of the heat pump speed from the PID controller. As a result, the occupants' preference has thus been "disabled" to allow an optimal control determined by the scheduler. To mimic the overriding of the room temperature setpoint by the occupants, the following algorithm was implemented in the MPC problem, and the pseudo code is shown below. Before each round of the optimization starts (Steps 1–2), if the occupant decided to change the setpoint (Step 3), the heat pump speed for the current timestep should be calculated to reach the setpoint instead of achieving the optimization objective (Steps 4–7). Otherwise, the optimization runs normally because no overriding happens (Step 7). After each optimization timestep, the flag

variables indicating the thermostat-changing actions need to be updated according to the concurrent room temperature (Step 8). It should be noted that in the optimization, no PID controller has been implemented, so we assumed that $T_{room}^{t} = T_{set}^{t}$ and the setpoint changes were directly added to the room temperature T_{room}^{t}.

Step 1. Start
Step 2. Initialization of flag variables: $increase = false, decrease = false$;
Step 3. If $increase = true$ or $decrease = true$: **Step 4.** $T_{room}^{t} = T_{room}^{t-1} + 1$ or $T_{room}^{t} = T_{room}^{t-1} - 1$; **Step 5.** Calculate the corresponding r_{hvac}^{t}; **Step 6.** Disable r_{hvac}^{t} from the optimization variables;
Step 7. Run MPC for timestep t;
Step 8. Update flag variables (i.e., $increase$ and $decrease$) according to T_{room}^{t};
Step 9. Repeat Steps 3–8 until the end of the MPC horizon of 48 hours;
Step 10. End

As mentioned above, the uncertainties in the occupants' thermostat-changing behavior are a probability function. In the scheduling optimization problem, the constraint directly affected by the occupants' thermostat-changing behavior is the room temperature bounds. The uncertainties related to the occupants' adjusting the thermostat could lead to the violation of the temperature bounds during the implementation of the developed control strategies. Furthermore, this could lead to other control-related performances being affected, including higher building load

unserved ratio and larger required battery size. To address this, we adopted the chance-constraint method.

By definition, the chance constraint allows the violation of a certain constraint with a small probability, which thus presents a systematic trade-off between control performance and the probability of constraint violations [223]. It can be expressed in general by the following equation:

$$Pr(g(x,\xi) \leq 0) \geq 1 - \epsilon, \tag{6.13}$$

where $g(x,\xi) \leq 0$ is the inequivalent constraint and ϵ is the maximum violation probability. Given the uncertainties in the occupants' thermostat-changing behavior, we assume that the temperature bounds can be satisfied with a probability of $(1 - \epsilon_T)$. For the lower temperature bounds, the chance constraint can thus be written as:

$$Pr\left(\underline{T}_{room} \leq T_{room}^{t+1}\right) \geq 1 - \epsilon_T. \tag{6.14}$$

Then, we rewrite it as:

$$Pr(\chi_T^{t+1} \leq 0) \geq 1 - \epsilon_T, \tag{6.15}$$

where $\chi_T^{t+1} = \underline{T}_{room} - T_{room}^{t+1}$. Let the indoor temperature be rewritten in terms of the prediction error: $T_{room}^t = T_{room,f}^t + T_{room,e}^t$ where $T_{room,f}^t$ is the predicted indoor room temperature and $T_{room,e}^t$ is the error caused by uncertainties. Similarly, $T_{room}^{t-1} = T_{room,f}^{t-1} + T_{room,e}^{t-1}$. For both timesteps, the room temperature distribution error follows the same distribution. The hypothetical error distributions can be in different forms and here we assume the distribution to be normal. Hence, it can be represented by:

$$T_{room,e}^{t,t-1} \sim \mathcal{N}(\mu_T^t, (\sigma_T^t)^2). \tag{6.16}$$

Therefore, χ_T^{t+1} is also normally distributed with the following mean μ^t and standard deviation σ^t:

$$\begin{aligned}\mu^t = \underline{T}_{room} - \beta_1(T_{room}^t + \mu_T^t) - \beta_2(T_{room}^{t-1} + \mu_T^t) - \beta_3 T_{amb}^t - \beta_4 T_{amb}^{t-1} - \beta_5 r_{hvac}^t \\ - \beta_6 Q_{sol}^t - \beta_7 Q_{sol}^{t-1} - \beta_8 Q_{gain}^t - \beta_9 Q_{gain}^{t-1},\end{aligned} \tag{6.17}$$

$$\sigma^t = \sqrt{(\beta_1 \sigma_T^t)^2 + (\beta_2 \sigma_T^t)^2}. \tag{6.18}$$

The chance constraint can thus be reformulated as:

$$Pr(\chi_T^{t+1} \leq 0) = \Phi\left(\frac{0 - \mu^t}{\sigma^t}\right) \geq 1 - \epsilon_T, \tag{6.19}$$

where $\Phi(\cdot)$ is the cumulative distribution function (CDF) of the standard normal distribution $\mathcal{N}(0,1)$. By taking the inverse CDF of both sides, we can get:

$$\frac{0 - \mu^t}{\sigma^t} \geq \Phi^{-1}(1 - \epsilon_T). \tag{6.20}$$

Rearrange the above equation and substitute μ^t and σ^t with Equations (6.17) and (6.18). Finally, we obtain the chance constraint for ensuring the indoor temperature will not fall below the lower bound of $\underline{T}_{room}$ with the probability of $(1 - \epsilon_T)$ as follows:

$$\begin{aligned}\beta_1(T_{room}^t + \mu_T^t) + \beta_2(T_{room}^{t-1} + \mu_T^t) + \beta_3 T_{amb}^t + \beta_4 T_{amb}^{t-1} + \beta_5 r_{hvac}^t + \beta_6 Q_{sol}^t + \beta_7 Q_{sol}^{t-1} \\ + \beta_8 Q_{gain}^t + \beta_9 Q_{gain}^{t-1} - \underline{T}_{room} \geq \Phi^{-1}(1 - \epsilon_T)\sqrt{(\beta_1 \sigma_T^t)^2 + (\beta_2 \sigma_T^t)^2}.\end{aligned} \tag{6.21}$$

Substituting Equation (6.3) into (6.21) and rearranging, we have:

$$T_{room}^{t+1} - \underline{T}_{room} \geq \Phi^{-1}(1 - \epsilon_T)\sqrt{(\beta_1 \sigma_T^t)^2 + (\beta_2 \sigma_T^t)^2} - (\beta_1 \mu_T^t + \beta_2 \mu_T^t). \tag{6.22}$$

Similarly, we have Equation (6.23) for the upper bound,

$$Pr\left(\overline{T}_{room} \geq T_{room}^{t+1}\right) \geq 1 - \epsilon_T. \tag{6.23}$$

Taking a similar derivation process as that in Equations (6.14) to (6.22), we can obtain the chance constraint for the temperature upper bound:

$$\overline{T}_{room} - T_{room}^{t+1} \geq \Phi^{-1}(1-\epsilon_T)\sqrt{(\beta_1\sigma_T^t)^2 + (\beta_2\sigma_T^t)^2} + (\beta_1\mu_T^t + \beta_2\mu_T^t). \tag{6.24}$$

The updated inequivalent constraints indicate that the temperature bounds for the optimization should be narrower than the original temperature bounds to account for the setpoint behavioral uncertainty, which is consistent with the expectations. Note that because the uncertainty-dealing method is focused on the temperature constraints, one possible limitation is that the above method might have a limited effect on the controller design for buildings that have larger thermal masses because the building temperature is insensitive to temperature constraints. More discussion of this point follows in Section 6.4.3.

6.4 Case Study

6.4.1 Studied Community

The case study community is a net-zero energy community located in Anna Maria Island, Florida, USA, which is a cooling-dominated region. The community buildings are installed with both roof-top PV panels and solar carports, which harvest about 85 MWh annually for the whole community. A centralized ground source heat pump system provides the HVAC needs of the whole community with high efficiency. Other sustainable features include well-insulated building envelopes, solar thermal

water heating, and rainwater recycling. This community achieved net-zero energy in the year 2014. In the community, there are various building types such as residential, small office, gift shop, etc. We would like to cover both residential and commercial buildings in the case study. So, we selected one residential and two small commercial buildings based on the measurement data quality. More specifically, the selected three buildings consist of a residential building (area: 93.8 m^2), an ice cream shop (area: 160.5 m^2), and a bakery (area: 410 m^2). The building layout of the community can be found in reference [151].

For the given community, a virtual testbed based on the object-oriented modeling language Modelica [27] was built and validated [16]. In the testbed, the TMY 3 data for a nearby city, Tampa, was adopted for this case study. The building thermal models are RC network models. For the optimal control in this work, the HVAC models were trained using one month (i.e., August) of the simulation data exported from the testbed. Table 6.2 lists the coefficients for the linear regression HVAC models, the RMSE of the models, as well as the corresponding nominal heat pump power. The N/A in the table represents a coefficient that is too small and thus has been neglected in the model. Three effective decimal places are provided.

Table 6.2 Coefficients and nominal power of the HVAC models.

		Residential	**Ice Cream Shop**	**Bakery**
Coefficients	T_{room}^{t}	1.429	0.502	0.977
	T_{room}^{t-1}	-0.432	0.498	0.0213
	T_{amb}^{t}	0.0263	0.000295	0.00405
	T_{amb}^{t-1}	-0.0232	-0.000193	-0.00196
	r_{hvac}^{t}	-0.210	-0.0114	-0.178
	Q_{sol}^{t}	0.0151	0.0000345	0.0107

		Residential	Ice Cream Shop	Bakery
	Q_{sol}^{t-1}	-0.00302	0.000181	-0.00621
	Q_{gain}^{t}	0.00852	N/A	N/A
	Q_{gain}^{t-1}	N/A	N/A	0.0140
RMSE (℃)		0.160	0.0205	0.114
Nominal Power (kW)		2.140	2.830	3.770

Additionally, Table 6.3 lists the load categorization for the studied buildings following the principles proposed in Section 5.2. A complete list of the building load capacities and their heat gains can be found in Appendix A.

Table 6.3 Building loads categorized into four types.

	Residential	Ice Cream Shop	Bakery
Sheddable	Computer	Coffee maker, soda dispenser, outdoor ice storage	Microwave
Modulatable	HVAC	HVAC	Mixer, unspecific room plug loads, HVAC
Shiftable	Range, washer, dryer	None	Range, oven, dishwasher
Critical	Lights, refrigerator	Lights, cooler, display case	Lights, cooler, display case

We designed three uncertainty levels (i.e., low, medium, high) as in Table 6.1 to evaluate the deterministic and preference-aware schedulers in this work. They are compared to the baseline scenario, where the deterministic scheduler is applied without occupant behavior uncertainties. The following results and discussion are all based on these scenarios. All scenarios were run in the three buildings for 48 hours with a timestep of 1 hour in the islanded mode.

6.4.2 Settings of Chance-constrained Controllers for Different Buildings

The preference-aware schedulers use chance-constrained controllers, whose settings depend on individual building properties and uncertainty levels. Following the method proposed in Section 6.3.2, this section provides the details of the chance-constrained controller settings for three individual buildings in the case study, which is based on the control outcome of the deterministic schedulers under three uncertainty levels.

Considering the occupant-preference-driven actions as the source of "prediction errors" for the room temperature, we extracted the distributions of the room temperature prediction errors. The Monte Carlo simulation method [224] was adopted, where 100 repeated simulations were run using the deterministic scheduler with three uncertainty levels. We used the room temperature of the deterministic baseline scenario as the benchmark to calculate the errors caused by the occupant setpoint-changing behavior. To describe the room temperature errors, three hypothetical distributions are proposed (i.e., fit distribution in Table 6.4). The normal distribution is mentioned in the derivation in Section 6.3.2. The half-normal distribution is a fold of a normal distribution at its mean. For the residential building medium uncertainty level, a half-normal distribution was adopted. This can be attributed to the fact that almost no temperature decrease action was observed and thus the errors were all above zero. Constants were used for the residential building and the bakery under the low uncertainty level because the frequency of the setpoint-changing is too low (nearly zero) to follow any distributions.

Chi-square goodness of fit tests [225] at a rejection level of 1% were conducted to evaluate whether the proposed hypothetical distributions fit well. The types of fitting distributions, p-values of the tests, and the distribution parameters are reported in Table 6.4. In the table, μ is the mean and σ is the standard deviation of the normal/half-normal distribution. The null hypothesis here is that the room temperature prediction error follows the hypothetical distribution. The p-value is the evidence against this null hypothesis. Since all p-values are greater than 99%, all error distributions failed to reject the hypothesis at the level of 1%. This means they all follow the corresponding hypothetical distribution.

Table 6.4 Chi-square goodness of fit test p-values and normal distribution parameters.

Building	Uncertainty	Fit Distribution	p-value	μ (°C)	σ (°C)
Residential	Low	Constant	1.0	-6.45E-05	N/A
	Medium	Half-normal	0.999	-3.57E-01	4.35E-01
	High	Normal	0.999	1.56E+00	8.17E-01
Ice Cream Shop	Low	Normal	0.999	-3.48E-03	7.86E-03
	Medium	Normal	0.999	-4.45E-03	8.59E-03
	High	Normal	0.999	1.60E-02	1.59E-02
Bakery	Low	Constant	1.0	-3.42E-03	N/A
	Medium	Normal	0.999	3.01E-02	1.05E-01
	High	Normal	0.999	5.33E-01	4.65E-01

The frequency histogram and probability density functions (PDFs) of each building under various uncertainty levels are plotted in Figure 6.6. In the figure, it can be seen that the higher the uncertainty, the wider the room temperature range. This is because, in scenarios with higher uncertainty, occupants change the thermostat more frequently, which expands the possible temperature ranges. We also noticed that the temperature range in the ice cream shop is relatively concentrated

compared to the other two buildings. This can be attributed to the large thermal mass of the building.

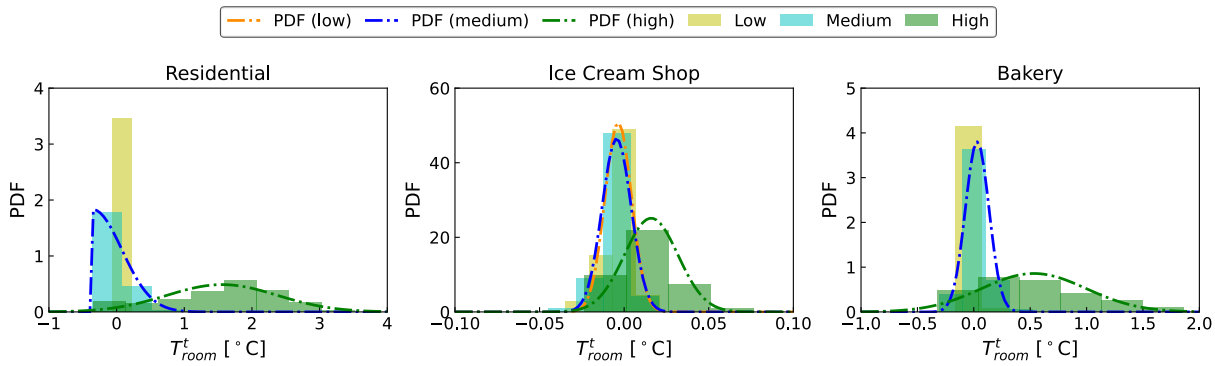

Figure 6.6 Room temperature prediction error PDFs obtained from the Monte Carlo simulations.

For the scenario where the temperature prediction error follows the half-normal distribution, we applied the chance constraint only to the upper bound because only increasing actions happen in this scenario. For the two scenarios where the room temperature error is estimated to be a constant, we adopted the original temperature bounds of [20°C, 25°C] because the estimated errors in both scenarios are smaller than 0.01°C. We choose the $\epsilon_T = 1\%$ to ensure a 99% probability of abidance of the temperature constraints (Equation (6.14)). Table 6.5 lists the updated room temperature lower and upper bounds for each building under different scenarios.

Table 6.5 Room temperature bounds for chance-constrained optimizations.

Building	Uncertainty	$\underline{T}_{room}$ (°C)	$\overline{T}_{room}$ (°C)
Residential	Low	20.000	25.000
	Medium	20.000	24.236
	High	20.547	21.343
Ice Cream Shop	Low	20.024	24.983
	Medium	20.027	24.982
	High	20.025	24.943
Bakery	Low	20.000	25.000
	Medium	20.240	24.700
	High	20.664	23.273

6.4.3 Results and Discussions

This section first quantifies the impact of introducing occupant behavior uncertainties to the optimal scheduling problem. Then, the deterministic and chance-constrained controllers are tested on the community virtual testbed. Their control performance in terms of the unserved load ratio, the required battery size, and the unmet thermal preference hours are then compared.

Figure 6.7 to Figure 6.9 depict the occupant thermal preference and the corresponding room temperatures. In the figures, the upper plots show the simulated stochastic thermostat-changing actions at different uncertainty levels, where increase means a setpoint increase action, and vice versa. The lower plots show the resulting room temperatures with dashed lines.

The results of the low uncertainty scenario overlap with that of the baseline scenario (i.e., the deterministic scheduler without uncertainty) mainly due to the low probability of setpoint-changing actions in this scenario. With the increase in the probability, we see more frequent setpoint-changing actions in all three buildings.

Further, the increase action happens more frequently than the decrease action. This is because, between the temperature range of 20°C and 24°C, the probability of increase is much higher than that of decrease (see Figure 6.4). This also implies that the occupants' temperature preference is closer to 24°C than 20°C. Additionally, for the residential building and the bakery, the temperature difference between scenarios is more noticeable than for the ice cream shop; this is attributable to the different building thermal masses of the three buildings.

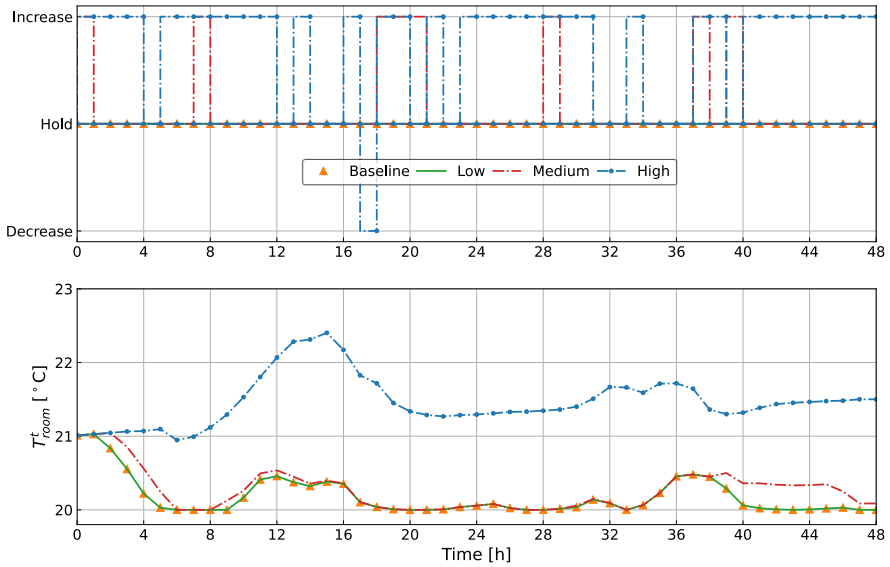

Figure 6.7 Residential building occupant thermostat changing actions (upper) and resulting room temperatures (lower) under three levels of uncertainty.

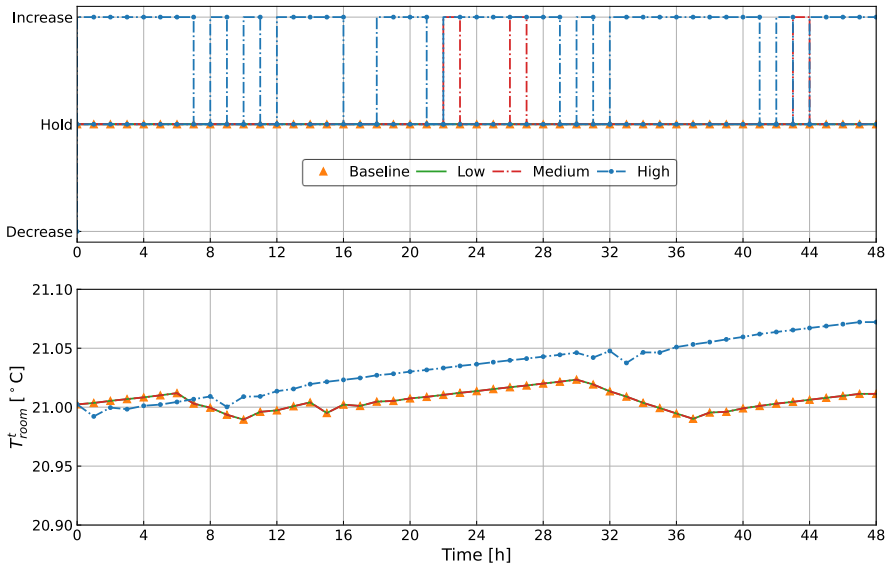

Figure 6.8 Ice cream shop occupant thermostat changing actions (upper) and resulting room temperatures (lower) under three levels of uncertainty.

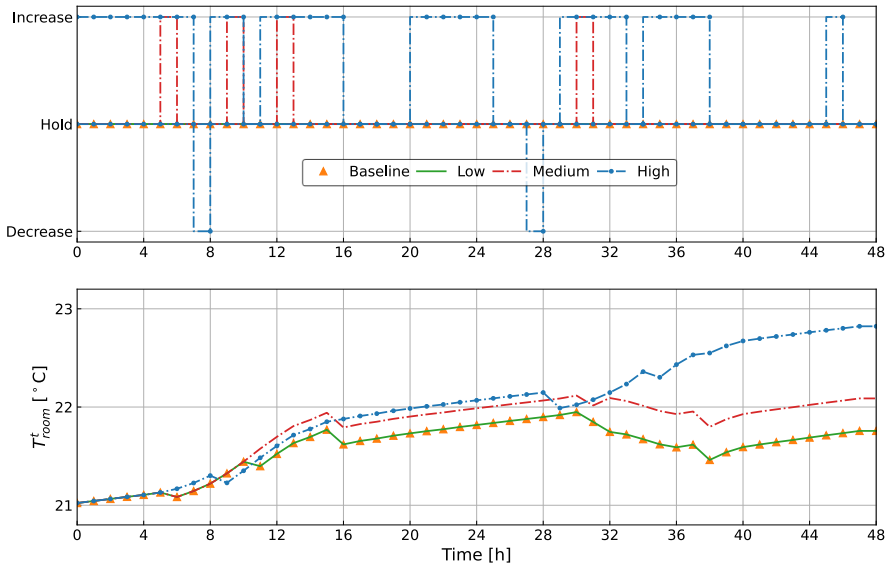

Figure 6.9 Bakery occupant thermostat changing actions (upper) and resulting room temperatures (lower) under three levels of uncertainty.

Table 6.6 lists the values of the KRIs in correspondence with Figure 6.7 to Figure 6.9. The HVAC energy and average room temperature over the optimization horizon are also provided to facilitate the analysis of the results.

Table 6.6 Key resilience indicators for studied buildings under different uncertainty levels.

Building	Scenario	Unserved Load Ratio	Battery Size [kWh]	HVAC Energy (kWh)	Mean Room Temperature (°C)
Residential	Baseline	0.0744	47.686	32.139	20.185
	Low	0.0744	47.686	32.139	20.185
	Medium	0.0744	47.168	32.099	20.271
	High	0.0744	38.541	21.400	21.468
Ice Cream Shop	Baseline	0.0215	99.139	32.703	21.006
	Low	0.0215	99.139	32.703	21.006
	Medium	0.0215	99.139	32.703	21.006
	High	0.0215	93.166	10.063	21.033
Bakery	Baseline	0.0247	80.007	35.144	21.579
	Low	0.0247	80.007	35.144	21.579
	Medium	0.0247	73.496	27.604	21.766
	High	0.0247	76.801	11.310	21.973

From the table, we see that the unserved load ratio remains the same across all scenarios for each building. This can be attributed to the fact that in the controller design phase, the optimization objective is set to minimize the unserved load ratio. Hence, the unserved load ratios for each building are already minimal and are not affected by the occupants' thermostat-overriding behavior uncertainties. Instead, the battery-charging/discharging behavior is affected, as reflected by the different required battery sizes in the table. Note that the unserved load ratios are minimal, but not zero, because of our assumption that each shiftable load operates once and only once per day.

For the rest of the metrics, note that the battery size, HVAC energy, and average room temperature remain the same for the baseline and low uncertainty scenarios in all buildings. This is because no setpoint-changing actions happened due

to the relatively low probabilities, as shown in the figures above. As for the medium uncertainty scenarios, both the residential building and the bakery show higher room temperatures and lower HVAC energy while the ice cream shop still has the same results as the baseline, given its large thermal mass.

In terms of the high uncertainty scenarios, due to the prominent increase in room temperatures, we noticed more HVAC energy savings in all buildings. Note that though the average room temperature increase is insignificant, the HVAC energy savings is large due to the cumulative effect over the many hours of setpoint increase. Overall, we see a positive correlation between the HVAC energy and the required battery size. When the PV generation and the other building loads remain the same, the more HVAC energy, the larger the required battery size. However, one opposite case was noted in the bakery high uncertainty scenario where the required battery size is slightly larger in the high uncertainty scenario than in the medium uncertainty scenario. This was caused by a setpoint decrease action at hour 28, which resulted in a battery discharging during the night and thus a smaller minimum SOC of the battery.

To summarize, occupant thermostat-changing behavior uncertainty needs to be considered when designing optimal schedulers for resilient buildings because it affects the indoor room temperature, the HVAC power, and thus the sizing of batteries. For the whole community, when considering the highest occupant behavior uncertainty, the consumed HVAC energy can be 57.2% less and the battery 8.08% smaller. Whereas the aforementioned impact depends on the uncertainty level (i.e.,

how frequently the occupants change the setpoint), heating or cooling season, and the occupants' actual preference for the indoor room temperature compared to the room temperature designed by the scheduler. In our case, a preferred higher indoor room temperature saves HVAC energy. During the heating season, the observations could be reversed.

To further evaluate the performance of the chance-constrained controller in comparison with the deterministic controller, tests were run on the virtual testbed [151] in a stochastic manner. In each of the studied buildings, both the deterministic controller and the chance-constrained controller were tested for two days (i.e., August 4 and 5) with the three levels of uncertainties. The testing method is similar to the method proposed in Section 6.3.2. Additionally, the precalculated optimal battery charging/discharging, as well as the optimized loads, are also implemented in the testbed. One hundred repeated Monte Carlo simulations were run for each scenario to better observe the controller performance. The KRIs of the unserved load ratio, the required battery size, and the unmet thermal preference hours are adopted for the performance evaluation.

The upper plot of Figure 6.10 depicts the predetermined optimal schedules of the heat pump speed ratio as the inputs of the test. The lower plot then shows the corresponding room temperatures predicted by the linear regression models in the optimization. The data for the residential building is adopted here for the analysis. The plots for the ice cream shop and the bakery can be found in Appendix A. From the figure, we see that the scheduled speed ratios in the low and medium uncertainty

scenarios overlap with that of the deterministic scheduler. Whereas the high uncertainty scenario tends to have lower speed ratios over the whole optimization horizon. This can be attributed to the controller settings shown in Table 6.5, where the temperature bounds set in the low and medium uncertainty scenarios are closer to the original bounds of [20°C–25°C]. Hence, the temperature constraints are not binding in these two scenarios. However, in the high uncertainty scenario, the temperature constraint is binding, which leads to speed ratio reductions. As a result, a higher room temperature can be seen in the high uncertainty scenario.

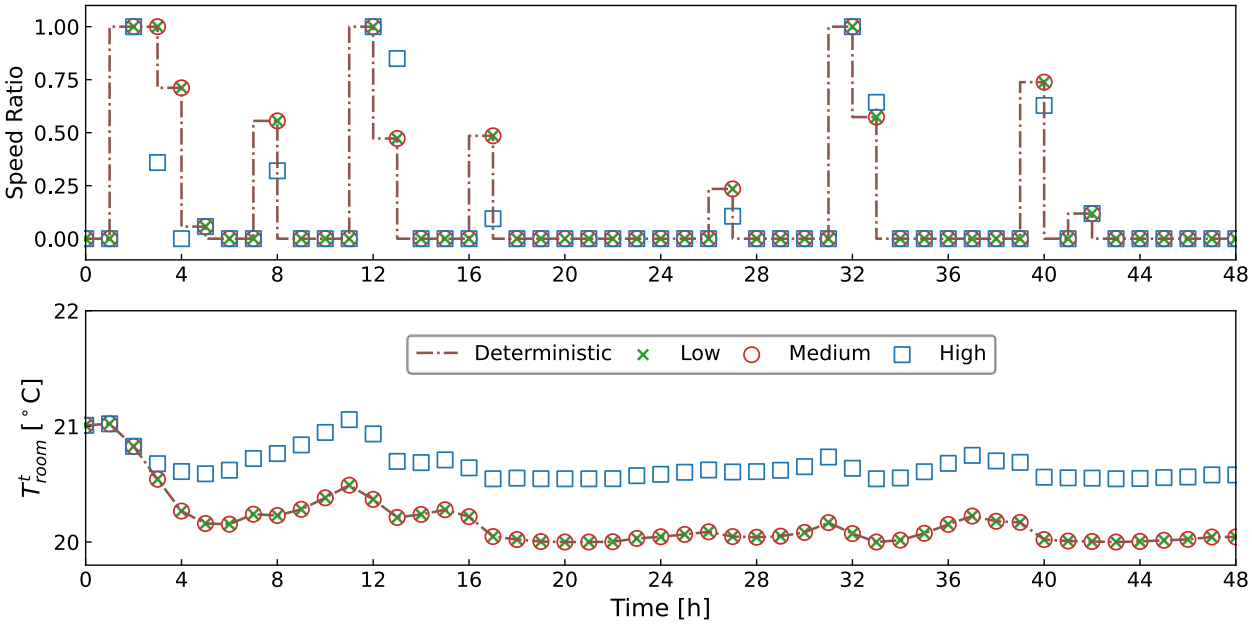

Figure 6.10 Optimal schedules of the heat pump speed ratio and predicted room temperatures by various schedulers (residential building).

Figure 6.11 to Figure 6.13 depict the room temperature boxplots as the controller testing outputs. The lower and upper borders of the boxes represent the 25th and 75th percentiles of the data, respectively. The longer the box, the more scattered the room temperature. The lines inside the boxes represent the median values. The lines beyond the boxes represent the minimum and maximum values

except for outliers, which are not shown in these figures. Note in the figures that the temperatures first concentrate together (shown as black lines) and then spread out (shown as boxes). This is because, at the beginning of the simulations, no overriding behavior of the setpoints happens and the heat pump operates following the scheduled speed ratio. Once the overriding happens at a certain timestep in some simulations, the room temperature trends start to deviate and become boxes. The occupant-preferred temperature lines are also shown as orange lines in these figures as a reference; they are average setpoints adjusted by the occupants in all the Monte Carlo tests.

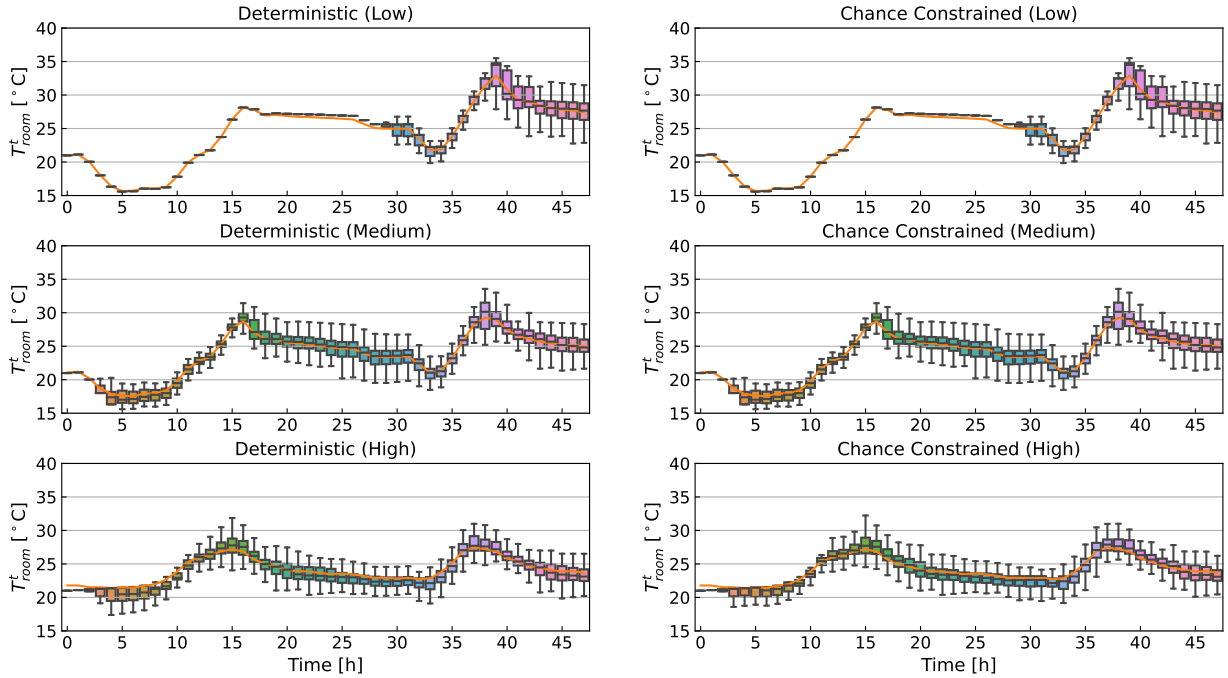

Figure 6.11 Residential building room temperature boxplots for control testing results.

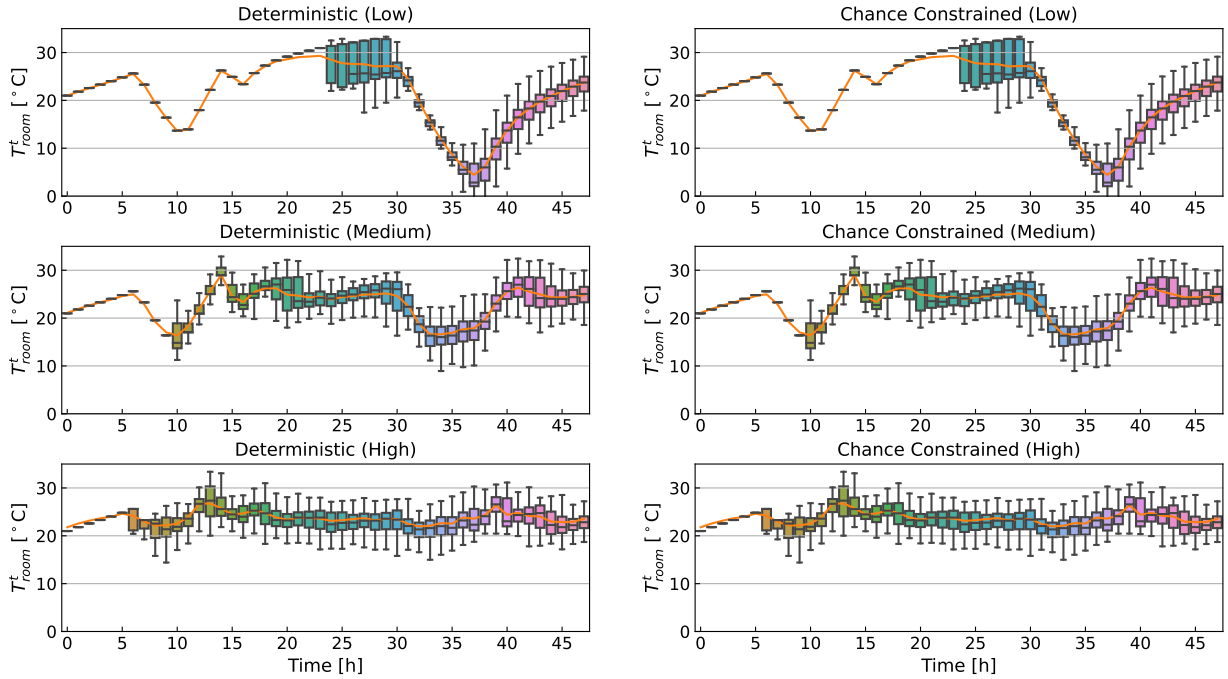

Figure 6.12 Ice cream shop room temperature boxplots for control testing results.

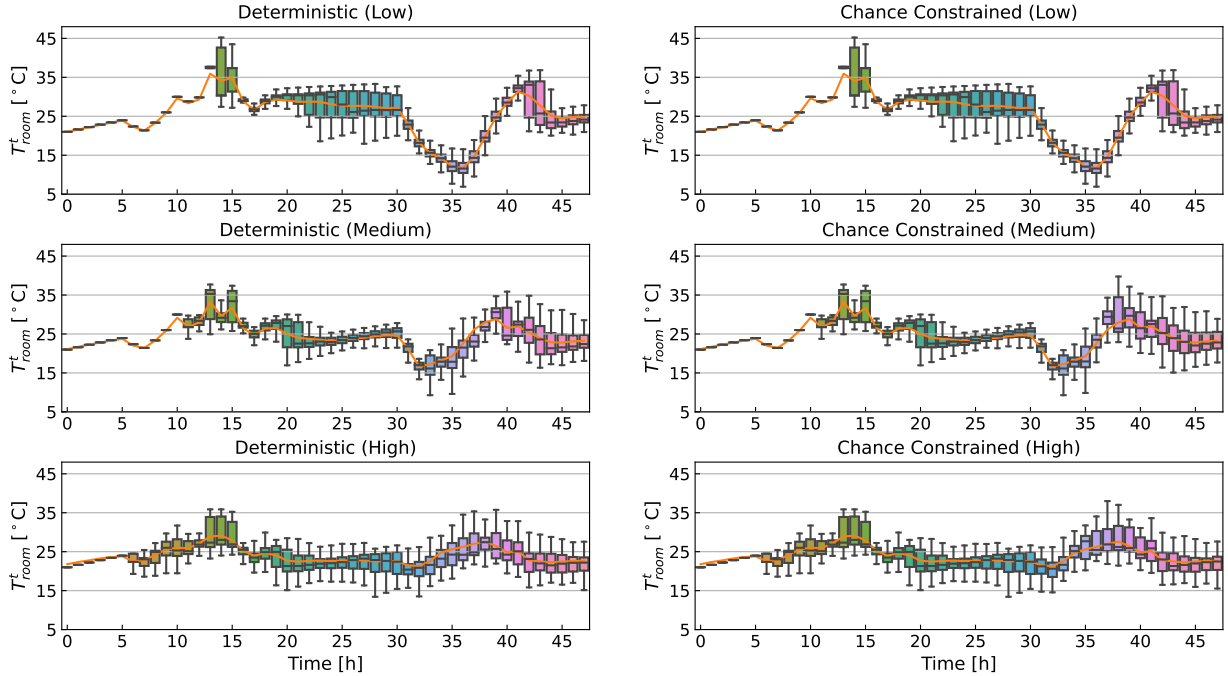

Figure 6.13 Bakery room temperature boxplots for control testing results.

In the figures, we see a general trend of narrower room temperature ranges from low uncertainty scenarios to high uncertainty scenarios. This is due to the

introduction of the occupant setpoint-overriding mechanism, which tends to moderate the extreme room temperatures. Also, there is a plant-model mismatch, which describes the parametric uncertainty of modeling that originates from neglected dynamics of the plant [216]. In our case, the mismatch exists as the simulated room temperatures in the testbed are slightly higher than those predicted by the reduced-order linear HVAC models. This is understandable because the physics-based testbed has much higher fidelity and simulates the non-linearity of the real mechanical systems.

Because the difference in the room temperature between the two controllers is not depicted in these figures, Table 6.7 and Table 6.8 provide further quantitative evaluations of the room temperatures along with other controller performances. Additionally, note that the optimal schedules of some scenarios remain the same because of the unbinding temperature constraints, which led to the same testing outputs. Here we only discuss the scenarios that have different inputs and outputs. A full list of all testing results is available in Table A.5.

Table 6.7 Comparison of controller performance in the residential building high uncertainty scenario.

Controller	**Unmet Thermal Preference Hours (ºC·hrs)**	**Mean Room Temperature (ºC)**	**Unserved Load Ratio**	**Required Battery Size (kWh)**
Deterministic	48.91	23.75	0.074	47.69
Chance-constrained	46.42	23.87	0.074	44.12

In Table 6.7, we see a larger value of unmet thermal preference hours in the deterministic controller than the chance-constrained one. This can be attributed to

the higher room temperatures regulated by the chance constraints to better satisfy the occupants' thermal preferences. Again, the same unserved load ratio is observed in both controllers because it is already minimal, which is enforced by the objective function. In terms of the battery size, the chance-constrained controller shows a smaller required battery size than the deterministic controller. This results from the fact that a higher room temperature has led to less consumed HVAC energy in the chance-constrained scenario. Thus, less discharging from the battery was happening, which led to smaller required battery size. For the bakery results shown in Table 6.8, the same trends for the battery size and the unserved load ratio as the residential building can be observed under each uncertainty level. Namely, smaller batteries and the same unserved load ratios.

Table 6.8 Comparison of controller performances in the bakery medium and high uncertainty scenarios.

Uncertainty	**Controller**	**Unmet Thermal Preference Hours (ºC·hrs)**	**Mean Room Temperature (ºC)**	**Unserved Load Ratio**	**Required Battery Size (kWh)**
Medium	Deterministic	88.80	24.27	0.025	80.01
	Chance-constrained	91.28	24.50	0.025	76.89
High	Deterministic	102.81	23.65	0.025	80.01
	Chance-constrained	101.61	23.89	0.025	76.89

As for the unmet thermal preference hours, different trends are witnessed in the medium and high uncertainty levels. At the medium level, the deterministic controller shows fewer unmet preference hours than the chance-constrained controller. Whereas in the high uncertainty level, an opposite trend is seen. This is

reasonable as we see a generally higher mean room temperature regulated by the chance-constrained controller under different uncertainty levels. However, in the medium scenario, a lower preference temperature line was obtained from the Monte Carlo testing, which is closer to the actual room temperatures of the deterministic controller. When the preference temperature rises in the high uncertainty scenario, the chance-constrained controller outperforms the deterministic controller with a higher actual room temperature and thus smaller unmet thermal preference hours.

When we compare different uncertainty levels in the bakery, we see that the mean room temperature decreases with the increase in uncertainty. This is because the lower temperature upper bounds shown in Table 6.5 have regulated the room temperature to sink when the uncertainty gets higher. Additionally, as seen in Figure 6.4, in the temperature range of 20ºC to 24ºC, the probability of increasing the temperature setpoint is much higher than that of decreasing it While above 24ºC, the probability to increase and to decrease is almost the same. This has caused the room temperatures to end up around 24ºC in the high uncertainty scenarios for all buildings (Table A.5). This reveals that with the increase in the occupant thermostat-changing uncertainties, the room temperatures tend to get closer to the occupants' preferred room temperature.

Though some improvement was noticed in the chance-constrained controller compared to the deterministic controller, the overall improvement was less than expected. This could be attributed to the following three factors. First, the impact of the uncertainty level on the controller performance improvement is prominent as we

observe higher performance improvement in high uncertainty scenarios. Second, the thermal property, especially the thermal mass, of the building itself also affects the results. Thermal mass serves as a thermal buffer to filter the impact of various HVAC supply temperatures. Hence, buildings with a larger thermal mass tend to experience less impact from the occupant thermal preference uncertainty. This can be demonstrated by the results of the ice cream shop, where the two controllers perform the same. Third, the plant-model mismatch also plays a significant role in the transition from the optimal scheduler design to its implementation. In the design phase, a series of control-oriented linear regression building models were used. However, the testing took place on a high-fidelity physics-based testbed, where the complex system dynamics of the whole buildings and HVAC systems were modeled with shorter simulation timesteps. This is a common source of uncertainty to be addressed for MPC design and implementation.

In our opinion, a joint effort from building scientists, modelers, and engineers is needed to facilitate implementing stochasticity in the building domain and ultimately better serve the occupants. For example, an open-source database focused on building performance-related stochasticities such as occupant behavior and weather forecast needs to be established. Further, readily available stochastic simulation tools need to be developed (e.g., Occupancy Simulator [226]). Finally, stochasticity needs to be incorporated into the whole process of building modeling and design in the form of boundary conditions or internal components.

6.5 Conclusion

In this work, we proposed a preference-aware scheduler for resilient communities. Stochastic occupant thermostat-changing behavior models were introduced into a deterministic load scheduling framework as a source of uncertainty. The impact of occupant behavior uncertainty on community optimal scheduling strategies was discussed. KRIs such as the unserved load ratio, the required battery size, and the unmet thermal preference hours were adopted to quantify the impacts of uncertainties. Generally, the proposed controller performs better in terms of the unmet thermal preference hours and the battery sizes compared to the deterministic controller. Though only tested on three buildings of the studied community, the methodology of introducing occupant behavior uncertainty into load scheduling and testing can be generalized and applied to other building and behavior types.

More specifically, we determined that occupant thermostat-changing behavior uncertainty should be considered when designing optimal schedulers for resilient communities. For the whole community, when considering the highest occupant behavior uncertainty, the consumed HVAC energy can be 57.2% less and the battery 8.08% smaller. During the controller testing phase, the proposed chance-constrained controller proves its advantage over the deterministic controller by better serving the occupants' thermal needs and demonstrating a savings of 6.7 kWh of battery capacity for the whole community. Additionally, we noticed that with the presence of occupant thermostat-changing uncertainties, the room temperatures tend to get closer to the occupants' preferred room temperature.

During the simulation experiments, we noticed some limitations of the proposed work. Because the proposed uncertainty method mainly deals with the uncertainty through the temperature constraints, it can be less effective for buildings of larger thermal mass due to the insensitivity to temperature constraints. Also, the plant-model mismatch was noticed in the controller testing phase, which is a common parametric uncertainty that originates from neglected dynamics of the plant [216]. Finally, we used the thermostat changing models developed based on data from private office spaces in different building types, which can be debatable. We note that the building types that we studied in this work were not necessarily the most representative, because for ice cream shops and bakeries, the largest portion of load (e.g., refrigeration and baking) does not rely on occupant behavior. However, the methodology proposed in this work can be transferred to and evaluated on other building types.

Future work for this research includes extending the scope to heating scenarios to further generalize the findings. Additionally, real-time stochastic MPC control techniques with occupant behavior models could be integrated into the framework to overcome the lack of flexibility in *a priori* designed controllers.

Chapter 7. Conclusions, Limitations, and Future Work

7.1 Conclusions

This dissertation aims to solve a few identified research questions surrounding low-carbon and resilient communities. To address the research gap of no readily available community modeling platforms that are capable of dynamic modeling and control, we built a Modelica-based community emulator and an open-source NZEC library. The emulator has the function of stochastic building occupant presence learning and reproducing based on lighting power data. Through the training and validation process, we noticed that logistic regression models are sensitive to the quality of the training data. Ideally, the training dataset should be more concentrated on the transitional region between the two states and the two classes should be well balanced. Further, increasing the number of independent features should help improve the fitness of the probability model. The stochastic simulation results showed that stochastic models can be very accurate for long-term energy predictions. However, they cannot predict uncommon events, and this can lead to large short-term power prediction errors.

In terms of the low-carbon community perspective of this dissertation, a carbon emission responsive control framework for thermostatically controlled loads was proposed. Within this framework, the four various controllers adjust thermostat setpoints according to projected carbon emission signals. Evaluating the impact of carbon net-metering, we found that controllers with carbon net-metering showed 2.5% to 3.0% less energy consumption and 5% to 12.7% less emission than controllers without carbon net-metering. This indicates the incentivizing impact of adopting carbon net-metering, as it encourages the exporting of power back to the grid. For controllers without carbon net-metering, higher annual energy consumption and carbon emissions result from attempting to increase the PV self-consumption rate. However, all controllers that do not consider carbon net-metering perform better in terms of the total cost. Due to the rebound effect, they tend to be shifting loads from on-peak hours to off-peak hours, causing the total cost to sink. Further, because more energy is consumed, non-net-metering controllers tend to create a more comfortable indoor environment for the occupants. All predictive controllers perform better than the momentary controllers in terms of energy consumption, carbon emission, and energy cost. This is attributed to the enhanced load shifting effect by the predictive controller design. Also, this finding verifies the claim made by Fischer [161] that predictive rule-based controllers are promising alternatives to optimization-based controllers because they are simpler and still effective.

To enhance community resilience, a novel decentralized control architecture for renewable resource allocation and load scheduling was proposed. This MPC-based

optimization architecture consists of a community operator layer that allocates the daily PV power generation to achieve the community-wide optimum and a building agent layer that schedules building loads to achieve its local optimum in each building. We found that the renewable resource allocation process is mostly constrained by the building load flexibility. More specifically, buildings with less load flexibility (i.e., higher critical loads) tend to be allocated more PV generation than other buildings. Additionally, when prioritizing buildings according to occupancy status, the building with a longer occupancy duration is allocated more PV power, which could lead to more PV curtailment. Additionally, through the analysis of different objective functions, we found that setting the objective to target at an appropriately selected indoor temperature setpoint will result in increased HVAC energy savings. However, in our case study, this did not lead to a lower unserved ratio for other load types. Instead, the PV curtailment increased. The two objectives have a competitive relationship: serving more HVAC power to increase thermal comfort will decrease the other served load. Therefore, it is necessary for the building agent to have multi-objective optimization to minimize the unserved load ratio and maximize comfort simultaneously. This will bring the benefit of less curtailment, a smaller unserved load ratio, assured thermal comfort, as well as smaller battery size. However, the weighting between the two objectives needs to be carefully selected as their scales are quite different.

Finally, the impact of occupant behavior uncertainty on community optimal scheduling strategies was discussed. Generally, the proposed controller performs

better in terms of the unmet thermal preference hours and the battery sizes compared to the deterministic controller. More specifically, we determined that occupant thermostat-changing behavior uncertainty should be considered when designing optimal schedulers for resilient communities. For the whole community, when considering the highest occupant behavior uncertainty, the consumed HVAC energy can be 57.2% less and the battery 8.08% smaller. During the controller testing phase, the proposed chance-constrained controller proves its advantage over the deterministic controller by better serving the occupants' thermal needs and demonstrating a savings of 6.7 kWh of battery capacity for the whole community. Additionally, we noticed that with the presence of occupant thermostat-changing uncertainties, the room temperatures tend to get closer to the occupants' preferred room temperature. Though only tested on three buildings of the studied community, the methodology of introducing occupant behavior uncertainty into load scheduling and testing can be generalized and applied to other building and behavior types.

7.2 Limitations

This work has the limitation of not having the ground truth data for occupant presence in the presence modeling part. The presence generated from lighting power can be delayed when people arrived and did not turn the lights on. This could be cross-validated with other appliance usage data in the future. In the best-case scenario, occupant surveys should be conducted to know their preferences and habits, and occupant sensors should be installed.

In the decarbonization control studies, we noticed that in some scenarios the emissions produced by space cooling and water heating are higher compared to the baseline due to the increased energy consumption from load shifting. This indicates that rule-based control solely informed by carbon emission signals may end up with higher emissions, which could be overcome by using optimization-based control methods such as MPC. Additionally, we note that another limitation of this work, which is also a general limitation of rule-based control, is that the rule thresholds might be case-dependent and thus need to be carefully selected for the specific use case.

Limitations of the proposed hierarchical load scheduling framework mainly lie in that all load models (e.g., HVAC system) have been linearized for the reduction of the computational effort, which can be improved in the future. Further, the decentralized MPC problem was not solved iteratively with data exchanged between the two layers. This is reasonable in this work because the same model was used for both prediction and evaluation. However, for more realistic cases, the problem should be solved iteratively with information exchanged at every timestep to better account for uncertainties. The limitation of the BAL is that though different objective functions, such as minimizing unserved load ratio and minimizing thermal discomfort, were compared, multi-objective optimizations were not implemented due to the time limit. Further, the application of this framework to normal grid-connected scenarios was not investigated.

In terms of the uncertainty impact studies, because the proposed uncertainty method mainly deals with the uncertainty through the temperature constraints, it can be less effective for buildings of larger thermal mass due to the insensitivity to temperature constraints. Also, the plant-model mismatch was noticed in the controller testing phase, which is a common parametric uncertainty that originates from neglected dynamics of the plant [216]. Finally, we used the thermostat changing models developed based on data from private office spaces in different building types, which can be debatable. We note that the building types that we studied in this work were not necessarily the most representative, because for ice cream shops and bakeries, the largest portion of load (e.g., refrigeration and baking) does not rely on occupant behavior. However, the methodology proposed in this work can be transferred to and evaluated on other building types.

7.3 Future work

Future work to better facilitate community decarbonization includes: Investigating better designs of the decarbonization control rules to achieve synergetic emission, energy, and cost reductions. Incorporating other types of controllable loads such as schedulable loads into the carbon emission responsive control framework. Comparing the performance of the developed rule-based control to optimization-based control. Incorporating real-time electricity pricing rates for the cost analysis to better reflect the relationship between carbon intensity and electricity price (i.e., lower intensity, lower price). Conducting lifecycle cost analysis for the controlled equipment to account for the impact of equipment short cycling on equipment life and

replacement cost. Discussing the trade-off between the reduction of operational carbon emissions and the potential sacrificing of equipment energy efficiency.

For improving the hierarchical control framework, future directions involve conducting multi-objective optimization for the building agent layer to investigate the trade-off between minimizing unserved load ratio and maximizing thermal comfort. The inclusion of other objectives such as decarbonization and minimizing energy costs for normal operation scenarios is also a promising direction. Uncertainty of PV generation should also be included to reflect the impact of different weather conditions. Nonlinear models for controllable devices could be incorporated into the framework to better reflect the system dynamics in the future.

In terms of the uncertainty study of occupant behavior in scheduling, future work includes extending the scope to heating scenarios to further generalize the findings. Additionally, real-time stochastic MPC control techniques with occupant behavior models could be integrated into the framework to overcome the lack of flexibility in *a priori* designed controllers.

Bibliography

[1] European Commission. Paris Agreement. https://ec.europa.eu/clima/policies/international/negotiations/paris_en (accessed Aug 29, 2021).

[2] The White House. FACT SHEET: President Biden Sets 2030 Greenhouse Gas Pollution Reduction Target Aimed at Creating Good-Paying Union Jobs and Securing U.S. Leadership on Clean Energy Technologies. https://www.whitehouse.gov/briefing-room/statements-releases/2021/04/22/fact-sheet-president-biden-sets-2030-greenhouse-gas-pollution-reduction-target-aimed-at-creating-good-paying-union-jobs-and-securing-u-s-leadership-on-clean-energy-technologies/ (accessed Oct 8, 2021).

[3] Xinhua Net. Xinhua Headlines: World's largest carbon trading market opens in Shanghai. http://www.xinhuanet.com/english/2021-07/17/c_1310066020.htm (accessed Aug 29, 2021).

[4] The Texas Tribune. Winter Storm 2021. https://www.texastribune.org/series/winter-storm-power-outage/ (accessed Apr 1, 2021).

[5] Campbell, A. F. It took 11 months to restore power to Puerto Rico after Hurricane Maria. A similar crisis could happen again. https://www.vox.com/identities/2018/8/15/17692414/puerto-rico-power-electricity-restored-hurricane-maria (accessed Apr 17, 2020).

[6] Satchwell, A.; Piette, M. A.; Khandekar, A.; Granderson, J.; Frick, N. M.; Hledik, R.; Faruqui, A.; Lam, L.; Ross, S.; Cohen, J. A National Roadmap for Grid-Interactive Efficient Buildings. **2021**.

[7] Xiang, Y.; Cai, H.; Liu, J.; Zhang, X. Techno-Economic Design of Energy Systems for Airport Electrification: A Hydrogen-Solar-Storage Integrated Microgrid Solution. Appl. Energy, **2021**, 283, 116374.

[8] Péan, T.; Costa-Castelló, R.; Salom, J. Price and Carbon-Based Energy Flexibility of Residential Heating and Cooling Loads Using Model Predictive Control. Sustain. Cities Soc., **2019**, 50, 101579.

[9] Olivieri, Z. T.; McConky, K. Optimization of Residential Battery Energy Storage System Scheduling for Cost and Emissions Reductions. Energy Build., **2020**, 210, 109787.

[10] Ghazzai, H.; Kadri, A. Joint Demand-Side Management in Smart Grid for Green Collaborative Mobile Operators under Dynamic Pricing and Fairness Setup. IEEE Trans. Green Commun. Netw., **2016**, 1 (1), 74–88.

[11] Renugadevi, T.; Geetha, K.; Muthukumar, K.; Geem, Z. W. Optimized Energy Cost and Carbon Emission-Aware Virtual Machine Allocation in Sustainable Data Centers. Sustainability, **2020**, 12 (16), 6383.

[12] Gasser, J.; Cai, H.; Karagiannopoulos, S.; Heer, P.; Hug, G. Predictive Energy Management of Residential Buildings While Self-Reporting Flexibility Envelope. Appl. Energy, **2021**, 288, 116653.

[13] Yan, D.; O'Brien, W.; Hong, T.; Feng, X.; Gunay, H. B.; Tahmasebi, F.; Mahdavi, A. Occupant Behavior Modeling for Building Performance Simulation: Current State and Future Challenges. Energy Build., **2015**, 107, 264–278.

[14] Warren, P. R.; Parkins, L. M. Window-Opening Behaviour in Office Buildings. Build. Serv. Eng. Res. Technol., **1984**, 5 (3), 89–101.

[15] Wang, J.; Fu, Y.; Huang, S.; Zuo, W. Net-Zero Energy Community Library https://bitbucket.org/sbslab-zuo/scc-nzec/branch/release/V1.1 (accessed Aug 30, 2021).

[16] Huang, S.; Wang, J.; Fu, Y.; Zuo, W.; Hinkelman, K.; Kaiser, M. R.; He, D.; Vrabie, D. An Open-Source Virtual Testbed for a Real Net-Zero Energy Community. Sustain. Cities Soc., **2021**, 103255.

[17] Hong, T.; Chen, Y.; Luo, X.; Luo, N.; Lee, S. H. Ten Questions on Urban Building Energy Modeling. Build. Environ., **2020**, 168, 106508.

[18] Lu, X.; Hinkelman, K.; Fu, Y.; Wang, J.; Zuo, W.; Zhang, Q.; Saad, W. An Open Source Modeling Framework for Interdependent Energy-Transportation-Communication Infrastructure in Smart and Connected Communities. IEEE Access, **2019**, 7, 55458–55476.

[19] Hinkelman, K.; Wang, J.; Zuo, W.; Gautier, A.; Wetter, M.; Fan, C.; Long, N. Modelica-Based Modeling and Simulation of District Cooling Systems: A Case Study; engrXiv, 2021.

[20] Hinkelman, K.; Wang, J.; Fan, C.; Zuo, W.; Gautier, A.; Wetter, M.; Long, N. A Case Study on Condenser Water Supply Temperature Optimization with a District Cooling Plant. In 14th International Modelica Conference; engrXiv, 2021.

[21] Hinkelman, K.; Huang, S.; Wang, J.; Lian, J.; Zuo, W. Enhancing the Implementation of a First-Order Equivalent Thermal Parameter Model to Enable Accurate and Robust Building Thermal Response Prediction. In Proceeding of the 16th Conference of International Building Performance Simulation Association (Building Simulation

2019); 2019.

[22] Polly, B.; El Kontar, R.; Charan, T.; Fleming, K.; Moore, N.; Goldwasser, D.; Long, N. URBANopt: An Open-Source Software Development Kit for Community and Urban District Energy Modeling; National Renewable Energy Lab.(NREL), Golden, CO (United States), 2020.

[23] Anderson, K. H.; Cutler, D. S.; Olis, D. R.; Elgqvist, E. M.; Li, X.; Laws, N. D.; DiOrio, N. A.; Walker, H. A. REopt: A Platform for Energy System Integration and Optimization; National Renewable Energy Lab.(NREL), Golden, CO (United States), 2017.

[24] Electric Power Research Institute. OpenDSS. 2021.

[25] Ali, U.; Shamsi, M. H.; Bohacek, M.; Purcell, K.; Hoare, C.; Mangina, E.; O'Donnell, J. A Data-Driven Approach for Multi-Scale GIS-Based Building Energy Modeling for Analysis, Planning and Support Decision Making. Appl. Energy, **2020**, 279, 115834.

[26] Yu, H.; Wang, M.; Lin, X.; Guo, H.; Liu, H.; Zhao, Y.; Wang, H.; Li, C.; Jing, R. Prioritizing Urban Planning Factors on Community Energy Performance Based on GIS-Informed Building Energy Modeling. Energy Build., **2021**, 249, 111191.

[27] The Modelica Association. Modelica. 2019.

[28] Wetter, M.; Bonvini, M.; Nouidui, T. S. Equation-Based Languages–A New Paradigm for Building Energy Modeling, Simulation and Optimization. Energy Build., **2016**, 117, 290–300.

[29] Wanner, G.; Hairer, E. Solving Ordinary Differential Equations II; Springer Berlin Heidelberg, 1996; Vol. 375.

[30] Zhou, G.; Ye, Y.; Wang, J.; Zuo, W.; Fu, Y.; Zhou, X. Modeling Air-to-Air Plate-Fin Heat Exchanger without Dehumidification. Appl. Therm. Eng., **2018**, 143, 137–148.

[31] Wang, J.; Huang, S.; Zuo, W. Cyber-Physical System Modeling Using Modelica for Smart and Sustainable Communities. In American Modelica Conference 2020 - Modelica Workshop; 2020.

[32] Clevenger, C. M.; Haymaker, J. The Impact of the Building Occupant on Energy Modeling Simulations. In Joint International Conference on Computing and Decision Making in Civil and Building Engineering, Montreal, Canada; Citeseer, 2006; pp 1–10.

[33] Wang, J.; Ye, Y.; Zuo, W.; New, J.; Rose, A. City-Scale Building Occupancy Prediction Using Geographic Information System Data; engrXiv, 2021.

[34] Hoes, P.; Hensen, J. L. M.; Loomans, M. G. L. C.; de Vries, B.; Bourgeois, D. User Behavior in Whole Building Simulation. Energy Build., **2009**, 41 (3), 295–302.

[35] Yan, D.; Hong, T. EBC Annex 66 Final Report-Definition and Simulation of Occupant Behavior in Buildings. **2018**.

[36] Wilke, U.; Haldi, F.; Scartezzini, J.-L.; Robinson, D. A Bottom-up Stochastic Model to Predict Building Occupants' Time-Dependent Activities. Build. Environ., **2013**, 60, 254–264.

[37] Erickson, V. L.; Lin, Y.; Kamthe, A.; Brahme, R.; Surana, A.; Cerpa, A. E.; Sohn, M. D.; Narayanan, S. Energy Efficient Building Environment Control Strategies Using Real-Time Occupancy Measurements. In Proceedings of the First ACM Workshop on Embedded Sensing Systems for Energy-Efficiency in Buildings; 2009; pp 19–24.

[38] D'Oca, S.; Hong, T. Occupancy Schedules Learning Process through a Data Mining Framework. Energy Build., **2015**, 88, 395–408.

[39] Energy in Buildings and Communities Programme (EBC). IEA-EBC Annex 66 Definition and Simulation of Occupant Behavior in Buildings https://annex66.org/ (accessed Apr 17, 2020).

[40] Page, J.; Robinson, D.; Morel, N.; Scartezzini, J.-L. A Generalised Stochastic Model for the Simulation of Occupant Presence. Energy Build., **2008**, 40 (2), 83–98.

[41] Dong, B.; Andrews, B.; Lam, K. P.; Höynck, M.; Zhang, R.; Chiou, Y.-S.; Benitez, D. An Information Technology Enabled Sustainability Test-Bed (ITEST) for Occupancy Detection through an Environmental Sensing Network. Energy Build., **2010**, 42 (7), 1038–1046.

[42] Richardson, I.; Thomson, M.; Infield, D. A High-Resolution Domestic Building Occupancy Model for Energy Demand Simulations. Energy Build., **2008**, 40 (8), 1560–1566.

[43] Andersen, P. D.; Iversen, A.; Madsen, H.; Rode, C. Dynamic Modeling of Presence of Occupants Using Inhomogeneous Markov Chains. Energy Build., **2014**, 69, 213–223.

[44] Wang, D.; Federspiel, C. C.; Rubinstein, F. Modeling Occupancy in Single Person Offices. Energy Build., **2005**, 37 (2), 121–126.

[45] Lawrence Berkeley National Laboratory. Modelica Buildings Library V6.0.0: Buildings.Occupants Package https://github.com/lbl-srg/modelica-buildings/tree/master/Buildings/Occupants (accessed Apr 17, 2020).

[46] Tahmasebi, F.; Mahdavi, A. The Sensitivity of Building Performance Simulation Results to the Choice of Occupants' Presence Models: A Case Study. J. Build. Perform. Simul., **2017**, 10 (5–6), 625–635.

[47] Zhou, X.; Yan, D.; Hong, T.; Ren, X. Data Analysis and Stochastic Modeling of Lighting Energy Use in Large Office Buildings in China. Energy Build., **2015**, 86, 275–287.

[48] Hunt, D. R. G. Predicting Artificial Lighting Use-a Method Based upon Observed Patterns of Behaviour. Light. Res. Technol., **1980**, 12 (1), 7–14.

[49] Newsham, G. R. Manual Control of Window Blinds and Electric Lighting: Implications for Comfort and Energy Consumption. Indoor Environ., **1994**, 3 (3), 135–144.

[50] Reinhart, C. F. Lightswitch-2002: A Model for Manual and Automated Control of Electric Lighting and Blinds. Sol. energy, **2004**, 77 (1), 15–28.

[51] Widén, J.; Nilsson, A. M.; Wäckelgård, E. A Combined Markov-Chain and Bottom-up Approach to Modelling of Domestic Lighting Demand. Energy Build., **2009**, 41 (10), 1001–1012.

[52] Love, J. A. Manual Switching Patterns in Private Offices. Int. J. Light. Res. Technol., **1998**, 30 (1), 45–50.

[53] Pigg, S.; Eilers, M.; Reed, J.; Works, T.; Pigg, S.; Eilers, M.; Reed, J. Behavioral Aspects of Lighting and Occupancy Sensors in Private Offices: A Case Study of a University Office Building. ACEEE 1996 Summer Study Energy Effic. Build., **1996**, No. 8, 161–170.

[54] Reinhart, C. F.; Voss, K. Monitoring Manual Control of Electric Lighting and Blinds. Light. Res. Technol., **2003**, 35 (3), 243–258.

[55] Gunay, H. B.; O'Brien, W.; Beausoleil-Morrison, I. Implementation and Comparison of Existing Occupant Behaviour Models in EnergyPlus. J. Build. Perform. Simul., **2016**, 9 (6), 567–588.

[56] Boyce, P. R.; Veitch, J. A.; Newsham, G. R.; Jones, C. C.; Heerwagen, J.; Myer, M.; Hunter, C. M. Occupant Use of Switching and Dimming Controls in Offices. Light. Res. Technol., **2006**, 38 (4), 358–376.

[57] Ecobee. Donate Your Data https://www.ecobee.com/donateyourdata/ (accessed Apr 17, 2020).

[58] Ren, X.; Yan, D.; Wang, C. Air-Conditioning Usage Conditional Probability Model for Residential Buildings. Build. Environ., **2014**, 81, 172–182.

[59] Corgnati, S. P.; D'Oca, S.; Fabi, V.; Andersen, R. K. Leverage of Behavioural Patterns of Window Opening and Heating Set Point Adjustments on Energy Consumption and Thermal Comfort in Residential Buildings. In Proceedings of the 8th International Symposium on Heating, Ventilation and Air Conditioning; Springer, 2014; pp 23–31.

[60] Gunay, H. B.; O'Brien, W.; Beausoleil-Morrison, I.; Bursill, J. Development and Implementation of a Thermostat Learning Algorithm. Sci. Technol. Built Environ., **2018**, 24 (1), 43–56.

[61] Haldi, F.; Robinson, D. On the Behaviour and Adaptation of Office Occupants. Build. Environ., **2008**, 43 (12), 2163–2177.

[62] Sun, K.; Hong, T. A Simulation Approach to Estimate Energy Savings Potential of Occupant Behavior Measures. Energy Build., **2017**, 136, 43–62.

[63] Hong, T.; D'Oca, S.; Taylor-Lange, S. C.; Turner, W. J. N.; Chen, Y.; Corgnati, S. P. An Ontology to Represent Energy-Related Occupant Behavior in Buildings. Part II: Implementation of the DNAS Framework Using an XML Schema. Build. Environ.,

2015, 94, 196–205.

[64] Hong, T.; D'Oca, S.; Turner, W. J. N.; Taylor-Lange, S. C. An Ontology to Represent Energy-Related Occupant Behavior in Buildings. Part I: Introduction to the DNAs Framework. Build. Environ., **2015**, 92, 764–777.

[65] Grandjean, A.; Adnot, J.; Binet, G. A Review and an Analysis of the Residential Electric Load Curve Models. Renew. Sustain. energy Rev., **2012**, 16 (9), 6539–6565.

[66] Swan, L. G.; Ugursal, V. I. Modeling of End-Use Energy Consumption in the Residential Sector: A Review of Modeling Techniques. Renew. Sustain. energy Rev., **2009**, 13 (8), 1819–1835.

[67] Tanimoto, J.; Hagishima, A.; Sagara, H. A Methodology for Peak Energy Requirement Considering Actual Variation of Occupants' Behavior Schedules. Build. Environ., **2008**, 43 (4), 610–619.

[68] Widén, J.; Wäckelgård, E. A High-Resolution Stochastic Model of Domestic Activity Patterns and Electricity Demand. Appl. Energy, **2010**, 87 (6), 1880–1892.

[69] Capasso, A.; Grattieri, W.; Lamedica, R.; Prudenzi, A. A Bottom-up Approach to Residential Load Modeling. IEEE Trans. power Syst., **1994**, 9 (2), 957–964.

[70] Gottwalt, S.; Ketter, W.; Block, C.; Collins, J.; Weinhardt, C. Demand Side Management—A Simulation of Household Behavior under Variable Prices. Energy Policy, **2011**, 39 (12), 8163–8174.

[71] Yamaguchi, Y.; Shimoda, Y.; Mizuno, M. Development of District Energy System Simulation Model Based on Detailed Energy Demand Model. In Proceeding of Eighth International IBPSA Conference; 2003; pp 1443–1450.

[72] Paatero, J. V; Lund, P. D. A Model for Generating Household Electricity Load Profiles. Int. J. Energy Res., **2006**, 30 (5), 273–290.

[73] Yilmaz, S.; Firth, S. K.; Allinson, D. Occupant Behaviour Modelling in Domestic Buildings: The Case of Household Electrical Appliances. J. Build. Perform. Simul., **2017**, 10 (5–6), 582–600.

[74] Page, J. Simulating Occupant Presence and Behaviour in Buildings; EPFL, 2007.

[75] Gunay, H. B.; O'Brien, W.; Beausoleil-Morrison, I.; Gilani, S. Modeling Plug-in Equipment Load Patterns in Private Office Spaces. Energy Build., **2016**, 121, 234–249.

[76] Wang, C.; Yan, D.; Jiang, Y. A Novel Approach for Building Occupancy Simulation. In Building simulation; Springer, 2011; Vol. 4, pp 149–167.

[77] Mahdavi, A.; Tahmasebi, F.; Kayalar, M. Prediction of Plug Loads in Office Buildings: Simplified and Probabilistic Methods. Energy Build., **2016**, 129, 322–329.

[78] Wang, Z.; Ding, Y. An Occupant-Based Energy Consumption Prediction Model for

Office Equipment. Energy Build., **2015**, 109, 12–22.

[79] US Energy Information Administration. U.S. Energy-Related Carbon Dioxide Emissions, 2019; 2020.

[80] Legorburu, G.; Smith, A. D. Incorporating Observed Data into Early Design Energy Models for Life Cycle Cost and Carbon Emissions Analysis of Campus Buildings. Energy Build., **2020**, 224, 110279.

[81] Cang, Y.; Luo, Z.; Yang, L.; Han, B. A New Method for Calculating the Embodied Carbon Emissions from Buildings in Schematic Design: Taking "Building Element" as Basic Unit. Build. Environ., **2020**, 185, 107306.

[82] Almeida, M.; Ferreira, M. Ten Questions Concerning Cost-Effective Energy and Carbon Emissions Optimization in Building Renovation. Build. Environ., **2018**, 143, 15–23.

[83] Garriga, S. M.; Dabbagh, M.; Krarti, M. Optimal Carbon-Neutral Retrofit of Residential Communities in Barcelona, Spain. Energy Build., **2020**, 208, 109651.

[84] Langevin, J.; Harris, C. B.; Reyna, J. L. Assessing the Potential to Reduce US Building CO2 Emissions 80% by 2050. Joule, **2019**, 3 (10), 2403–2424.

[85] Fathy, A.; Salib, A.; Krarti, M. Transitioning From Net-Zero Energy Homes to Carbon-Neutral Grid-Connected Communities. J. Eng. Sustain. Build. Cities, **2020**, 1 (4), 41003.

[86] Lou, Y.; Yang, Y.; Ye, Y.; Zuo, W.; Wang, J. The Effect of Building Retrofit Measures on CO2 Emissions Reduction–A Case Study with US Medium Office Buildings; 2021.

[87] Jin, X.; Baker, K.; Christensen, D.; Isley, S. Foresee: A User-Centric Home Energy Management System for Energy Efficiency and Demand Response. Appl. Energy, **2017**, 205, 1583–1595.

[88] Leerbeck, K.; Bacher, P.; Junker, R. G.; Tveit, A.; Corradi, O.; Madsen, H.; Ebrahimy, R. Control of Heat Pumps with CO2 Emission Intensity Forecasts. Energies, **2020**, 13 (11), 2851.

[89] Clauß, J.; Stinner, S.; Sartori, I.; Georges, L. Predictive Rule-Based Control to Activate the Energy Flexibility of Norwegian Residential Buildings: Case of an Air-Source Heat Pump and Direct Electric Heating. Appl. Energy, **2019**, 237, 500–518.

[90] Holling, C. S. Resilience and Stability of Ecological Systems. Annu. Rev. Ecol. Syst., **1973**, 4 (1), 1–23.

[91] Cutter, S. L.; Ash, K. D.; Emrich, C. T. The Geographies of Community Disaster Resilience. Glob. Environ. Chang., **2014**, 29, 65–77.

[92] Bocchini, P.; Frangopol, D. M.; Ummenhofer, T.; Zinke, T. Resilience and Sustainability of Civil Infrastructure: Toward a Unified Approach. J. Infrastruct. Syst.,

2014, 20 (2), 4014004.

[93] Gama Dessavre, D.; Ramirez-Marquez, J. E.; Barker, K.; Dessavre, D. G.; Ramirez-Marquez, J. E.; Barker, K. Multidimensional Approach to Complex System Resilience Analysis. Reliab. Eng. Syst. Saf., **2016**, 149, 34–43.

[94] Bie, Z.; Lin, Y.; Li, G.; Li, F. Battling the Extreme: A Study on the Power System Resilience. Proc. IEEE, **2017**, 105 (7), 1253–1266.

[95] Watson, J.-P.; Guttromson, R.; Silva-Monroy, C.; Jeffers, R.; Jones, K.; Ellison, J.; Rath, C.; Gearhart, J.; Jones, D.; Corbet, T. Conceptual Framework for Developing Resilience Metrics for the Electricity Oil and Gas Sectors in the United States. Sandia Natl. Lab. Albuquerque, NM (United States), Tech. Rep, **2014**.

[96] Hosseini, S.; Barker, K.; Ramirez-Marquez, J. E. A Review of Definitions and Measures of System Resilience. Reliab. Eng. Syst. Saf., **2016**, 145, 47–61.

[97] Francis, R.; Bekera, B. A Metric and Frameworks for Resilience Analysis of Engineered and Infrastructure Systems. Reliab. Eng. Syst. Saf., **2014**, 121, 90–103.

[98] Carlson, J. L.; Haffenden, R. A.; Bassett, G. W.; Buehring, W. A.; Collins III, M. J.; Folga, S. M.; Petit, F. D.; Phillips, J. A.; Verner, D. R.; Whitfield, R. G. Resilience: Theory and Application.; Argonne National Lab.(ANL), Argonne, IL (United States), 2012.

[99] Meerow, S.; Newell, J. P.; Stults, M. Defining Urban Resilience: A Review. Landsc. Urban Plan., **2016**, 147, 38–49.

[100] Razafindrabe, B. H. N.; Parvin, G. A.; Surjan, A.; Takeuchi, Y.; Shaw, R. Climate Disaster Resilience: Focus on Coastal Urban Cities in Asia. Asian J. Environ. Disaster Manag. - Focus. Pro-active Risk Reduct. Asia, **2009**, 01 (01), 101.

[101] McManus, S.; Seville, E.; Brunsden, D.; Vargo, J. Resilience Management: A Framework for Assessing and Improving the Resilience of Organisations. **2007**.

[102] Roege, P. E.; Collier, Z. A.; Mancillas, J.; McDonagh, J. A.; Linkov, I. Metrics for Energy Resilience. Energy Policy, **2014**, 72, 249–256.

[103] Huang, C.-N.; Liou, J. J. H.; Chuang, Y.-C. A Method for Exploring the Interdependencies and Importance of Critical Infrastructures. Knowledge-Based Syst., **2014**, 55, 66–74.

[104] Buldyrev, S. V; Parshani, R.; Paul, G.; Stanley, H. E.; Havlin, S. Catastrophic Cascade of Failures in Interdependent Networks. Nature, **2010**, 464 (7291), 1025–1028.

[105] Bollinger, L. A. Evolving Climate-Resilient Energy Infrastructures; TU Delft, 2011.

[106] Arif, A.; Wang, Z.; Wang, J.; Chen, C. Power Distribution System Outage Management with Co-Optimization of Repairs, Reconfiguration, and DG Dispatch. IEEE Trans. Smart Grid, **2017**, 9 (5), 4109–4118.

[107] Yuan, W.; Wang, J.; Qiu, F.; Chen, C.; Kang, C.; Zeng, B. Robust Optimization-Based Resilient Distribution Network Planning Against Natural Disasters. IEEE Trans. Smart Grid, **2016**, 7 (6), 2817–2826.

[108] Ding, T.; Lin, Y.; Li, G.; Bie, Z. A New Model for Resilient Distribution Systems by Microgrids Formation. IEEE Trans. Power Syst., **2017**, 32 (5), 4145–4147.

[109] Liu, Z.; Chen, Y.; Zhuo, R.; Jia, H. Energy Storage Capacity Optimization for Autonomy Microgrid Considering CHP and EV Scheduling. Appl. Energy, **2018**, 210, 1113–1125.

[110] Manshadi, S. D.; Khodayar, M. E. Resilient Operation of Multiple Energy Carrier Microgrids. IEEE Trans. Smart Grid, **2015**, 6 (5), 2283–2292.

[111] Dudenhoeffer, D. D.; Permann, M. R.; Manic, M. CIMS: A Framework for Infrastructure Interdependency Modeling and Analysis. In Proceedings of the 2006 winter simulation conference; IEEE, 2006; pp 478–485.

[112] Pederson, P.; Dudenhoeffer, D.; Hartley, S.; Permann, M. Critical Infrastructure Interdependency Modeling: A Survey of US and International Research. Idaho Natl. Lab., **2006**, 25, 27.

[113] Keirstead, J.; Samsatli, N.; Shah, N. SynCity: An Integrated Tool Kit for Urban Energy Systems Modelling. Energy Effic. cities Assess. tools benchmarking Pract., **2010**, 21–42.

[114] Li, G.; Bie, Z.; Kou, Y.; Jiang, J.; Bettinelli, M. Reliability Evaluation of Integrated Energy Systems Based on Smart Agent Communication. Appl. Energy, **2016**, 167, 397–406.

[115] Bompard, E.; Napoli, R.; Xue, F. Analysis of Structural Vulnerabilities in Power Transmission Grids. Int. J. Crit. Infrastruct. Prot., **2009**, 2 (1–2), 5–12.

[116] Ji, C.; Wei, Y.; Mei, H.; Calzada, J.; Carey, M.; Church, S.; Hayes, T.; Nugent, B.; Stella, G.; Wallace, M. Large-Scale Data Analysis of Power Grid Resilience across Multiple US Service Regions. Nat. Energy, **2016**, 1 (5), 1–8.

[117] Larsen, P. H.; LaCommare, K. H.; Eto, J. H.; Sweeney, J. L. Assessing Changes in the Reliability of the US Electric Power System. **2015**.

[118] Erdener, B. C.; Pambour, K. A.; Lavin, R. B.; Dengiz, B. An Integrated Simulation Model for Analysing Electricity and Gas Systems. Int. J. Electr. Power Energy Syst., **2014**, 61, 410–420.

[119] Chen, C.; Wang, J.; Qiu, F.; Zhao, D. Resilient Distribution System by Microgrids Formation after Natural Disasters. IEEE Trans. Smart Grid, **2015**, 7 (2), 958–966.

[120] Yuan, C.; Ng, E.; Norford, L. K. Improving Air Quality in High-Density Cities by Understanding the Relationship between Air Pollutant Dispersion and Urban Morphologies. Build. Environ., **2014**, 71, 245–258.

[121] Panteli, M.; Mancarella, P. Modeling and Evaluating the Resilience of Critical Electrical Power Infrastructure to Extreme Weather Events. IEEE Syst. J., **2015**, 11 (3), 1733–1742.

[122] Cadini, F.; Agliardi, G. L.; Zio, E. A Modeling and Simulation Framework for the Reliability/Availability Assessment of a Power Transmission Grid Subject to Cascading Failures under Extreme Weather Conditions. Appl. Energy, **2017**, 185, 267–279.

[123] Chen, B.; Chen, C.; Wang, J.; Butler-Purry, K. L. Sequential Service Restoration for Unbalanced Distribution Systems and Microgrids. IEEE Trans. Power Syst., **2017**, 33 (2), 1507–1520.

[124] Nezamoddini, N.; Mousavian, S.; Erol-Kantarci, M. A Risk Optimization Model for Enhanced Power Grid Resilience against Physical Attacks. Electr. Power Syst. Res., **2017**, 143, 329–338.

[125] Chen, G.; Dong, Z. Y.; Hill, D. J.; Zhang, G. H. An Improved Model for Structural Vulnerability Analysis of Power Networks. Phys. A Stat. Mech. its Appl., **2009**, 388 (19), 4259–4266.

[126] Page, J.; Basciotti, D.; Pol, O.; Fidalgo, J. N.; Couto, M.; Aron, R.; Chiche, A.; Fournié, L. A Multi-Energy Modeling, Simulation and Optimization Environment for Urban Energy Infrastructure Planning. In Proceedings of the 13th conference of international building performance simulation association, Chambéry, France; 2013; pp 26–28.

[127] Hines, P.; Cotilla-Sanchez, E.; Blumsack, S. Do Topological Models Provide Good Information about Electricity Infrastructure Vulnerability? Chaos An Interdiscip. J. Nonlinear Sci., **2010**, 20 (3), 33122.

[128] Chen, G.; Dong, Z. Y.; Hill, D. J.; Zhang, G. H.; Hua, K. Q. Attack Structural Vulnerability of Power Grids: A Hybrid Approach Based on Complex Networks. Phys. A Stat. Mech. its Appl., **2010**, 389 (3), 595–603.

[129] Lin, Y.; Bie, Z. Tri-Level Optimal Hardening Plan for a Resilient Distribution System Considering Reconfiguration and DG Islanding. Appl. Energy, **2018**, 210, 1266–1279.

[130] Wooldridge, M.; Jennings, N. R. Intelligent Agents: Theory and Practice. Knowl. Eng. Rev., **1995**, 10 (2), 115–152.

[131] Bonabeau, E. Agent-Based Modeling: Methods and Techniques for Simulating Human Systems. Proc. Natl. Acad. Sci., **2002**, 99 (suppl 3), 7280–7287.

[132] Reynolds, C. W. Flocks, Herds and Schools: A Distributed Behavioral Model. In Proceedings of the 14th annual conference on Computer graphics and interactive techniques; 1987; pp 25–34.

[133] Casalicchio, E.; Galli, E.; Tucci, S. Agent-Based Modelling of Interdependent Critical Infrastructures. Int. J. Syst. Syst. Eng., **2010**, 2 (1), 60–75.

[134] Zhou, Z.; Zhao, F.; Wang, J. Agent-Based Electricity Market Simulation With Demand

Response From Commercial Buildings. IEEE Trans. Smart Grid, **2011**, 2, 580–588.

[135] Solanki, J. M.; Khushalani, S.; Schulz, N. N. A Multi-Agent Solution to Distribution Systems Restoration. IEEE Trans. Power Syst., **2007**, 22 (3), 1026–1034.

[136] Solanki, J.; Solanki, S.; Schulz, N. Multi-Agent-Based Reconfiguration for Restoration of Distribution Systems with Distributed Generators. Integr. Comput. Aided. Eng., **2010**, 17, 331–346.

[137] Zhang, P.; Peeta, S. A Generalized Modeling Framework to Analyze Interdependencies among Infrastructure Systems. Transp. Res. Part B Methodol., **2011**, 45 (3), 553–579.

[138] Farzin, H.; Fotuhi-Firuzabad, M.; Moeini-Aghtaie, M. Role of Outage Management Strategy in Reliability Performance of Multi-Microgrid Distribution Systems. IEEE Trans. Power Syst., **2017**, 33 (3), 2359–2369.

[139] Fishman, G. Monte Carlo: Concepts, Algorithms, and Applications; Springer Science & Business Media, 2013.

[140] Kroese, D. P.; Brereton, T.; Taimre, T.; Botev, Z. I. Why the Monte Carlo Method Is so Important Today. WIREs Comput. Stat. , **2014**, 6 (6), 386–392.

[141] Li, G.; Zhang, P.; Luh, P. B.; Li, W.; Bie, Z.; Serna, C.; Zhao, Z. Risk Analysis for Distribution Systems in the Northeast US under Wind Storms. IEEE Trans. Power Syst., **2013**, 29 (2), 889–898.

[142] Gillette, J. L.; Fisher, R. E.; Peerenboom, J. P.; Whitfield, R. G. Analyzing Water/Wastewater Infrastructure Interdependencies.; Argonne National Lab., IL (US), 2002.

[143] Toole, G. L.; McCown, A. W. Interdependent Energy Infrastructure Simulation System. Wiley Handbook of Science and Technology for Homeland Security. January 1, 2008, p 1.

[144] Yan, S. C.; D., S. C.; Lucio, S.; Scott, M. H.; H., G. J.; Keith, D.; Sandra, M. Data Management for Geospatial Vulnerability Assessment of Interdependencies in U.S. Power Generation. J. Infrastruct. Syst., **2009**, 15 (3), 179–189.

[145] Kirkwood, C. W. System Dynamics Methods. Coll. Bus. Arizona State Univ. USA, **1998**.

[146] Scott, G. Protecting the Nation http://www.ga.gov.au/ausgeonews/ausgeonews200509/cip.jsp (accessed Nov 8, 2021).

[147] ten Raa, T. Input-Output Economics: Theory and Applications; WORLD SCIENTIFIC, 2009.

[148] Historic Green Village. Historic Green Village https://www.historicgreenvillage.com/ (accessed Apr 11, 2019).

[149] Li, P.; Li, Y.; Seem, J. E.; Qiao, H.; Li, X.; Winkler, J. Recent Advances in Dynamic

Modeling of HVAC Equipment. Part 2: Modelica-Based Modeling. HVAC&R Res., **2014**, 20 (1), 150–161.

[150] Wetter, M.; Zuo, W.; Nouidui, T. S.; Pang, X. Modelica Buildings Library. J. Build. Perform. Simul., **2014**, 7 (4), 253–270.

[151] He, D.; Huang, S.; Zuo, W.; Kaiser, R. Towards to the Development of Virtual Testbed for Net Zero Energy Communities. In SimBuild 2016: Building Performance Modeling Conference; Salt Lake City, UT, USA, 2016; Vol. 6.

[152] Wang, J.; Zuo, W.; Rhode-Barbarigos, L.; Lu, X.; Wang, J.; Lin, Y. Literature Review on Modeling and Simulation of Energy Infrastructures from a Resilience Perspective. Reliab. Eng. Syst. Saf., **2019**, 183, 360–373.

[153] Wu, D.; Hao, H.; Fu, T.; Kalsi, K. Regional Assessment of Virtual Battery Potential from Building Loads. In 2018 IEEE/PES Transmission and Distribution Conference and Exposition (T&D); 2018; pp 1–5.

[154] Zhao, L.; Zhang, W.; Hao, H.; Kalsi, K. A Geometric Approach to Aggregate Flexibility Modeling of Thermostatically Controlled Loads. IEEE Trans. Power Syst., **2017**, 32 (6), 4721–4731.

[155] Luo, X.; Lam, K. P.; Chen, Y.; Hong, T. Performance Evaluation of an Agent-Based Occupancy Simulation Model. Build. Environ., **2017**, 115, 42–53.

[156] Kim, Y.-S.; Heidarinejad, M.; Dahlhausen, M.; Srebric, J. Building Energy Model Calibration with Schedules Derived from Electricity Use Data. Appl. Energy, **2017**, 190, 997–1007.

[157] Chawla, N. V; Bowyer, K. W.; Hall, L. O.; Kegelmeyer, W. P. SMOTE: Synthetic Minority over-Sampling Technique. J. Artif. Intell. Res., **2002**, 16, 321–357.

[158] ASHRAE. ASHRAE Guideline 14-2002: Measurement Of Energy And Demand Savings; 2002.

[159] Zhang, X.; Wang, Y. How to Reduce Household Carbon Emissions: A Review of Experience and Policy Design Considerations. Energy Policy, **2017**, 102, 116–124.

[160] Alimohammadisagvand, B.; Jokisalo, J.; Sirén, K. Comparison of Four Rule-Based Demand Response Control Algorithms in an Electrically and Heat Pump-Heated Residential Building. Appl. Energy, **2018**, 209, 167–179.

[161] Fischer, D.; Madani, H. On Heat Pumps in Smart Grids: A Review. Renew. Sustain. Energy Rev., **2017**, 70, 342–357.

[162] Palmintier, B.; Krishnamurthy, D.; Top, P.; Smith, S.; Daily, J.; Fuller, J. Design of the HELICS High-Performance Transmission-Distribution-Communication-Market Co-Simulation Framework. In 2017 Workshop on Modeling and Simulation of Cyber-Physical Energy Systems (MSCPES); IEEE, 2017; pp 1–6.

[163] Blonsky, M.; Maguire, J.; McKenna, K.; Cutler, D.; Balamurugan, S. P.; Jin, X. OCHRE: The Object-Oriented, Controllable, High-Resolution Residential Energy Model for Dynamic Integration Studies. Appl. Energy, **2021**, 290, 116732.

[164] Gagnon, P.; Frazier, W.; Hale, E.; Cole, W. Cambium Documentation: Version 2020; NREL/TP-6A20-78239. Golden, CO: National Renewable Energy Laboratory. https …, 2020.

[165] ASHRAE. ASHRAE Standard 169-2006; 2006.

[166] Aspen/Pitkin County Housing Authority. Basalt Vista housing https://www.apcha.org/374/Basalt-Vista-Housing/.

[167] Air Conditioning Contractors of America (ACCA). Manual J: Residential Load Calculation; 2008.

[168] Sparn, B.; Hudon, K.; Christensen, D. Laboratory Performance Evaluation of Residential Integrated Heat Pump Water Heaters; National Renewable Energy Lab.(NREL), Golden, CO (United States), 2014.

[169] Wilson, E. J.; Christensen, C. B.; Horowitz, S. G.; Robertson, J. J.; Maguire, J. B. Energy Efficiency Potential in the US Single-Family Housing Stock; National Renewable Energy Lab.(NREL), Golden, CO (United States), 2017.

[170] Holy Cross Energy. Holy Cross Energy electric service tariffs, rules and regulations https://www.holycross.com/wp-content/uploads/2018/12/Electric-Service-Tariffs-Rules-and-Regulations-12.17.2018.pdf (accessed Aug 7, 2021).

[171] ASHRAE. ASHRAE Standard 55-2017 Thermal Environmental Conditions for Human Occupancy; ASHRAE: PeachTree Corners, USA, 2017.

[172] Maguire, J. How Hot Is Hot Enough? Quantifying Unmet Loads in Simulation. In 2020 ACEEE Hot Water Forum; 2020.

[173] Sun, K.; Specian, M.; Hong, T. Nexus of Thermal Resilience and Energy Efficiency in Buildings: A Case Study of a Nursing Home. Build. Environ., **2020**, 106842.

[174] Wang, J.; Garifi, K.; Baker, K.; Zuo, W.; Zhang, Y. Optimal Operation for Resilient Communities through a Hierarchical Load Scheduling Framework. In Proceedings of 2020 Building Performance Analysis Conference & SimBuild; Virtual Conference, 2020.

[175] Marnay, C.; Venkataramanan, G.; Stadler, M.; Siddiqui, A. S.; Firestone, R.; Chandran, B. Optimal Technology Selection and Operation of Commercial-Building Microgrids. IEEE Trans. Power Syst., **2008**, 23 (3), 975–982.

[176] Bozchalui, M. C.; Sharma, R. Optimal Operation of Commercial Building Microgrids Using Multi-Objective Optimization to Achieve Emissions and Efficiency Targets. In 2012 IEEE Power and Energy Society General Meeting; IEEE: San Diego, CA, USA, 2012; pp 1–8.

[177] Hussain, A.; Bui, V.-H.; Kim, H.-M. Microgrids as a Resilience Resource and Strategies Used by Microgrids for Enhancing Resilience. Appl. Energy, **2019**, 240, 56–72.

[178] Kallel, R.; Boukettaya, G.; Krichen, L. Demand Side Management of Household Appliances in Stand-Alone Hybrid Photovoltaic System. Renew. Energy, **2015**, 81, 123–135.

[179] Ayodele, T. R.; Ogunjuyigbe, A. S. O.; Akpeji, K. O.; Akinola, O. O. Prioritized Rule Based Load Management Technique for Residential Building Powered by PV/Battery System. Eng. Sci. Technol. an Int. J., **2017**, 20 (3), 859–873.

[180] Garifi, K.; Baker, K.; Touri, B.; Christensen, D. Stochastic Model Predictive Control for Demand Response in a Home Energy Management System. In 2018 IEEE Power & Energy Society General Meeting (PESGM); Portland, OR, USA, 2018; pp 1–5.

[181] Zhao, Z.; Lee, W. C.; Shin, Y.; Song, K.-B. An Optimal Power Scheduling Method for Demand Response in Home Energy Management System. IEEE Trans. Smart Grid, **2013**, 4 (3), 1391–1400.

[182] Pathak, A. K.; Chatterji, D. S.; Narkhede, M. S. Artificial Intelligence Based Optimization Algorithm for Demand Response Management of Residential Load in Smart Grid. Int. J. Eng. Innov. Technol., **2012**, 2 (4).

[183] Zhang, D.; Li, S.; Sun, M.; O'Neill, Z. An Optimal and Learning-Based Demand Response and Home Energy Management System. IEEE Trans. Smart Grid, **2016**, 7 (4), 1790–1801.

[184] Mazzeo, D.; Oliveti, G.; Baglivo, C.; Congedo, P. M. Energy Reliability-Constrained Method for the Multi-Objective Optimization of a Photovoltaic-Wind Hybrid System with Battery Storage. Energy, **2018**, 156, 688–708.

[185] Maslow, A. H. Motivation and Personality; Harper & Brothers: New York City, USA, 1954.

[186] Tolić, D.; Palunko, I.; Ivanović, A.; Car, M.; Bogdan, S. Chapter Twelve - Decentralized Cooperative Control in Degraded Communication Environments; Vamvoudakis, K. G., Jagannathan, S. B. T.-C. of C. S., Eds.; Butterworth-Heinemann: Oxford, UK, 2016; pp 373–395.

[187] Luncean, L.; Becheru, A. Communication and Interaction in a Multi-Agent System Devised for Transport Brokering. In Proceedings of the 2015 Balkan Conference on Informatics: Advances in ICT, Craiova, Romania; 2015; pp 2–4.

[188] Javaid, N.; Ullah, I.; Akbar, M.; Iqbal, Z.; Khan, F. A.; Alrajeh, N.; Alabed, M. S. An Intelligent Load Management System with Renewable Energy Integration for Smart Homes. IEEE Access, **2017**, 5, 13587–13600.

[189] Garifi, K.; Baker, K.; Christensen, D.; Touri, B. Control of home energy management systems with energy storage: Nonsimultaneous charging and discharging guarantees https://arxiv.org/pdf/1805.00100.pdf.

[190] Zakula, T.; Armstrong, P. R.; Norford, L. Modeling Environment for Model Predictive Control of Buildings. Energy Build., **2014**, 85, 549–559.

[191] Garifi, K.; Baker, K.; Christensen, D.; Touri, B. Stochastic Home Energy Management Systems with Varying Controllable Resources. In 2019 IEEE Power & Energy Society General Meeting (PESGM); IEEE: Atlanta, GA, USA, 2019; pp 1–5.

[192] SiteSage. Historic Green Village Submetering Data. https://sitesage.net/home/management/index.php (accessed Oct 7, 2020).

[193] National Renewable Energy Laboratory. National Solar Radiation Data Base 1991-2005 Update: Typical Meteorological Year 3. Office of Scientific and Technical Information: Oak Ridge, USA 2019.

[194] Gurobi 9.0. Gurobi Optimization https://www.gurobi.com/ (accessed Oct 29, 2020).

[195] Tang, H.; Wang, S.; Li, H. Flexibility Categorization, Sources, Capabilities and Technologies for Energy-Flexible and Grid-Responsive Buildings: State-of-The-Art and Future Perspective. Energy, **2020**, 119598.

[196] Kou, X.; Li, F.; Dong, J.; Olama, M.; Starke, M.; Chen, Y.; Zandi, H. A Comprehensive Scheduling Framework Using SP-ADMM for Residential Demand Response with Weather and Consumer Uncertainties. IEEE Trans. Power Syst., **2020**.

[197] Faraji, J.; Ketabi, A.; Hashemi-Dezaki, H.; Shafie-Khah, M.; Catalão, J. P. S. Optimal Day-Ahead Self-Scheduling and Operation of Prosumer Microgrids Using Hybrid Machine Learning-Based Weather and Load Forecasting. IEEE Access, **2020**, 8, 157284–157305.

[198] Wang, J.; Garifi, K.; Baker, K.; Zuo, W.; Zhang, Y.; Huang, S.; Vrabie, D. Optimal Renewable Resource Allocation and Load Scheduling of Resilient Communities. Energies. 2020.

[199] Yu, M. G.; Pavlak, G. S. Assessing the Performance of Uncertainty-Aware Transactive Controls for Building Thermal Energy Storage Systems. Appl. Energy, **2021**, 282, 116103.

[200] Liang, Z.; Huang, C.; Su, W.; Duan, N.; Donde, V.; Wang, B.; Zhao, X. Safe Reinforcement Learning-Based Resilient Proactive Scheduling for a Commercial Building Considering Correlated Demand Response. IEEE Open Access J. Power Energy, **2021**, 8, 85–96.

[201] Ahmad, A.; Khan, J. Y. Real-Time Load Scheduling, Energy Storage Control and Comfort Management for Grid-Connected Solar Integrated Smart Buildings. Appl. Energy, **2020**, 259, 114208.

[202] E Silva, D. P.; Salles, J. L. F.; Fardin, J. F.; Pereira, M. M. R. Management of an Island and Grid-Connected Microgrid Using Hybrid Economic Model Predictive Control with Weather Data. Appl. Energy, **2020**, 278, 115581.

[203] Yundra, E.; Surabaya, U. N.; Kartini, U.; Wardani, L.; Ardianto, D.; Surabaya, U. N.; Surabaya, U. N.; Surabaya, U. N. Hybrid Model Combined Fuzzy Multi-Objective Decision Making with Feed Forward Neural Network (F-MODMFFNN) For Very Short-Term Load Forecasting Based on Weather Data. Int. J. Intell. Eng. Syst., **2020**, 13 (4), 182–195.

[204] Lu, M.; Abedinia, O.; Bagheri, M.; Ghadimi, N.; Shafie-khah, M.; Catalão, J. P. S. Smart Load Scheduling Strategy Utilising Optimal Charging of Electric Vehicles in Power Grids Based on an Optimisation Algorithm. IET Smart Grid, **2020**, 3 (6), 914–923.

[205] Khalid, Z.; Abbas, G.; Awais, M.; Alquthami, T.; Rasheed, M. B. A Novel Load Scheduling Mechanism Using Artificial Neural Network Based Customer Profiles in Smart Grid. Energies, **2020**, 13 (5), 1062.

[206] Kerboua, A.; Boukli-Hacene, F.; Mourad, K. A. Particle Swarm Optimization for Micro-Grid Power Management and Load Scheduling. Int. J. Energy Econ. Policy, **2020**, 10 (2), 71.

[207] Kaur, R.; Schaye, C.; Thompson, K.; Yee, D. C.; Zilz, R.; Sreenivas, R. S.; Sowers, R. B. Machine Learning and Price-Based Load Scheduling for an Optimal IoT Control in the Smart and Frugal Home. Energy AI, **2021**, 3, 100042.

[208] Chung, H.-M.; Maharjan, S.; Zhang, Y.; Eliassen, F. Distributed Deep Reinforcement Learning for Intelligent Load Scheduling in Residential Smart Grids. IEEE Trans. Ind. Informatics, **2020**, 17 (4), 2752–2763.

[209] Aftab, M.; Chen, C.; Chau, C.-K.; Rahwan, T. Automatic HVAC Control with Real-Time Occupancy Recognition and Simulation-Guided Model Predictive Control in Low-Cost Embedded System. Energy Build., **2017**, 154, 141–156.

[210] Lim, B.; Van Den Briel, M.; Thiébaux, S.; Backhaus, S.; Bent, R. HVAC-Aware Occupancy Scheduling. In Proceedings of the AAAI Conference on Artificial Intelligence; 2015; Vol. 29.

[211] Jin, Y.; Yan, D.; Zhang, X.; An, J.; Han, M. A Data-Driven Model Predictive Control for Lighting System Based on Historical Occupancy in an Office Building: Methodology Development. In Building Simulation; Springer, 2020; pp 1–17.

[212] Wang, J.; Zuo, W.; Huang, S.; Vrabie, D. Data-Driven Prediction of Occupant Presence and Lighting Power: A Case Study for Small Commercial Buildings. In American Modelica Conference; 2020.

[213] Chen, X.; Wang, Q.; Srebric, J. Model Predictive Control for Indoor Thermal Comfort and Energy Optimization Using Occupant Feedback. Energy Build., **2015**, 102, 357–369.

[214] West, S. R.; Ward, J. K.; Wall, J. Trial Results from a Model Predictive Control and Optimisation System for Commercial Building HVAC. Energy Build., **2014**, 72, 271–279.

[215] Wang, J.; Huang, S.; Zuo, W.; Vrabie, D. Occupant Preference-Aware Load Scheduling for Resilient Communities. Energy Build., **2021**.

[216] Drgoňa, J.; Arroyo, J.; Figueroa, I. C.; Blum, D.; Arendt, K.; Kim, D.; Ollé, E. P.; Oravec, J.; Wetter, M.; Vrabie, D. L. All You Need to Know about Model Predictive Control for Buildings. Annu. Rev. Control, **2020**.

[217] Zhang, X.; Schildbach, G.; Sturzenegger, D.; Morari, M. Scenario-Based MPC for Energy-Efficient Building Climate Control under Weather and Occupancy Uncertainty. In 2013 European Control Conference (ECC); IEEE, 2013; pp 1029–1034.

[218] The Engineering ToolBox. Metabolic Heat Gain from Persons. https://www.engineeringtoolbox.com/metabolic-heat-persons-d_706.html (accessed Feb 19, 2021).

[219] Hosni, M. H.; Beck, B. T. Updated Experimental Results for Heat Gain from Office Equipment in Buildings. ASHRAE Trans., **2011**, 117 (2).

[220] ASHRAE. ASHRAE Handbook — Fundamentals 2017; 2017.

[221] Lawrence Berkeley National Laboratory. Home Energy Saver & Score: Engineering Documentation - Internal Gains. http://hes-documentation.lbl.gov/calculation-methodology/calculation-of-energy-consumption/heating-and-cooling-calculation/internal-gains (accessed Feb 16, 2021).

[222] Roth, A.; Reyna, J.; Christensen, J.; Vrabie, D.; Adetola, V. GEB Technical Report Webinar Series: Whole-Building Control, Sensing, Modeling & Analytics https://www.energy.gov/sites/default/files/2020/05/f74/bto-geb-webinar-CSMA-051920.pdf.

[223] Heirung, T. A. N.; Paulson, J. A.; O'Leary, J.; Mesbah, A. Stochastic Model Predictive Control—How Does It Work? Comput. Chem. Eng., **2018**, 114, 158–170.

[224] Mooney, C. Z. Monte Carlo Simulation; Sage, 1997.

[225] Statistics Solutions. Chi-Square Goodness of Fit Test. https://www.statisticssolutions.com/chi-square-goodness-of-fit-test/ (accessed Feb 25, 2021).

[226] Chen, Y.; Hong, T.; Luo, X. An Agent-Based Stochastic Occupancy Simulator. In Building Simulation; Springer, 2018; Vol. 11, pp 37–49.

Appendix A

Supplementary Tables and Figures

Table A.1 Community average annual carbon emission per household for different controllers across simulated years (non-net-metered; percentage values are changes relative to the corresponding baseline).

Year	Baseline (kg/yr.)	MO-0	MO-1	PR-0	PR-1
2022	8,318	-5.1%	-4.0%	-5.4%	-4.4%
2030	7,201	-4.6%	-3.4%	-4.9%	-3.8%
2038	7,476	-5.0%	-3.6%	-5.3%	-4.0%
2046	7,793	-5.4%	-4.0%	-5.8%	-4.3%

Figure A.1 Community average annual energy on- and off-peak costs of controlled loads for different controllers in 2030.

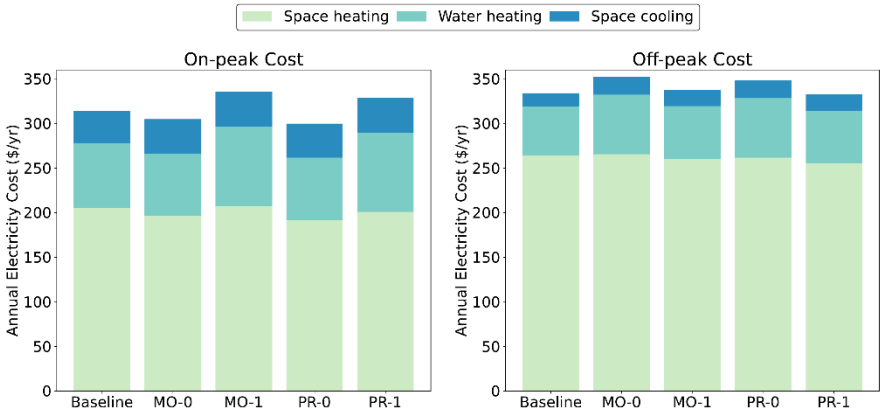

Figure A.2 Community average annual energy on- and off-peak costs of controlled loads for different controllers in 2038.

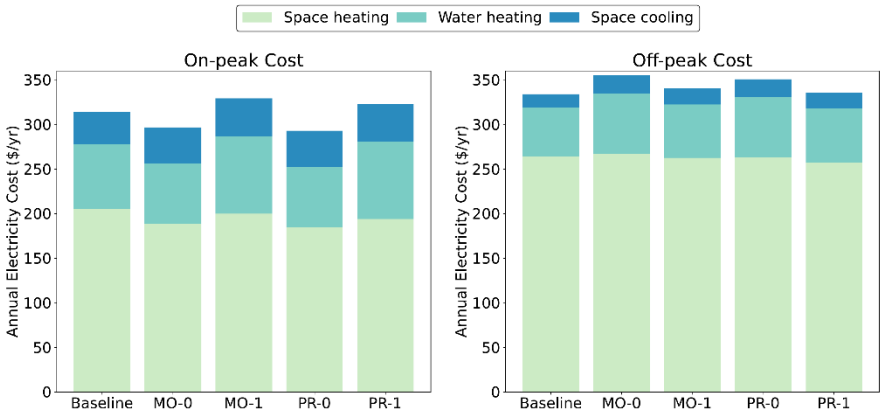

Figure A.3 Community average annual energy on- and off-peak costs of controlled loads for different controllers in 2046.

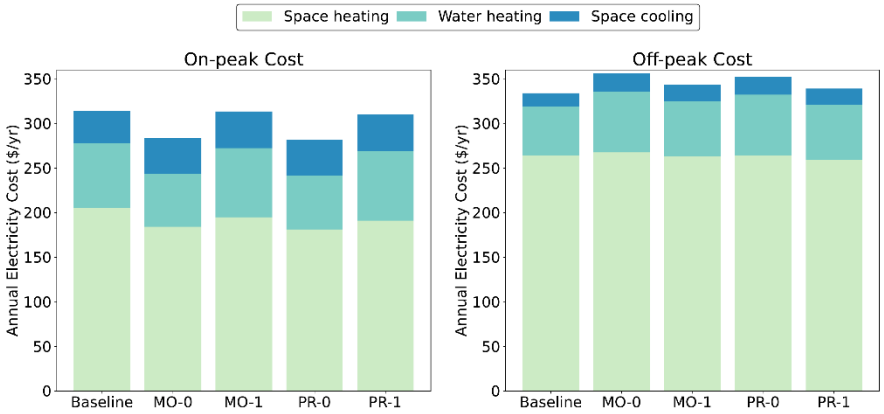

Table A.2 Community average indoor discomfort values for each simulation scenario based on ASHRAE Standard 55.

Year	Heating (°C-hrs./yr.)				
	Baseline	MO-0	MO-1	PR-0	PR-1
2022	8	24	27	30	33
2030	8	34	40	31	36
2038	8	69	79	64	73
2046	8	55	66	51	59

Table A.3 Detailed KPIs for each building and community overall of each scenario.

		Temperature Deviation (℃)	PV Curtailment Ratio	Unserved Load Ratio					Battery Size (kWh)
				Sheddable	Shiftable	Modulatable	Critical	Overall	
S11	R	1.34	0.00%	0.00%	19.92%	N/A	0.00%	5.99%	34.71
	I	2.62	0.00%	0.00%	N/A	N/A	0.00%	0.00%	89.81
	B	0.77	0.00%	0.00%	8.18%	0.00%	0.00%	0.38%	75.28
	Community	3.04	0.00%	0.00%	10.94%	0.00%	0.00%	0.27%	199.80
S21_R	R	2.76	31.25%	0.00%	19.92%	N/A	0.00%	5.99%	45.57
	I	2.65	0.00%	0.00%	N/A	N/A	0.00%	0.00%	75.85
	B	1.34	0.00%	0.00%	8.18%	0.00%	0.00%	0.38%	94.13
	Community	4.05	8.31%	0.00%	10.94%	0.00%	0.00%	0.27%	215.55
S21_I	R	0.79	0.00%	0.00%	19.92%	N/A	0.00%	5.99%	35.56
	I	2.62	0.00%	0.00%	N/A	N/A	0.00%	0.00%	93
	B	0.50	0.00%	0.00%	8.18%	0.00%	0.00%	0.38%	81.08
	Community	2.78	0.00%	0.00%	10.94%	0.00%	0.00%	0.27%	209.64
S21_B	R	1.45	0.00%	0.00%	19.92%	N/A	0.00%	5.99%	35.56
	I	2.62	0.00%	0.00%	N/A	N/A	0.00%	0.00%	87.79
	B	0.79	0.00%	0.00%	8.18%	0.00%	0.00%	0.38%	71.26
	Community	3.10	0.00%	0.00%	10.94%	0.00%	0.00%	0.27%	194.61
S31	R	2.06	5.50%	0.00%	19.92%	N/A	0.00%	5.99%	38.79
	I	2.69	0.00%	0.00%	N/A	N/A	0.00%	0.00%	77.67
	B	0.80	0.00%	0.00%	8.18%	0.00%	0.00%	0.38%	66.45
	Community	3.48	1.03%	0.00%	10.94%	0.00%	0.00%	0.27%	182.91
S12	R	0.29	0.00%	86.50%	19.92%	N/A	0.00%	10.80%	28.99
	I	0.28	0.00%	63.72%	N/A	N/A	0.00%	12.74%	124.68
	B	0.34	0.00%	99.03%	8.18%	68.89%	0.00%	4.32%	64.4
	Community	0.53	0.00%	64.14%	10.94%	68.89%	0.00%	9.25%	218.07
S22_R	R	0.29	49.57%	31.49%	19.92%	N/A	0.00%	7.74%	39.81
	I	0.28	0.00%	65.17%	N/A	N/A	0.00%	13.03%	90.25
	B	0.34	0.00%	100.00%	8.18%	77.00%	0.00%	4.77%	111.99
	Community	0.53	13.18%	65.06%	10.94%	77.00%	0.00%	9.54%	242.05
S22_I	R	0.29	0.00%	85.89%	19.92%	N/A	0.00%	10.77%	32.82
	I	0.28	0.00%	63.72%	N/A	N/A	0.00%	12.74%	127.86
	B	0.34	0.00%	99.03%	8.18%	72.83%	0.00%	4.54%	77.23
	Community	0.53	0.00%	64.13%	10.94%	72.83%	0.00%	9.34%	237.91
S22_B	R	0.29	0.00%	86.50%	19.92%	N/A	0.00%	10.80%	28.37
	I	0.28	0.00%	63.72%	N/A	N/A	0.00%	12.74%	122.66
	B	0.34	0.00%	99.03%	8.18%	69.23%	0.00%	4.34%	59.16
	Community	0.53	0.00%	64.14%	10.94%	69.23%	0.00%	9.26%	210.19
S32	R	0.29	28.93%	46.01%	19.92%	N/A	0.00%	8.55%	35.33
	I	0.28	0.00%	65.47%	N/A	N/A	0.00%	13.09%	90.88
	B	0.34	0.00%	100.00%	8.18%	73.64%	0.00%	4.58%	73.31
	Community	0.53	5.43%	65.49%	10.94%	73.64%	0.00%	9.51%	199.52

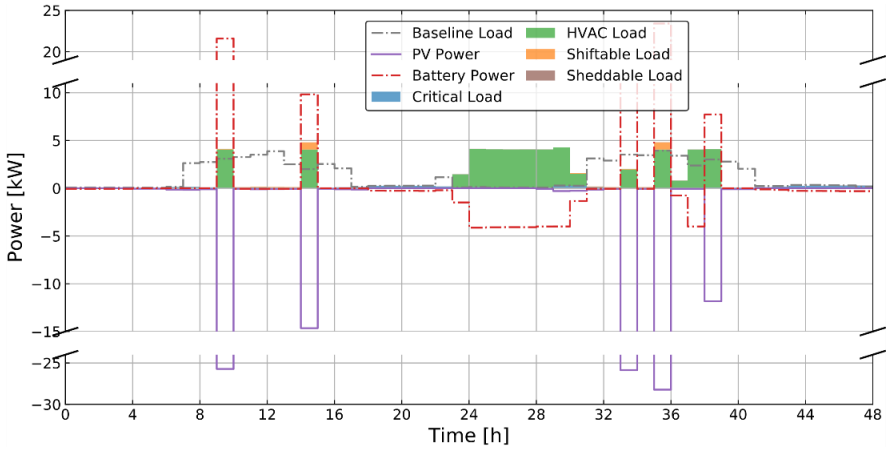

Figure A.4 Residential building load shape, battery behavior, and PV power (S31: occupancy-based weighting, minimizing unserved load ratio).

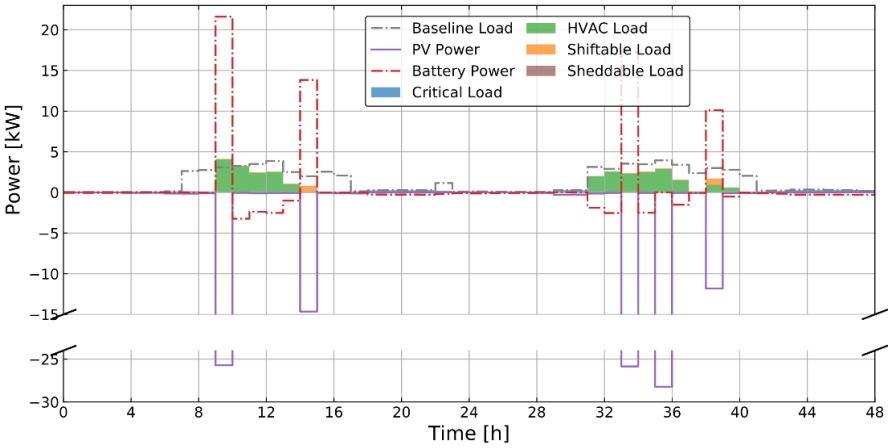

Figure A.5 Residential building load shape, battery behavior, and PV power (S32: occupancy-based weighting, maximizing thermal comfort).

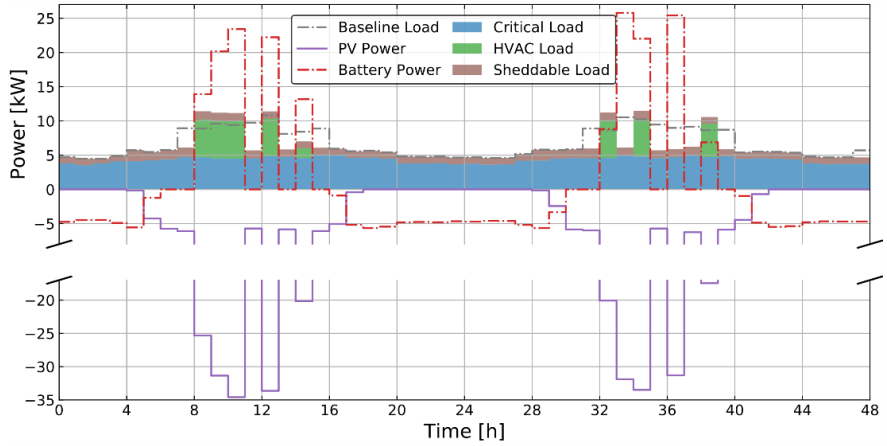

Figure A.6 Ice cream shop load shape, battery behavior, and PV power (S21_I: prioritizing ice cream shop, minimizing unserved load ratio).

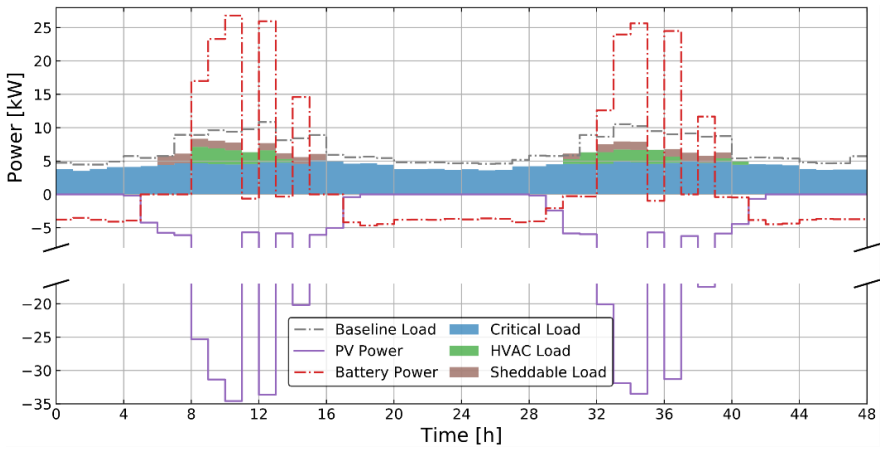

Figure A.7 Ice cream shop load shape, battery behavior, and PV power (S22_I: prioritizing ice cream shop, maximizing thermal comfort).

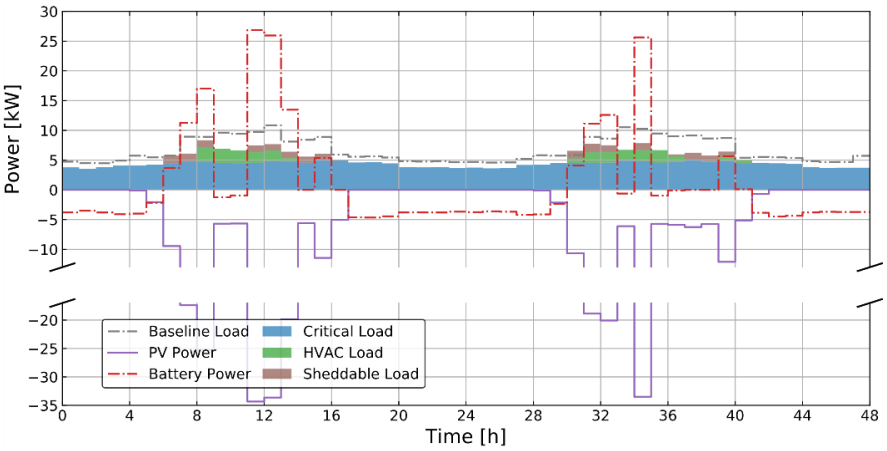

Figure A.8 Ice cream shop load shape, battery behavior, and PV power (S32: occupancy-based weighting, maximizing thermal comfort).

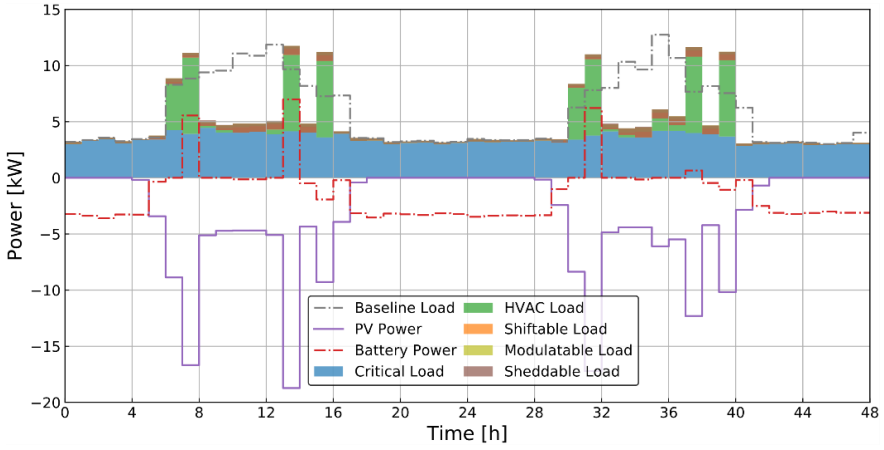

Figure A.9 Bakery load shape, battery behavior, and PV power (S21_B: prioritizing bakery, minimizing unserved load ratio).

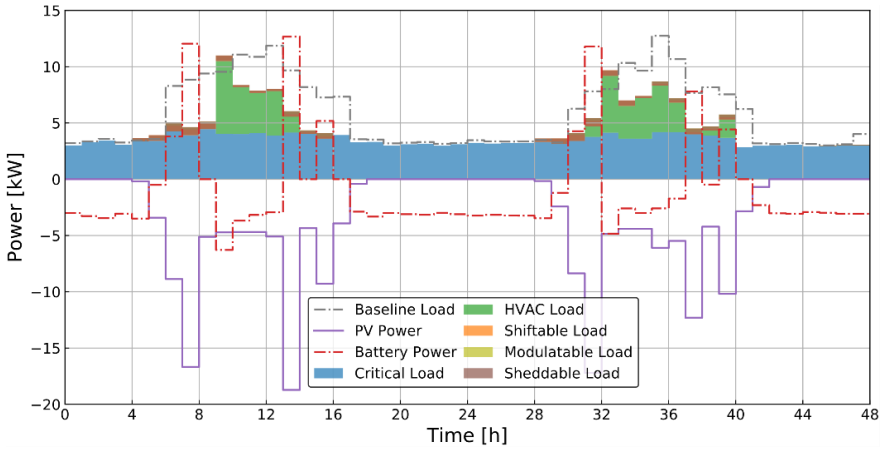

Figure A.10 Bakery load shape, battery behavior, and PV power (S22_B: prioritizing bakery, maximizing thermal comfort).

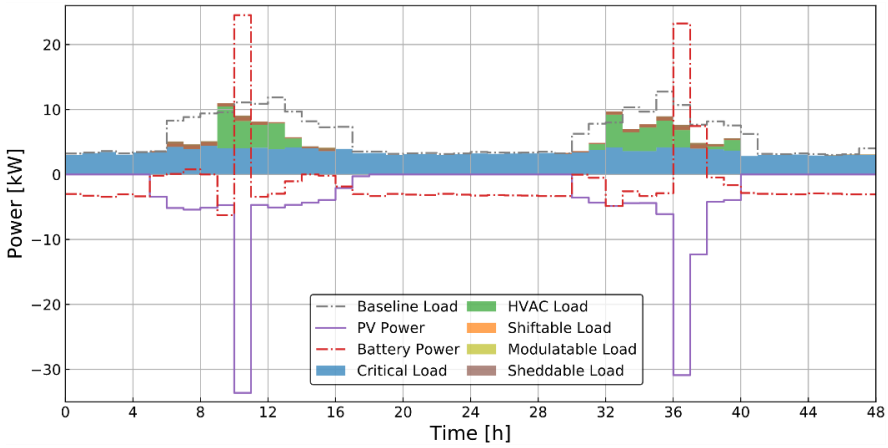

Figure A.11 Bakery load shape, battery behavior, and PV power (S32: occupancy-based weighting, maximizing thermal comfort).

Table A.4 Complete list of building loads and heat gain coefficients [219–221].

Building	No.	Load	Capacity (W)	Heat Gain Coefficient	Heat Gain (W)	Weighted Average Coefficient
Residential	1	Lights	293	0.8	234.4	0.31
	2	Refrigerator	494	0.4	197.6	
	3	Computer	18	0.15	2.7	
	4	Range	1775	0.34	603.5	
	5	Washer	438	0.8	350.4	
	6	Dryer	2795	0.15	419.25	
Ice Cream Shop	1	Lights	135	0.8	108	0.35
	2	Coolers	7394	0.4	2957.6	
	3	Display case	280	0.4	112	
	4	Coffee maker	2721	0.3	816.3	
	5	Soda dispenser	201	0.5	100.5	
	6	Outdoor ice storage	1127	0	0	
Bakery	1	Lights	1859	0.8	1487.2	0.38
	2	Coolers	4161	0.4	1664.4	
	3	Display case	1011	0.4	404.4	
	4	Range	4065	0.15	609.75	
	5	Mixer	521	0.31	161.51	
	6	Gas oven	761	0.2	152.2	
	7	Room plugs	377	0.5	188.5	
	8	Microwave	1664	0.67	1114.88	
	9	Dishwasher	1552	0.15	232.8	

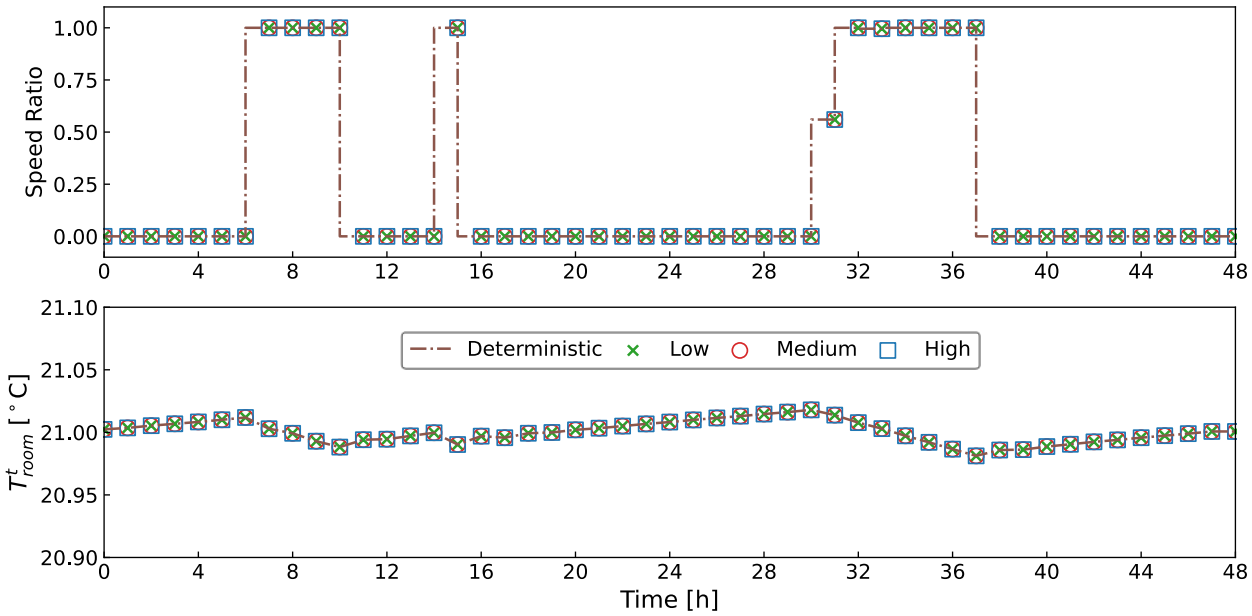

Figure A.12 Optimal schedules of the heat pump speed ratio and predicted room temperatures by various schedulers (ice cream shop).

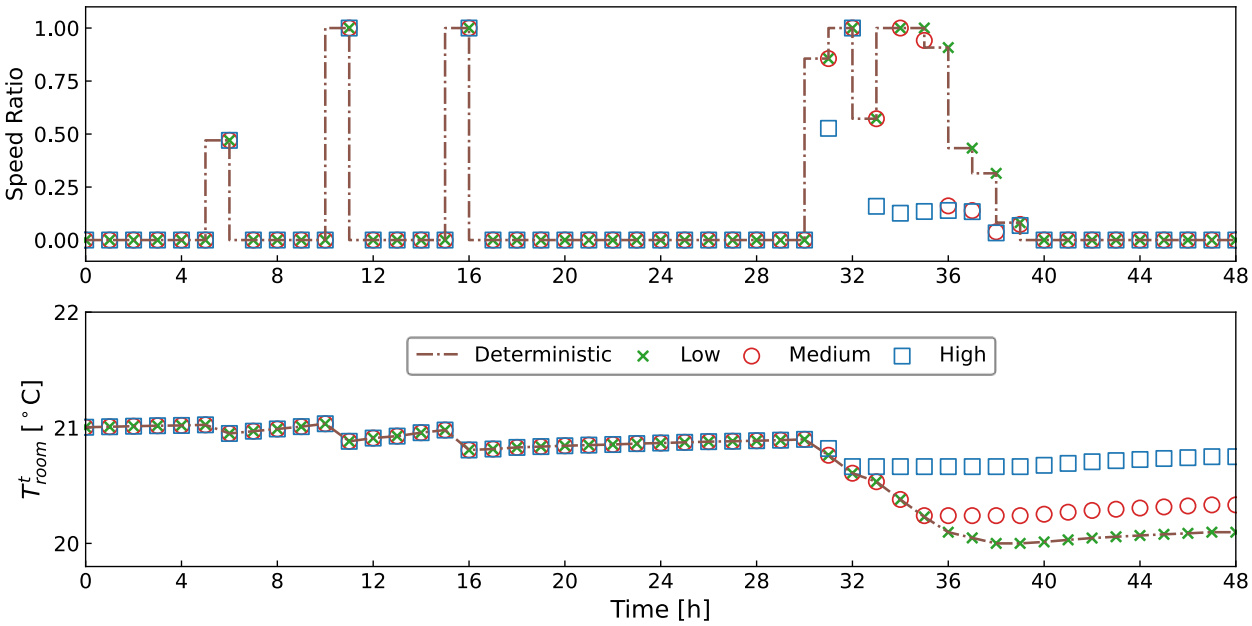

Figure A.13 Optimal schedules of the heat pump speed ratio and predicted room temperatures by various schedulers (bakery).

Table A.5 Full comparison of controller performances under different uncertainty levels in all three buildings.

KRIs	Controller	Residential			Ice Cream Shop			Bakery		
		Low	Medium	High	Low	Medium	High	Low	Medium	High
Unmet Thermal Preference Hours (°C·hrs)	Deterministic	33.70	47.19	48.91	70.69	85.61	86.87	89.03	88.80	102.81
	Chance-constrained	33.70	47.19	46.42	70.69	85.61	86.87	89.03	91.28	101.61
Mean Room Temperature (°C)	Deterministic	24.38	23.69	23.75	21.23	22.87	23.38	25.34	24.27	23.65
	Chance-constrained	24.38	23.69	23.87	21.23	22.87	23.38	25.34	24.50	23.89
Unserved Load Ratio	Deterministic	0.074			0.022			0.025		
	Chance-constrained	0.074	0.074	0.074	0.022	0.022	0.022	0.025	0.025	0.025
Required Battery Size (kWh)	Deterministic	47.69			99.14			80.01		
	Chance-constrained	47.69	47.69	44.12	99.14	99.14	99.14	80.01	76.89	76.89